THE UNIVERSITY *of* EDINBURGH

Antennas And Beam-steering Arrays For Polarization Diversity And Full-duplex Applications

by

Maksim Kuznetcov

Submitted for the degree of

Doctor of Philosophy

ELECTRICAL, ELECTRONIC AND COMPUTER ENGINEERING
SCHOOL OF ENGINEERING & PHYSICAL SCIENCES
HERIOT-WATT UNIVERSITY

October 2022

Abstract

This thesis presents new designs for polarization diverse dielectric resonator antennas (DRAs) as well as antennas that can offer efficient full-duplex (FD) functionality. Basically, this research effort has been completed to meet the demands of modern tracking systems as well as in-band full-duplex communication systems. For these applications antenna polarization control, compatibility, co-location, and isolation are the important parameters to support these high-performance systems.

The first part of the thesis covers the challenges of modern radio frequency (RF) environments where the proposed polarization reconfigurable antennas are introduced. At first, a multi-port DRA is outlined as a possible candidate for the global positioning system (GPS) and the Global Navigation Satellite System (GNSS). To further advance this original design, and in an effort to reduce the size whilst maintaining polarization control, an integrated circuit was also proposed and tested.

Advancing from the research work of phase polarization control using DRAs, the second part of the thesis studies other new antennas which are suitable for FD communications. Those antennas offer high isolation which makes the signal recoverable for those FD systems. To advance the state-of-the-art, an H-shaped slot antenna arrangement with parasitic patches and dual-differential feeding was proposed. The antenna architecture was investigated with both external and integrated feed systems and both prototypes offer high isolation levels. The single-element was further integrated into a 1×4 antenna array which was shown to offer similar isolation levels and with the capability to beam steer.

Further research included high isolation antennas for operation in the 5G mm-wave band. In particular, a new FD pattern reconfigurable antenna was proposed which can be used in dual-polarized radars and other FD systems. Depending on the input phase excitation, the beam pattern control can be established with sum or difference patterns or both. Also, the antenna concept was further extended into a novel FD antenna array. This array has a similar common and/or differential feeding which can provide sum or difference patterns in the far-field. Also, an external Butler matrix was used to investigate the beam-steering capabilities of the array. These antenna systems also have applications for dual-polarized radars, retro-directive arrays, and other beam-tracking scenarios which require high inter-port isolation.

Dedication

To my parents and relatives who raised me and supported me over such a challenging and exciting teaching and research path. Also to my uncle and friends who further supported me financially. To my grandparents, especially my grandfather Alexander Timofeyevich. I am sad that you were not able to see the day when I hopefully graduate. I miss you very much.

To everyone at Heriot-Watt and The University of Edinburgh who gave me opportunities and helped me along the way.

Bolshoe Spasibo!

Acknowledgements

I would like to express my sincere gratitude to Dr. Symon Podilchak. Together we did a lot of things over my Ph.D. and during the last years of my M.Eng. degree. Your support over those challenging times was great. It was a big mental challenge with uncertainties of the future, visas issues, then COVID and now the war in Ukraine. Sometimes it seems that I'm like a squirrel in a wheel. If not for your help, all the achievements would never have happened.

I would like to thank Prof. Mathini Sellathurai for assisting with my Ph.D. and helping with my life plans. Without your help this Ph.D. would not be possible. I am very grateful to you both, and I hope that you will help other students in the same way to achieve their dreams. Special thanks to Prof. Alexander Belyaev. I'm very glad I could talk to you. Especially in difficult times.

Thanks to Prof. George Goussetis and Dr. Dimitris Anagnostou for your help during my Ph.D. Especially the 3-month opportunity before my Ph.D. which not only was an interesting project and prepared me for further research.

A special thanks to my colleagues and friends at Heriot-Watt and Edinburgh University. Especially to Zain Shafiq, Grant Gourley, Cristian Alistarh, Callum Hodgkinson, Kostas, Rahil, Victoria, Ariel, Pascual...I am sure I have missed people, sorry! It was a long and challenging journey over those 8 years. It was a great pleasure to work with you and learn things together.

Finally, a special thanks goes to Davide from Sapienza University.

Research Thesis Submission

Please note this form should be bound into the submitted thesis.

Name:	Maksim Kuznetcov		
School:	School of Engineering and Physical Sciences		
Version: *(i.e. First, Resubmission, Final)*	Final	Degree Sought:	PhD

Declaration

In accordance with the appropriate regulations I hereby submit my thesis and I declare that:

1. The thesis embodies the results of my own work and has been composed by myself
2. Where appropriate, I have made acknowledgement of the work of others
3. The thesis is the correct version for submission and is the same version as any electronic versions submitted*.
4. My thesis for the award referred to, deposited in the Heriot-Watt University Library, should be made available for loan or photocopying and be available via the Institutional Repository, subject to such conditions as the Librarian may require
5. I understand that as a student of the University I am required to abide by the Regulations of the University and to conform to its discipline.
6. I confirm that the thesis has been verified against plagiarism via an approved plagiarism detection application e.g. Turnitin.

ONLY for submissions including published works

Please note you are only required to complete the Inclusion of Published Works Form (page 2) if your thesis contains published works)

7. Where the thesis contains published outputs under Regulation 6 (9.1.2) or Regulation 43 (9) these are accompanied by a critical review which accurately describes my contribution to the research and, for multi-author outputs, a signed declaration indicating the contribution of each author (complete)
8. Inclusion of published outputs under Regulation 6 (9.1.2) or Regulation 43 (9) shall not constitute plagiarism.

* *Please note that it is the responsibility of the candidate to ensure that the correct version of the thesis is submitted.*

Signature of Candidate:	MBK	Date:	4/10/2022

Submission

Submitted By *(name in capitals):*	MAKSIM KUZNETCOV
Signature of Individual Submitting:	MBK
Date Submitted:	4/10/2022

For Completion in the Student Service Centre (SSC)

Limited Access	Requested	Yes		No		Approved	Yes		No	
E-thesis Submitted ***(mandatory for final theses)***										
Received in the SSC by *(name in capitals):*						Date:				

Inclusion of Published Works

Please note you are only required to complete the Inclusion of Published Works Form if your thesis contains published works under Regulation 6 (9.1.2)

Declaration

This thesis contains one or more multi-author published works. In accordance with Regulation 6 (9.1.2) I hereby declare that the contributions of each author to these publications is as follows:

Citation details	"Printed Leaky-Wave Antenna With Aperture Control Using Width-Modulated Microstrip Lines and TM Surface-Wave Feeding by SIW Technology," in IEEE Antennas and Wireless Propagation Letters, vol. 18, no. 9, pp. 1809-1813, Sept. 2019. link)
Maksim V. Kuznetcov	Design, analysis, simulations, measurements, post processing, paper writing.
Victoria Gómez-Guillamón Buendía;	Supervision, guidance
Zain Shafiq	Theoretical analysis, assistance
Ladislau Matekovits	Theoretical analysis, assistance
Symon K. Podilchak	Supervision, guidance, corrections.
Signature:	MBK
Date:	15/09/2022

Citation details	"Dual-Polarized Aperture-Coupled Patch Antennas With Application to Retrodirective and Monopulse Arrays," in IEEE Access, vol. 8, pp. 7549-7557, 2020
Paul Le Bihan	Design, analysis, simulations, measurements, post processing, paper writing
Pascual D. Hilario Re	Design, analysis, simulations
Davide Comite	Analysis, assistance
Maksim Kuznetcov	Analysis, assistance
Symon K. Podilchak	Supervision, guidance, corrections.
Colum Tucker	Theoretical analysis, assistance
Kieran Maccoll	Assistance
Yelzhas Zhaksylyk	Assistance
María García-Vigueras	Assistance
Mathini Sellathurai	Assistance
George Goussetis	Assistance, guidance
Signature:	MBK
Date:	15/09/2022

Citation details	"Wideband Array-Fed Fabry-Perot Cavity Antenna for 2-D Beam Steering," in IEEE Transactions on Antennas and Propagation, vol. 69, no. 2, pp. 784-794, Feb. 2021.
Davide Comite	Design, analysis, simulations, paper writing
Symon K. Podilchak	Supervision, guidance, corrections.
Maksim Kuznetcov	analysis, simulations, measurements, post processing
Victoria Gómez-Guillamón Buendía	analysis, simulations
Paolo Burghignoli	Theoretical analysis
Paolo Baccarelli	Theoretical analysis
Alessandro Galli	Theoretical analysis
Signature:	MBK
Date:	15/09/2022

Please included additional citations as required.

Citation details	Directive 2-D Beam Steering by Means of a Multiport Radially Periodic Leaky-Wave Antenna," in IEEE Transactions on Antennas and Propagation, vol. 69, no. 5, pp. 2494-2506
Davide Comite	Design, analysis, simulations, paper writing
Maksim Kuznetcov	Analysis, simulations, measurements, post processing
Victoria Gómez-Guillamón Buendía	Analysis, simulations
Symon K. Podilchak	Supervision, guidance, corrections.
Paolo Burghignoli	Theoretical analysis
Paolo Baccarelli	Theoretical analysis
Alessandro Galli	Theoretical analysis
Signature:	MBK
Date:	15/09/2022

Citation details	"Hybrid Dielectric Resonator Antenna for Diversity Applications With Linear or Circular Polarization," in IEEE Transactions on Antennas and Propagation,
Maksim V. Kuznetcov	Analysis, simulations, paper writing.
Symon K. Podilchak	Design, analysis, simulations, corrections.
Michel Clénet	Guidance
Yahia M. M. Antar	Guidance
Signature:	MBK
Date:	15/09/2022

Citation details	"Planar Feeding Circuit Integrated With a Compact Dielectric Resonator for Polarization Diversity," in IEEE Transactions on Microwave Theory and Techniques,
Maksim V. Kuznetcov	Analysis, simulations, paper writing.
Symon K. Podilchak	Analysis, simulations, corrections.
Jonathan C. Johnstone	Design, analysis, measurements
Michel Clénet	Guidance
Yahia M. M. Antar	Guidance
Signature:	MBK
Date:	15/09/2022

Citation details	"Dual-Polarized High-Isolation Antenna Design and Beam Steering Array Enabling Full-Duplex Communications for Operation Over a Wide Frequency Range," in IEEE Open Journal of Antennas and Propagation, vol. 2, pp. 521-532, 2021.
Maksim V. Kuznetcov	Design, analysis, theoretical considerations, measurements, post processing, paper writing
Symon K. Podilchak	Supervision, Guidance, paper corrections.
Ariel J. McDermott	Paper corrections.
Mathini Sellathurai	Supervision, Guidance,
Signature:	MBK
Date:	15/09/2022

Citation details	"Dual-Polarized Antenna With Dual-Differential Integrated Feeding for Wideband Full-Duplex Systems," in IEEE Transactions on Antennas and Propagation, vol. 69, no. 11, pp. 7192-7201, Nov. 2021
Maksim V. Kuznetcov	Design, analysis, theoretical considerations, measurements, post processing, paper writing
Symon K. Podilchak	Supervision, Guidance, paper corrections.
Ariel J. McDermott	Paper corrections.
Mathini Sellathurai	Supervision, Guidance,
Signature:	MBK
Date:	15/09/2022

Citation details	"Compact Leaky-Wave SIW Antenna With Broadside Radiation and Dual-Band Operation for CubeSats," in IEEE Antennas and Wireless Propagation Letters, vol. 20, no. 11, pp. 2125-2129, Nov. 2021
Maksim V. Kuznetcov	Simulations, additional measurements, post processing, paper writing
Symon K. Podilchak	Supervision, Guidance, paper corrections.
Miguel Poveda-García	Theoretical analysis, measurements, post processing, assistance, guidance

Pascual Hilario	Measurements assistance
Cristian A. Alistarh	Measurements
George Goussetis	Guidance
José Luis Gómez-Tornero	Guidance
Signature:	MBK
Date:	15/09/2022

Table of Contents

List of Tables

Figure table

Glossary

ACS Aperture Coupled Slots.

AP Antenna Port.

BW Bandwidth.

CP Circular Polarization.

DRA Dielectric Resonator antenna.

DRCS Dielectric Resonator and Circuit System.

DUT Device Under Test.

FD Full-duplex.

GNSS Global Navigation Satellite System.

GPRS General Packet Radio Service.

GPS Global Positioning System.

IBFD In-Band Full-Duplex.

LH Left-Hand.

LP Linear Polarization.

MIMO Multiple-Input Multiple-Output.

PCB Printed Circuit Board.

RH Right-Hand.

RX Receiver.

SIW Substrate Integrated Waveguide.

SNR Signal-to-Noise Ratio.

TX Transmitter.

UAV Unmanned Aerial Vehicle.

List of Publications

Articles Published in International Journals:

1. M. V. Kuznetcov, S. K. Podilchak, A. J. McDermott and M. Sellathurai, "Dual-Polarized Antenna With Dual-Differential Integrated Feeding for Wideband Full-Duplex Systems," in IEEE Transactions on Antennas and Propagation, vol. 69, no. 11, pp. 7192-7201, Nov. 2021.

2. M. V. Kuznetcov, S. K. Podilchak, A. J. McDermott and M. Sellathurai, "Dual-Polarized High-Isolation Antenna Design and Beam Steering Array Enabling Full-Duplex Communications for Operation Over a Wide Frequency Range," in IEEE Open Journal of Antennas and Propagation, vol. 2, pp. 521-532, 2021.

3. M. V. Kuznetcov, S. K. Podilchak, M. Clénet and Y. M. M. Antar, "Hybrid Dielectric Resonator Antenna for Diversity Applications With Linear or Circular Polarization," in IEEE Transactions on Antennas and Propagation, vol. 69, no. 8, pp. 4457-4465, Aug. 2021.

4. M. V. Kuznetcov, S. K. Podilchak, J. C. Johnstone, M. Clénet and Y. M. M. Antar, "Planar Feeding Circuit Integrated With a Compact Dielectric Resonator for Polarization Diversity," in IEEE Transactions on Microwave Theory and Techniques, vol. 69, no. 4, pp. 2229-2240, April 2021.

5. Kuznetcov, Maksim V. and Podilchak, Symon K. and Poveda-García, Miguel and Hilario, Pascual and Alistarh, Cristian A. and Goussetis, George and Gómez-Tornero, José Luis, "Compact Leaky-Wave SIW Antenna With Broadside Radiation and Dual-Band Operation for CubeSats," in IEEE Antennas and Wireless Propagation Letters, vol. 20, no. 11, pp. 2125-2129, Nov. 2021

6. Comite, Davide and Podilchak, Symon K. and Kuznetcov, Maksim and Buendía, Victoria Gómez-Guillamón and Burghignoli, Paolo and Baccarelli, Paolo and Galli, Alessandro, "Wideband Array-Fed Fabry-Perot Cavity Antenna for 2-D Beam Steering," in IEEE Transactions on Antennas and Propagation, vol. 69, no. 2, pp. 784-794, Feb. 2021.

7. Comite, Davide and Kuznetcov, Maksim and Buendía, Victoria Gómez-Guillamón and Podilchak, Symon K. and Baccarelli, Paolo and Burghignoli, Paolo and Galli, Alessandro, "Directive 2-D Beam Steering by Means of a Multiport Radially Periodic Leaky-Wave Antenna," in IEEE Transactions on Antennas and Propagation, vol. 69, no. 5, pp. 2494-2506, May 2021.

8. Le Bihan, Paul and Hilario Re, Pascual D. and Comite, Davide and Kuznetcov, Maksim and Podilchak, Symon K. and Tucker, Colum and Maccoll, Kieran and Zhaksylyk, Yelzhas and García-Vigueras, María and Sellathurai, Mathini and Goussetis, George, "Dual-Polarized Aperture-Coupled Patch Antennas With Application to Retrodirective and Monopulse Arrays," in IEEE Access, vol. 8, pp. 7549-7557, 2020.

9. Kuznetcov, Maksim V. and Buendía, Victoria Gómez-Guillamón and Shafiq, Zain and Matekovits, Ladislau and Anagnostou, Dimitris E. and Podilchak, Symon K., "Printed Leaky-Wave Antenna With Aperture Control Using Width-Modulated Microstrip Lines and TM Surface-Wave Feeding by SIW Technology," in IEEE Antennas and Wireless Propagation Letters, vol. 18, no. 9, pp. 1809-1813, Sept. 2019.

Articles Presented in International Conferences:

1. Z. Shafiq, M. Kuznetcov, V. G. Buendia, D. E. Anagnostou and S. K. Podilchak, "A Planar Horn Antenna for TM Surface Wave Launching using Substrate Integrated Waveguide Technology," 2019 13th European Conference on Antennas and Propagation (EuCAP), 2019. pp. 1-3.

2. V. G. -G. Buendía, D. Comite, S. K. Podilchak, M. Kuznetcov, A. P. Freundorfer and Y. M. M. Antar, "2-D Planar Leaky-Wave Antenna with Fixed Frequency Beam Steering Through Broadside," 2020 14th European Conference on Antennas and Propagation (EuCAP), 2020. pp. 1-4.

3. M. Kuznetcov, S. K. Podilchak and M. Sellathurai, "High-Isolation Dual-Polarized Antenna for Wideband Full-Duplex Systems," 2020 IEEE International Symposium on Antennas and Propagation and North American Radio Science Meeting, 2020. pp. 487-488.

4. M. Kuznetcov, M. Clénet, S. K. Podilchak and Y. M. M. Antar, "Dielectric Resonator Antenna with 8-Ports for Polarization Diversity Applications," 2020 IEEE International Symposium on Antennas and Propagation and North American Radio Science Meeting, 2020. pp. 1743-1744.

5. M. Kuznetcov, S. K. Podilchak, A. McDermott and M. Sellathurai, "Dual-Polarization Multi-Layer Antenna by Patch Asymmetry with Simple Integrated Feeding for In-Band Full-Duplex Systems," 2021 15th European Conference on Antennas and Propagation (EuCAP), 2021. pp. 1-4.

6. M. Kuznetcov, S. K. Podilchak, J. C. Johnstoney, M. Clénet and Y. M. M. Antar, "Agile Dielectric Resonator Antenna with an Integrated Feeding Circuit for Polarization Diversity," 2021 15th European Conference on Antennas and Propagation (EuCAP), 2021. pp. 1-5.

7. M. Kuznetcov, S. K. Podilchak and M. Sellathurai, "Antenna Integrated with Dual-Differential Feeding for In-Band Full-Duplex Applications," 2021 International Symposium on Antennas and Propagation (ISAP), 2021. pp. 1-2.

8. B. Alshammari, K. Alrushud, M. Kuznetcov, Y. Li and S. K. Podilchak, "Dual-Band Dually-Polarized Compact Folded-Shorted Patch Array for Small Satellites," 2021 IEEE International Symposium on Antennas and Propagation and USNC-URSI Radio Science Meeting (APS/URSI), 2021. pp. 707-708.

9. K. Kossenas, M. V. Kuznetcov, D. Comite and S. K. Podilchak, "Remote Destruction of the Coronavirus by Dual-Polarized Wireless Power Transmission," 2021 IEEE International Symposium on Antennas and Propagation and USNC-URSI Radio Science Meeting (APS/URSI), 2021. pp. 459-460.

10. M. Kuznetcov and S. K. Podilchak, "Printed SIW Horn and Aperture Design for Surface-Wave Control and Power Routing by Genetic Algorithm Optimization," 2021 IEEE International Symposium on Antennas and Propagation and USNC-URSI Radio Science Meeting (APS/URSI), 2021. pp. 1651-1652.

11. M. Kuznetcov et al., "One-Sided Leaky-Wave Antenna with TM Surface Wave Feeding and Open-Stopband Suppression," 2021 IEEE International Symposium on Antennas and Propagation and USNC-URSI Radio Science Meeting (APS/URSI), 2021. pp. 1563-1564.

12. M. Kuznetcov, V. G. -G. Buendía, K. Alrushud and S. K. Podilchak, "Simple Matching Technique using Finite Metasurface to Control Surface Waves," 2022 16th European Conference on Antennas and Propagation (EuCAP), 2022. pp. 1-5.

Articles Under Review:

1. M. V. Kuznetcov, S. K. Podilchak, A. J. McDermott and M. Sellathurai, "SIW Sub-arrays with Dual-polarized Monopulse Patterns for Full-duplex or Diversity Applications," in IEEE Antennas and Wireless Propagation Letters, 2022.

Awards

1. Deputy Principal's Award 2018
2. Deputy Principal's Award 2019
3. James Watt Scholarship for International Students
4. Radio Frequency Pipeline Communications Short List Award
5. Honorable Mention APS 2020 Student Paper Competition
6. 1st year Postgraduate Research Prize
7. Honorable Mention APS 2021 Student Paper Competition
8. 2nd year Postgraduate Research Prize

Chapter 1

Introduction

In the process of organizing communications, sound and television broadcasting, antennas are widely used to provide radiation and reception of radio waves. Modern wireless communication systems are fundamentally impossible without the use of these electromagnetic waves in free-space and, therefore, devices that would ensure their radiation and reception are a crucial part of said system. Today, antenna solutions are used in many promising technologies such as 5G networks, radar installations and other communication transmission systems. Moreover, antenna systems are becoming more and more complex. There is also a need to adopt such systems for a certain type of activity. Areas of recent interest within academia, government, military, and industry include polarization-diverse antenna systems and full-duplex data transmission systems. These antennas are also applicable to global satellite systems, for example. This thesis focuses on new designs of such of antennas for these complex systems.

1.1 Brief Historical Overview of GPS and GNSS Systems and Polarization Diversity Challenges

The GPS system appeared in 1973 in the US [1], [2]. Mostly it was used in military operations and tracking systems. With further development, GPS systems were extended for civilian use particularly aerospace and naval systems. This first generation system worked by line-of-sight, and obstructions reduced signal quality. Also, the GPS tracker recorded all the data in memory and transmitted them to the server upon the arrival of vehicles at the base station via a wired or wireless interface [3].

In the second generation, short message service mechanisms were used to organize communication between GPS terminals and the server. One or more cellular communication modules were installed on the server, allowing users to receive SMS or data calls. Such systems were distinguished by a long period of time between transmissions of positional data and on-demand modes when receiving data. With the widespread use of mobile internet users, these second-generation systems have become obsolete.

In the third generation, General Packet Radio Services (GPRS) was used as a transport network, which makes it possible to reduce the cost of transmitting location data and this led to systems with a more real-time tracking [4]. In such systems, the server is installed directly at the client in the local office network, which provides better efficiency and data security, but requires regular support of the server by the client. Also, server maintenance requires a certain qualification of maintenance personnel on the client side and specialized softwar is needed to be installed on users workstations. Some systems allow you to rent server resources from a monitoring service provider. To date, such systems not only provide careful tracking of objects but also have increased quality of service when compared to previous generations. Particular improvements are: 1) help to decrease budget costs for transportation and vehicle fleets, 2) improved discipline of drivers in working routes, 3) tracking traffic and stopping points, 4) control over the degree of fuel filling and consumption, and, 5) increased efficiency and productivity at work.

The reliability of these networks are based on radio frequency (RF) systems which support nonstop continuous tracking and communications [5]. However, the signal can be simply distorted by weather conditions or other obstacles that can affect the received data and sometimes even completely blocked. Additionally, the signal can be simply jammed or even blocked by obstacles [6]. An example of the propagation challenges could be seen in Fig. 1.1. Thus, an antenna solution would require robust and continuous data transfer. Additionally, for commercial applications, those systems need to be compact, low-cost, and efficient. This makes the antenna in these systems to be challenging to design, and as such, diversity systems have also been recently adopted to ensure robust communications [7], [8]. For example, diversity in the exploited polarization or antenna beam pattern shape [9], [10]. Another more advanced approach is using co-located antennas for different functions. A specific example of this is simultaneous transmission and reception, defines full-duplex communications [11].

1.2 Brief Historical Overview of Full-duplex

For a long time, Alexander Bell worked on the creation of a telegraph, and during the experiments, he came up with the idea of creating a telephone [12]. On June 2, 1875, he heard a faint echo coming from a telegraph receiver, and this event prompted him to work on the creation of a telephone. He ordered his assistant Thomas Watson

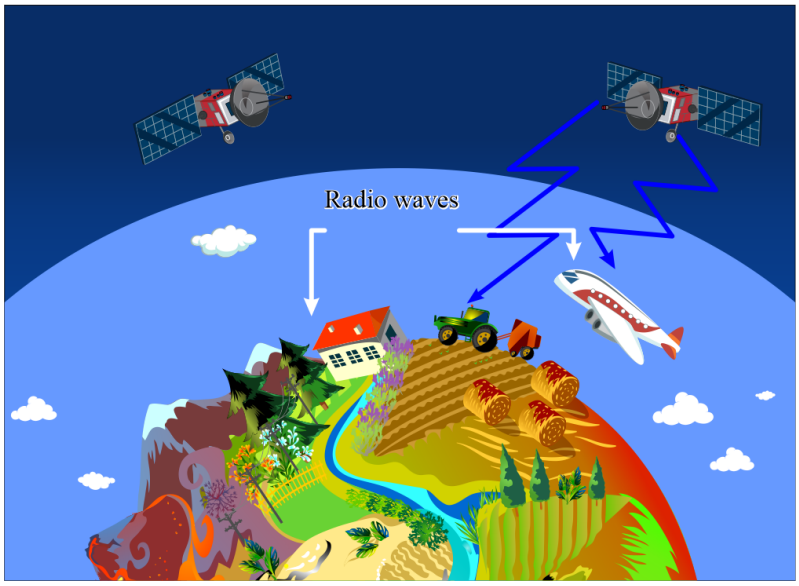

Figure 1.1: An example of GPS and GNSS interferences during transmission based on [6].

to make an apparatus for transmitting sound, and the next day a prototype telephone was ready. The device, tested on June 3, 1875, worked very poorly and could not serve for stable communication. Thomas Watson called this phone a 'bitter disappointment', and communication historians and collectors called it the gallows for the technology. Following this development, on March 10, 1876, Alexander Bell and his assistant Thomas Watson successfully tested a telephone set in the United States.

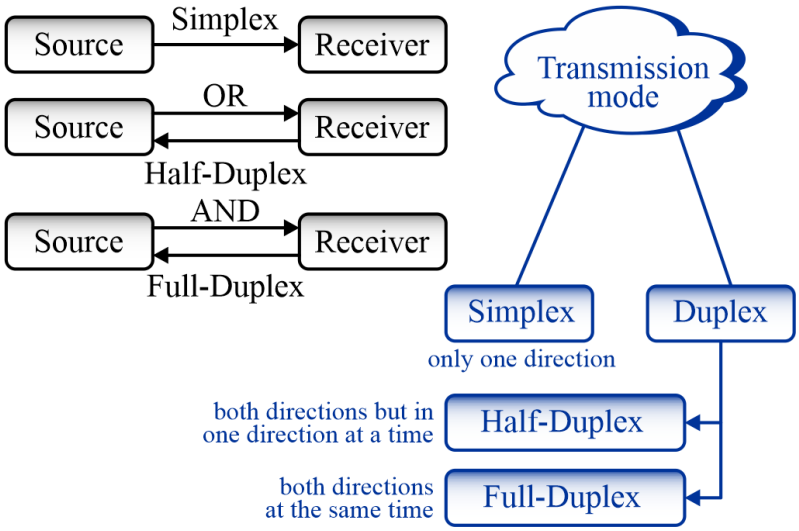

Figure 1.2: Development and types of the duplex systems.

This is how the very first communication based on a duplex system appeared, called simplex (one way only) and half-duplex (one way at a time). Today, each of us has a

cell phone or a computer that transmits and receives data. While simplex and half-duplex are well developed, full-duplex (two ways at the same time) was not developed well due to technological limitations [13]. These limitations were related to the isolation between the transmitter and receiver and the possible range. The visual representation of duplex systems is depicted in Fig. 1.2.

The first full-duplex systems appeared in the 1950s in the form of continuous wave radars, but the system was not used for data transmission as the received signal was not possible to recover as the signal strength of the transmitted signal was a thousand times stronger [14]. Moreover, the range of those radars was limited as the transmitted signal (in the form as feedback) caused interference. To improve the response and ranges, the antenna separation was increased and the free-space path loss was reduced. This was because circulators were not very well developed. Thus, the transmitted power was reduced which made limitations in the range. In the 1960s a block of massive and heavy ferrite rotators was used to achieve acceptable isolation levels thus advancing circulatory technology [15]. Since then radar systems have advanced further with the required isolation levels to be lower in comparison to full-duplex data communication systems.

Due to these technological limitations, full-duplex data communication systems were generally abandoned for a long time as the requirements for those systems were higher in comparison to the radar counterpart; i.e. lower levels of isolation were required [16]. Only recently, due to the advancements in digital, analog, and antenna isolation enhancement and signal cancellation techniques, have these communication systems once again started to be considered. Basically, the return of full-duplex communications can be seen in the number of publications on this topic, with the main focus on antenna co-location, high-isolation between the transmitter and receiver, and high bandwidths of operation. Figure 1.3 illustrates such a full-duplex antenna.

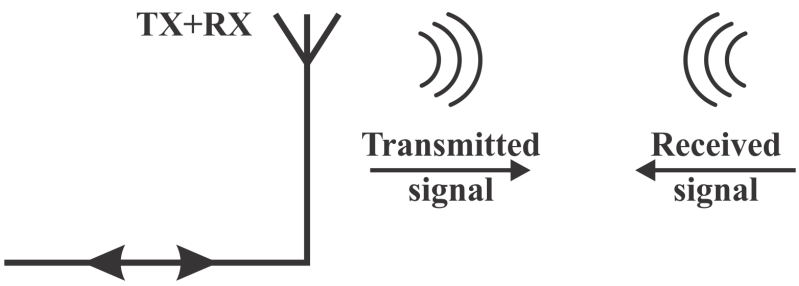

Figure 1.3: Example of a co-located full-duplex antenna system.

1.3 Thesis Motivation

Following these developments and the need for diversity antennas and full-duplex systems, the main purpose of this thesis is to design, analyze, and test such antennas while also, developing further the state-of-the-art. The basic aim of the antenna research is to expand the capabilities of these polarization diverse and FD systems. In addition, polarization diversity or antenna polarization reconfigurability, as well as, dual-polarization antennas (with high isolation) are considered in this thesis. These types of novel antenna technologies which advance existing, can provide solutions to the aforementioned system problems in RF challenging environments for example [17], as well as reduce self-interference within full-duplex antennas [18]. Effectively signal polarization diversity and orthogonality can be generated in the far-field by these types of antennas, and this can be advantages to enable more efficient system operation and data communications at microwave and millimeter-wave frequencies. Applications include modern polarization diverse radar, satellite communications, and 5G/6G systems.

Particularly, the attractive characteristics such as efficiency, design compactness, and simplicity, make dielectric resonator antennas (DRAs) suitable for such diverse applications and RF-challenged environments. In order to effectively control the polarization, it is necessary to control the orientation and phase of the fields applied to the DR. This creates some challenges in that an integrated or dedicated feeding circuit for signal and field control is required. These different antenna features can be useful in RF challenging environments where the optimal polarization scheme might not be known apriori, and, by proper polarization selection and agility given by the available antenna operating states, improved system reliability can be made possible.

Antenna designs based on a signal shift at its various ports, were also investigated for full-duplex. These designs offered high isolation and dual-polarization functionality for signal transmission and reception at the same frequency, defining in-band operation, or in-band full-duplex (IBFD). As also further examined in the thesis the problem of self-interference (SI) was also further alleviated using dual-differential feeding and the appropriate supporting feeding circuit. Based on these design concepts, new antennas are proposed which can offer high inter-port isolation; i.e. reduced SI. This can be useful for 5G/6G wireless networks, radar, and other IBFD systems.

Following these advancements, the new possibility of beam steering systems for IBFD is also proposed at microwave and millimeter-wave frequencies. Finally, IBFD will

also be investigated with the possibility of diversity in the beam pattern; i.e. by using monopulse, sum and difference patterns. These types of beam patterns are required for conventional monopulse radar and it was recently reported in [19], that there is a need to generate sum/difference patterns for 5G point-to-point communication systems. As further described in [19], this technique exploits a sum beam and a difference beam to accurately determine the direction of arrival for data signals to support efficient 5G communications. Basically such an antenna design follows more conventional monopulse radar and tracking principles to help ensure precise signal tracking and stable data communication links between antennas.

1.4 Thesis Objectives

The first main objective of the thesis is to investigate existing approaches and trends in communication systems and the required antennas. This activity also has the motivation to extend existing designs and advance the state-of-the-art in antenna technology in terms of diversity and differential feeding. For example, dielectric resonator antennas are well studied in the literature, but not many of these antennas have been reported to offer polarization diversity and reconfigurability. Also, in this dissertation, an important objective was to consider real-life scenarios and thus the necessary adjustments such as size, simplicity, and complexity of the circuit feeding system. Thus, the antenna development from a multi-port arrangement to a 2-port system was shown to be beneficial for advancing DRA technology.

The second main objective is related to the understanding, characteristics, architecture design, and the relevant parameters for FD systems. This is because these systems can suffer from self-interference which requires suppressing these values to around 100 dB. The higher the suppression of the antenna SI, the more relaxed the analog and digital cancellation systems can be. Basically, the main objective of FD antennas is to maximize the isolation between the transmitter and receiver of the antenna system, and possibility, improve the operating bandwidth. The secondary objectives are design simplicity, beam pattern control, and reconfigurability. Thus, antenna arrays and the supporting integrated circuit systems are great tools to achieve these goals.

1.5 Thesis Contributions

This thesis have following contributions:

1. Investigated and evaluated proposed dielectric resonator antennas for polarization diversity proposed in the literature review.
2. Highlighted requirements for those antennas and possible solutions. Investigated phase control for polarization diversity.
3. Proposed polarization diverse resonator antenna and further modifications of the antenna design, making it suitable for real-life applications. Investigated the circuit feeding system, and its efficiency and proposed further improvements.
4. Using the experience from the dielectric resonator antenna and dual-differential antenna systems some design considerations for Full-duplex systems were highlighted.
5. Proposed Full-duplex antenna in the S-band, validation of the isolation levels, and further integration into the antenna array for beam-steering. Additional integration of the feeding system was designed and analyzed.
6. Simple 5G Full-duplex antenna system with the possibility of reconfigurable beam-pattern characteristics was proposed.
7. Redesigned the system into the array with a similar capability and tested with Butler Matrix.

1.6 Thesis Overview

The thesis is organized as follows:

1.6.1 Chapter 2

In this chapter, new DRAs will be investigated and these designs have applications to polarization diversity scenarios and RF challenged environments. Particularly, information about the operation and mode control will be discussed. The polarization control using an 8-port configuration will be proposed and manufactured showing the possibility

of multiple polarization states [20]. While the proposed antenna showed high reconfigurability, the design was also further expanded and integrated into a simple 2-port configuration [21] with a similar capability to above mentioned the 8-port system [20]. More details will follow in Chapter 2.

1.6.2 Chapter 3

This chapter focuses on other antennas for full-duplex systems. Firstly, more details on the different classifications for FD will be outlined and the existing antenna approaches (as found in the literature) which can offer high-isolation, will be discussed and compared. A new in-band antenna design approach will also be proposed with an external feed which realizes a simple design and with high isolation. Furthermore, a circuit system will be more integrated with the antenna realizing a single unit while also maintaining similar isolation levels. Finally, a FD antenna array which can beam steer and this proposed design can be used in tracking systems and other IBFD scenarios.

1.6.3 Chapter 4

This last technical chapter focuses on novel antenna designs for operation at millimeter-wave frequencies while still offering in-band full-duplex operation. Particularly, design approaches using substrate integrated waveguide technologies are exploited due the isolation metrics that can be achieved. More specifically, a co-located array for dual-polarization and high-isolation is first discussed. Then design concepts are extended to a 16-port antenna array for beam steering scenarios, which is achieved using a butler matrix beamformer.

1.6.4 Chapter 5

This chapter summarizes the thesis research and provides possible future work.

Chapter 2

Dielectric Resonator Antennas Offering Polarization Diversity

2.1 Introduction

In this chapter, dielectric resonator antennas (DRA) for polarization diversity will be investigated. The first part of the chapter will provide information about the polarizations available and the ones widely used in challenged RF environments and some theoretical considerations for DRAs. The second part of the chapter will provide a brief overview of the available DRAs and the importance of polarization diversity for such systems. Typically, those requirements need to be accommodated in the Global Navigation Satellite System (GNSS) and the Global Positioning System (GPS) for applications such as unmanned aerial vehicles (UAVs) and other applications for target tracking.

Next, a new 8-port antenna configuration that supports right-hand (RH), left-hand (LH), and two orthogonal linear polarizations (LPs) will be proposed. Detailed information about the antenna design will also be discussed. In particular, two antenna designs will be proposed depending on the antenna gain which can be useful depending on the employed digital signal processing, or multiplexing for example [7]. The particular challenges with multi-port feeding will be investigated for the antennas, and possible external feed configurations will also be outlined to achieve the different polarizations. Afterward, as further discussed, the dielectric resonator part of the antenna was further modified to have a higher dielectric for a more compact design and a new feeding structure was integrated to support dual-CP radiation, and, with the possibility to employ external delay lines for two orthogonal LPs. Such integrated feeding generally simplifies the antenna and makes it more practical. Finally, the chapter will be concluded by highlighting the achievements of the proposed design and discussing the possibility to employ such antennas for in-band full-duplex communication systems.

Finally, the chapter will be concluded by highlighting the achievements of the proposed design and discussing the possibility to employ such antennas for IBFD communication system configurations.

2.2 Antenna Polarizations, Depolarization Effects in the Atmosphere and Jamming

In antenna systems there are the following types of polarizations: linear, circular (left or right handed) and elliptical [22], [23] (see Fig 2.1). In a linearly polarized electromagnetic plane-wave in the far-field, the vectors of the vertical electric $\vec{E}$ and magnetic $\vec{H}$ fields at each moment of time are oriented in space and are perpendicular. The direction of the electric field lines when at a significant distance from the antenna determines the polarization of the electromagnetic plane wave. For example, a dipole is a linearly polarized antenna in which the electric field lines are parallel to the dipole axis. Similarly, for circular polarization, the signal propagates in both planes (vertical and horizontal) with a phase shift of 90 degrees. Finally, for elliptical polarization, the electric field maximum moves in the shape of an ellipse. Each type of polarization has its advantages and disadvantages. In general, linear polarization is ideal for long distances, it is the simplest to generate. However, if there is no perfect angle alignment some additional polarization mismatches might appear. Circularly polarized waves generally enable a communications link regardless of the angle between the transmitting and receiving antennas. This also assumes that the beam pattern maximums of the transmitting and receiving antennas are generally aligned.

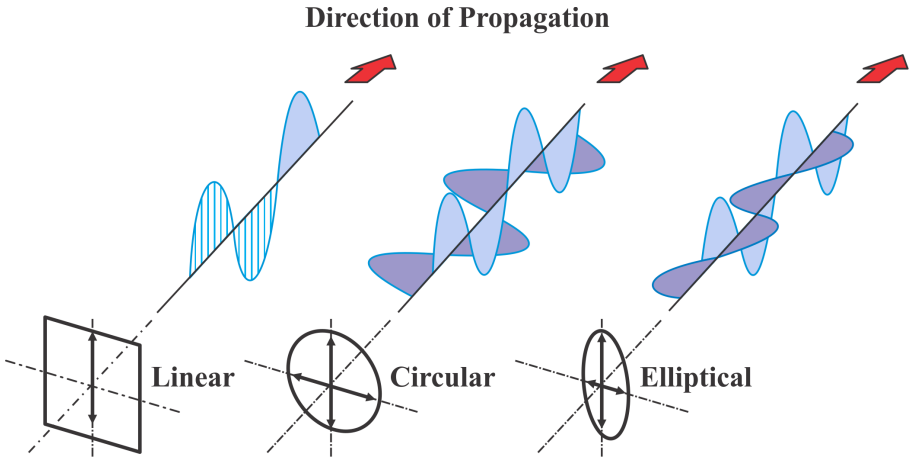

Figure 2.1: Polarization types: each polarization has a different vector for the Electric and Magnetic fields. Reproduced from [22].

For antennas, polarization control can be achieved in various ways. Firstly, by applying a specialized design approach, for example, by clipping two corners from a printed patch resonator, the fields and currents can rotate in a circular orientation. Secondly, multi-port antenna configurations can be used to control the phase distribution for circu-

larly polarized radiation. For example, if a four-port system has a phase shift of 90°, the signals will have a delay which forces circular polarization of the fields near the antenna. Using these different methods, and other similar approaches to manipulate the currents and fields near the antenna, polarization control can be achieved.

As stated in [24] the weather effects and other Earth's atmosphere conditions can cause changes in the polarization produced by the antennas. This effect causes depolarization of the electromagnetic wave. The most common type and affected below 3 GHz is the multipath propagation effect which is caused by the tropospheric or ionospheric, channel fading effects are also typically caused by rain or other hydrometeor factors. Such weather conditions not only make it difficult to receive and transmit data but also can completely give incorrect position data for a GPS system, for example it can also change the propagation of the electric and magnetic fields making the polarization be converted into an orthogonal mode (cross-polarization) which degrades signal reception.

Some attention also needs to be given to jamming techniques [25]. To date there are different types of jamming techniques that exist such as constant, deceptive, and random. All of them involve different DSP techniques which are outside the topic of this thesis. The important factor of jamming is that the antenna type requires the use of a single-channel. Thus, if the antenna system is configurated into a two-channel mode with different employed polarization states, the reliability and stability of the system can be improved. This technique can also be used in tracking systems such as the Global Positioning System (GPS) and the Global Navigation Satellite System (GNSS).

As the focus of this thesis is to work in RF challenged environments, pattern diversity in antennas could also be a great option in the case where a particular blocking object is preventing data transmission. Thus, bypassing the obstacle, the signal could be re-directed. However, in some RF environments, the propagation of the signal with a particular polarization could be completely blocked and pattern reconfiguration would not provide enough degrees of freedom. Thus, in this scenario, polarization reconfiguration would be the only choice to achieve stable data communications.

2.3 General Antenna Considerations

One of the oldest types of antennas is a dielectric resonator antenna (DRA) which can be defined by a square or cylindrical shape using dielectric materials [26], [27]. The relative dielectric of the element ε_r can control the size of the antenna and has the following

dependency as in [27]:

$$L = \frac{\lambda_0}{\varepsilon_r} \tag{2.1}$$

where L is the size of the dielectric element, and λ_0 is the free-space wavelength defining resonance. Also, by choosing ε_r higher than 20 it is possible to design a compact DRA for low or high frequency applications. The basic cylindrical DRA representation can be observed in Fig. 2.2. As there is no conductor loss in dielectric resonators, radiation efficiency can be very high and on the order of 90% or above. In comparison to simple microstrip antennas, the DRA can offers wider impedance bandwidth as the DRA radiates over the surface of the dielectric, but not the ground plane. It also does not excite parasitic surface waves, which can reduce performance as in microstrip structures.

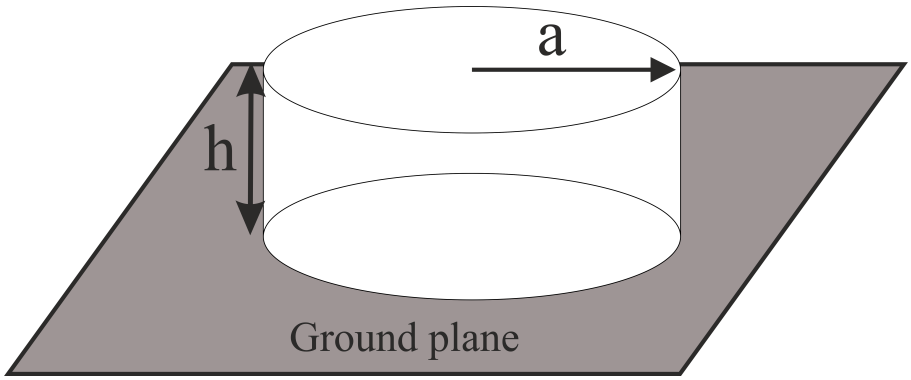

Figure 2.2: Overview of the cylindrical dielectric resonator antenna consisting of dielectric element and ground plane. Based on [27].

Another important characteristic of the DRA is the excitation modes. Following the conventional square shape waveguide, the DRA with the shape of a square, the mathematical waveguide model can also be used to determine modes. For instance, the different resonant frequencies can be calculated as follows [28]:

$$f_0 = \frac{c}{2\pi\sqrt{\varepsilon_r}}\sqrt{k_x^2 + k_y^2 + k_z^2} \tag{2.2}$$

$$k_x = \frac{\pi}{a} \tag{2.3}$$

$$k_z = \frac{\pi}{2b} \tag{2.4}$$

where a and b are dimensions of the square resonator, k_i are the component vectors de-

pending on the antenna dimensions as presented in Fig. 2.2 and c is the speed of light.

Similarly for cylindrical DRAs, the modes can be calculated using following equations [28]:

$$f_{TE_{npm}} = \frac{c}{2\pi\sqrt{\varepsilon_r \mu_r}} \sqrt{\left(\frac{X_{np}}{a}\right)^2 + \left(\frac{(2m+1)\pi}{2h}\right)^2} \tag{2.5}$$

$$f_{TM_{npm}} = \frac{c}{2\pi\sqrt{\varepsilon_r \mu_r}} \sqrt{\left(\frac{X'_{np}}{a}\right)^2 + \left(\frac{(2m+1)\pi}{2h}\right)^2} \tag{2.6}$$

where TE and TM are transverse electric and transverse magnetic modes, npm is the mode number, a is the radius of the dielectric, h is the height of the dielectric and X'$_{np}$ and X$_{np}$ are roots of Bessel functions of the first kind. Other possible shapes are available, but calculations are more complicated and advanced. For more information on DRAs, please see [28] and [29], for example.

Each mode has different field distributions which defines far-field and impedance characteristics. The coupling feeding circuit also dictates the excited modes. Using probe feeding, aperture coupling slot or monopole parasitic excitation, the desired radiation configuration can be achieved. Thus, a real challenge comes with the design of the feeding system to achieve multiple polarization states and wideband response. Most of the recent studies found in the literature are focused on new feeding techniques and wide-bandwidth designs suitable for polarization control which will be further explored in this thesis.

2.4 Literature Review of Existing DRAs

Dielectric resonator antennas (DRAs) have received considerable attention for different RF communication systems and satellite applications. They are generally compact, provide high radiation efficiencies, can be excited using various feeding techniques, and provide high gain. Recent developments focus on new types of DRAs including dual-band operation with high impedance bandwidth [30], new feeding techniques [31] and new shapes for the radiating elements such as the T-shape [32], L-shape [33], stair-shape [34], [35] and others (see Fig. 2.3). However, achieving wide bandwidth with a compact design, the feeding system can be challenging. Moreover, difficulties can arise when trying to achieve wide bandwidth and high polarization diversity at the same time.

This is because most DRA feeding systems are focused on the efficient excitation of only one type of polarization, being either linearly polarized (LP) or circularly polarized (CP).

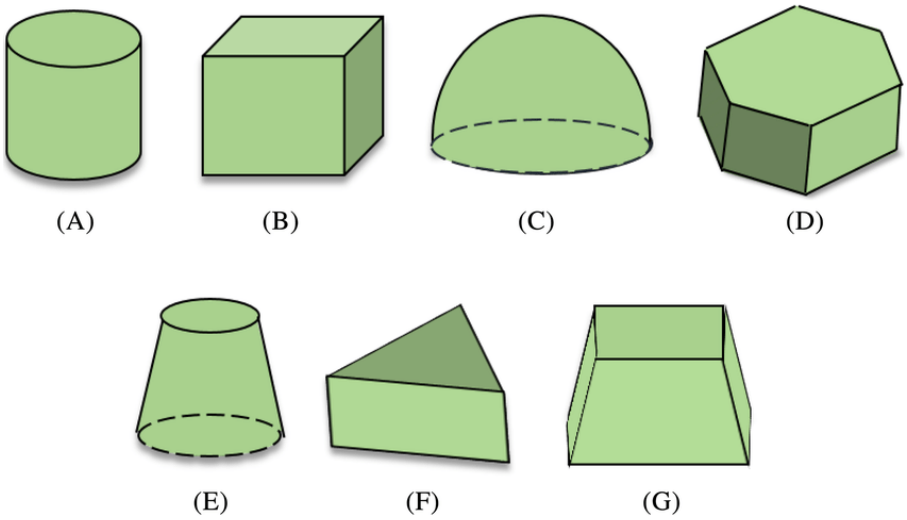

Figure 2.3: Dielectric resonator shapes in the literature review. From typical cylindrical shape, to non conventional octagon shapes. Reproduced from [26].

It is well known that the polarization of the generated far-field radiation pattern for a DRA is mostly dependent on its feeding mechanism. For example, one of the earliest and most common feeding systems to achieve CP over a wide beamwidth is the quadrature feed described in [36] where microstrip lines were positioned on the dielectric resonator to excite two orthogonal modes. In the same way, the antenna described in [37] uses two vertical strips with quadrature phase excitation to excite TE_{111} and TE_{113} modes simultaneously to achieve CP. The DRA operated from 2.7 GHz to 3.76 GHz where the reported maximum gain was 6.8 dBic and where the axial ratio was below 4 dB. The antenna also utilized a large (205 mm by 205 mm) ground plane to improve antenna performance. Similar feeding was employed in the antenna described in [35] where a bottom microstrip line fed a ground plane slot with a stair-like dielectric structure on the top aperture defining the DRA. The CP antenna achieved an axial ratio below 3 dB from 9.3 GHz to 10.3 GHz.

Another type of feeding scheme for DRAs is substrate integrated waveguide (SIW) technology [38]. Typically the dielectric resonator antenna is placed on top of a slot etched on top of a SIW transmission line. The antenna in [31] represented a dual-layer PCB with low permittivity and with slot coupling on the bottom layer and an integrated resonator placed on top. The antenna design frequency was 35 GHz with a gain of about 5 dBi, and only offered LP radiation by excitation of the TE_{111} mode. SIW technology was

also used in [39], where DRA elements were employed to form an array. In particular, SIW was used to produce a corporate feeding system to excite 64 dielectric elements. The final DRA array provided high efficiency of 89 % and a realized gain of 21.6 dBi while the structure operated in the frequency range from 35 to 37 GHz.

Another degree of freedom is to use unconventionally shaped dielectric resonators. In [40] an H-shaped resonator was presented with a side-attached trapezoidal-like patch. In that structure, truncation and cuts allowed for better impedance matching and caused multiple resonances over frequency enabling antenna operation from 3.61 GHz to 6.85 GHz. In a similar feeding approach, an L-shaped DRA [33] operated from 1.71 to 2.51 GHz. Due to that structured shape, the excited mode was $HEM_{11\partial}$ which can offer stable radiation patterns over the intended frequency range while the measured maximum gain was 8.7 dBi. Similarly, the U-shaped feeding technique reported in [41] with a stair-like dielectric resonator offered better impedance matching. This compact antenna generated an omnidirectional pattern covering the ultra-wide band frequency range from 3.14 to 10.9 GHz with a maximum gain of 4.2 dBi.

2.5 Polarization Diversity

As one main focus of this thesis is polarization diversity, it is important to consider the polarization reconfigurability of the antenna. Of interest is also polarization diversity antennas which can offer a higher degree of freedom by ensuring two or more polarization states. These antennas can be used in wireless communication systems to minimize fading losses caused by multipath effects as well as in satellite systems for geolocation. Diversity antennas can also offer frequency reuse when combined with polarization modulation techniques as reported in [42] - [44]. Using such polarization diversity, the antenna system can be less affected by different signal obstacles, improving the reliability and accuracy of the transmitting data. For example, in [7], to reduce power consumption and the signal bit-error rate (BER), a dynamic polarization diversity antenna system was implemented and compared. In that work, [7], which mainly considered the signal-to-noise ratio (SNR), a method to switch between two antennas while only one antenna was activated was implemented. Another diversity scenario was reported in [8], where antennas with equal gain were used to distinguish between small-scale and large-scale fading signals. Due to the fluctuating signal strengths in [8], the wake-up packet reception rate could be jeopardized, and by using antenna diversity, those effects could be mitigated.

An antenna switching approach could also be implemented using antennas with diverse gain [45]. In this methodology, if the signal level power drops for one polarization, signals received from another polarization state can be employed to recover the data link. Using this approach, one polarization state will be active at a certain time. Similarly, an equal gain combiner (ECG) technique can be implemented [46], where the signals can be combined using all active polarization states.

Most of the recent findings in the literature report on single-antenna units for diversity applications with new multi-port feeding configurations whilst offering good isolation between the ports. Moreover, and by following the previously mentioned advancements in feeding approaches for DRAs, a few polarization-diverse DRA structures have been reported with multiple port feeding or made reconfigurable with two or more polarizations. In particular, the structure described in [47], was a 2-port DRA using coplanar waveguide technology to excite two TE_{111} orthogonal modes. The antenna provided 7 % and 11.6 % bandwidth for port one and port two, respectively, with a maximum gain of 6.45 dBi for its two polarization states. Similarly, a two-port dual-LP reconfigurable DRA was reported in [48]. The structure employed inverted-trapezoid patches and skywork switches along with applied phase shifts to the two ports to control the TE_{111} and TM_{111} modes for radiation from about 5 GHz to 6 GHz. This resulted in the control of the pattern while the reported maximum gain was 10.3 dBi at 5.5 GHz.

2.6 Hybrid Dielectric Resonator Antenna for Diversity Applications With Linear or Circular Polarization

Advancing on these findings for antenna diversity and the aforementioned DRA feeding approaches, this thesis reports on a new 8-port antenna design achieving simultaneously dual-CP or dual-LP polarization. The single-antenna unit is defined by a square arrangement of aperture coupled slots (ACSs) hybridized with the radiation of a cylindrical dielectric resonator to achieve polarization control. More specifically, two distinct microstrip lines drive each of the four ACSs (see Fig. 2.4), defining the 8-port antenna, for radiation of degenerate $HE_{11\partial}$ modes. To the best knowledge of the author, no similar slot array feeding scheme, DRA concept and results have been reported. Basically, it will be shown that high polarization diversity is possible for the proposed 8-port DRA allowing for the generation of various LP states, as well as RHCP and LHCP, by the appropriate excitation of the relevant ports. Moreover, new and more efficient LP states

are simulated and measured when compared to [49] by differential-like feeding. This work also addresses inter-port coupling and antenna efficiency where it will be shown that values approaching 90 % are possible.

To demonstrate these concepts, two different, yet also similar, antenna structures are designed and examined for comparison having a center frequency of 1.5 GHz. Both offer an input impedance bandwidth of more than 40 % and distinct characteristics which may be of practical interest for diversity applications; for example, when requiring varied gain values for the different polarization states (Design A), similar to [45], or, more consistent realized gain and matching over frequency when considering the possible LP and CP operational states (Design B). Both structures might be useful within the aforementioned systems [7, 8, 45, 46], but depend on the specific requirements of the antenna. However, results for Design B are fully reported herein, mainly due to its achieved antenna performances in terms of radiation efficiency, similar matching at the ports as well as its relatively consistent gains for the achieved polarization states. In the following regardless, both antennas are compared whilst measurements are provided, demonstrating proof-of-concept for the 8-port antenna concept.

2.6.1 Antenna Design and Polarization Considerations

The proposed DRAs offer gain and polarization diversity, and this agile feature, can be useful in communication or satellite systems such as the Global Navigation Satellite System (GNSS). Basically, in these scenarios, the proposed diversity antennas can support signal processing approaches as in [7, 8, 45, 46] to improve overall system performance whilst employing only a single antenna unit.

The hybrid DRAs, Design A and Design B (see Figs. 2.4 and 2.5) consist mainly of three parts: (1) the dielectric resonator with ε_r = 10, radius and height of 31.75 mm and 22 mm, respectively, glued on top of the four ACSs; (2) the FR-4 substrate with thickness h = 0.8 mm and ε_r = 4.3; and (3) eight 50-Ω microstrip lines which are perpendicular to the four ACSs and angled 45° at the open stub terminations. Details on the optimized dimensions for the two designs and the layout parameters can be seen in Fig. 2.5 and Table 2.2.

In the next sections, the external feeding system and these two different antenna designs will be reported in detail: Design A and Design B. The former offers different peak antenna gains for its different polarization states while the latter offers similar antenna

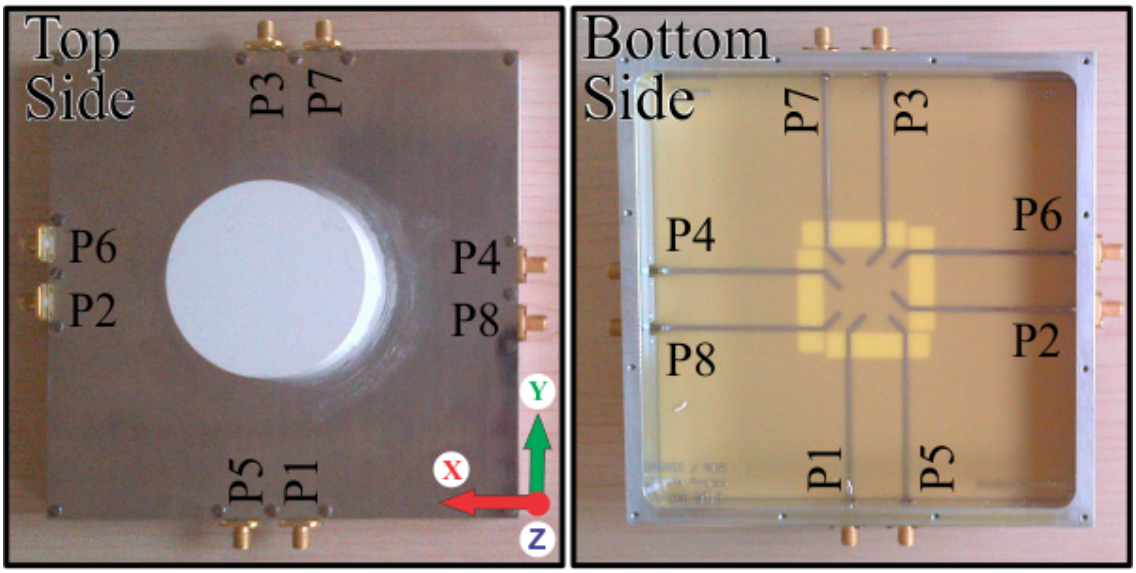

Figure 2.4: Manufactured DRA: (left) The dielectric resonator element glued to the top metalized side which defines the ground plane platform. (right) The feeding network on the bottom side is shown with eight 50-Ω SMA connector jacks which excite the square array of four ACSs; i.e. two microstrip lines per slot defining the 8-port antenna.

Table 2.1: Feed definitions to achieve the possible polarization states

Port	LP (Horizontal)	LP (Vertical)	RHCP	LHCP
P1	$1\angle 0°$	0	$1\angle 0°$	0
P2	0	$1\angle 0°$	$1\angle 90°$	0
P3	$1\angle 180°$	0	$1\angle 180°$	0
P4	0	$1\angle 180°$	$1\angle 270°$	0
P5	$1\angle 0°$	0	0	$1\angle 0°$
P6	0	$1\angle 0°$	0	$1\angle 270°$
P7	$1\angle 180°$	0	0	$1\angle 180°$
P8	0	$1\angle 180°$	0	$1\angle 90°$

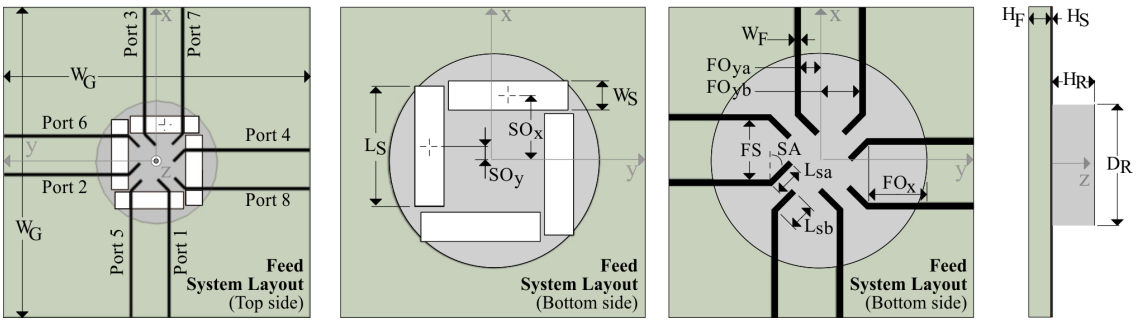

Figure 2.5: Top, bottom and side layout views of the proposed DRAs (relevant to both Designs A and B). Dimensional details are described in Table 2.2.

matching values at all its eight ports with consistent gain values. This is because the structure, Design B, is symmetric. Regardless, depending on the specific polarization or gain diversity application, Design A or Design B may be more suitable. As further

described in Table 2.1, each polarization state of the DRA is made possible by exciting different ports and applying the relevant phase shifts. In addition, both Design A and Design B were optimized using the commercial full-wave simulator Ansys HFSS and CST microwave Studio. HFSS was mainly used to refine the structure dimensions and simulate the radiation performances, while CST was used to compute the active S-parameter (or F-parameter) response, beam patterns, realized gain, and antenna efficiency.

Antenna Operation: Design A

Circular Polarization: RHCP (P1 to P4), LHCP (P5 to P8)

In this configuration the antenna was excited using ports 1 to 4 or ports 5 to 8 with the applied phase shift of 90° (i.e. sequential rotation [50]) with respect to each port (see Table 2.1). As a result, RHCP and LHCP radiation was made possible defining the CP polarization states.

During the simulations and structure optimizations in HFSS, the relevant dimensions near the ACSs for the 50-Ω microstrip lines were varied such that ports 1 to 4 provided the best possible matching (see Fig. 2.6(a)), while still making it possible to operate the antenna when using ports 5 to 8 for the other polarization state. As a result, the RHCP state provided better active F-parameter matching when compared to the LHCP state (see Figs. 2.6(b) and 2.7(a), respectively). For example, the active F-parameters for the RHCP state showed a -10 dB matching (or better) over a bandwidth from 1 to 1.58 GHz, while LHCP was only able to reach -9 dB from 1.05 to 1.45 GHz with only -8 dB at the center frequency of 1.5 GHz. Since the coupling to the non-active ports is minimized at the 1.5 GHz design frequency whilst good matching is achieved for the RHCP state, an efficiency maximum of 82 % is achieved. On the other hand, an efficiency of 74 % is possible for the LHCP state (see Figs. 2.6(b) and 2.7(a)). Consequently, maximum realized gains for the RHCP state reached 4.9 dBic, while the LHCP state only reached 3.2 dBic (see Table 2.3).

This general design goal for Design A, to achieve a higher CP gain for one polarization state, impacted the matching for ports 5 to 8; i.e. the reflection coefficient values (passive) were about -7 dB over the operating band of the DRA (see Fig. 2.6(a)). As expected, the active LHCP state is also not well matched; i.e. the active F-parameters are greater than -10 dB (see Fig. 2.7(a)). Looking at the simulated beam patterns for the LHCP and RHCP states (see Fig. 2.8) the diversity in the CP gains can be observed. Also, for both RHCP and LHCP, the cross-polarization level is well below -50 dBic at

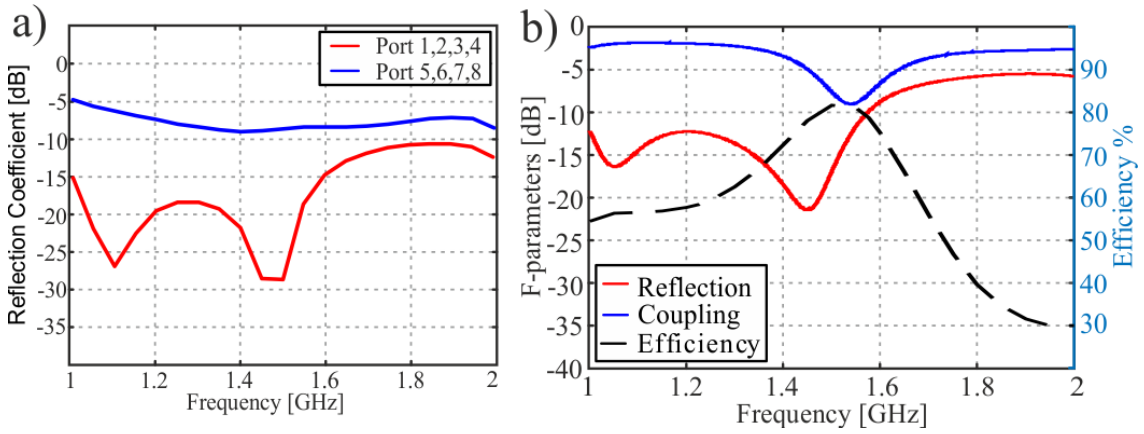

Figure 2.6: Design A: (a) Simulated reflection coefficients (passive) for all eight ports. Reflection coefficient values for ports 1 to 4 are below -10 dB over entire range, however matching for ports 5 to 8 did not reach -10 dB. (b) The F-parameters and antenna efficiency for the RHCP state (ports 1 to 4).

broadside.

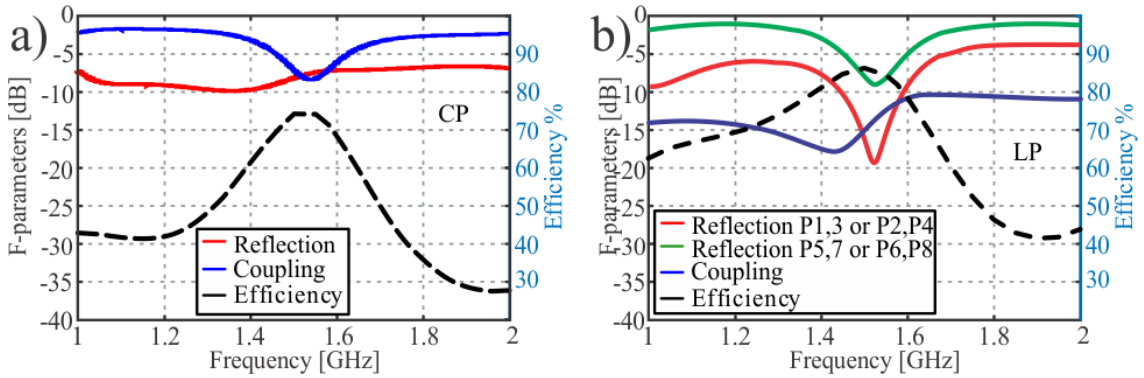

Figure 2.7: Design A: (a) simulated active S-parameters (or F-parameters from CST defining the active reflection coefficient in dB as well as the coupling to the non-activated ports) for the LHCP state (ports 5 to 8). It can be observed that increased reflections are generated for the active S-parameters when compared to the RHCP state (see Fig. 2.6(b)). (b) Simulated F-parameters for the LP states (Horizontal: Ports 1, 3, 5, and 7; Vertical: Ports 2, 4, 6, and 8). The antenna is matched better for the horizontal state.

Linear Polarization: Horizontal (P1, P3, P5, and P7) Vertical (P2, P4, P6, and P8)

In this state the antenna was excited using ports 1, 3, 5, 7 or 2, 4, 6, 8 with a 0° and 180° phase shift applied to the ports as defined in Table 2.1. Using this approach two

Table 2.2: DRA Dimensions (all values in millimeters, see Fig. 2.5)

	W_g	H_F	H_S	H_R	D_R	W_S	L_S	SO_x	SO_y
Design A	160	0.762	0.035	22	63.5	8.8	36	19.4	4
Design B	160	0.762	0.035	22	63.5	8.8	36	19.4	4
	W_F	FO_{ya}	FO_{yb}	FO_x	FS	SA	L_{sa}	L_{sb}	
Design A	1.45	3.275	14.475	16.75	17.75	45°	7.5	8.3	
Design B	1.45	5.675	12.775	16.75	18.45	45°	7.5	8.5	

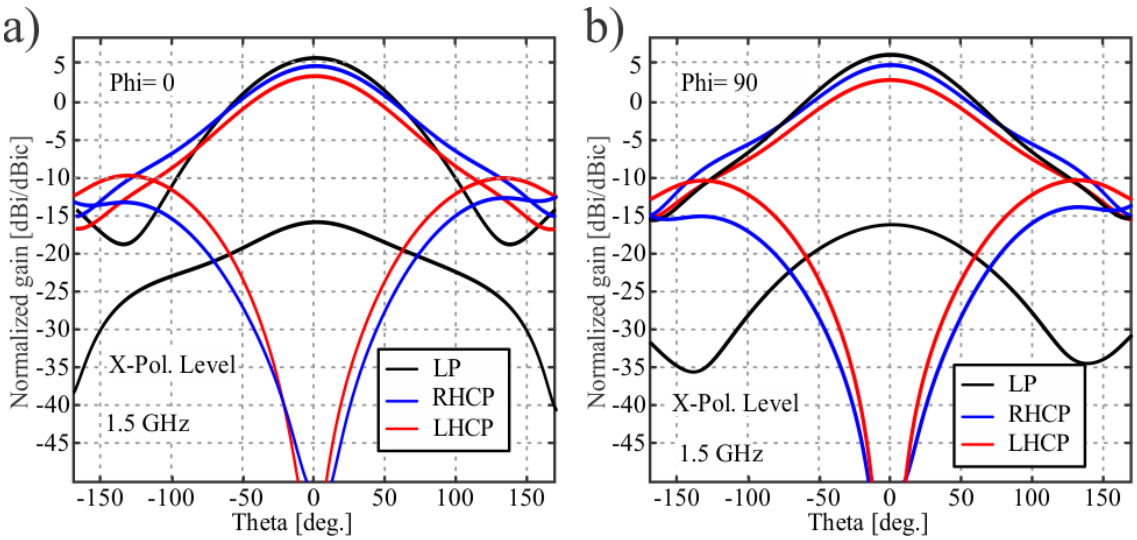

Figure 2.8: Design A: simulated beam patterns and cross-polarization levels for the antenna operating states as defined in Table 2.1 in the (a) $\phi = 0°$ and (b) $\phi = 90°$ planes. As mentioned, Design A provides variation of the gains for its different polarization states.

ACS slots will be activated only. When compared to the case when only one feed line per slot was driven (; i.e. port 1 or 5, and ports 2 or 6), the differential feeding outlined in Table 2.1 showed to offer the most efficient LP states with a radiation efficiency of 88 % at 1.5 GHz (see Fig. 2.7(b)). The simulations of the F-parameters confirmed that the active reflection coefficient reaches -20 dB at the design frequency for ports 1 and 3 or ports 2 and 4. Similar to the LHCP state, ports 5, 6, 7 and 8 were actively matched with values of about -7 dB. Also, simulated beam patterns in Fig. 2.8 showed that the cross-polarization level is well below -15 dBi with the maximum realized gain at 1.5 GHz as expected.

Using this design approach, different gains for the different polarization states can be achieved defining a type of antenna offering polarization-gain diversity. As can be observed in the plot of the realized gain versus frequency for the different polarization cases as in Fig. 2.9(a), a diversity gain of about 2 dB can be achieved for Design A at its center frequency of 1.5 GHz.

Table 2.3: Design A: Simulation Results for the Polarization States

Pol. State	Max Gain (Real.)	X-pol. Level ($\theta = 0°$)	3dB HPBW	Rad. Eff.	Active Impedance Matching at 1.5 GHz
RHCP	4.9 dBic	<-50 dB	85°	81 %	P5,6,7,8 -17 dB
LHCP	3.2 dBic	<-50 dB	83°	74 %	P1,2,3,4 -8 dB
LP (Hor.)	5.3 dBi	<-18 dB	81°	88 %	P1,3 -14.8 dB P5,7 -8 dB
LP (Ver.)	5.3 dBi	<-18 dB	81°	88 %	P2,4 -14.8 dB P6,8 -8 dB

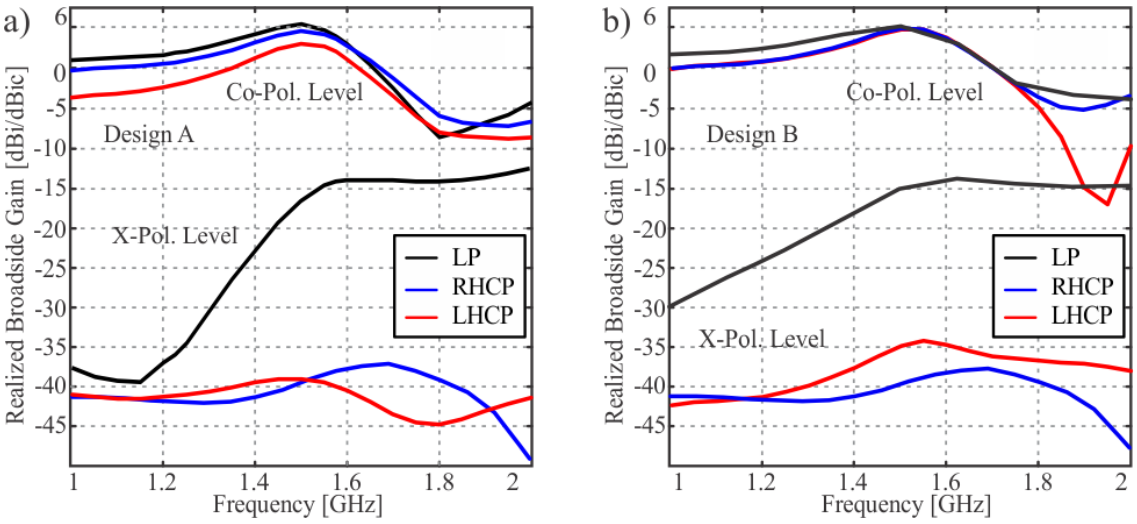

Figure 2.9: Simulated realized gain versus frequency for Design A (a) and Design B (b) considering the defined port definitions in Table 2.1. It should be mentioned that Design A (a) provides different realized gain for its states, while Design B (b) achieves consistent gain values of about 5 dBi and 5 dBic at 1.5 GHz.

Antenna Operation: Design B

Circular Polarization: RHCP (P1 to P4), LHCP (P5 to P8)

For Design B the microstrip terminations near the ACSs slots were optimized to achieve similar passive matching at all the ports whilst achieving port coupling (passive) well below -15 dB for the ports connected to non-parallel microstrip feed lines (see Figs. 2.10 and 2.11).

As a result, the RHCP and LHCP states also provide consistent active F-parameters (see Fig. 2.12(a)). Overall, the F-parameters showed a -10 dB (or better) impedance matching over a bandwidth from 1.1 to 1.55 GHz. Additionally, the coupling to the non-activated ports is minimized at the 1.5 GHz design frequency. This results in an efficiency maximum of 80 % (see Fig. 2.12(a)). This is related to the fact that two microstrip lines feed the same ACS, defining the proposed co-located antenna feeding structure. Also, by using this symmetric feeding approach the realized gain for the DRA is consistent for both CP states; i.e. simulated realized gain peaks were about 5 dBic for the LHCP and RHCP states, respectively, as reported in Fig. 2.9(b).

Linear Polarization: Horizontal (P1, P3, P5, and P7) Vertical (P2, P4, P6, and P8)

The F-parameters for the LP states are presented in Fig. 2.12(b) and generally provide a more narrow -10 dB impedance bandwidth when compared to the CP states for Design B in that the structure is only well matched from 1.45 to 1.55 GHz. Additionally, the

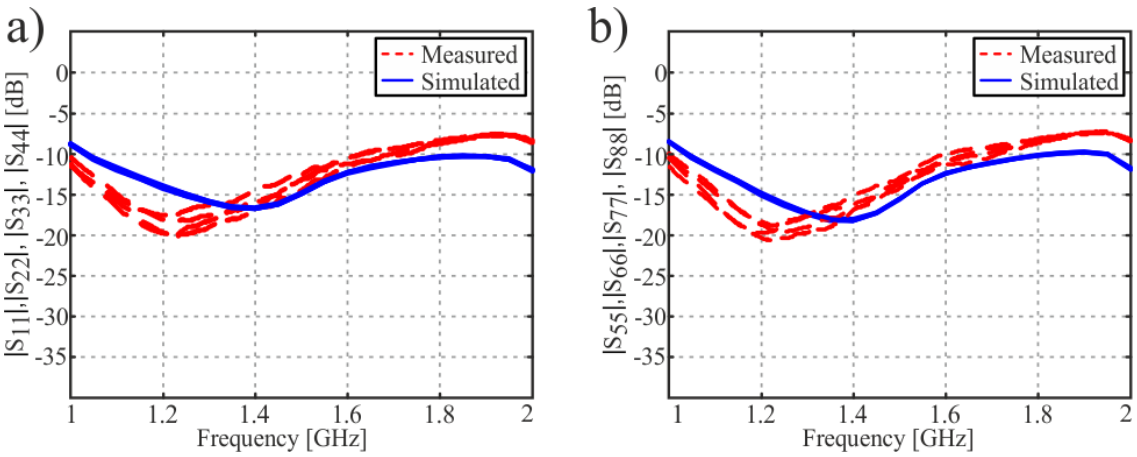

Figure 2.10: Design B: simulated and measured reflection coefficients (passive) for all eight ports. Reflection coefficient values are -14 dB at the 1.5 GHz design frequency. It is important to note that the reflection coefficients for all eight ports are consistent. This is due to the symmetric antenna structure.

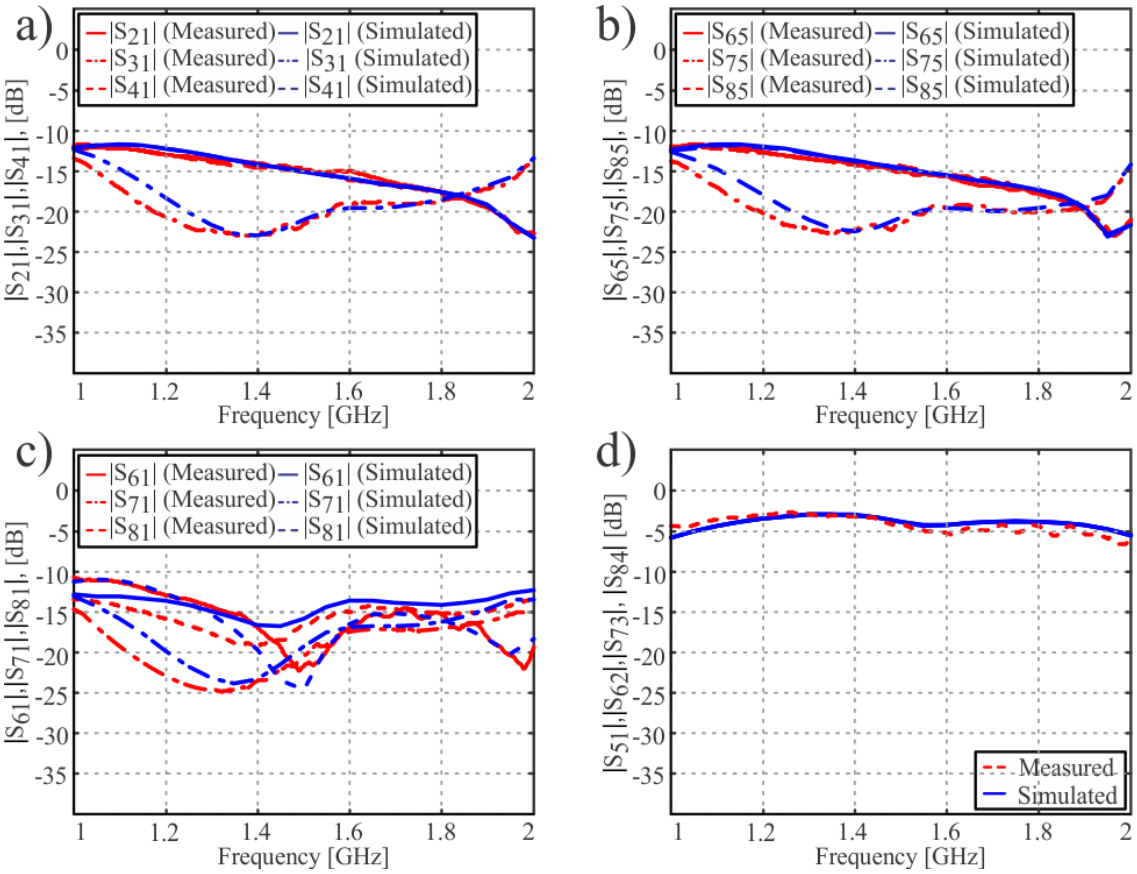

Figure 2.11: Design B: simulated and measured passive coupling between the ports. Coupling values are about -15 dB or below at 1.5 GHz (a)-(c), except for cases when the ports are connected to microstrip lines which feed the same slot (d).

coupling is generally lower than the CP configurations over the operating band of the antenna while the maximum antenna efficiency is 88 % at 1.5 GHz.

The antenna simulations also suggest that high polarization purity is also possible. This is because low cross-polarization levels of -20 dB or better can be observed for

the LP states at broadside (see Fig. 2.13). Similarly for RHCP and LHCP. Also, the simulated beam patterns in Fig. 2.13 suggest that the half-power beam width (HPBW) is approximately 85° while the maximum realized gain is more than 5 dBi at 1.5 GHz (see Fig. 2.9(b) and Table 2.4).

Table 2.4: Design B: Simulation Results for the Polarization States

Polarization State	Max Gain (Real.)	X-pol. Level ($\theta = 0°$)	3dB HPBW	Rad. Eff.	Active Impedance Matching at 1.5 GHz
RHCP	4.9 dBic	<-50 dB	85°	80 %	P5,6,7,8 -12 dB
LHCP	4.8 dBic	<-50 dB	83°	80 %	P1,2,3,4 -12 dB
LP (Hor.)	5.2 dBi	<-20 dB	81°	88 %	P1,3,5,8 -14 dB
LP (Ver.)	5.2 dBi	<-20 dB	81°	88 %	P2,4,6,8 -14 dB

2.6.2 Measurements and Discussions

To validate the proposed diversity antennas, Design A and Design B were both manufactured and measured. For brevity, only results for Design B are fully reported in this section. This is because Design B offers better matching for both of its LP states. On the other hand, the RHCP state for Design A offers best matching as well as higher gain and efficiency when compared to its LHCP state making the proposed antenna (i.e. Design A) suitable for diversity gain scenarios [45] enabling a co-located antenna system and thus not requiring the need to switch to different antennas which offer different gains. However, Design B offers good matching for all its ports and consistent gains for its LP and CP states making it suitable for perhaps polarization diversity applications as in [7, 8, 46] and where a single-antenna unit is required enabling lower system implementation costs.

The S-parameters (passive) for Design A and B were measured using an Anritsu 37377C Vector Network Analyzer and results were in agreement with the simulations (see results in Figs. 2.10 and 2.11). Far-field antenna measurements were completed in a calibrated anechoic chamber and values show a good agreement with the full-wave simulations (see Figs. 2.12-2.17). In addition, external coupler circuits and combiners (as in [49], [51] and references therein) were employed for the far-field measurements to achieve the desired phase at the ports while non-activated ports were terminated in 50-Ω loads. Given this experimental setup, particular measured realized gain patterns were plotted for different azimuth angles as well as the antenna response with respect to frequency. Beam patterns, the matching and the coupling responses, axial ratios, and cross-polarization levels are also reported.

Port Matching and Coupling

Measured and simulated passive S-parameters are presented in Figs. 2.10 and 2.11 for Design B. Results indicate that the DRA offers a good impedance bandwidth with reflection coefficients below -10 dB from 1.1 to 1.8 GHz (which is more than 40 %). The coupling between ports 3 and 1 is also below -15 dB over the entire frequency range while the coupling between ports 1 and 2 is below -10 dB (see Fig. 2.11(a)). This increase in coupling is related to the port locations; i.e they are opposite to each other. In a similar way ports 6, 7, and 8 have coupling values to port 1 below -10 dB. However, the inter-port coupling between the microstrip lines which drive the same ACS can reach up to -4 dB (see Fig. 2.11(d)). This is consistent with the simulations for both Design A and Design B (all results not reported for brevity). It is also important, to follow the port definitions as described in Table 2.1 for the various polarization states. This is because after significant comparisons and simulation trials (not fully reported here for simplicity), these port definitions offered the best radiation efficiency performances for all the defined polarization states as well as improved matching, reduced coupling and when the active S-parameters or F-parameters were considered as in Fig. 2.6(b), 2.7, and 2.12 and in Tables 2.3 and 2.4 for the same DRA structure.

CP Antenna Operation: RHCP and LHCP

The antenna simulations and measurements demonstrate high polarization purity with low cross polarization levels at broadside for every CP state (see Figs. 2.13-2.16). For Design A and B, the different CP gain values can be observed in Fig. 2.14 for the RHCP and LHCP states, respectively. Also, the measured maximum realized gain is about 5 dBic at 1.5 GHz for Design B (both polarization states) and the antenna offers a HPBW of approximately 80° (see Figs. 2.14(b) and 2.15, respectively). Measured axial ratios are also well below 3 dB considering an angular range of more than ±50° as reported for different azimuth angles as in Fig. 2.16. In general, the simulation results are in close agreement with the measurements.

LP Antenna Operation: Horizontal and Vertical

For Design B the antenna simulations and measurements demonstrated good polarization purity with cross polarization levels of -15 dBi or less at broadside for every LP state (see Fig. 2.17). Measured maximum realized gain is at 1.5 GHz with a value of almost 5 dBi which is consistent with the simulations as reported in Table 2.4. Additionally, the realized gain over frequency is shown in Fig. 2.17(a) while the HPBW is approximately

88° as observed in Fig. 2.17(b).

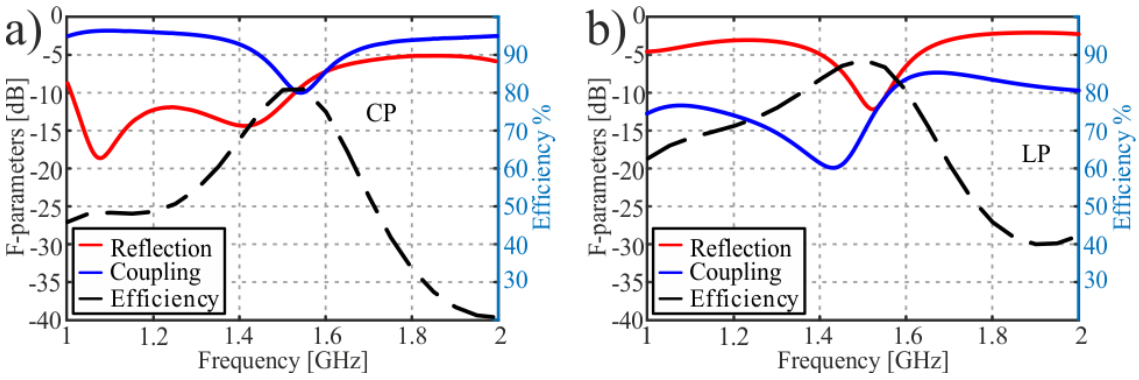

Figure 2.12: Design B: simulated active S-parameters (or F-parameters from CST) defining the active reflection coefficient in dB as well as the coupling to the non-activated ports for the CP (a) and LP (b) states. The efficiency is also reported in (a) where it is observed that when the coupled power to the non-active ports is reduced, antenna efficiency increases. In addition, the active reflection coefficients demonstrate values of -10 dB (or less) at 1.5 GHz.

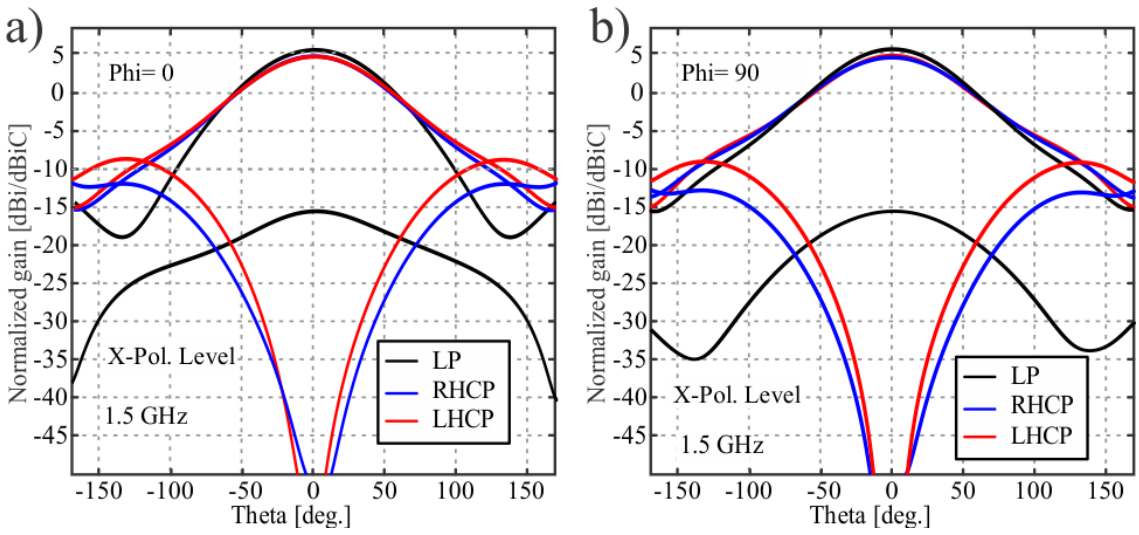

Figure 2.13: Design B: simulated beam patterns and cross-polarization levels for the antenna operating states as defined in Table 2.1.

2.6.3 General Discussions

Discrepancies between simulations and measurements for Design A and Design B could be related to manufacturing tolerances or by imbalances in the power combiners and external hybrid couplers employed to generate the required phase shifts at the ports (see Table 2.1). More specifically, in the simulations the applied port voltage (magnitude and phase) were considered ideal. It should also be mentioned that higher than expected cross-polarization levels were observed and are likely related to the commercial reference

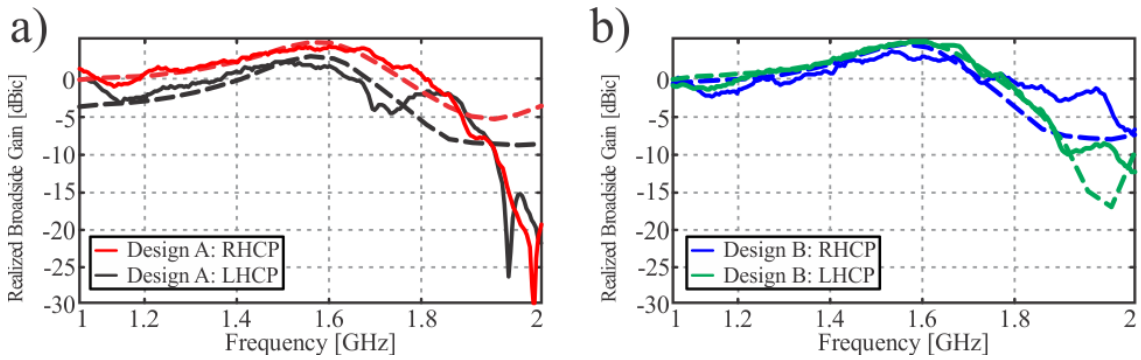

Figure 2.14: Design A (a) and Design B (b) simulated and measured broadside gain versus frequency for the RHCP and LHCP states. Simulations and measurements are continuous and dashed lines, respectively.

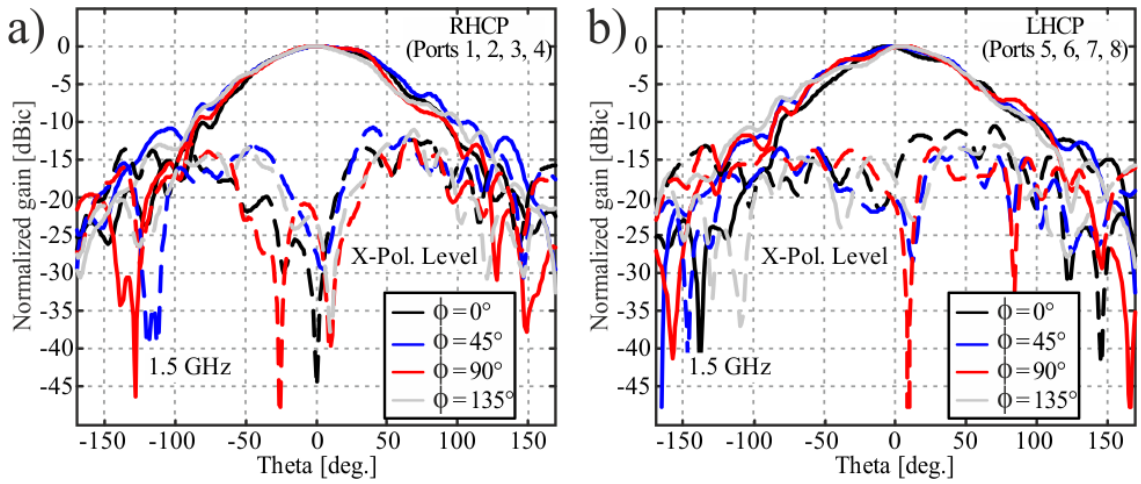

Figure 2.15: Design B: RHCP (a) and LHCP (b) measured beam patterns at 1.5 GHz. Cross-polarization levels are also shown.

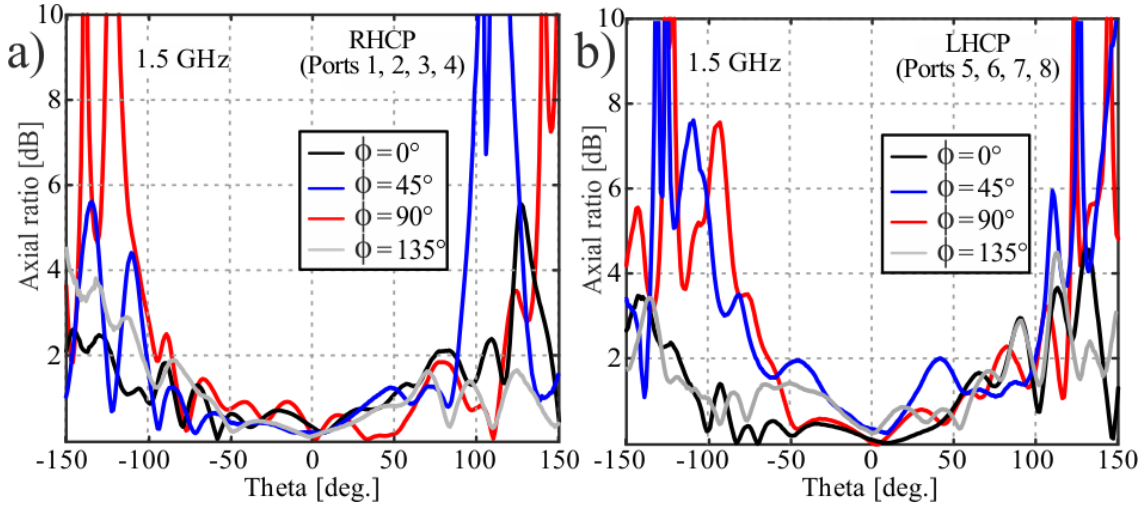

Figure 2.16: Design B: measured axial ratios for the RHCP and LHCP states.

antennas which also have relatively high cross-polarization values (10 dB below the main co-pol. beam maximum) at the measurement frequencies as well unwanted scattering from the metallic antenna tower. Regardless of these practicalities, measurements and

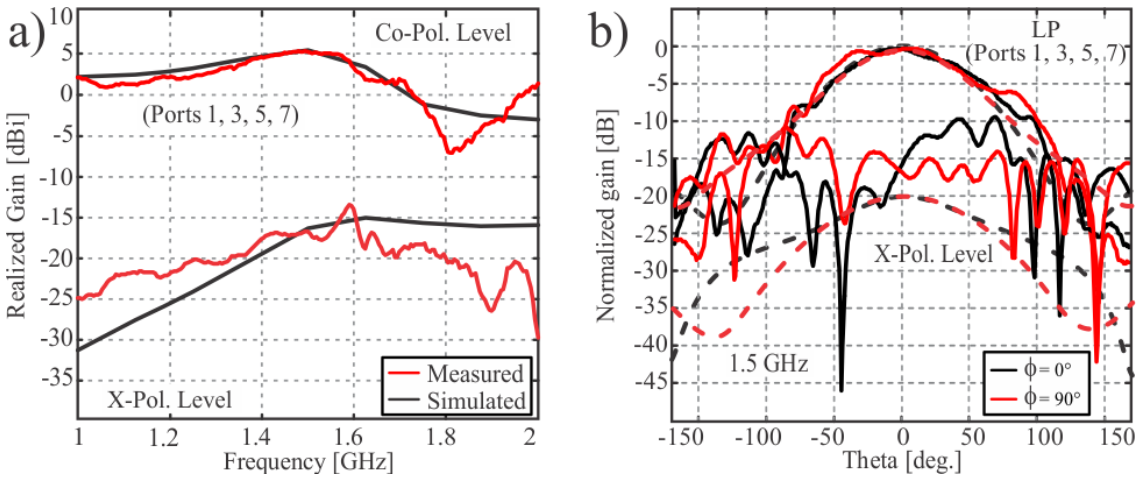

Figure 2.17: Design B: LP (vertical) realized gain versus frequency (a) and beam pattern (b). For (b) simulations and measurements are continuous and dashed lines, respectively. Very similar results are observed for Design A, LP (vertical and horizontal) as well as Design B, LP (horizontal). All results not shown for brevity.

simulations are generally in good agreement for the proposed L-band diversity antennas.

2.6.4 Feeding System Discussions

To generate circularly polarized radiation, approximately phased signals need to be applied to ports 1 to 4 or ports 5 to 8; i.e. an applied phase delay of 90° is required. Similarly, for the LP states, the DRA needs to be excited using ports 1, 3, 5, 7 or 2, 4, 6, 8 with a 0° and 180° phase shift; i.e. differential. To achieve these phase shifts different combinations of external hybrid couplers can be used, defining a supporting coupler system. The simplest implementation could be one 180° coupler and two 90° couplers for the CP states. For LP, only one hybrid coupler with a 180° output phase difference is required.

Possible circuit schematics are detailed in Fig. 2.18 for the CP and LP cases and examples of such couplers can be found in [52] or [53]. For simplicity, the coupler system from [51] (see specifically Fig. 5, from [51]) was employed for the DRA measurements in this paper; i.e. for the fabricated antenna prototype as in Fig. 2.4, enabling polarization diversity. Moreover, this external 5-port coupler system offered reduced imbalances at the ports from about 1 to 1.8 GHz. For example, the magnitude imbalance is less than about 1 dB over the majority of this frequency range whilst offering the required 90° sequential rotation [51].

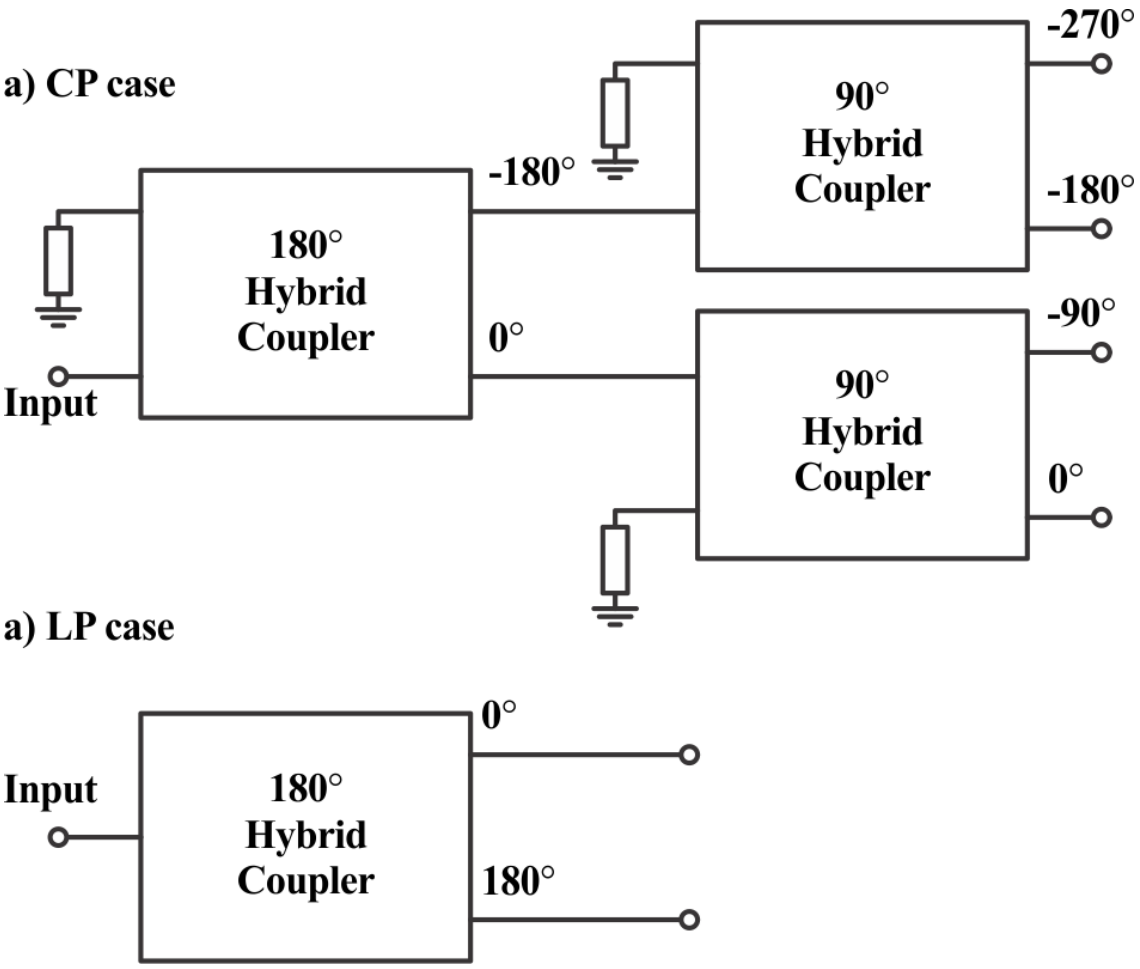

Figure 2.18: Possible circuit combinations to generate CP, (a), where one 180° and two 90° hybrid couplers are required, and (b), LP, where only 180° coupler is needed. As further described in the text, a 5-port coupler system (see Fig. 5 from [51]) can be employed for both CP or LP DRA measurements. For example, for LP measurements, the 0° and 180° output circuit ports are only needed, from (a), while the -90° and -270° ports can be terminated in matched loads. Phased matched cables are also required when connecting this type of external coupler system to the appropriate ports of the DRA (see Table 2.1).

2.6.5 Conclusion, Achievements and Discussions

A novel 8-port dielectric resonator antenna (DRA) was presented for gain and polarization diversity applications. The antenna design consists of eight 50-Ω microstrip lines feeding 4 slots (with unconventionally 2 feed lines per slot), and a dielectric resonator element on top with a relative permittivity of ε_r = 10 which exploits degenerate $HE_{11\partial}$ modes. This DRA structure offers dual-linear and dual-circularly polarized radiation by its flexible port arrangement. Maximum gains of 5.2 dBi and 4.9 dBic are obtained for the linear and circular polarization states, respectively. For proof-of-concept, two distinct prototypes were fabricated and experimentally verified (Design A and Design B). Further advancements could be the realization of a higher dielectric constant for the resonator for

size reduction, as briefly studied in [54], as well as an integrated feeding circuit. The proposed antenna can be used in various communication systems where antenna gain and polarization diversity are required such as in geolocation or other wireless systems.

Therefore, while the 8-port DRA achieves a relatively compact design, it is possible to further reduce the size of the antenna by choosing a higher dielectric. Additionally, the feeding which required additional coupler circuits could be not desirable in practice as it creates an additional microwave element. Thus, a more practical feeding circuit integration would require integrating commercial coupler systems on the same feeding PCB could be a great solution for this antenna.

2.7 Planar Feeding Circuit Integrated with a Compact Dielectric Resonator for Polarization Diversity

Given the previous findings, investigations to simplify the overall design of the DRA whilst reducing the feeding network complexity was also of interest. For example, motivations where to simplify the previous 8-port DR structure for polarization diversity applications which generated LHCP, RHCP, and LP. Such an antenna system required a network of external couplers and an 8-port feeding configuration. To advance this design, a similar antenna system (but with only 4-ports) was made more efficient and compact in [51] by using a meandered slot ring with a metallic cavity backing. In particular, the DR element was reduced in size by using a high relative dielectric constant material, and similar to [49], CP radiation over a wide frequency band (35 %) was achieved only for the 4-port antenna by using external couplers.

Most of the feeding systems for polarization control or reconfigurability can be divided into active or passive circuit solutions. An example of such a passive system was presented in [55], where a dually-polarized waveguide coupler system was presented which operated at 60 GHz. The proposed feeding system enabled an efficient power split ratio which can be useful in base station applications. Also in that work a dual-polarized Butler Matrix feeding system was adopted, verifying the capabilities of the beam-forming network.

Another reconfigurable system was presented in [56]. The described waveguide antenna feeder provided an efficient signal rotation between LHCP and RHCP. Also, by utilizing piezo-motors integrated within the waveguide system, the authors were able to achieve a compact design while maintaining a high efficiency power split ratio. The re-

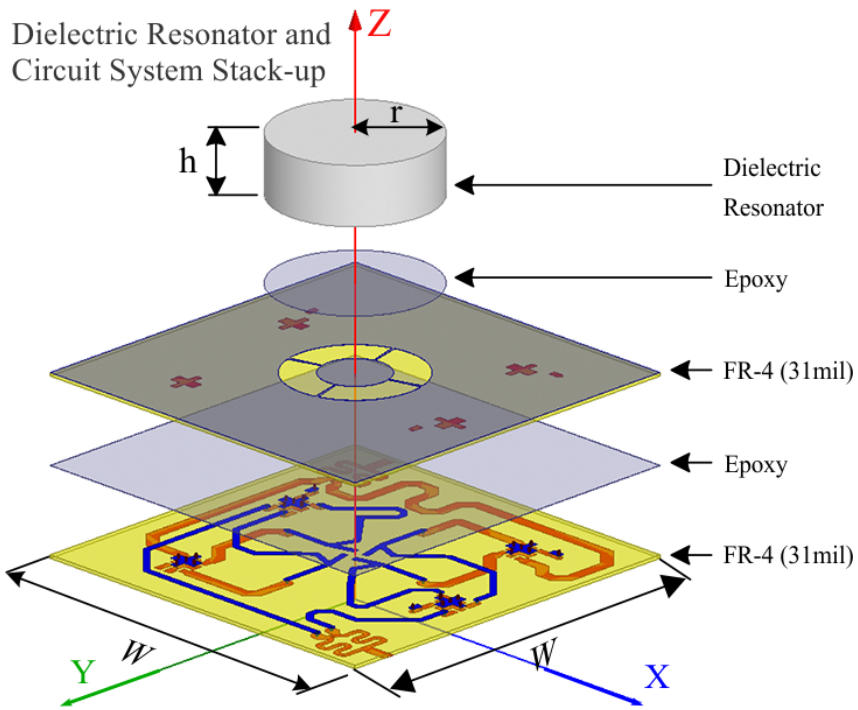

Figure 2.19: Complete stack-up for the proposed dielectric resonator and circuit system (DRCS) defined by two 31 mil FR-4 substrates, two epoxy layers, surface mount components and the cylindrical DR itself. Dimensions h, W, and r are 18.1 mm, 90 mm, and 19.05 mm, respectively. In terms of size with respect to the wavelength, the total structure is 0.54 λ_0 by 0.54 λ_0 by 0.1 λ_0 (at the higher operational frequency range which is about 1.8 GHz).

ported polarizer operated from about 13 to 15 GHz with an axial ratio below 3 dB. An example of an active system could be reconfigurable elements based on p-i-n switches. The antenna design presented in [57] utilized such a diode system to control beam properties of the dipole antenna array. This structure operated from about 24 to 27.5 GHz with a maximum realized gain of 10 dBi and a 90 % efficiency. The antenna was also integrated within a mobile phone model suggesting that such a structure could be applicable for 5G communication systems.

Following these developments, in this thesis a new L-band dielectric resonator circuit system; i.e. a DRCS, with only 2 external ports which offers RHCP, LHCP and two orthogonal LP operating states is also reported (see Figs. 2.19, 2.20, and 2.21). As a starting point in our design, the preliminary efforts in [58] for the simulated 8-port DR antenna were reviewed and studied. Expanding on these findings, a totally new feeding system was designed and fully integrated under the DR ground plane (see Fig. 2.19). Then this DRCS was fabricated and experimentally verified to demonstrate polarization agility. The particular choice of the L-band frequency range, whilst offering polarization diversity, can support connectivity to the Global Navigation Satellite System (GNSS), the

Global Positioning System (GPS), and other wireless communication systems where polarization diversity and polarization purity is of interest [59]. Using this antenna diversity and the supporting signal processing techniques as outlined in [60], [61], noise effects can be reduced and channel fading mitigated.

The antenna circuit system reported in this paper, for operation in the L-band, offers similar compactness to [51], but also, with the noted integrated feeding (see Fig. 2.20(b)). In addition and as further discussed in this thesis, a more complicated DR excitation approach enabling polarization diversity is employed. With such compactness into a single antenna unit, there are many benefits when adopting such a DRCS for real-life scenarios. However, as further outlined herein, there are also some minor design constraints. This includes acceptable coupling within the circuit and reduced DRCS total efficiency, the need for an external combiner and phase shifter for LP operation, and, reduced realized antenna gains when using commercial printed circuit board (PCB) dielectric materials of low-cost; i.e. FR-4. As further discussed in the paper, solutions include re-designing the feeding network, to better support LP operation, at the cost of an enlarged circuit layout size and using lower-loss PCB substrates to enhance DRCS efficiency.

Regardless of these points, the fabricated and measured DRCS reported for proof-of-concept is well matched between 1.25 and 1.9 GHz defining the -10 dB impedance reflection coefficient bandwidth (which is in excess of 40 %). Also, the simulated total DRCS efficiency (antenna and feeding system) for all polarization states is about 70% or more. Measured beam patterns are documented as well as the realized gain over frequency with results in agreement with full-wave simulations. Simulated and measured axial ratios for the LHCP and RHCP states are also well below 3 dB over the DRCS operational frequency range. To the best knowledge of the authors, no similar antenna structure with an integrated feeding system has been reported offering comparable functionality in terms of overall compactness, broadband operation, and polarization diversity.

2.7.1 Dielectric Resonator & Circuit System Design

As an initial step in the design and development of the proposed DRCS, the cylindrical DR with the basic feeding system from [58] is reviewed. That preliminary feeding system was defined by a network of eight microstrip lines etched on the bottom side of the substrate to feed four aperture coupled slots (ACSs) which were positioned on the bottom side of the DR (see inset of the 8-port feeding system in Fig. 2.22). This 8-port

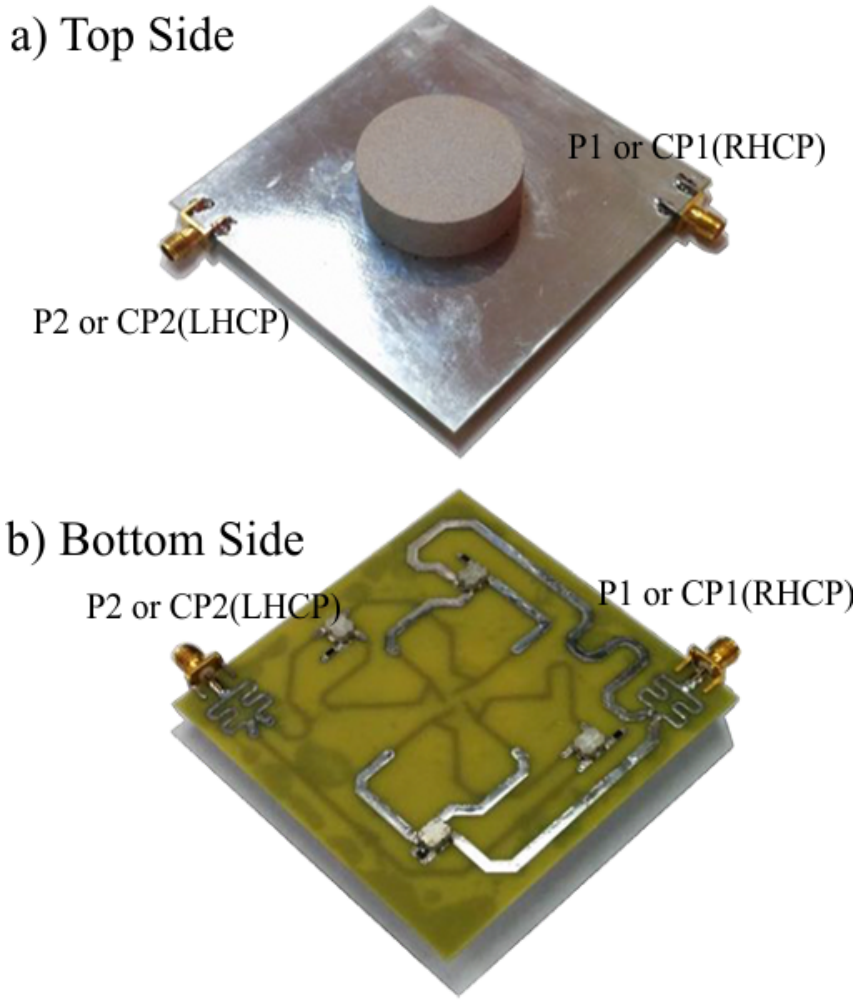

Figure 2.20: (a) Top view and (b) bottom view for the fabricated DRCS (total dimensions: 90 by 90 by 19.7 mm^3, excluding connectors); see the multilayer stack-up for the relevant circuit and ground plane layers as shown in Fig. 2.19.

structure was able to provide a high-degree of freedom and when applying the appropriate (and fixed) phase shifts to the ports (see Table 2.5), the excitation and control of degenerate $HE_{11\delta}$ modes were made possible. As a result, an agile 8-port polarization diverse antenna [58] was simulated and optimized which offered LP, LHCP and RHCP radiation.

The realized gains in the far-field for the polarization states described in Table 2.5 can also be plotted versus frequency as in Fig. 2.22 considering a relative dielectric constant (ε_r) of 27 for the DR. While polarization diversity can be observed for the 8-port DR antenna, see Fig. 2.22, and some preliminary simulations were reported in [58] with ε_r = 30 for the DR (whilst both adopting ideal port excitation), no practical feeding circuit was developed. As further described herein, a new feeding system with only 2 external ports is designed for complete DRCS integration, allowing for dual-CP and dual-LP operation.

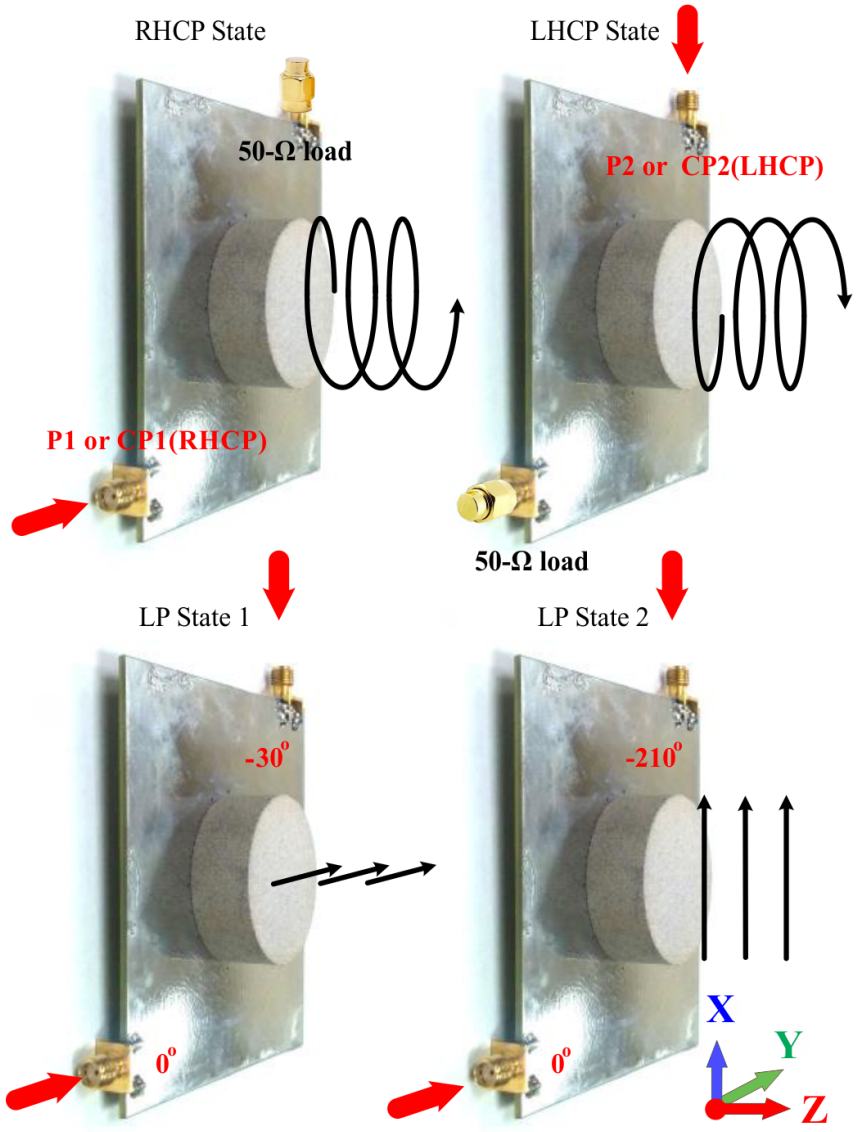

Figure 2.21: Illustration of the possible polarization states for the 2-port DRCS where the relevant ports are driven and the non-active ports are terminated with 50-Ω loads: a) RHCP, b) LHCP, c) LP state 1 (dominant in the y-z plane), and d) LP state 2 (dominant in the x-z plane).

2.7.2 General DRCS Structure Overview

The proposed DRCS consists of an optimized cylindrical DR ($\varepsilon_r = 27$) having a radius of 19.05 mm and a height of 13.80 mm (see Figs. 2.19 to 2.21). This DR and its ground plane are placed on top of two 31 mil square FR-4 substrates, each having dimensions of 90 mm by 90 mm. The four radiating $HE_{11\delta}$ modes of the DR are excited by four radial ACSs. The slots are driven by the aforementioned feeding circuit (see Fig. 2.23) which shares the ground plane of the top cylindrical DR element. Basically, each port of the DRCS when driven generates either RHCP or LHCP. These external ports define the input connections to two distinct planar circuits, and given the compact implementation,

Table 2.5: Feed Definitions for the Polarization States (see Fig. 2.22)

Port	RHCP	LHCP	LP (Horizontal)	LP (Vertical)
P1	$1\angle 0°$	0	$1\angle -30°$	$1\angle -210°$
P2	$1\angle 270°$	0	$1\angle 240°$	$1\angle 60°$
P3	$1\angle 180°$	0	$1\angle 150°$	$1\angle -30°$
P4	$1\angle 90°$	0	$1\angle 60°$	$1\angle -120°$
P5	0	$1\angle 0°$	$1\angle 180°$	$1\angle 210°$
P6	0	$1\angle 90°$	$1\angle 270°$	$1\angle 300°$
P7	0	$1\angle 180°$	$1\angle 0°$	$1\angle 30°$
P8	0	$1\angle 270°$	$1\angle 90°$	$1\angle 120°$

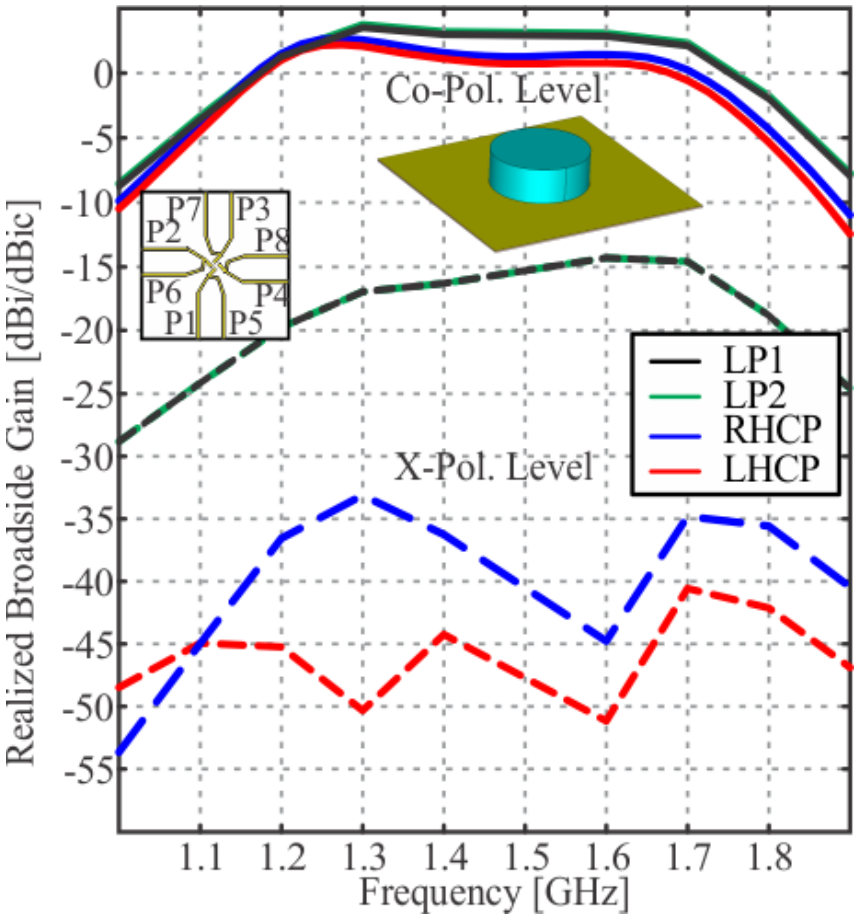

Figure 2.22: Simulated gain and cross-polarization levels for a representative 8-port DR structure (see inset for the bottom view and top view), whilst considering the (ideal) port definitions as outlined in Table 2.5 from 1 to 2 GHz. Note that no feeding circuit, as in Fig. 2.20(b), was included in the simulation model.

these circuits become co-located.

As outlined in Figs. 2.19 and 2.20, these RHCP and LHCP feeding circuits are realized by a bottom microstrip transmission line layer and an inner strip layer (or buried microstrip). This ensures overall structure compactness and full integration with the top DR element. Additionally, for some practical applications and when interference from

other radiation sources can be problematic, the bottom side of the DRCS can be covered with a metal sheet or the feeding system can be placed inside a cavity as in [51]. Full-wave simulations suggest that an air gap of at least 6 mm between the bottom PCB (of the DRCS) and any additional metal sheeting for shielding purposes is required. This can help to minimize any unwanted coupling effects and de-tuning of the microstrip line-based feed system (all results not reported for brevity).

It can be noted that the realized gain traces in Fig. 2.22 consist of two peaks: one located at about 1.25 GHz and the other at 1.65 GHz. The 1.25 GHz peak is related to the resonances of the ACSs which are driven by the feeding circuit. These slots also transfer power to the DR for hybridized radiation into the far-field. The 1.65 GHz peak can be attributed to strong $HE_{11\delta}$ mode excitation. It is the combination of these two complementary radiation mechanisms which supports the broadband DRCS performance whilst it is the high relative dielectric constant material for the resonator and its PCB feeding circuit which dictates overall DRCS compactness.

2.7.3 Design & Operation of the Feed Circuit

The antenna feeding circuit layout overview for overall DRCS design purposes, can be seen in Fig. 2.23 and the motivation for this structure was primarily to achieve CP operation by either a sequential +90° or -90° applied to the four ACSs. However, LP operation can be made possible using external phase shifters and will also be described herein.

Circularly Polarized Radiation

to achieve LHCP for example, a +90° sequential phase shift is achieved by taking power incident on a single port (see Figs. 2.20 and 2.21) and then having it divided through a meandered and compact Wilkinson power divider in order to achieve a 3 dB power split. Each of these two split signals is then routed to a 90° surface mount hybrid coupler (Anaren model XC1400P-03S) which further splits the input power while also adding a 90° delay. This results in four signal paths; i.e. two signals in phase and two signals with a 90° relative phase shift. However, sequential +90° is required at the ACSs for LHCP operation; i.e. 0°, +90°, +180°, and +270°. These last two phase shifts are obtained by passing one of the two signal lines from the Wilkinson power divider through a 180° long trace or delay line (designed with a 1.3 GHz centre frequency) prior to another 90° hybrid coupler. Similarly, a sequential -90° phase shift (i.e. 0°, -90°, -180°, -270°)

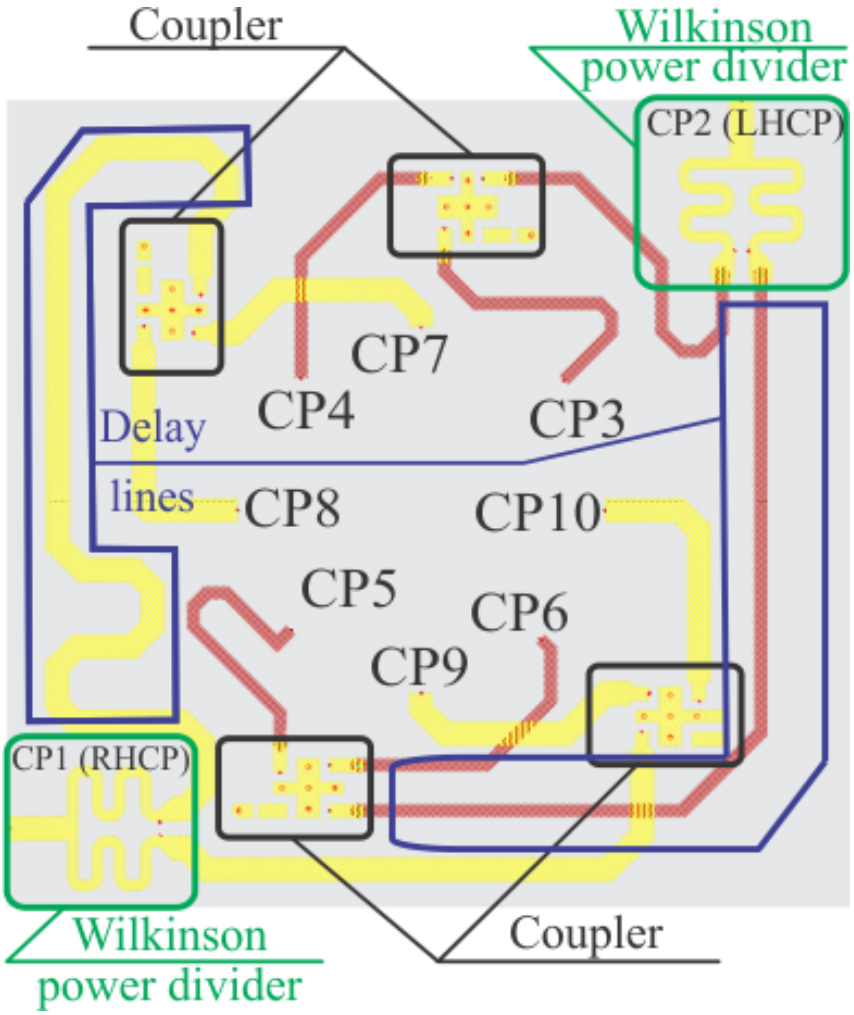

Figure 2.23: Intermediate layout of the feeding network for design and simulation purposes; for the final PCB circuit dimensions, see Fig. 2.28 and Table 2.6, respectively. As outlined in Fig. 2.19, the feed circuit is composed of two FR-4 dielectric layers having a common ground plane and 10 circuit ports; i.e. CPi where $i \in$ [1,10]. Microstrip transmission lines (yellow trace) are attached to the two external ports (i.e. P1 or CP1 and P2 or CP2, see Fig. 2.20) while the inner strip transmission lines or buried microstrip (red trace), are connected to the eight internal ports for DR feeding: CP3, CP4, CP5, CP6, CP7, CP8, CP9, and CP10. It should be mentioned that the microstrip and strip lines were electrically connected by metalized vias while ideal magnitude and phase responses were defined for the four surface mount couplers during simulations.

for RHCP is achieved by a separate and co-located circuit enabling this opposite polarization state. The primary differences being that auxiliary ports on the hybrid couplers are connected to the traces from the power divider.

Linearly Polarized Radiation

is achieved by employing an external power divider and simultaneous excitation of both the LHCP and RHCP ports. However, an external phase shifter providing an offset of either -210° or -30° should be connected to P2 (LHCP) in order to account for path length differences between the two feeding circuits. The two options (-210° or -30°) will provide orthogonal orientations of the radiated fields (see Fig. 2.21), defining LP state 1

and LP state 2 for the DRCS, respectively.

It should be mentioned that other phase offsets are possible such as 0° and 180° (or 90° and -90°), however, full-wave simulations for the DRCS suggest that -210° and -30° offered increased realized gain values in the far-field. These phase requirements are related to the asymmetry within the feeding circuit, unwanted phase offsets incurred due to electromagnetic coupling within the PCB and transmission line meandering. This transmission line meandering was needed to ensure a compact feeding circuit implementation.

2.7.4 Feeding of the Radial Aperture Coupled Slots (ACSs)

By inspection of the feeding circuit and the slots positioned under the DR element (see Figs. 2.19 and 2.20), it can be observed that two transmission lines which originate from the hybrid couplers, drive each of the four ACSs, for example, CP3 and CP7 or CP4 and CP8. The radial positioning of these slots, and the resulting physical connection of the lines, was required due to the high relative dielectric constant of the DR (ε_r = 27) which enabled overall structure compactness. This resulted in an eight-point feed arrangement for the cylindrical DR element. It should also be mentioned that, whilst considering these design constraints, a parametric optimization for the relevant dimensions of the DR (such as radius and height of the DR as well as the radius, orientation and position of the ACSs, whilst excluding and then including the feeding circuit) was completed using a commercial full-wave simulator. Results suggest that the best possible matching was achieved from about 1.1 GHz to 1.7 GHz with maximum realized gain values as reported in Fig. 2.22 for the case without the integrated feeding circuit.

It should be mentioned that coupling is not significantly increased with these physical connections of the transmission lines near the ACSs (see Figs. 2.19 and 2.20(b)), when compared to more classic open circuited stub matching techniques as adopted in [49]. This is because the majority of any coupling is mainly generated by the adjacently positioned strip lines, which feed the common slots, and not the connected stubs positioned near the origin. In fact, it was found that during our design work, the connected transmission lines under the DR, provide some reactive loading and can be utilized when matching and improving power delivery to the slots for hybridized radiation of the ACSs with the DR.

2.7.5 Feed Circuit & DRCS Simulations

To further design the feeding network, the PCB circuit in Fig. 2.23 was optimized using a commercial circuit simulator. In particular, dimensions of the Wilkinson power dividers, the placement of the via interconnections, and, the equal phase delay lines positioned between couplers and other connection points. There are also two 180° delay transmission line (see Fig. 2.22) considering a centre frequency of 1.3 GHz to achieve the required phase delays (see Table 2.5) at the feed points of DR element. In addition, similar circuit performances were also desired from about 1.1 GHz to 1.7 GHz. The simulations were initially completed having no DR element placed on top of the structure whilst using the circuit as illustrated in Fig. 2.23.

The feed system was also carefully designed and optimized by considering the possible electromagnetic coupling effects between transmission lines and any unwanted phase offsets accrued due to meandering. In particular, traces were separated as much as possible while corner chamfers, due to the meanders and 90° bends, were taken into consideration during the DRCS optimization. This ensures phase stability and improves the overall response of the circuit system. In the following, simulation results for the various circuit parts are reported realizing the various polarization states as well as the generated electric field within the PCB for the RHCP state (see Figs. 2.24 to 2.27). Detailed dimensional layouts for the final and fabricated feeding circuit are outlined in Fig. 2.28 and Table 2.6. Simulated losses, phase imbalances, and total DRCS efficiency values are also reported in Figs. 2.29 and 2.30 as well as Table 2.7.

Excitation of DRCS Port 1 or CP1 for RHCP

The first external port, CP1, divides the input signal to circuit ports CP7, CP8, CP9 and CP10 for RHCP. The feeding network magnitude and phase imbalances can be seen in Fig. 2.24. It should be noted that the magnitude imbalance is no more than 0.8 dB across the entire simulated range, from 1 to 2 GHz, which is slightly higher than the magnitude imbalance for the LHCP feeding circuit (see Fig. 2.26).

The different electrical lengths for the transmission lines connected to CP 7,8 and CP 9,10 provide the required phase at 1.3 GHz as per design (see Fig. 2.24). For example, it can be seen that a sequential 90° phase shift is achieved at that frequency (as required with reference to Table 2.5 for the RHCP state). For other frequencies, the electrical lengths of the microstrip lines are naturally different due to dispersion and it can be observed that at 1.1 GHz and 1.5 GHz the required sequential phase difference is offset by about 25°

(see Fig. 2.24). Similar phase responses are observed for the LHCP circuit-part.

The observed minor magnitude and phase imbalances in Fig. 2.24, which is unwanted and can detune DRCS operation, is related to the signal cross-talk between the co-located LHCP and RHCP feed circuits. A full-wave simulation of the electric field within the PCB for this polarization state confirms that unavoidable electromagnetic coupling occurs at the cross-over sections of the microstrip and strip lines near CP4 and CP7 as well as CP6 and CP9 (see insets in Fig. 2.25). The simulated cross-coupled power from 1 GHz to 2 GHz showed values below -20 dB for both cases. It should be mentioned that the full-wave simulator did account for this coupling during the feeding circuit optimization; i.e. the refinement of the detailed metallic patterning features such as the transmission line bends and meandering (see Fig. 2.28 and Table 2.6). However, this unavoidable coupling within the co-located RHCP and LHCP circuit-parts can still moderately detune circuit performance for the different external port excitations (which enable the various polarization states) contributing to the observed magnitude and phase imbalances reported in Fig. 2.24.

By inspection of Fig. 2.25 it can be observed that such coupled power would be absorbed at the resistive loads connected to the hybrid couplers decreasing efficiency. These E-field simulations for the RHCP state in Fig. 2.25 are very similar to the LHCP case and are not reported for brevity. Regardless of these points, the losses for the RHCP circuit-part are less than 1 dB at the circuit design frequency of 1.3 GHz when considering no losses for the PCB as well as for $\tan\delta = 0.02$ as reported in Fig. 2.29. Efficiency values for the complete DRCS range from 74 % to 83 % when all PCB loss cases are compared (see Fig. 2.30 and Table 2.7) whilst considering common conductor losses associated with the copper traces and the ground plane.

Excitation of DRCS Port 2 or CP2 for LHCP

When circuit port 2 (CP2) of the DRCS is driven, LHCP radiation can be made possible. Basically the input signal is mostly divided equally to circuit ports CP3, CP4, CP5 and CP6, and ideally, with the phase delays as outlined in Table 2.5. Also for this state, simulations suggest that the imbalance of those ports can reach maximum values which are less than 0.5 dB at 1.3 GHz (see Fig. 2.26). Close to ideal phase imbalances can also be observed at 1.3 GHz. This is related to the optimized electrical lengths of the transmission lines connected to CP3, CP4, CP5, and CP6.

The overall circuit losses for this LHCP state are compared to other states (see Fig.

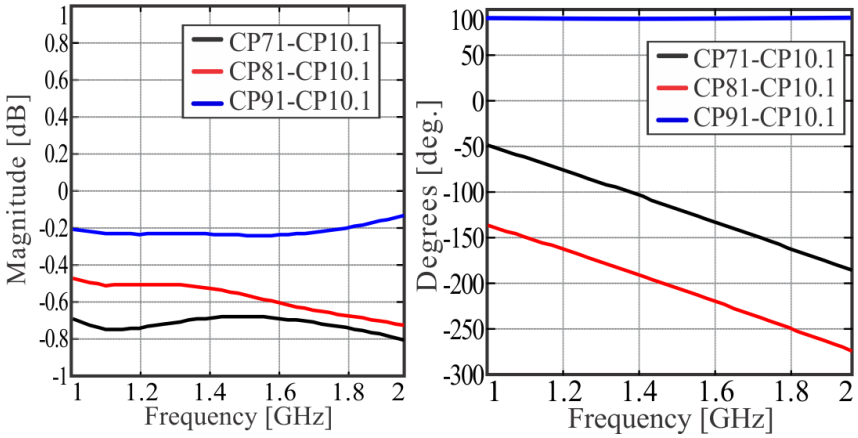

Figure 2.24: Simulated response of the feeding network for the RHCP state without the DR (see Fig. 2.23). The maximum magnitude imbalance is approximately 0.7 dB at the 1.3 GHz circuit centre frequency, which is slightly higher when compared to the RHCP state (see Fig. 2.26). Phase differences are ±90° or -180° at 1.3 GHz which is similar to the RHCP state.

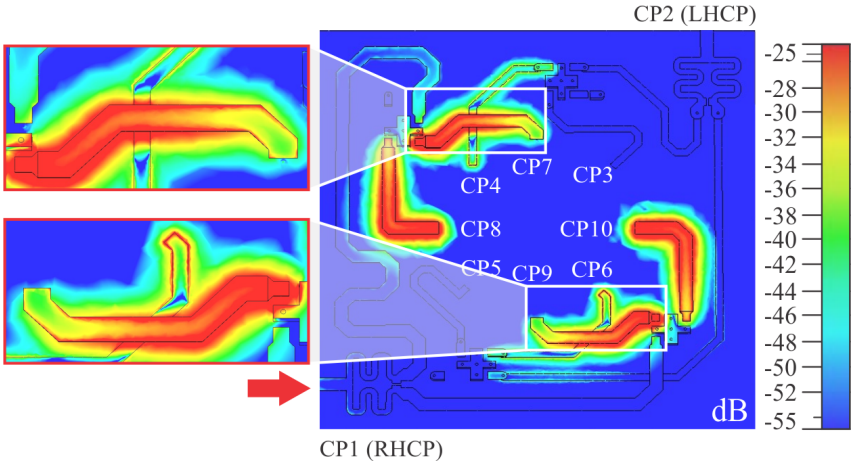

Figure 2.25: Simulated E-field at 1.3 GHz within the central part of the feeding circuit (bottom view) for the RCHP state and where power is injected into P1 or CP1. Due to the compactness of the structure, the microstrip and strip lines cross-over in particular sections. This allows for unwanted (minor) cross-coupling between the two main CP circuits (see insets) and this can be observed between the transmission lines connected to internal ports CP4 and CP7, CP6 and CP9 (whose S-parameter coupling values are below 20 dB). Similar observations were made for the LHCP and LP states (all results not reported for brevity).

2.29) considering a lossless and lossy FR-4 feeding circuit structure. Maximum efficiency for the LHCP state can be seen at 1.35 GHz with a value of 73 %. Simulations in Table 2.7 also report different values of $\tan\delta$ for the two FR-4 PCB layers (no loss with $\tan\delta = 0$, low-loss; i.e. where $\tan\delta = 0.002$ representing a hypothetical dielectric PCB material, and standard FR-4 with $\tan\delta = 0.02$). It can be observed that when comparing the maximum feed circuit imbalances for different values of $\tan\delta$, the total DRCS efficiency increases (see Fig. 2.30) for lower dielectric losses. This makes sense since

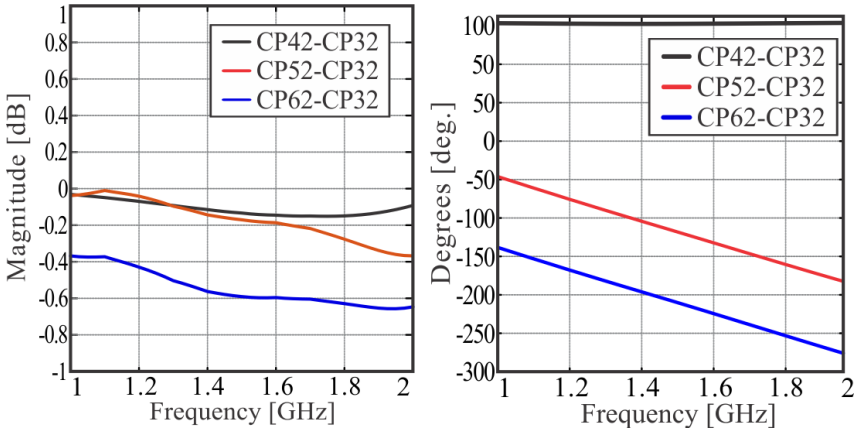

Figure 2.26: Simulated response of the feeding network for the LHCP state without the DR (see Fig. 2.23). The magnitude imbalance is about 0.6 dB for 1.7 GHz (or below) while the general phase response is similar to the LHCP case (see Fig. 2.24) but with a reverse sequential phase rotation.

the signal along the circuit path accrues higher losses (for larger values of $\tan\delta$) which dictate a larger magnitude imbalance for the entire feeding circuit. For example, for $\tan\delta$ = 0 [$\tan\delta = 0.02$] the maximum simulated circuit imbalances are 0.50 dB [0.62 dB] while the total peak DRCS efficiency is 80 % [68 %] for the LHCP state.

It is also important to note that the circuit and DRCS efficiency is generally improved for the RHCP state when compared to the LHCP state. This is related to the fact that the majority of the RHCP circuit-part is defined by a conventional microstrip transmission line (see the red trace in Fig. 2.28(a)) with the signal path defined by an air-dielectric medium versus the strip lines (or the microrstrip immersed in dielectric) for the LHCP circuit-part (see the blue trace in Fig. 2.28(b)). Basically the LHCP circuit-part accrues more dielectric and conductor losses for this compact circuit configuration.

Simultaneous Excitation of DRCS Ports 1 and 2 for LP

In this state both DRCS ports are activated (RCHP port and LHCP port). However, to obtain the required phases for the two LP states as defined in Fig. 2.21 and Table 2.5, external phase shifters and power combiners are required. To simulate the circuit response, an ideal phase shift of -30° for LP1 and -210° for LP2 were considered in the simulation model from 1 to 2 GHz and by assigning the required port definitions. For brevity, only the results for the -30° case are reported in Fig. 2.27; i.e. the LP1 state, as similar results were observed for the LP2 state.

For both LP states, the magnitude imbalance is less than 0.5 dB at 1.3 GHz while the phases are offset by about 20° or less and this is related to the aforementioned coupling between the LHCP and RHCP circuit-parts. However, the overall DRCS performance

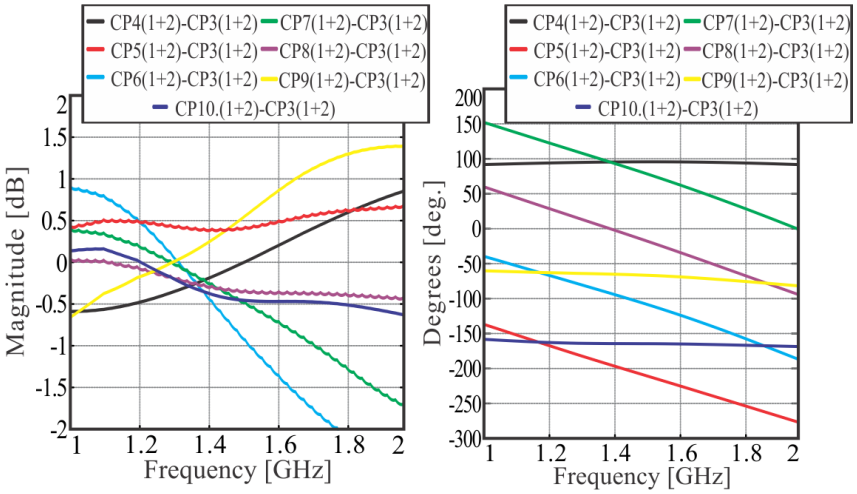

Figure 2.27: Simulated response of the feeding network for the LP1 state without the DR considering the circuit in Fig. 2.23. It is important to note that due to the asymmetry of the design and its compactness, the phase response needs to be corrected so that the phase shifts, as described in Table 2.5, are achieved at the internal ports. Basically, in this simulation an ideal phase shift of -30° was defined (to represent any external mechanical phase shifter). It is important to note that the magnitude imbalances are ±0.5 dB at about 1.35 GHz while phase differences are near 0, ±90°, or ±180°.

is acceptable for the LP states (see Figs. 2.29 and 2.30 as well as Table 2.7) and the optimized circuit-parts, as shown in Fig. 2.28, which achieved the required wideband performance within the commercial simulator. Moreover, it was not possible to achieve the required phase for all the possible polarization states and over the frequency range from 1.1 GHz to 1.7 GHz. From these studies it is likely that the LP states will have more narrow band performance when compared to the LHCP or RHCP states in practice. Mainly because the noted phase offsets of -30° for LP1 and -210° for LP2 can be difficult to achieve with an external phase shifter and power divider combination whilst over the required frequency range to enable broadband LP operation.

The simulated losses for these LP states is about the mean for the RHCP and the LHCP states (see Fig. 2.29 and Table 2.7). For example, the simulated efficiency of the DRCS considering LP operation is slightly lower than the RHCP state with values ranging from 72 % to 81 % for the various PCB loss cases as outlined in Table 2.7. Regardless of these results, simulations suggest that the LP states can be made possible.

2.7.6 DRCS Structure Considerations & Simulations

It should be noted that the DRCS was originally designed considering ε_r = 30 for the DR element as in [58]. However, after further experimental study and by following [51], the relative dielectric for the DR was defined as 27 for the full-wave simulations (in

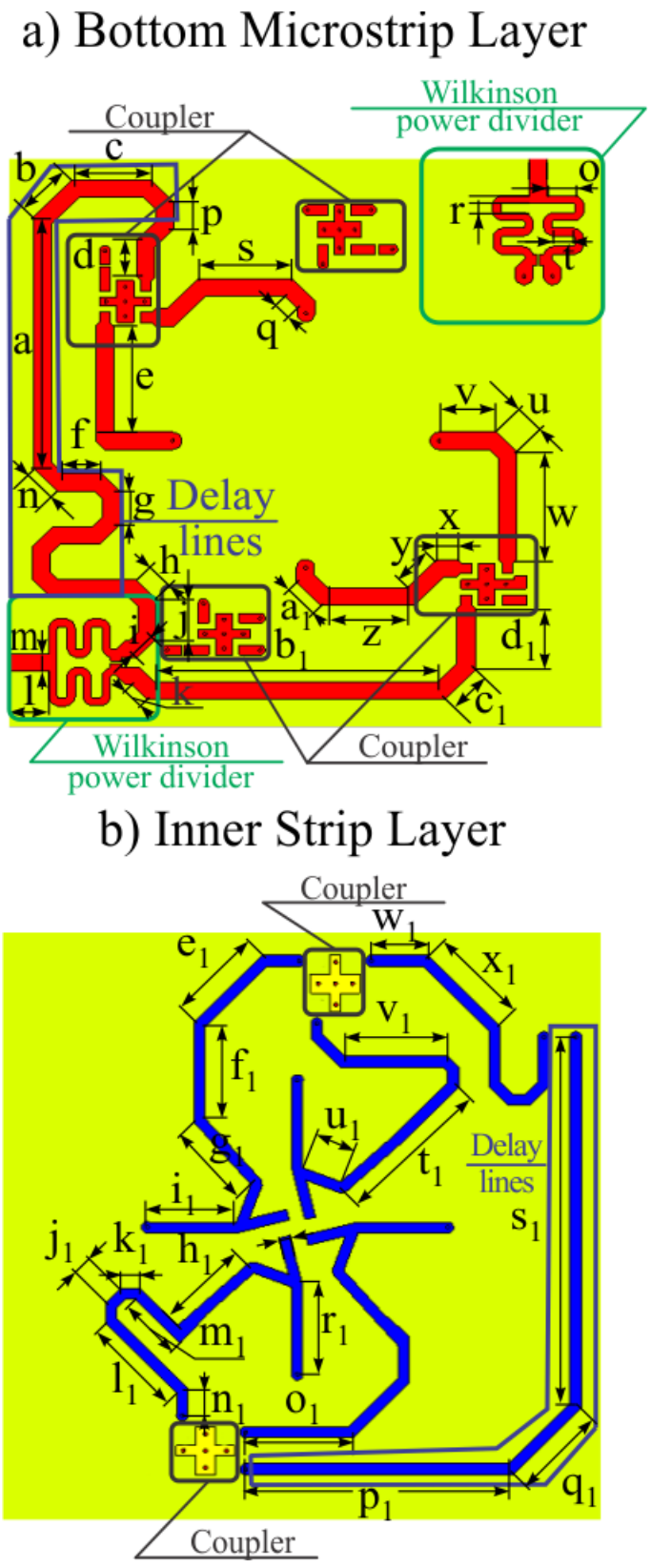

Figure 2.28: Final layout of the feeding circuit (relevant dimensions in Table 2.6). (a): The bottom 31 mil thick FR-4 layer and where the top-face of the microstrip lines are shown. (b): The middle strip trace layer. This layout defines the inner layer which employs microstrip covered by 31 mil thick FR-4; i.e. a strip layer.

Table 2.6: DRCS feeding circuit dimensions as Illustrated in Fig. 2.28
(all values in millimeters)

a	**b**	**c**	**d**	**e**	**f**	**g**	**h**	**i**
39.5	8.2	11.8	5.8	16.7	5.5	5.1	4.3	4
j	**k**	**l**	**m**	**n**	**o**	**p**	**q**	**r**
6.2	2	6.2	2.7	5	3.9	4.0	2.6	1.4
s	**t**	**u**	**v**	**w**	**x**	**y**	**z**	$\mathbf{a}_1$
14	2.8	4.2	8.6	17	3.1	6.2	12	4.9
$\mathbf{b}_1$	$\mathbf{c}_1$	$\mathbf{d}_1$	$\mathbf{e}_1$	$\mathbf{f}_1$	$\mathbf{g}_1$	$\mathbf{h}_1$	$\mathbf{i}_1$	$\mathbf{j}_1$
42.6	9.7	9.7	12.9	12.4	12.9	12.7	11.6	2.8
$\mathbf{k}_1$	$\mathbf{l}_1$	$\mathbf{m}_1$	$\mathbf{n}_1$	$\mathbf{o}_1$	$\mathbf{p}_1$	$\mathbf{q}_1$	$\mathbf{r}_1$	$\mathbf{s}_1$
2.6	13.4	8.3	3.5	14.2	35	12.7	11.7	50.3
$\mathbf{t}_1$	$\mathbf{u}_1$	$\mathbf{v}_1$	$\mathbf{w}_1$	$\mathbf{x}_1$				
20.7	5.4	13.5	7.3	13.7				

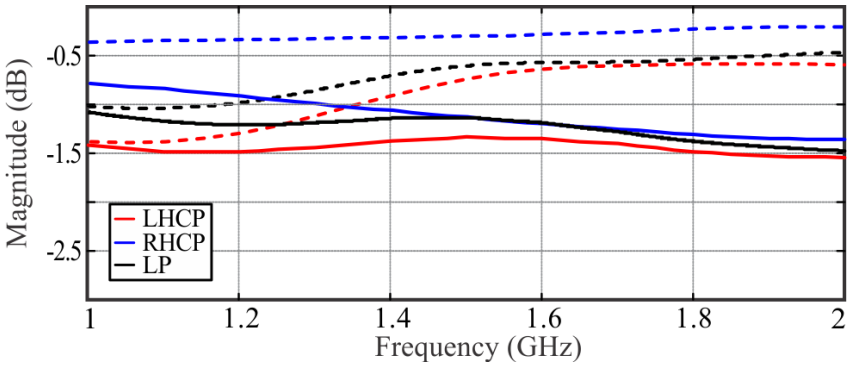

Figure 2.29: Simulated losses for the feeding network without the DR element (see Fig. 2.23). Dashed lines considers no PCB dielectric losses; i.e. $\tan\delta = 0$ while the solid lines defines the employed FR-4 material ($\tan\delta = 0.02$). It can be observed that the LHCP circuit-part has increased losses when compared to both the RHCP and LP states. Note: both LP states offer consistent losses.

Table 2.7: Simulated PCB Feeding Circuit Performance & DRCS Efficiency (see Fig. 2.30) Considering Different Values for $\tan\delta$

	RHCP State		LHCP State		LP States	
PCB $\tan\delta$	Maximum Feed Circuit Imbalance	Peak DRCS Efficiency	Maximum Feed Circuit Imbalance	Peak DRCS Efficiency	Maximum Feed Circuit Imbalance	Peak DRCS Efficiency
0.000 (ideal)	0.48 dB	83 %	0.50 dB	80 %	1.10 dB	81 %
0.002	0.52 dB	82 %	0.51 dB	79 %	1.50 dB	80 %
0.020 (FR-4)	0.78 dB	74 %	0.62 dB	68 %	2.00 dB	72 %

Figs. 2.22 and 2.30), rather than 30, the nominal value reported by the manufacturer on the material data sheet. This is related to the given rated variance specification for the dielectric material, $\varepsilon_r = 30 \pm 10$ % (Eccostock HiK500F). Given these findings, all simulations results provided in this paper are those for a dielectric resonator with $\varepsilon_r = 27$, and not 30, providing a valid comparison with any measurements.

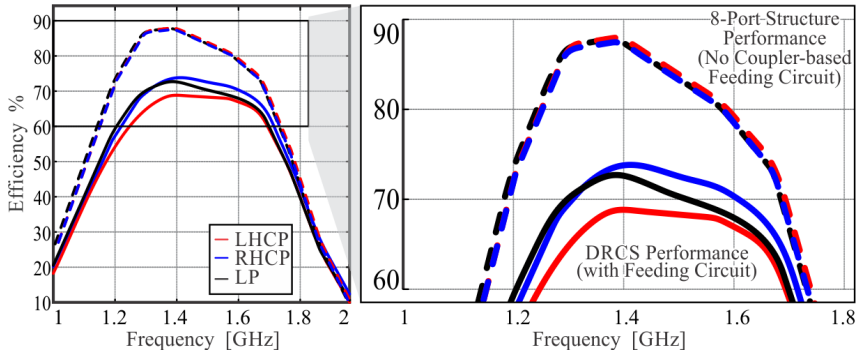

Figure 2.30: Simulated efficiency for the DRCS without (see Fig. 2.22) and with the feeding circuit system. Values are 65 % or more from 1.25 GHz to 1.70 GHz considering the employed FR-4 substrate defined by $\tan\delta = 0.02$. Improved efficiency is possible with PCB substrates having reduced dielectric losses (see Table 2.7).

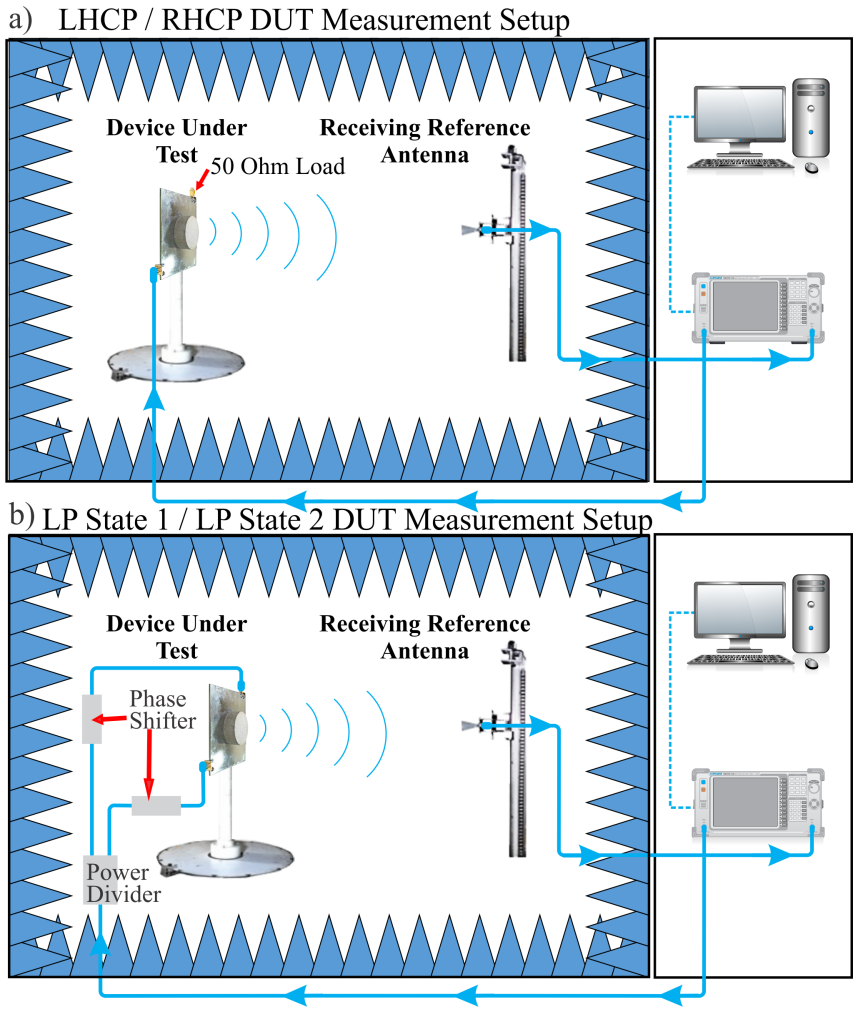

Figure 2.31: The far-field measurement setup: a) one-port configuration for CP and b) two-port for LP. For the CP states, one of the ports was terminated with a 50-Ω load as shown in Fig. 2.21. An external power divider and mechanical phase shifters were used to excite both ports for the LP states (see Fig. 2.21). It should be highlighted that two equivalent phase shifters were employed in the LP measurements and that the relative phase differences were defined as required; i.e. -30° and -210° for LP state 1 and LP state 2, respectively.

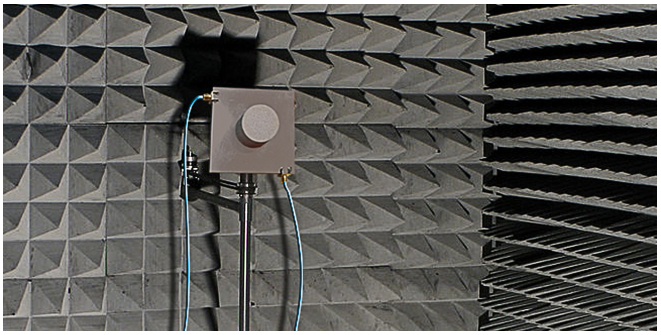

Figure 2.32: Photo of the DUT for far-field characterization: DRCS defined by a top cylindrical DR element and its integrated PCB feed circuit.

2.7.7 Results & Discussion

The proposed DRCS (see Figs. 2.19 and 2.20) was fabricated and then measured using the anechoic chamber facilities at The Royal Military College of Canada. The DRCS measurement setup can be better understood in Fig. 2.31 while a photograph of this device under test (DUT) positioned within the anechoic chamber can be observed in Fig. 2.32. The DRCS was measured in transmit mode where the reference horn antenna was used as the receiver (see Fig. 2.31). The measurements were completed from 1 GHz to 2 GHz with steps of 8 MHz. As discussed previously, to measure the DRCS response when considering CP operation, one of the ports was terminated with a 50-Ω load (see Fig. 2.21). For both LP cases, external phase shifters (mechanical) were employed as well as a power divider. The resulting far-field beam patterns, realized gains, axial ratios, and port matching values are reported in Figs. 2.33 to 2.37. The minimum and maximum ripples in the beam patterns are most likely related to the raw highly sampled measurements and overall measurement tolerances such as some minor misalignment and unwanted phase noise in the samples due to possible cable bending and twisting.

Referring to Fig. 2.33(a), the LHCP port of the DRCS, has a measured -10 dB reflection coefficient bandwidth from 1.11 GHz to above 1.90 GHz. The peak gain is 0.0 dBic with a 3 dB bandwidth from 1.25 GHz to 1.62 GHz. On the other hand, it can be observed that the RHCP port of the measured DRCS, was matched with a -10 dB impedance reflection coefficient bandwidth of 41 % from 1.25 GHz to 1.90 GHz (although $|S_{22}|$ does rise above -10 dB slightly at 1.35 GHz). Additionally, the peak gain of the DRCS is 1.20 dBic occurring at 1.35 GHz, with a 3 dB bandwidth from 1.25 GHz to 1.83 GHz. The reduced realized gain for the LHCP state is expected and inline with the full-wave simulations since the DRCS efficiency is less than 70 % (see Fig. 2.30). On the other hand, efficiency

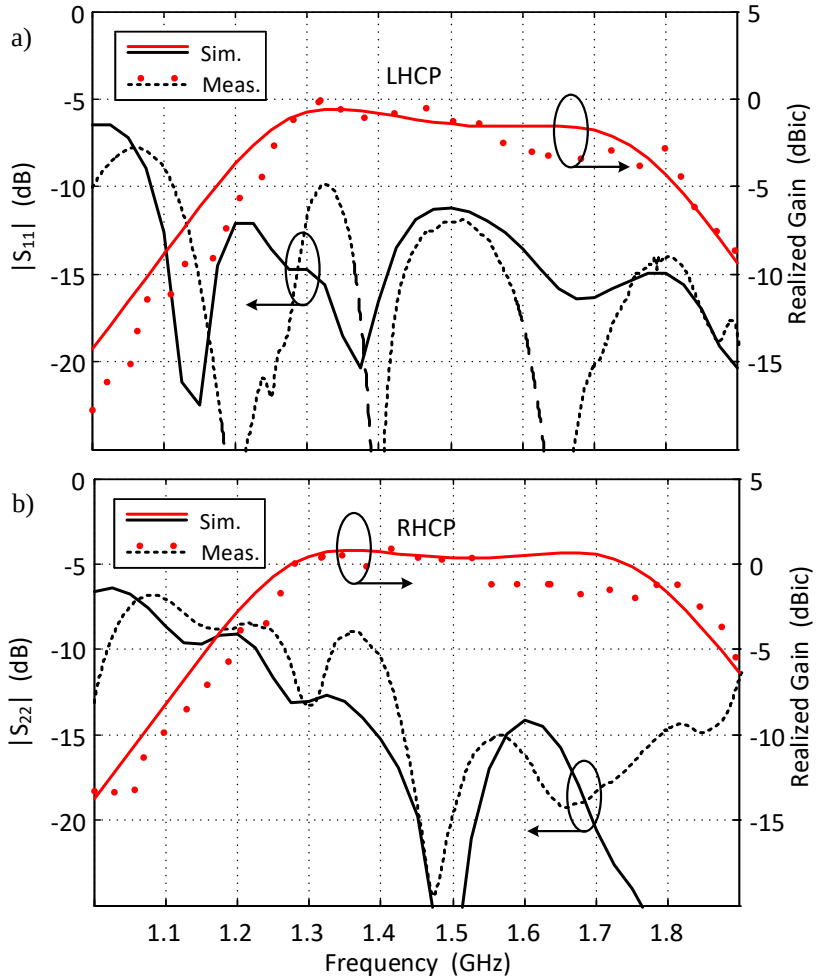

Figure 2.33: (a) Simulated and measured LHCP gain and reflection coefficient. (b) Simulated (solid) and measured (dashed/dotted) reflection coefficient and realized RHCP gain at broadside versus frequency.

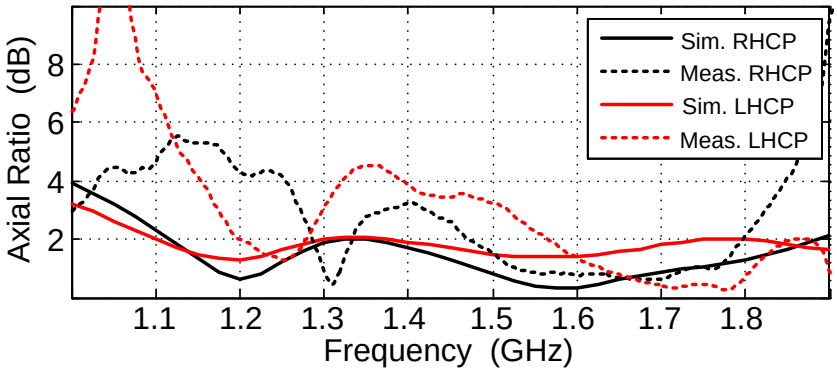

Figure 2.34: Simulated (solid) and measured (dashed) axial ratios at broadside for the LHCP (red) and RHCP (black) states as compared to frequency.

values are above 70 % from 1.3 GHz to 1.6 GHz for the RHCP state. Improved realized gain values are expected for a PCB substrate with less loss than FR-4 (see Figs. 2.29 and 2.30 as well as Table 2.7).

Referring to the axial ratio results in Fig. 2.34, simulation results are well below 3

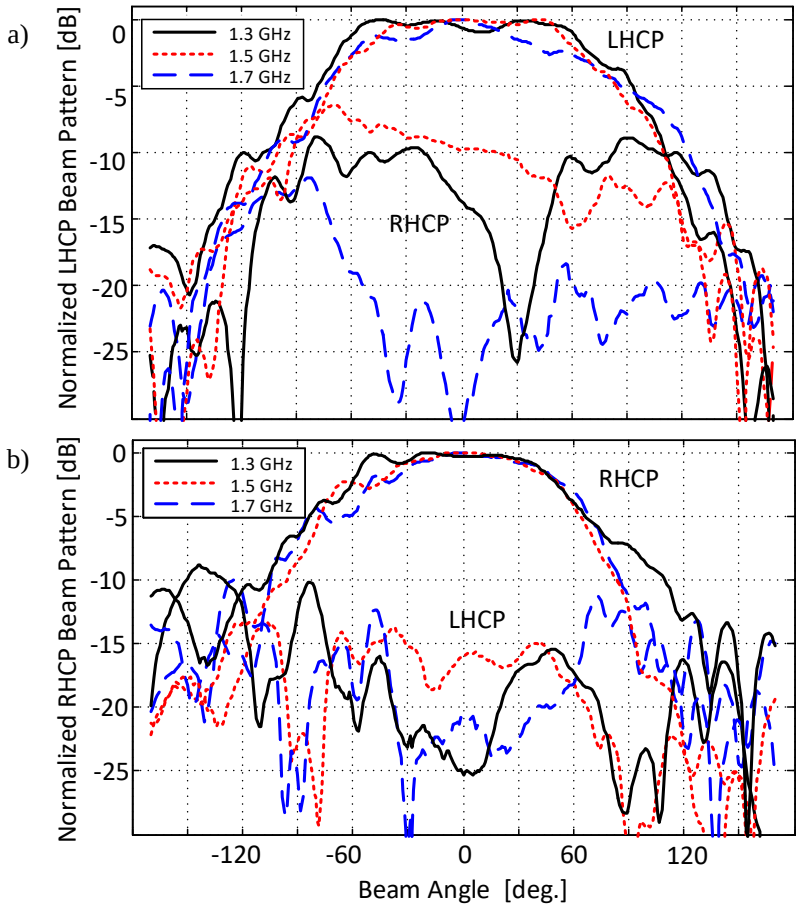

Figure 2.35: Measured LHCP and RHCP beam patterns in the $\phi = 0^\circ$ plane. Normalized patterns are shown at 1.3 GHz, 1.5 GHz, and 1.7 GHz (similar patterns were observed over the operating band of the DRCS).

dB over the entire operating band of the DRCS. For the measurements, axial ratio values are about 4 dB or below. This minor discrepancy can be related to some fabrication and assembly tolerances in that the DR element was likely not perfectly positioned on top of the four ACSs.

The RHCP and LHCP radiation patterns were measured and are reported in Fig. 2.35. It can be observed that when excited for RHCP radiation, the DRCS offers a 3 dB beam width greater than 120° in the elevation plane, and a cross-polarization level of -13 dB (at worst) below the co-polarized values at broadside. When excited for LHCP operation, the 3 dB angular beam width is similar to the RHCP case.

As mentioned previously, in addition to RHCP and LHCP, the 2-port DRCS is capable of generating two orthogonal LP states (see Fig. 2.21). This is achieved through simultaneous excitation of both the RHCP and LHCP ports. Results for these LP states were also measured and the resulting gain is presented as a function of frequency in Fig. 2.36 while the normalized beam patterns are reported in Fig. 2.37.

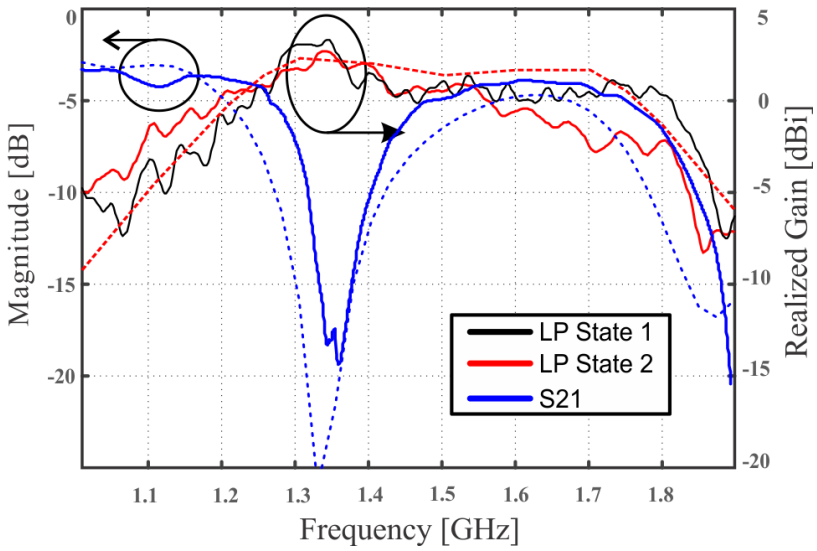

Figure 2.36: Measured (solid lines) and simulated (dash lines) LP gains versus frequency for both states. Calibrated phase offsets defined at 1.35 GHz, which provided the needed -30° and -210° phase offset at the ports, were achieved using a tunable mechanical phase shifter. It can be observed that when the (passive) port coupling $|S_{21}|$ is minimized, the realized LP gain increases.

Comparing Figs. 2.33 and 2.36, it can be observed that the LP peak gains are higher than those of both the RHCP and LHCP cases (as also reported in Fig. 2.22). This is because, during LP operation, the power from both ports is combined (see Fig. 2.21(c) and (d)), resulting in an overall higher realized gain. Similar results were observed for the full-wave simulations in Fig. 2.22. Additionally, note that the gain profile versus frequency for the studied LP case in Fig. 2.36 has more variation over frequency than those for the CP cases reported in Fig. 2.33. This is attributed to several factors including phase mismatches between the RHCP and the LHCP ports. This was because the required phase offset was provided through an external and tunable phase shifter (which does have some frequency dependance), and, unequal amplitudes at the LHCP and RHCP ports (caused by the practically realized and non-symmetric feed system). These factors likely caused different signal amplitudes and minor phase offsets for the two main signal paths.

When considering possible real-life applications for the reported L-band DRCS, such as GNSS/GPS systems, the cross-coupling between the LHCP and RHCP ports is not much of a concern. This is because it can be expected that the same signal will be received at the two ports from the far-field (albeit at different power levels). Also, the polarization of the incoming signal might be elliptical. This would realize an unequal power split ratio onto the antenna, of the same far-field signal, for collection at the external ports. This makes the coupled signal (between ports) of little significance. However, in the case of

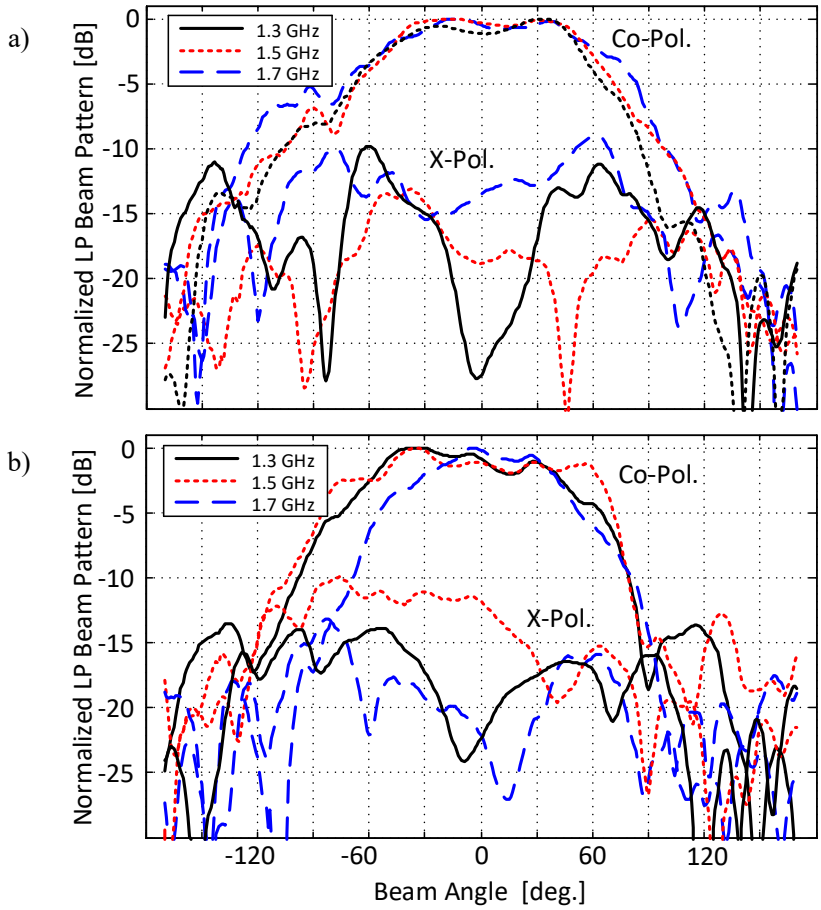

Figure 2.37: Measured LP beam patterns generated by excitation of both DRCS ports (see Fig. 2.21): a) LP state 1 and b) LP state 2. Normalized patterns are shown at 1.3 GHz, 1.5 GHz, and 1.7 GHz. It should be mentioned that the required phase shifts were achieved using a calibrated phase shifter at these three frequencies.

other RF systems with two different incoming signals onto the antenna, and with different polarizations, the circuit coupling within the DRCS should be taken into account. This can possibly be accommodated by introducing some type of filtering within the feed system, or, by applying some other signal processing techniques. These approaches could help to mitigate any unwanted cross-talk.

Studying the beam patterns in Fig. 2.37 it can be observed that both LP antenna states have a -3 dB beam width of approximately 120°. Furthermore, the cross-polarization levels for the LP states were measured to be (at most) less than 12 dB below the co-polarization levels at broadside, and as low as -27 dB depending on the observed frequency.

2.7.8 Conclusions and Achievements

In this chapter a single dielectric resonator (DR) and feeding circuit system (CS); i.e. a DRCS were presented. This antenna structure is capable of right-handed circular polar-

ization (RHCP), left-handed circular polarization (LHCP), and two orthogonal linearly polarized operating states. The two ports of the DRCS were measured to have -10 dB impedance reflection coefficient bandwidths of 41 % and 53 %, which are representative of the RHCP and LHCP antenna operational states, respectively. Additionally, the DRCS was measured and offers peaks gains of 1.2 dBic, 0.0 dBic, 3.6 dBi, and 2.6 dBi for RHCP, LHCP, and both linear polarization (LP) orientations, respectively. Furthermore, all CP and LP states were found to have a beamwidth greater than 120° in the elevation plane and cross-polarization levels are typically in excess of -10 dB.

Improvements which could be made to the DRCS include a modified feeding circuit considering a dielectric substrate with reduced losses when compared to FR-4. This would improve DRCS realized gain values and efficiency. In addition, a modified feeding circuit that includes both the additional transmission line lengths of -210° or -30° could be designed to achieve both, LP and CP radiation, and thus not requiring an external combiner/divider and phase shifter as in the LP case. However, this would require additional delay lines and printed circuit parts which could increase the physical size of the network and thus the entire antenna system. Furthermore, additional feeding circuit losses would be observed due to the added transmission line lengths to achieve such dual-CP and dual-LP operation. To avoid this problem a dielectric substrate with lower loss could be employed; i.e. not FR-4 as mentioned previously. However, in some cases, only dual-CP operation (and not both dual-CP and dual-LP) might be the main design motivation for the compact DRCS, in that both LHCP and RHCP using two distinct ports is of main interest, as demonstrated in this work.

Overall this DRCS functionality has been made possible by a compact wideband antenna structure and a low-cost feeding circuit implementation for dual-CP. External phase shifters were employed to demonstrate dual-LP operation as well, and in the main effort to circumvent the aforementioned losses in the FR-4 feeding circuit.

2.8 Full-duplex, Compatability of the Polarization Diverse Antennas for In-band Full-duplex Systems

Another main recent focus of the antennas and propagation society, is In-band Full-duplex systems, also known as simultaneous transmit and receive (STAR). Those systems can double spectrum efficiency and reduce the congested frequency spectrum of wireless systems. Such systems have increased requirements for isolation and antenna systems

requiring two orthogonal polarizations. Typically the minimum isolation needs to be around 100 to 110 dB for the combined analogue, digital and antenna cancellation systems [62]. Thus appropriate levels for antennas are typically in the range of 30 to 40 dB as the minimum would be sufficient.

Thus, it is possible to use in some cases the proposed DRAs in this chapter, however, additional constraints and further isolation requirements for analogue and digital cancellations would be needed. This increases the cost of the systems and increases the constraints of the analogue and digital cancellation network. Moreover, the beam-steering would be a great addition to Full-duplex systems which is not possible with the reported single-element resonator antennas.

2.9 Chapter Summary

In this chapter, the achieved multiple polarization states and multi-port antenna configurations can indeed support FD systems. However, those DRAs have a significant drawback when it comes to isolation levels. The inter-port coupling between polarization states is at best below -20 dB making it not suitable and challenging to integrate into Full-duplex communication systems. Such as the required level of isolation needs to be increased at least to 30-40 dB with high as possible bandwidth. Additionally, the beam-steering approach could be challenging to integrate into those DRAs however, the use of different frequency bands for STAR is another possible line of research.

Thus different antenna solutions were explored. Therefore, in the next chapters, this thesis further investigates the types of FD systems with a motivation to improve isolation levels, increase bandwidth, and offer beam-steering functionality using arrays.

Chapter 3

H-shaped Slot Antennas for In-band Full-duplex Systems

3.1 Introduction

In this chapter, Full-duplex antennas will be investigated and new solutions for in-band Full-duplex systems will be proposed. The first part will be focused on the existing antenna approaches using coupler-based solutions and how isolation can be enhanced by employing differential-based feeding. Some important antenna technologies such as slot and H-shaped slots will also be investigated and antenna array configuration analyzed.

Afterward, the new external feeding H-shaped slot antenna system for S-band in-band Full-duplex is proposed. An additional effort was done to design a new slot-line coupler with a highly stable phase-response to improve isolation levels. While the antenna achieves high isolation levels, the connections need to be co-located at times and ideally designed within a single PCB. This can make system integration challenging as a chain of connections is typically required, making the system bulky. Because of these challenges, conventional solutions employ external feeding systems as the first step.

To improve and simplify the required antenna feeding, a new dual-differential H-shaped antenna for IBFD applications with a fully integrated feeding system was designed. The isolation level was slightly lower but offered a simple two-port approach for transmitting and receiving making the system significantly more compact. Additionally, the antenna arrays used external feeding (2×2) and internal feeding (4×1) were proposed with options for beam-steering configurations. The antenna arrays were analyzed and a 4×1 antenna array was manufactured. Finally, the conclusions and achievements for those Full-duplex antennas are discussed in detail.

3.2 Duplex Classification

In order to understand the problem of FD systems, it is necessary to review the existing data receptions and transmission schemes. When transmitting data or some other relevant information between two connected devices over a network, the antenna, supporting

RF hardware, and digital backbone; i.e. the system can be considered in transmission mode [63]. This transmission mode indicates the direction of signal flow between two connected devices. Currently, there are three categories of transmission modes [64], [65]:

- Simplex
- Half-Duplex (two-frequency simplex)
- Full-Duplex

In simplex communications, the signal is transmitted in one way only and within the same communication channel. The transmitter turns on when transmitting and turns off when receiving. Most Very High Frequency (VHF) and Single Side Band (SSB) radio stations operate in simplex mode. Similarly, in television and radio broadcasting, information flows only from the site of the transmitter to several receivers. The transmission medium (radio signal over the air) can carry information in only one direction. More modern communications systems generally require two-way data exchange, but simplex is a one-way exchange, so there is no communication of data between devices.

In Half-Duplex mode, each device can transmit and receive data. A message flow can go in both directions, but not simultaneously. All communication channel bandwidth is used in one direction at a time. In this mode, the sender sends the data and waits for their confirmation, and if there is any error, the recipient may require him to re-transmit this data. Because of this, any possible error detection is possible. An example of a half-duplex mode could be a walkie-talkie. In the walkie-talkie, on the one hand, an operator speaks into the microphone of the device, and on the other, someone is listening. After a pause, another speaks and the first person listens. The disadvantage of this approach is the delay in sending data at the same time because when one device sends data, the other must wait for the data to be sent.

In FD mode, communication is bi-directional, which means that the data flow goes in both directions at the same time. From both ends, data reception and transmission are possible simultaneously. FD mode has two physically separate transmission paths, one of which is designed for traffic in one direction and the other for traffic in the opposite direction. This is one of the fastest ways to communicate between devices.

3.3 Full-Duplex Classification

One of the difficulties in FD systems is the separation of channels for receiving and transmitting data. Currently, there are three types of FD systems:

- Frequency Division Duplex (FDD) [66]
- Time Division Duplex (TDD) [67]
- In Band Full-Duplex (IBFD) [68]

Frequency Division Duplex (FDD) is the type of the communication where the transmitter and receiver operate at different carrier frequencies. The method is often used in simple radio transmitters, where the operator tries to use a repeater station [69]. A relay station must be able to transmit and receive at the same time, and does so by slightly changing the frequency at which it sends and receives; i.e. the up-link and down-link frequencies. The advantage of frequency division duplex is that it makes radio planning easier and more efficient since the base stations do not interfere between each other (because they transmit and receive in different sub-bands).

Time Division Duplex (TDD) is a time division multiplexing application to separate outward and returned signals. It emulates FD half- line duplex communication [70]. Duplex time division is flexible when asymmetries exist between the up-link and the down-link data rate. As the amount of up-link data increases, more communication capabilities can be dynamically distributed and as traffic load becomes easier, capacity can be taken away. The same applies in the down-link direction.

In Band Full-Duplex (IBFD) is the type of transmission where the transmitter and the receiver operate at the same frequency, and, at the same time, [14]. This solution is more attractive due to the same frequency reuse, but challenging for the transmitter and the receiver due to the bi-directional nature of the communications. Usually, this type of transmission scheme uses either different polarizations or circulators to avoid interference between the transmitted and the received signals.

3.4 Full-duplex Antennas

Full-duplex (FD) antennas are the type of antennas that accommodate two ports to transmit and receive, have high isolation, and can use two different polarization states. This could be using different frequencies (OBFD) or by using the same frequency (IBFD), but with isolation techniques applied. The main focus of this thesis is antennas with an In-band frequency approach. The problem of IBFD is the antenna self-interference (SI) where the signal strength of the transmitted signal interferes with the desired received signal. In particular, in IBFD systems, the transmitted signal is received with a very high

power level compared to the desired received signal power and suppresses the signal of interest at the receiver, thus making data reception very challenging.

When developing FD antennas it is important to take into account polarization control. Thus, polarization diversity antennas are another focus of this thesis in the previous chapter. These types of antennas are widely used in systems where stable communication could be challenging i.e in a challenging radio frequency (RF) environment. Thus, the antenna supports different polarizations and can be switched into the mode where the signal is less affected by the environment. Usually, such antennas required a multi-port configuration with additional phase control circuitry connected to them.

The main contribution of this thesis is to present new types of FD and polarization-diverse antennas. Such design approaches can be well adapted to the FD systems. The main advantage of those systems are:

1) The antenna can relax analogue and digital cancellation systems in the FD system. Thus, making wireless transfer cheaper and more available. 2) The reconfigurability and polarization diversity can be well used in the radar and RF challenges environment. 3) Potential applicability in the radar systems with beam-tracking as an option should it be needed.

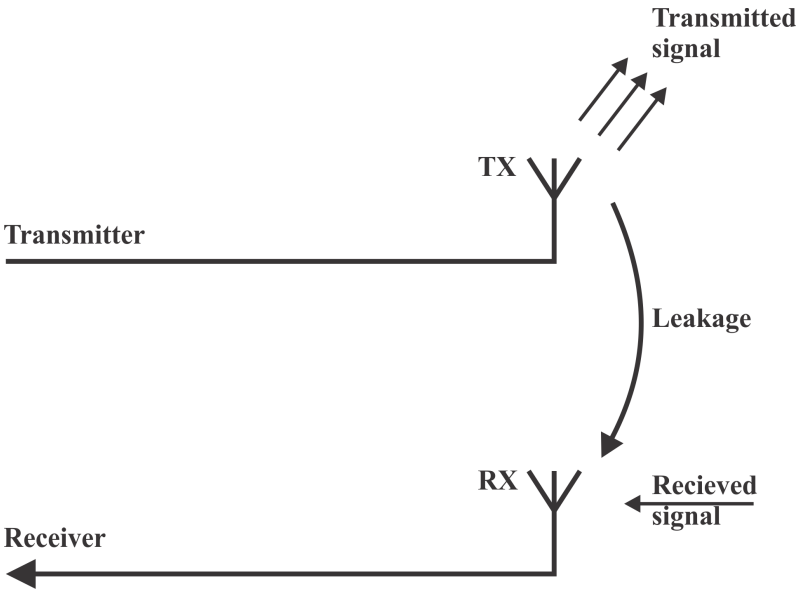

Figure 3.1: Self-inteference between transmitter and receiver.

3.5 Coupler Based Systems on Full-duplex

Some attractive solutions are antennas based on hybrid coupler systems. Recently, different structures have been reported which consist of hybrid couplers and one resonating patch antenna [71], [72]. These designs are based on a single- and double-differential signal shift, where the input signals applied to the couplers input port, provide a phase shift of 180° between ports 2 and 4, while port 3 is terminated by a 50-Ω load. With this feeding, SI is reduced and high isolation of 40 to 50 dB can be achieved. Moreover, due to the field cancellation effect, i.e signal difference in 180°, the cross-polarization due to the field cancellation effect can also be improved. However, the majority of the presented papers based on this technique have offered narrow bandwidths whilst the antenna presented in [73], which operated at 5 GHz, was able to provide a bandwidth of 22% achieving isolation levels of over 50 dB and only having one slot-line type hybrid coupler.

It should be noted that the dual-polarization control in [73] was achieved by a single-differential feeding approach. In this antenna array, port one of the coupler provided equal signal phase shift, and coupler port two provided the differential signal shift. Thus, when the equal phase shift occurred, the produced field configuration with the 0° shifts on the active transmitted ports, and a null in the cross-polarization can be observed. This possibly deteriorated the antenna performance when the second port of the coupler when the 0° signal split was used. Moreover, the -10 dB impedance bandwidth over frequency of ports one and two were not the same.

According to [71], the coupling reduction mechanism considering the various transmitted current signals with double-differential feeding for a 4-port system (see Fig. 3.2) can be described as [71]:

$$I_{Tx1} = \frac{I_{Tx}}{\sqrt{2}}$$

$$I_{Tx3} = \frac{I_{Tx}}{\sqrt{2}} e^{j180^\circ}$$

The total current I_{Rx} using differential ports will be as in [71]:

$$I_{Rx} = \frac{1}{\sqrt{2}} (I_{Rx2} + e^{j180^\circ} I_{Rx4})$$

Which can be re-written to:

$$I_{Rx} = \frac{I_{Tx}}{\sqrt{2}}[(S_{21} - S_{23}) - (S_{41} - S_{43})]$$

Which leads to:

$$\frac{I_{Tx}}{I_{Rx}} = \frac{2}{(S_{21} - S_{23}) - (S_{41} - S_{43})}$$

Which looking at the figure Fig. 3.2, the coupling between ports is S_{21}=S_{23}=S_{41}=S_{43} is similar. As described above, when the phase and amplitude for the differential case is ideal, the cancellation effect tends to be infinite. However, in real-life applications, this is not possible. The coupler stability will never be ideal, some small amount of power can leak into the signal paths reducing the isolation.

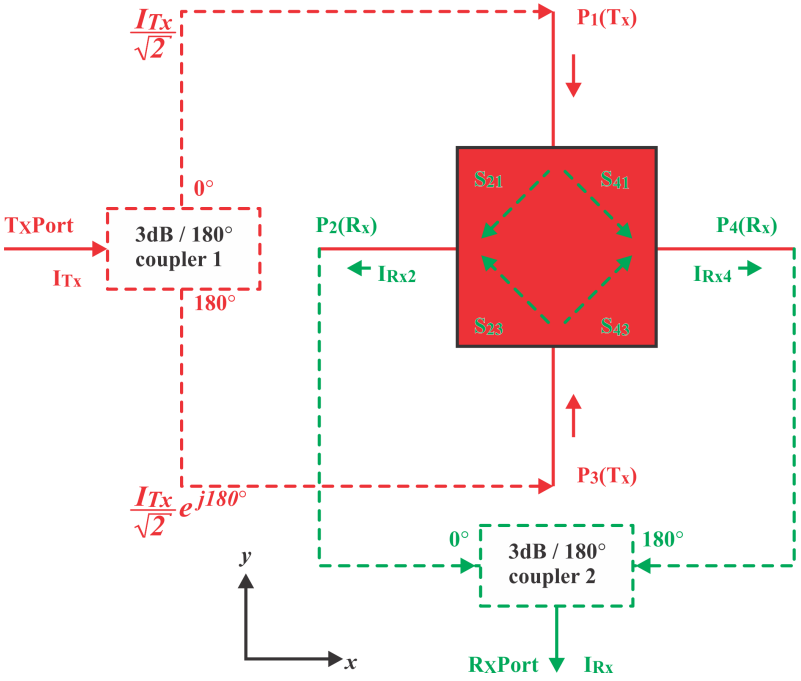

Figure 3.2: Equivalent circuit and signal path definitions for SI suppression based on the technique from [71] considering four excitation points of a rectangular patch. This configuration achieves dual-polarization linear. Concepts can also be applied to other symmetric antenna elements having four points of excitation.

As described above, the antenna design is important for isolation enhancement. Also, the antenna is required to offer two different polarizations and high port-to-port isolation. By achieving the highest possible isolation, some other isolation techniques such as digital or analogue can be relaxed. In particular, as outlined in [14] and [16], the primary goal of any IBFD communication system is that the required level of isolation needs to

be around 100 dB. Such isolation levels allow for the recovery of the signal without a reduction in the transmitted power. The secondary focus of that system is bandwidth. It should be noted that in-band or out-of-band antennas and H-shaped slots are relevant ideas that can be used to achieve new and novel antenna designs.

3.6 The Radiating Slot

An elementary slot antenna is a slot cut in a perfectly conducting flat screen of unlimited dimensions (see example in Fig 3.3). The slot cut in the wall of the waveguide is excited by currents flowing along its inner surface [22]. The distribution of the surface current is determined by the type of wave propagating in the waveguide, and the intensity of the slot excitation depends on the number of current lines crossing it. The greater the projection of the gap on the normal to the current lines and the greater its density, the stronger the gap is excited and the greater the field strength is radiated by it. The maximum current density is obtained on the narrow walls of the waveguide and the edges of its wide sides adjacent to them.

The slot antenna also follows Babinet's principle, which states that two complementary screens generate a similar diffraction pattern [74]. Following this, the structure of the slot antenna and the half-wave dipole structure cut out from the conducting sheet are operating in a similar fashion. Thus, the operating principle of slot antennas is very similar to the operation of $\lambda/2$ dipole antennas.

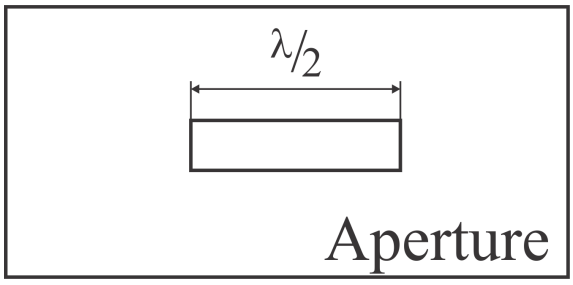

Figure 3.3: Representation of the ideal slot radiator on the metallic waveguide. Based on [22].

The length of the slot L_{slot} at an air-dielectric interface can be calculated using the following [22]:

$$L_{slot} = \frac{\lambda_0}{\sqrt{2(\varepsilon_r + 1)}} \tag{3.1}$$

where λ_0 is the free space wavelength, and ε_r is the permittivity of the dielectric.

From [74] using Babinet's principle and the intrinsic impedance of free space, the dominant field component (in the far-field) radiated by the slot antenna can be written as:

$$E_\phi = \frac{E_0 sin\theta}{\eta} \tag{3.2}$$

where η is the intrinsic impedance of free space and $E_0 \sin\theta$ the is the field component for dipole-like radiation.

Similarly, the impedance of the slot Z_s can be calculated using following [74]:

$$Z_s = \frac{\eta^2}{4Z_D} \tag{3.3}$$

where Z_D is the impedance of the dipole.

3.7 Slot Antennas

Slot antennas are understood to mean antennas whose radiation is associated with the radiation of electromagnetic waves from holes cut in metal screens [22], [65]. Typically a slot antenna, can be made in the form of a coaxial line [75], a cavity resonator [76], a flat metal sheet (screen), or in a conductive surface with cut holes (slots) [77]. These apertures serve to emit (or receive) radio waves. Radiation occurs as a result of the excitation of gaps: in a wave, resonator, and coaxial lines, in an internal electromagnetic field, in flat screens, by means of a radio frequency cable connected directly to the edges of the gap. Since the polarization of the radiation field coincides with the direction of the electric lines within such slot antennas, the horizontal gap will emit vertically polarized waves.

The radiation patterns of this antenna will approximately coincide with the patterns of its dipole counter-part, with the exception of the position in space of the field vectors $\vec{E}$ and $\vec{H}$, which, based on a slot implementation, will be interchanged. Slot length in terms of $\lambda/2$ determines the resonant frequency (see Fig. 3.3). To date, slot antennas are popular due to their simplicity, high gain, small side lobes, and possibly high radiation efficiency. These types of antennas are commonly used in radar applications such as passive electronic scanning arrays or ones with electronic phase shifters as illustrated in Fig. 3.5.

To improve radiation performance and provide polarization control, the conventional rectangular-shaped slot has been modified in the literature [78], [79], [80]. Some of the

most popular shapes are U-shaped, H-shaped and T-shaped. Depending on the feeding system, different slots begin to act as capacitors and inductors. Thus, the equivalent circuit elements can be determined, in which all real elements are replaced by their equivalent circuits such as capacitors or inductors.

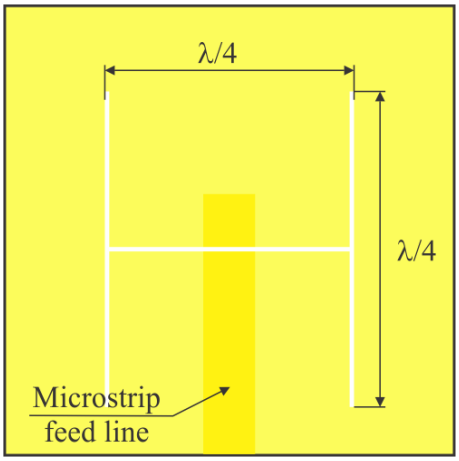

Figure 3.4: Example of the H-shaped slot placed on the substrate and excited using a 50-Ω microstrip line.

Nevertheless, when considering such planar-based slot antennas, size and practicality play an important role. One of the very first papers, see [81], mentions the design of H-shaped slots on PCB substrates using micrsotrip feed lines. In that work the authors conducted experiments using different types of slots and were able to derive formulas to calculate the input impedance for different shapes. The proposed structure showed that the $\lambda/2$ size slot can be modified into a combination of shapes with $\lambda/4$ sizes to present an H-shaped slot (see example in Fig. 3.4). This made it possible to reduce the length of the slot, improve the structure bandwidth whilst having good efficiency. To date, the H-shaped slot can be found in many various antennas implementations such as the: coaxial feed type H-shaped slot antenna in [82], and where a leaky-wave antenna based on H-shaped slots were studied.

3.8 Antenna Array Systems and Beam-Steering

An array is a type of antenna consisting of a set of individual antennas (radiating elements) [74] (see Fig. 3.5). The radiation pattern is formed as a result of the constructive interference of waves transmitted by those elements. If the elements are identical and equally oriented, then the total far-field pattern can be represented as the product of the

patterns of those elements and the array factor. The array factor is invariant on antenna type but is mainly related to the physical spacing between elements and the relative current (magnitude and phase) driving each element. Generally, the array factor (AF), can be described as in [74]:

$$AF = 1e^{j0} + 1e^{j\beta}e^{jkdcos\theta} + ... + 1e^{j(N-1)\beta}e^{j(N-1)kdcos\theta} \tag{3.4}$$

Where: N = Number of elements, k - wave number, θ - elevation angle, d - element spacing and β - phase excitation. As a result, the antenna parameters such as gain, beam directionality, or cross-polarization can be calculated theoretically and improved (in comparison to a single element). A fundamental feature of the antenna array is the ability to control its beam direction (beam steering) when changing the complex amplitudes and/or polarization of the waves radiated by the elements.

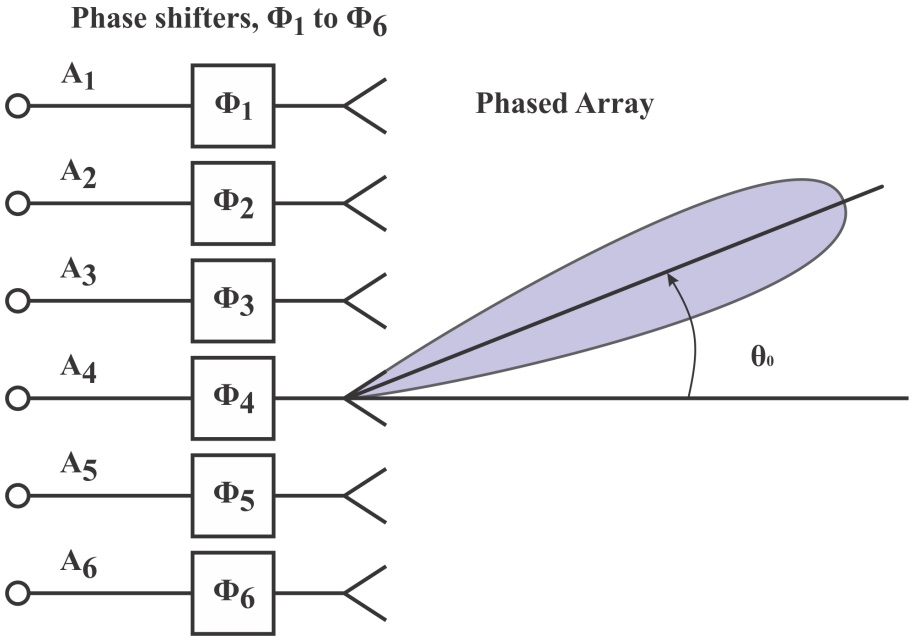

Figure 3.5: 6 element Antenna array structure with introduced beam steering. Based on [22].

Two main types of systems based on phased antenna arrays should be distinguished; i.e. passive and active antenna arrays [22]. The main difference is this. In passive antenna arrays there is a single transceiver, whose signal is divided into all channels, conditionally there is only one fixed phase shifting mechanism to control the beam. In active phased arrays, the channel of each element of the array has its own transceiver. Each of the concepts has its pros and cons: passive are much cheaper, but require the use of high powerful signal sources, which, in turn, require a complex power supply and cooling

circuit system. Active arrays have a huge margin of safety, for example, the failure of one transceiver does not lead to a breakdown of the entire system, but the number of components used and the complexity of control, and synchronization. In the end, the cost of the active devices for the system can exceed the cost of just the passive array.

The best way to analyze the antenna array in the commercial simulators is to apply consecutive phase shift, where the applied phase to the ports allows the beam direction to change (see Fig. 3.5). This phase difference can be calculated as in [74]:

$$\Delta\varphi = \frac{360^{\circ} d sin(\theta_0)}{\lambda}$$

Where: $\Delta\ \varphi$ - applied relative phase shift to the ports, d - elements spacing, θ_0 - main beam position in the far-field. It should be noted that the phase shift must be carefully tuned and ideally be simulated in the commercial full-wave simulations and prior to any measurements to ensure that the desired beam pattern is realized.

3.9 Literature Review of Existing Full-duplex Antennas

One of the earliest designs of an inter-port antenna with high isolation was a circular patch design in [83]. In that paper, two antenna designs were investigated. Both consisted of two H-shaped slots and circular shaped patches elevated above the ground plane. As a result, the antennas offered bandwidths of 8% with isolation values of only 31.3 dB. In that same work [83] the authors extended the system to four H-shaped slots and a feeding circuit consisting of two Wilkinson power dividers. Using this approach, the authors were able to improve the antenna bandwidth to 17% and the port-to-port isolation to 34 dB. The antenna gains reached 6.8 dBi with cross-polarization levels of 14 dB at the center frequency.

Another method to achieve high isolation between the transmitting and receiving ports is to design a Dual-Band (Out-of-Band) system. Antennas in such systems are less affected by SI due to having different transmitting and receiving frequencies. One such antenna was proposed in [84]. In that design the data was transmitted at a center frequency of 4.7 GHz and a received frequency of 6 GHz. The antenna consisted of coupled-resonators with a patch placed on top. The reported antenna -10 dB impedance bandwidth was about 5.5% with isolation values around 35 dB and a maximum gain of 6.7 dBi. The antenna was further expanded into a 2×2 array system which slightly re-

duced the isolation to 30 dB and increased the gain to a maximum of 12 dBi. In a similar fashion, the dual-polarized antenna reported in [85] utilized a four-port system to achieve dual-band operation at 1.8 GHz and 2.0 GHz for transmitting and receiving, respectively. The proposed antenna consisted of resonator-based filtering channels, slot lines, and a radiating patch. The reported gain was 7.2 dBi and the isolation was greater that 23 dB.

Following these recent developments, in-band full-duplex (IBFD) antennas are generally of greater interest than their dual-band counterparts, for reasons of their single frequency re-use and doubled spectral efficiency [14]. The main focus of recent research studies was to achieve wider bandwidths, high as possible inter-port isolation, and to operate using dual-polarization. Previous FD antennas, which operate over a wide frequency range, as proposed in the literature are generally complex, might require careful feed and design considerations, and possibly can be expensive to manufacture. One such antenna was proposed in [86]. The involved design consisted of four T-shape parasitic elements mounted on a metallic ground plane. However, the antenna provided an impressive bandwidth of 98% and operated at frequencies between 0.6 to 1.75 GHz with isolation values below 40 dB. Maximum realized gain for the receive and transmitting mode was approximately 7 dBi and 6 dBi, respectively, and with an omnidirectional-like radiation pattern. Similarly, a metallic-based, four-port antenna was reported in [87]. It provided an wider bandwidth of 108% and operated from 0.8 GHz to 2.7 GHz. The antenna design consisted of resonating metallic ring elements with dipole-like arms, producing a monopole-like radiation pattern. The reported maximum realized gain was 7 dBi with inter-port isolation values of 37 dB over the entire operating range.

These antennas are suitable for use in base station applications due to their wide operational bandwidth and their physical size. However, simpler and lower-cost solutions using printed circuit board (PCB) manufacturing techniques, for example, can be more attractive for use in more basic or low-power radio transmission links for day-to-day communication systems such as Wi-Fi.

Recently, different structures have been reported which consist of hybrid couplers and a single resonating patch antenna [72], [71]. These designs are based on a single- and double-differential signal shift, where a phase shift of 180° is achieved between two coupler ports while a third port is terminated by a 50-Ω load. With this feeding, SI is reduced and a high isolation of 40 to 50 dB can be achieved whilst the antenna system is matched. Moreover, due to the signal cancellation effect at the coupler, i.e. the 180° phase

shift, the antenna cross-polarization in the far-field is also improved. However, previous designs [71], [72] which have implemented this technique have offered narrow isolation bandwidths. On the other hand, the antenna presented in [73], which operated at 5 GHz, achieved isolation levels of over 50 dB with a bandwidth of about 9%. That antenna system [73] was implemented using only one slot-line type hybrid coupler supported by a network of power dividers making it a single-differential feeding approach. In that work, port one of the coupler provided an equal signal phase shift, while port two provided a differential shift. This possibly limited the antenna performance and increased the cross-polarization levels. Moreover, the -10 dB impedance bandwidth over frequency for ports 1 and 2 were not the same.

Another IBFD dual-CP antenna based on a sequential rotation array (SRA) and an additional phase compensation control circuit was proposed in [88]. The system consisted of four circularly polarized patches, two 180° hybrid couplers, and an additional circuit on the receiver port with an attenuator and phase shifter. The reported radiation bandwidth was 10% with a maximum realized gain of 10 dBic. In addition, the developed cancellation circuit on the receiver side, integrated on a separate board, compensated the phase instabilities of the cables and the hybrid coupler. This improved the isolation beyond 50 dB.

3.10 Dual-Polarized High-Isolation Antenna Design and Beam Steering Array Enabling Full-Duplex Communications for Operation Over a Wide Frequency Range

Following these developments as outlined in this thesis, a new and low-cost antenna and array are proposed in the following. These structures offer high inter-port isolation and this can be useful for future wireless networks and RF-IBFD systems. The design process is outlined in the following sections.

By the inclusion of simple antenna excitation approaches for improved bandwidths, double-differential feeding, and by adopting different isolation techniques not explored previously in the literature for FD antennas, the problem of SI can be further alleviated whilst offering an advancement from previous studies. For example, isolation values in excess of 60 dB are observed for a corresponding 10% impedance bandwidth for the developed antenna (see Fig. 3.31). To explore the design attributes and to report these findings, a few prototypes are simulated and measured. In addition, a new and compact

slot-line coupler with high phase and magnitude stability is also developed (see Section 3.8.3) for improved IBFD antenna and system performances.

3.10.1 Antenna Design, Simulations, and General Considerations for the Single-element

The proposed IBFD antenna consists of four H-shaped slots connected to 50-Ω microstrip lines and two parasitic patch antennas placed on top of the slot arrangement (see Figs. 4.2 and 3.6(a)) for improved bandwidth. Initially two Rat-Race couplers, as in Fig. 3.6(b), were included for the simulated antenna feeding system and the elevated patches were positioned with no mechanical fixtures. Then foam spacers and nylon screws were included defining the first and second prototypes, respectively. The antenna design dimensions can be seen in Fig. 3.7 and Table 3.1 for the structure using foam with simulations and measurements in Figs. 3.8 to 3.12. A photo of the second prototype using nylon screws is also shown in Fig. 3.13. Both the foam spacer and the nylon screw-based designs are compared to understand the benefits of the different structures as well as to outline the design evolution to a final single-element which can offer significantly better IBFD antenna operation when compared to other structures as found in the literature. See Tables 3.2 and 3.3 where results are compared in terms of bandwidth, isolation, cross-polarization levels, and manufacturing simplicity.

To reduce leakage effects and improve the isolation, the H-shaped slots in both designs were surrounded by a network of metalized vias (see Fig. 3.13) with a diameter and periodicity of 2 mm and 3.3 mm, respectively. The antenna PCB design design material was FR-4 (see Fig. 4.2, for stacked patch # 1 and # 2) with a relative permittivity of 4.6 and thickness of 1.6 mm. The H-shaped slots serve as an excitation mechanism for the top radiating patches [89] with square dimensions of 48.3 mm for the bottom patch and 42.5 mm for the top patch. This multilayer configuration can increase the bandwidth of the antenna system. The overall dimensions of the system are 150 mm by 150 mm (which corresponds to $1.13\lambda_0$ by $1.13\lambda_0$ at the lowest operating frequency of 2.25 GHz, where λ_0 is the free-space wavelength). The choice of the relatively large ground plane size increases the antenna gain whilst reducing the sidelobe levels (SLLs) caused by any parasitic radiation from the the H-shaped slots.

Table 3.1: Antenna dimensions as outlined in Fig. 4.2 (all values in millimeters)

a	*b*	*c*	*d*	*e*	*f*	*g*	*h*	*i*	*j*	*k*	*l*	*m*	*n*	*o*	*p*	*q*
16	2	19	1.3	4.3	0.2	14.6	150	42.5	51.7	150	58.3	33.3	14.6	3.1	4.2	9.4

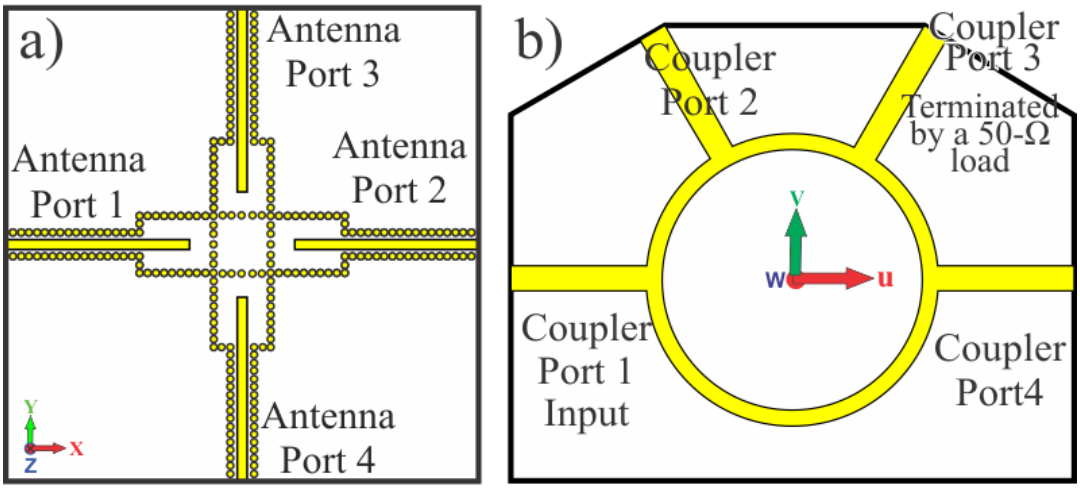

Figure 3.6: Bottom view of the feed system and coupler layout. a) Bottom view: 50-Ω microstrip lines are printed on the bottom to feed the H-shaped slots which are isolated using vias. b) Rat-Race coupler: Coupler Port 1 is the input port to the antenna and feeding network and system, Coupler Ports 2 and 4 are connected using external cables to Antenna Ports 1 and 2 to provide a 180° phase shift; i.e. differential feeding while Coupler Port 3 is terminated with a 50-Ω load. A second coupler and analogous connections are required for Antenna Ports 3 and 4.

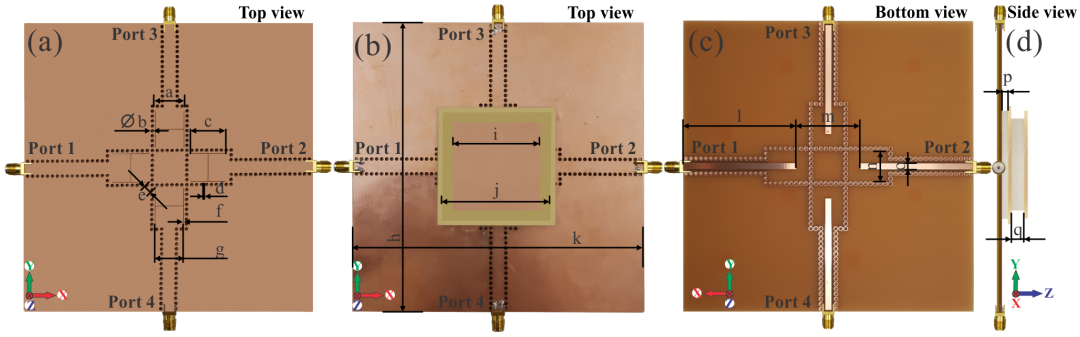

Figure 3.7: Fabricated antenna design considering foam spacers (see dimensions in Table 3.1): (a) top view: four H-shaped slots with embedded vias. (b) Top view: loaded parasitic patches on top of the four H-shaped slots. (c) Bottom view: four 50 Ω lines with connectors. (d) Side view: two parasitic patches and the foam placed in between.

As a first step in the feeding system design a basic microstrip-based hybrid coupler was employed (see Fig. 3.6). This enables double-differential external feeding making the feeding network for the single-element consist of two simple Rat-Race couplers. These couplers were designed and manufactured using a Taconic TLY-5A substrate which has a relative permittivity of approximately 2.2 and a thickness of 1.6 mm. With this external feeding approach, the two driven Antenna Ports (1 and 2, or 3 and 4, see Figs. 4.2 and 3.6) will have a 180° phase shift. This antenna and feed configuration can provide two orthogonal linear polarizations with a main beam radiating at broadside. For example, by driving Antenna Ports 1 and 2, the generated far-fields in the *x*-*z* plane will be

linearly polarized. Similarly, by exciting antenna ports 3 and 4, the dominant fields in the *y-z* plane will also be linearly polarized. Moreover, when the two couplers have perfect phase balance and the same amplitude; i.e. minimal magnitude imbalance, the inter-port leakage of the transmitted and the received signal can be minimized.

The antenna and hybrid couplers were designed and simulated in the commercial full-wave simulator CST microwave studio. Since the antenna ports will be driven simultaneously, the proposed structure was initially optimized and analyzed using active F-parameters (i.e active S-parameters), with the applied 0° and 180° shifts and without the external hybrid coupler system. Simulations suggest that the antenna is well matched between about 2.2 GHz to 2.46 GHz where the reflection coefficient is below -10 dB. Also, the corresponding port isolation is below 60 dB in this frequency range (see Fig. 3.8). This defines an operating bandwidth of about 10%. The simulated maximum realized gain can be observed at 2.3 GHz in Fig. 3.8 with a value of 7.8 dBi. Also, the antennas and couplers were simulated independently which allowed us to use the S-parameter combination tool in CST. Isolation values of more than 70 dB over the operating frequency range of the antenna and coupler system can be observed (see Fig. 3.9).

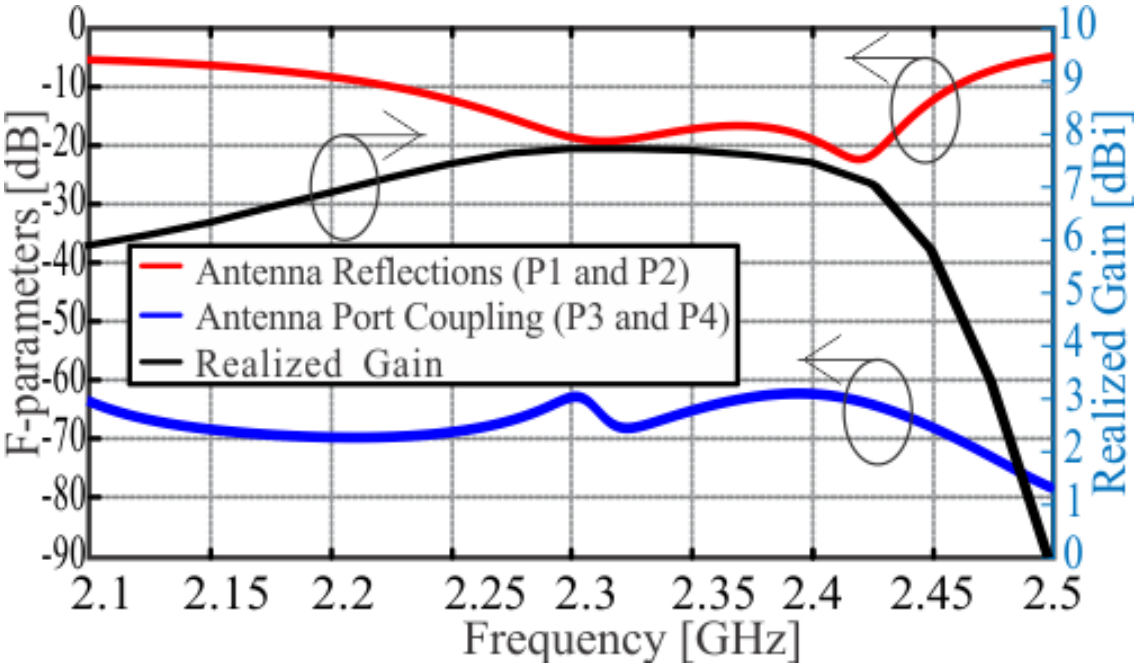

Figure 3.8: Simulated antenna F-parameters from CST considering 0° and 180° phase shifts applied to Antenna Ports 1 and 2, respectively (see Figs. 4.2 and 3.6). Similar results are observed when applying analogous feeding to Antenna Ports 3 and 4, but with an opposite polarization for the radiated far-fields. Realized gain values approach 8 dBi (see right axis).

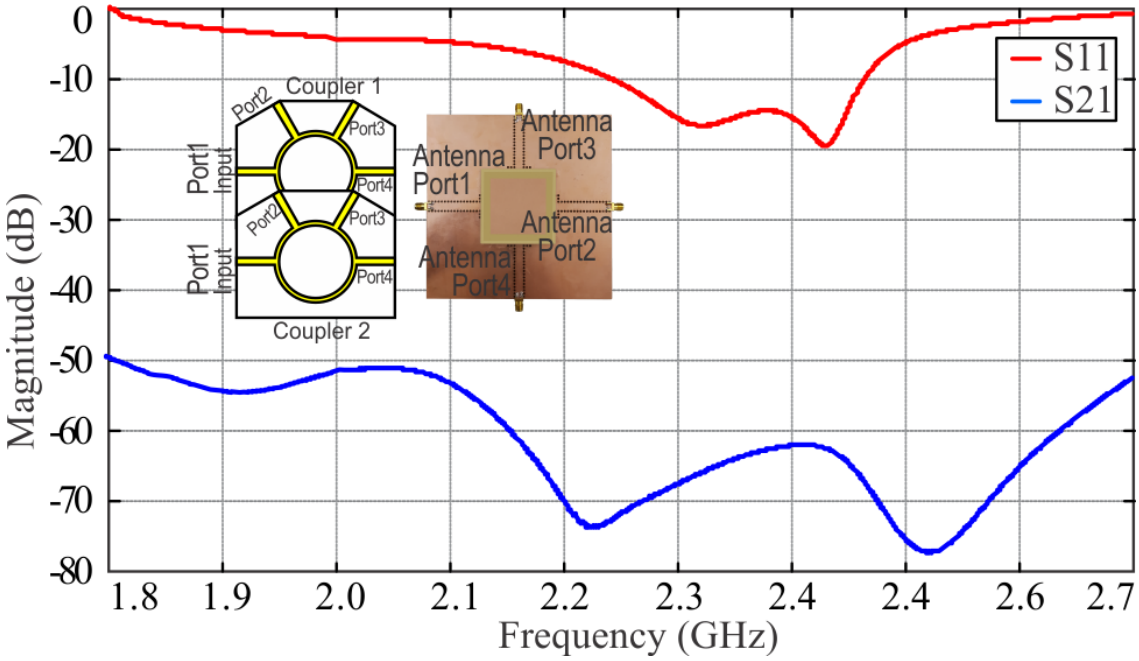

Figure 3.9: Simulated ideal antenna (air spacing for the patches whilst considering dielectric substrate losses, and ideal connections; i.e. no physical cable connections) response with the external coupler system (see Fig. 3.6). Antenna Ports 1 and 2 where connected to Ports 2 and 4 of Coupler 1. Likewise Antenna Ports 3 and 4 where connected to Ports 2 and 4 of Coupler 2. The |S11| is the port reflection coefficient at Port 1 of Coupler 1 (analogous results were observed for Coupler 2). The plotted |S21| is the coupling between Coupler 1 and Coupler 2 (connected to Port 1 for both). Port 3 of both couplers are loaded with 50-Ω.

3.10.2 Single-element Fabrication and System Measurements

The proposed prototype IBFD antenna and couplers were manufactured and measured. A photograph of the antenna prototype with foam spacers and nylon screws can be seen in Figs. 3.7 and 3.13, respectively. The S-parameter measurements were done using Keysight PNAs N5225A and 5234A. The antenna was loaded with the elevated patches. Ideally the H-shaped slots and the patches would by spaced apart by air layers. For implementation of the first prototype, Laird Eccostock PP-4 type foam with a relative permittivity of 1.06 was used as a spacer between the patches and the H-shaped slots.

To verify the beam pattern performance in the far-field, the antenna measurement system DAMS 7100 Diamond Engineering was used in the anechoic chamber at Heriot-Watt University. As a reference antenna, a Flann Horn (type 08240) was employed. The simulated and measured beam patterns can be observed in Fig. 3.10 while the antenna gain (measured in both receive and transmit modes) is reported in Fig. 3.11. It should be mentioned that the maximum measured realized gain was 7.3 dBi at 2.3 GHz, which is

slightly less than what was simulated by about 0.5 dBi. Measured realized gain from ports one and two, and three and four, are similar since the antenna is fully symmetrical. However, in receive mode, the measured gain was slightly lower. These minor discrepancies could be related to measurement tolerances or interactions with the antenna positioner. Regardless, the normalized beam patterns for the operating frequencies can be seen in Fig. 3.10 which match the simulations. Measured cross-polarization levels are more than 20 dB from the main beam maximum at the broadside.

Subsequent simulations which took into account the foam materials, some possible misalignments, and other fabrication tolerances showed that the frequency was shifted by about 50 MHz which better matched the S-parameter measurements (see Fig. 3.12). Due to these practicalities, the inter-port isolation was reduced by about 5 to 10 dB over the frequency range of interest. To circumvent this practical design challenge and improve the isolation, the second antenna prototype was optimized and manufactured using nylon screws with extended substrate layers for the top patches. This helped to improve the alignment and positioning of the various layers (see Fig. 3.13). The antenna F-parameters were simulated to validate the coupling of these approaches as reported in Fig. 3.14. From the simulations, it was observed that when the foam is used as the separation between elements, more energy leaks threw the foam to the H-shaped slots. Moreover, it is also required to be glued which introduces further manufacturing complications. Vias could help to reduce parasitic leakage caused by substrate and improve isolation levels. It can be observed that the antenna with the nylon screws and vias provided the best isolation suggesting structure fabrication and further testing for this design.

During the measurements of these antenna systems, it was also observed that the phase-matched cables and port connectors (which were made consistent for all antennas), introduced additional phase imbalances, which likely resulted in reduced isolation levels between the antenna ports. The full system S-parameter simulations and measurements including the cables, the couplers, and the antenna for the foam prototype are presented in Fig. 3.12 with results for both structures in Table 3.2. In these measurements, two short low-loss (phase-matched) cables were used. It is important to note that due to the long 50-Ω microstrip feeding lines, coaxial cables were required to feed the signals to the coupler ports. These additional cable lengths and the required connector ports, which is not possible to avoid with the external couplers, introduced some practical phase and magnitude imbalances and reduced port-to-port isolation.

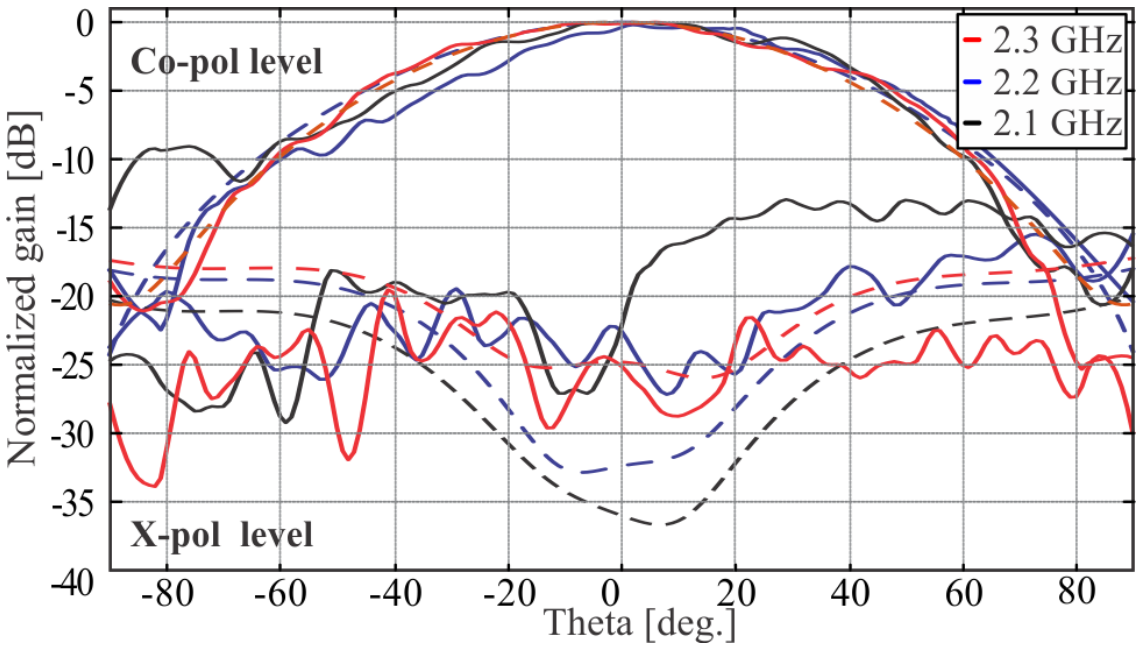

Figure 3.10: Simulated (dashed lines) and measured (solid lines) normalized beam patterns at the operating frequencies for the antenna as in Fig. 3.7. The beam patterns are in agreement with the cross-polarization levels which are below 20 dB at boresight.

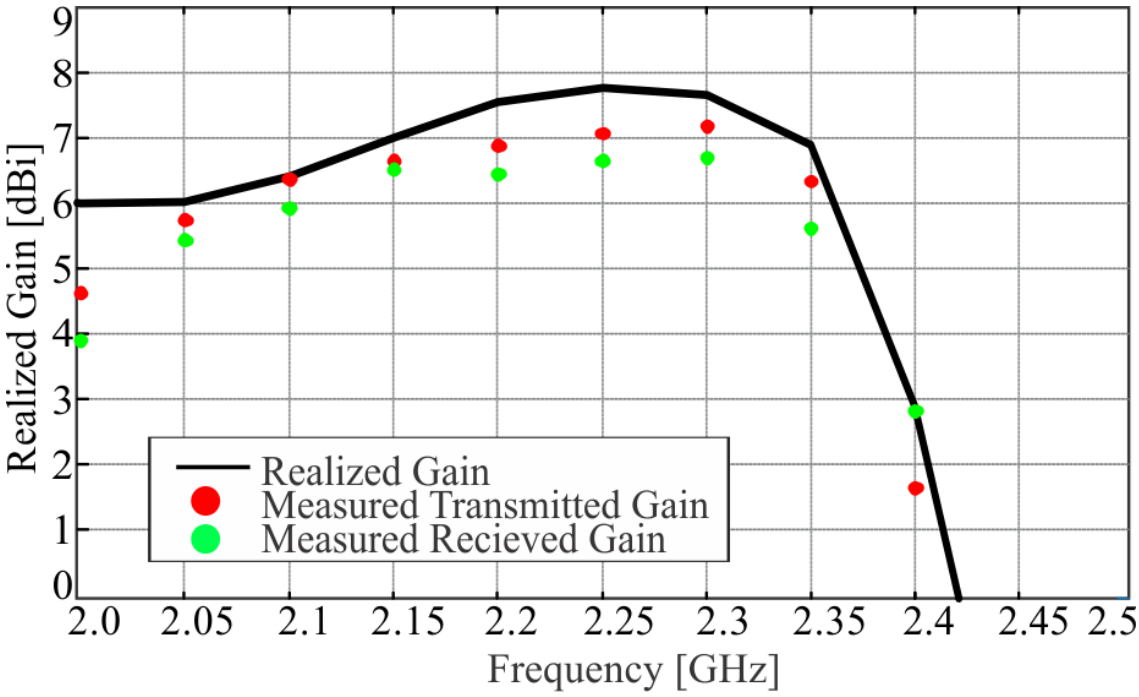

Figure 3.11: Simulated (black line) and measured (red/green dots) realized gains for the antenna system considering foam spacers (see Fig. 3.7). It should be noted that the single-element was measured in both transmit and receive mode.

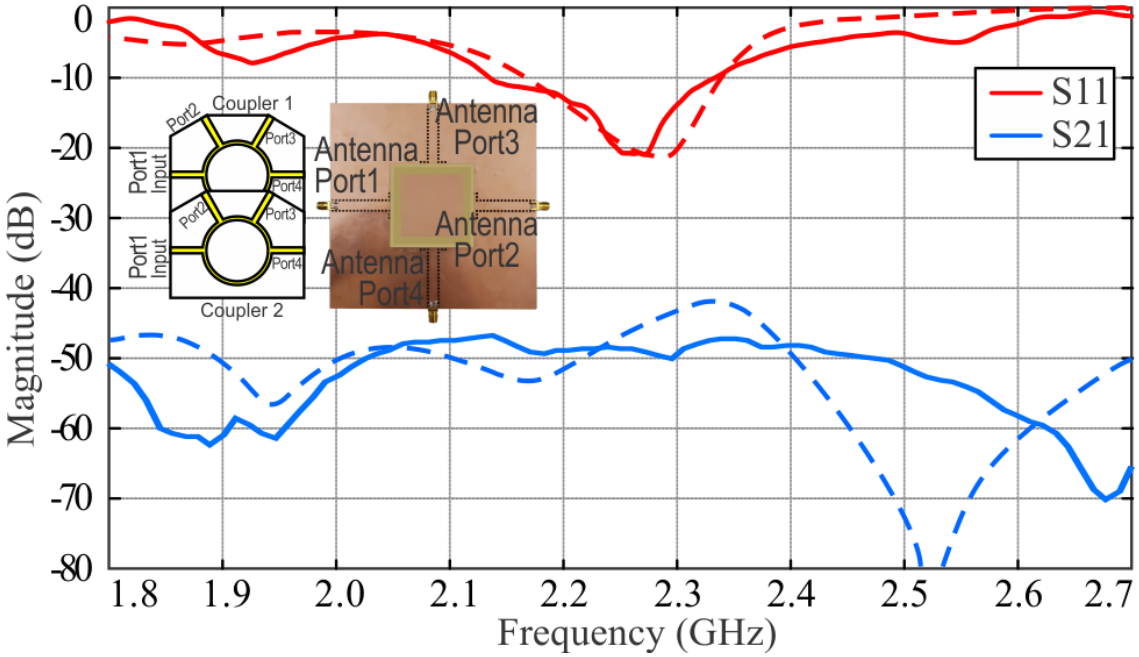

Figure 3.12: Simulated (dashed lines) and measured (solid lines) S-parameters of the antenna with the couplers and cables (foam spacer design, Fig. 3.7). In particular, the S-parameter combination tool in CST was employed which included simulation and measurement results of the couplers, the phase matched cables, and the four-port antenna. This provided the combined simulation and measurements of the final two-port antenna system.

Table 3.2: Prototype Comparisons Considering the Cables and Couplers

Developed Prototype	Measured / Simulated	Frequency Range	Percentage Bandwidth	Corresponding Isolation Range
Foam Spacer	Simulated	2.15 to 2.34 GHz	10%	45 to 49 dB
Foam spacer	Measured	2.15 to 2.35 GHz	9%	48 to 49 dB
Nylon Screws	Simulated	2.25 to 2.45 GHz	10%	60 to 70 dB
Nylon Screws	Measured	2.14 to 2.42 GHz	11%	48 to 60 dB

It is also important to note that at low frequencies the environmental noise could also be problematic (even in a fully enclosed anechoic chamber) when trying to achieve low isolation responses which are inline with the simulations (all results not reported for brevity). Regardless, from the simulations and measurements, the antenna with nylon screws provided a similar response, but with improved isolation as outlined in Table 3.2. For example, the measured isolation range, when the antennas are matched (i.e. the external port reflection coefficients are -10 dB or less), is higher than 49 dB and 60 dB for the antenna prototype with foam spacers and nylon screws, respectively.

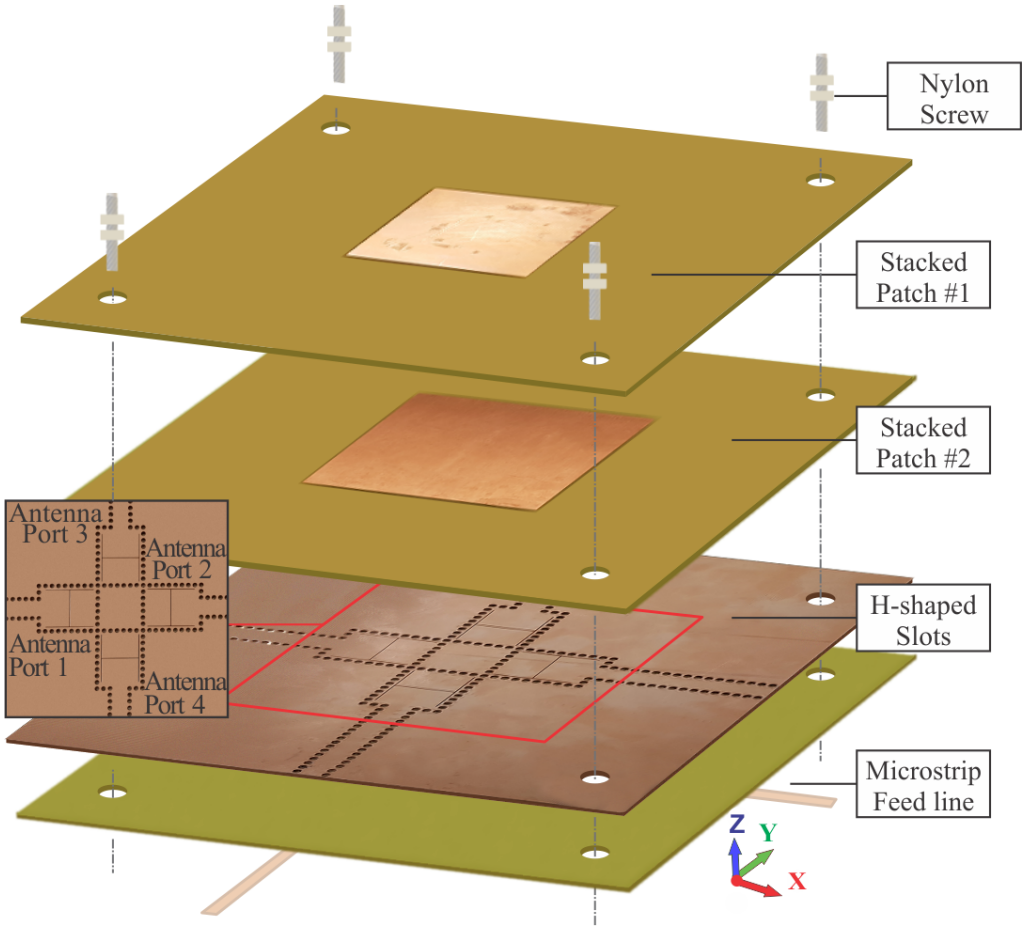

Figure 3.13: Exploded view of the antenna prototype design (using nylon screws).

Overall, the prototypes show that the measurements and simulations are in agreement when all the cables and couplers where taken into consideration. Some comparisons to other types of IFBD antennas are presented in Table 3.3, were it can be observed that the single-element can provide some benefits over the existing FD antennas in terms of simplicity and low-cost manufacturing, while maintaining a better operating bandwidth whilst providing high levels of isolation.

3.10.3 Slot-line Coupler for Phase Stability and Improved Full-duplex Antenna Operation

During the design work as outlined in the previous section, it was realized that antenna operation could be improved when required for FD systems. One such improvement could be the integration of a slot-line based coupler to replace the Rat-race coupler. This is because it is generally well known that microstrip transmission lines are dispersive and that Rat-Race couplers can be relatively narrow band. On the other hand, slot-based structures are less dispersive [65]. The inclusion of a slot-based coupler would reduce

Table 3.3: Comparison to other High Isolation Antennas Found in the Literature

Reference	Frequency	[1]Impedance Bandwidth	Cross-pol. at Boresight	[2]Corresponding Isolation Range	Element Size (Lowest Freq.)	Ground Plane Size (Lowest Freq.)	Max Gain (Realized)	Feeding Technique	Polarization	Single-element or Array	Multilayer
[71]	2.38 to 2.43 GHz	2%	<-50 dB	72 to 98 dB	0.23 by 0.23 λ_0	1 by 0.67 λ_0	4 dBi	Double-Diff.	dual-LP	Planar (Single)	No
[72]	2.45 to 2.55 GHz	4%	<-20 dB	40 to 75 dB	0.22 by 0.22 λ_0	N/A	4.4 dBi	Single-Diff.	dual-LP	Planar (Single)	No
[73]	4.75 to 5.18 GHz	9%	<-20 dB	50 to 58 dB	N/A	3 by 2 λ_0	10.5 dBi	Single-Diff.	dual-LP	Planar (Array)	No
[86]	0.5 to 2 GHz	98%	<-10 dB	40 to 55 dB	3.5 by 3.5 λ_0	6 by 6 λ_0	5.5 dBi	-	dual-LP	Metal (Array)	Yes
[88]	2.4 to 2.5 GHz	4%	<-30 dB	50 to 65 dB	0.3 by 0.3 λ_0	1.6 by 1.6 λ_0	10 dBic	SRA	dual-CP	Planar (Array)	Yes
[90]	2.3 to 2.7 GHz	16%	<-20 dB	37 to 45 dB	0.36 by 0.36 λ_0	N/A	8 dBi	-	dual-LP	Planar (Single)	Yes
[91]	2.25 to 2.6 GHz	16%	<-25 dB	41 to 54 dB	0.32 by 0.32 λ_0	2 by 2 λ_0	10.5 dBic	SRA	dual-CP	Planar (Array)	No
[92]	2.7 to 2.9 GHz	7%	<-32 dB	52 to 80 dB	0.25 by 0.25 λ_0	N/A	5.2 dBi	Double-Diff.	dual-LP	Non-Planar (Single)	Yes
[93]	5.62 to 6.11 GHz	8.5%	<-20 dB	35 to 70 dB	0.21 by 0.15 λ_0	0.85 by 0.75 λ_0	5.8 dBi	-	dual-LP	Planar (Single)	Yes
This work - Sim.	2.25 to 2.45 GHz	10%	<-27 dB	60 to 70 dB	0.32 by 0.32 λ_0	1.13 by 1.13 λ_0	7.8 dBi	Double-Diff.	dual-LP	Planar (Single)	Yes
This work - Meas. (Foam)	2.15 to 2.35 GHz	9%	<-20 dB	48 to 49 dB	0.32 by 0.32 λ_0	1.13 by 1.13 λ_0	7.3 dBi	Double-Diff.	dual-LP	Planar (Single)	Yes
This work - Meas. (Nylon)	2.14 to 2.42 GHz	11%	<-30 dB	48 to 60 dB	0.32 by 0.32 λ_0	1.13 by 1.13 λ_0	7.5 dBi	Double-Diff.	dual-LP	Planar (Single)	Yes

[1]The transmit and receive ports -10 dB impedance bandwidth (shared bandwidth); i.e. -10 dB impedance bandwidth for ports 1 and 2 of the antenna system.

[2]The corresponding isolation range refers to the external port isolation for the antenna system while the port reflection coefficients are -10 dB (or better).

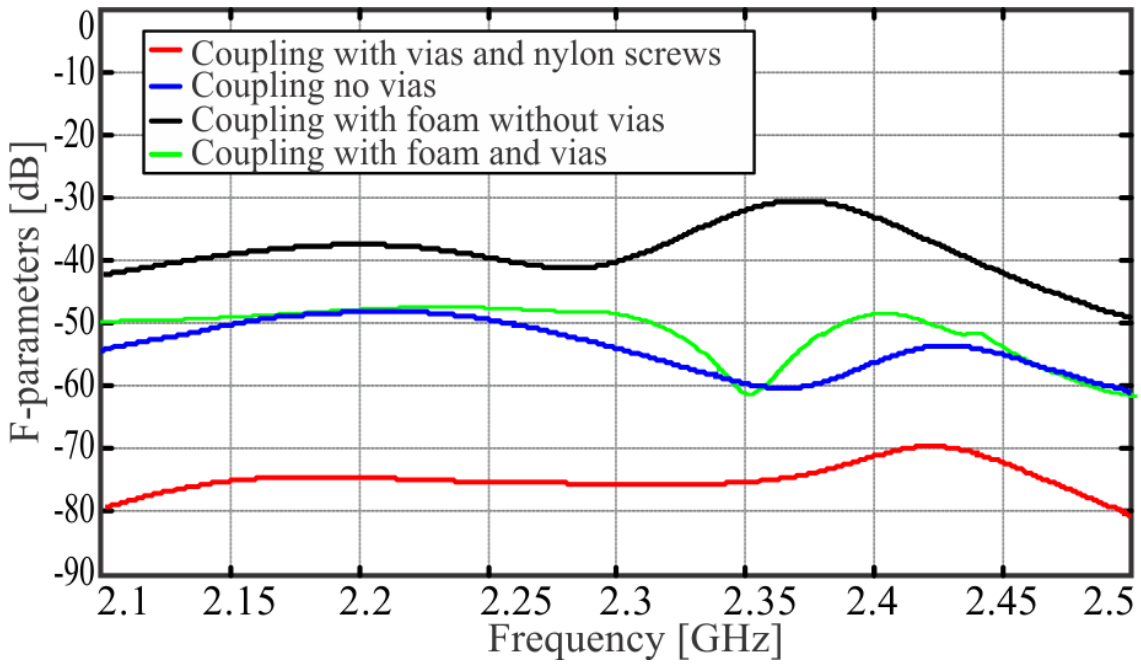

Figure 3.14: Simulated F-parameter coupling of the antenna designs considering different isolation techniques (see legend) and common design features. In these simulations no external feeding systems were considered.

the phase imbalances introduced to the antenna by the feeding network. Such imbalances can be seen in Fig. 3.10 where the beam pattern measurements are slightly squinted and the cross-polarization is higher than simulated.

To improve these results, a slot-based coupler was designed using transmission line meandering for compactness (see Fig. 3.15). From the simulations of the designed slot-line coupler, the phase imbalance is less that 0.5° while the magnitude imbalance is less than 0.2 dB (see Fig. 3.16). In the case of Rat-Race couplers, and thus for the antenna design reported in the previous section, it can be observed that the coupler is narrow-band and can only deliver stable operation at the center frequency (see Fig. 3.16). Moreover, it can be seen that the magnitude imbalances can reach as high as 1 dB while phase imbalances reach higher than 5°. As described in the following sections, the proposed slot-line based couplers can also be used to improve the phase and magnitude responses as applied to the antenna in transmit and receive mode.

Slot-line Coupler Design Approach using Meandering

One of the earliest slot-line based coupler designs can be found in [94] where magic-T slot-line based stubs were used to control the even and odd modes of operation. Addition-

ally, the structure consisted of coplanar waveguide (CPW) connections and a hybrid-like ring. Using this approach the authors were able to achieve wideband operation from 2.4 to 6 GHz with maximum phase imbalances of 2.5° and a magnitude imbalance of 0.4 dB. Another similar example of such a coupler, but based on microstrip technology can be seen in [52] where a similar magic-T like structure was presented. The placement of the slots above the feeding line provided a stable power split. The authors claimed that by carefully balancing the impedances of the system, by using open stubs and stepped circular rings, the currents can be exploited to enable good operation of the hybrid coupler. The designed structure was able to achieve an almost 80% bandwidth (center frequency of 10 GHz) with maximum magnitude imbalances of 0.25 dB and phase imbalances of 1°. It should also be mentioned that generally slot-line based couplers operate and have better performance at higher frequencies [65].

Advancing on these works we designed a new slot-line / microstrip-based coupler to operate with a 2.3 GHz center frequency. Meandering of the transmission lines was applied for compactness (see Fig. 3.15). Also, the initial size of the non-meandered coupler was $a = 0.38\ \lambda_0$ by $b = 0.5\ \lambda_0$ (considering lambda at the center frequency of 2.3 GHz). This was reduced to $c = 0.17\ \lambda_0$ by $d = 0.26\ \lambda_0$ (see Fig. 3.17) for the meandered structure which was fabricated and measured as reported in Figs. 3.18 to 3.20.

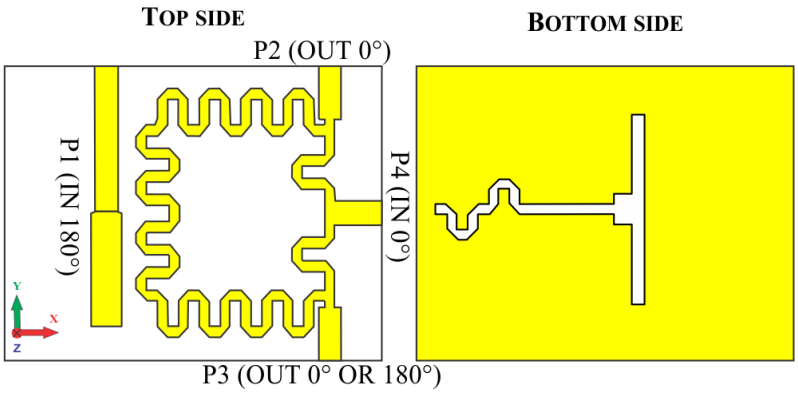

Figure 3.15: Top and bottom view of the proposed slot-line meandered hybrid coupler. It should be noted that the coupler can operate as a 0° divider when port 4 is driven. However, when port 1 is excited, a 180° phase difference can be observed at ports 2 and 3.

Coupler Performance and Antenna Results

The meandered coupler was designed using CST microwave studio. The reflections for all ports are minimal at port 1 which is matched from 1.9 to 2.6 GHz, and at port 4 which

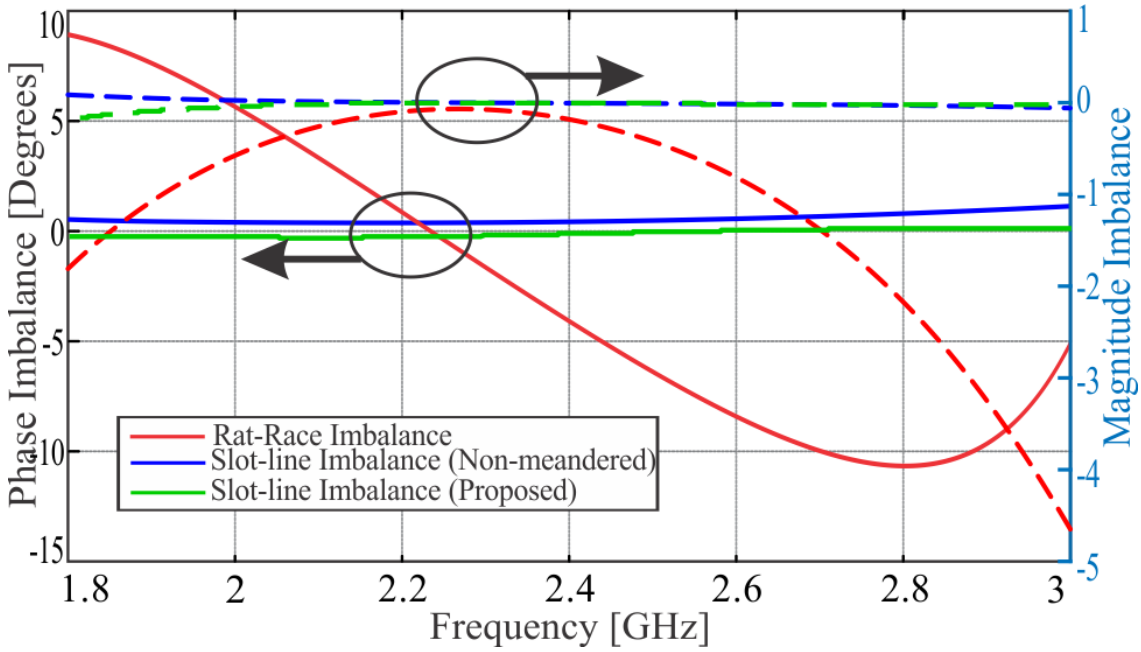

Figure 3.16: Simulated phase and magnitude imbalances (active ports for a 180° phase shift) of the hybrid couplers: Rat-Race type (considered for the single-element antenna, Fig. 3.6) as well as the non-meandered and the proposed compact, meandered slot-line type (see Fig. 3.17). It can be seen that the slot-line coupler has less than a 0.5° phase imbalance and a 0.2 dB magnitude imbalance.

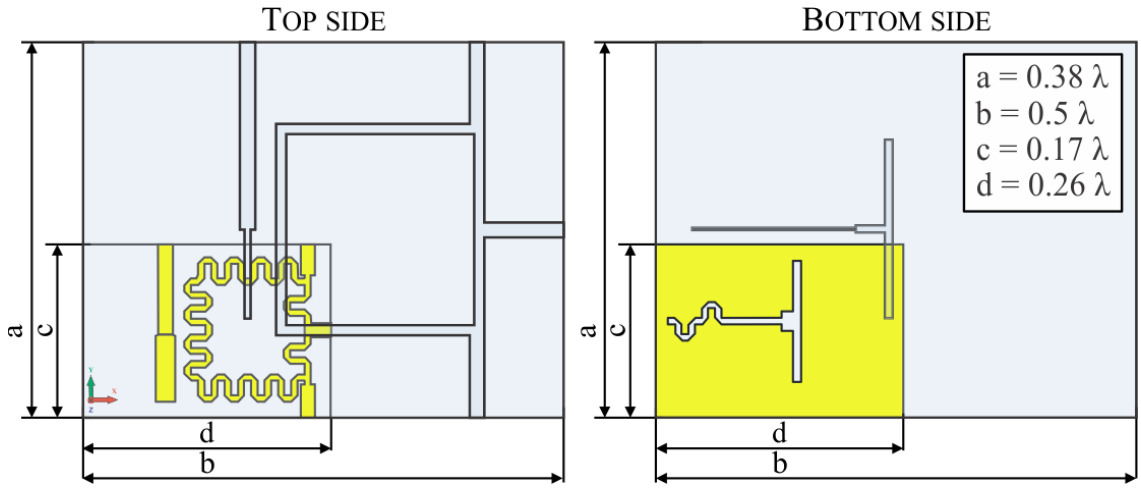

Figure 3.17: Size comparison between the meandered and non-meandered couplers. It can be seen that the size is almost three times smaller for the meandered version.

is matched from 2.1 GHz to 3 GHz (see Figs. 3.19 and 3.20). The highest magnitude and phase imbalances are around 0.1 dB and 1°, respectively. The isolation between ports 1 and 4 is well below 40 dB. The hybrid coupler was compared to existing devices in the literature (see Table 3.4) and it can be observed that the developed coupler offers improved

compactness, port isolation, and operating bandwidths. These features are important for low-cost, FD antenna systems.

The slot-line coupler was manufactured and measured for the 0° and 180° division input modes (see Fig. 3.18). For an input into port 1, the coupler divides the signal with the phase shifts of 0° and 180°, while for input into coupler port 4, an equal phase output can be generated. Simulations and measurements are in good agreement. Port 1 is matched from 1.9 to 2.6 GHz while port 4 is matched from 2.1 GHz to 3 GHz (see Figs. 3.19 and 3.20). The isolation between ports is also below 40 dB.

The antenna with the foam spacers was simulated considering the phase shifts due to the slot-line and Rat-Race couplers. Results show that the beam tilt and cross-polarization values are improved due to the slot-line coupler (see Table 3.5). For example, unwanted beam squints can be observed with the Rat-Race coupler, while improved cross-polarization levels are observed with the slot-line coupler for all cases. Also, when two of these compact, slot-line couplers were used to feed the antenna with nylon screws, measured isolation values were about 50 dB (or better) as shown in Fig. 3.21. These results demonstrate a clear advantage when using the slot-line couplers in terms of enabling no beam squint over frequency and generally providing lower cross-polarization levels as well as sustained isolation for the practical antenna.

3.10.4 Conclusion and Achievements

In this thesis part a new IBFD dual-polarized antenna element was presented for S-band applications. Two different single-element prototypes based on foam spacers and nylon screws were discussed and the presented designs offer improvements in terms of isolation and bandwidth when compared to similar structures previously reported (see Table 3.3). Two simple external hybrid-couplers were manufactured and used with the combined antenna system. The measured single element isolation was around 45 dB for the foam spacer and approached 70 dB for the nylon screw system complimenting the design approach. Most notably, a meandered slot-line based coupler to reduce the magnitude and phase imbalances feeding the antenna was also demonstrated, and this coupler offers better performances when compared to other structures in the literature in terms of bandwidth, isolation, and reduced coupler imbalances (see Table 3.4).

The antenna isolation might be improved by considering a larger ground plane, mainly to increase gain and reduce any leakage currents and unwanted coupling to the feeding

Table 3.4: Comparison of Existing Hybrid Couplers

Reference	Center Frequency	Size at Centre Wavelength, λ_c	Max Amplitude Imbalance	Max Phase Imbalance	Port Isolation	Impedance Bandwidth (-10 dB)	Transmission Line Technology
[52]	10 GHz	0.34x0.5	<0.25 dB	<1°	<29 dB	70%	Slot-line/Microstrip
[53]	1.575 GHz	0.012x0.02	<0.14 dB	<40.9°	<30 dB	34%	Balun Type
[95]	1.4 GHz	0.29x0.29	<0.5 dB	<5°	<25 dB	50%	Microstrip
[96]	14.1 GHz	2.8x1.8	<0.24 dB	<1.5°	<30 dB	18%	Slot-line/SIW
[97]	2.4 GHz	0.25x0.25	<0.5 dB	<5°	<25 dB	33%	Microstrip
This work, Rat-Race	2.3 GHz	0.72x0.68	<4.8 dB	<11°	<15 dB	66%	Slot-line/Microstrip
This work, Non-meandered	2.3 GHz	0.38x0.5	<0.1 dB	<1°	<48 dB	75%	Slot-line/Microstrip
This work, Meandered	2.3 GHz	0.17x0.26	<0.1 dB	<1°	<40 dB	32%	Slot-line/Microstrip

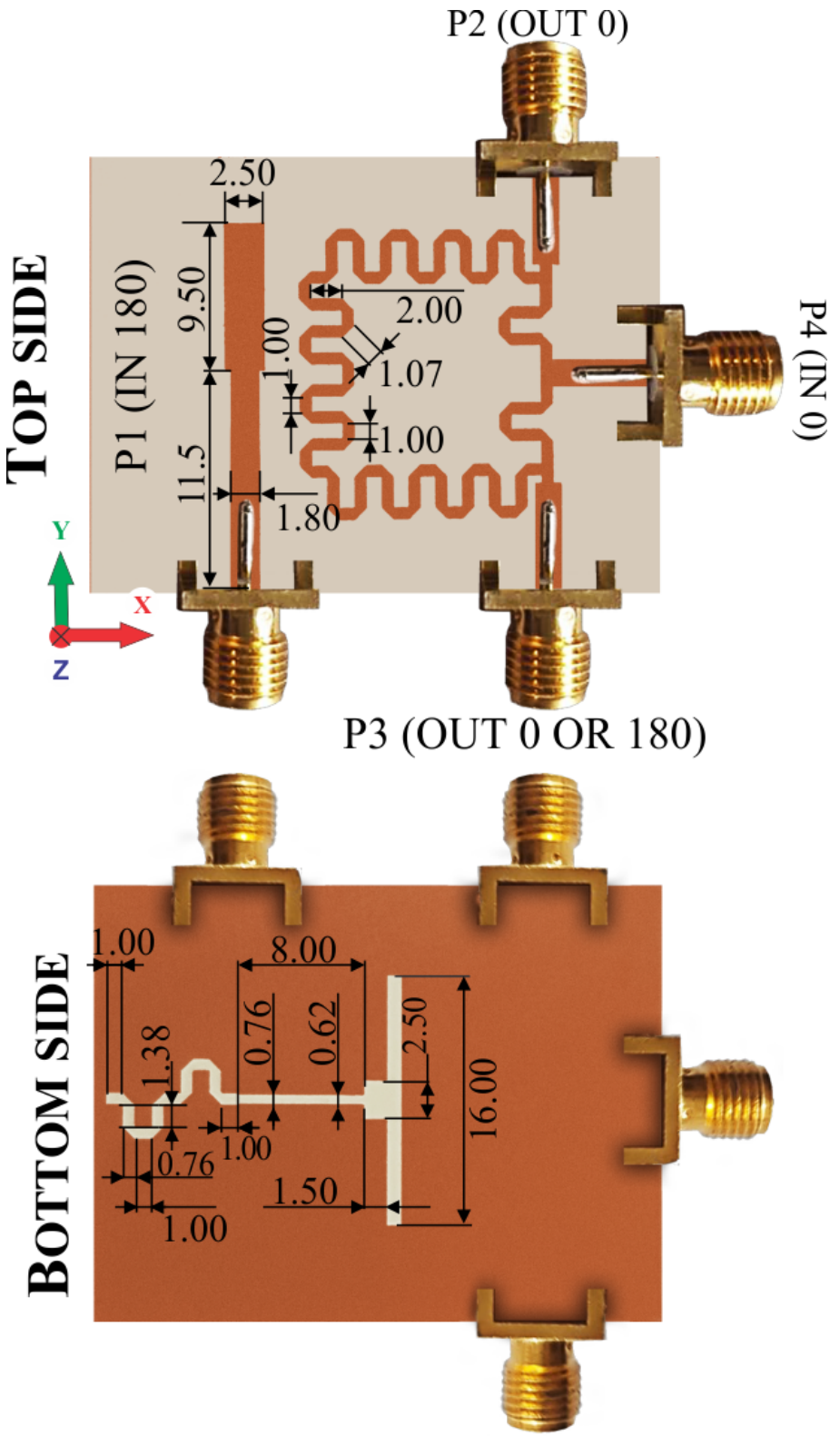

Figure 3.18: Top and bottom view of the manufactured slot-line meandered hybrid coupler. Coupler port 1 provides a differential phase shift at the output, while port 4 provides an equal phase shift. Final dimensions of the coupler are defined in millimeters.

system and network analyzer. Basically, an increase in ground plane size might improve practical isolation levels, however, the aim was to achieve a compact structure that is

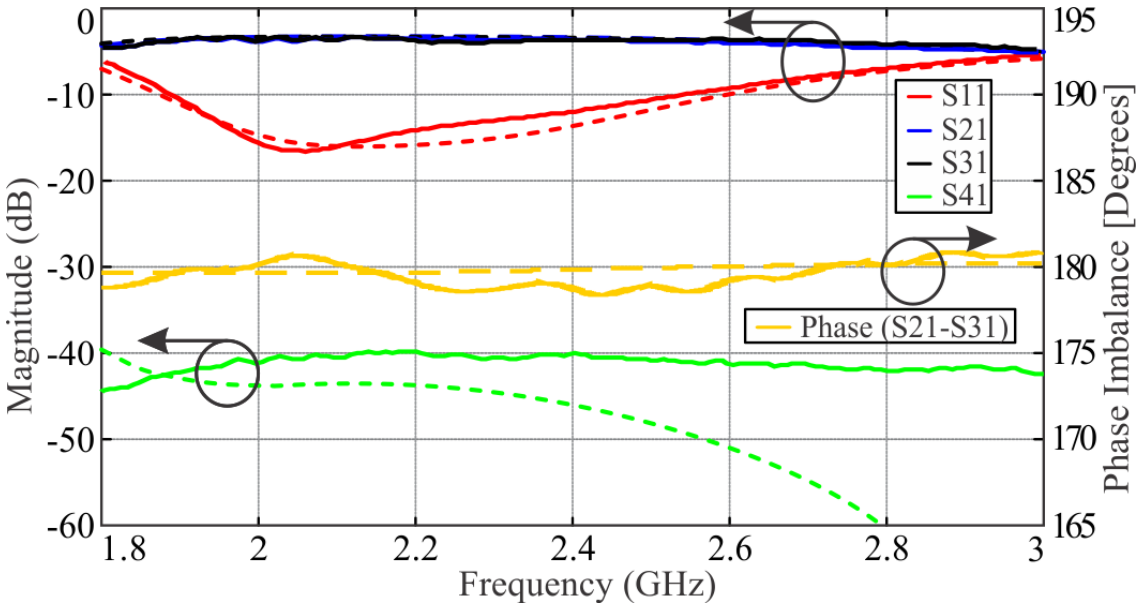

Figure 3.19: Simulated (dashed lines) and measured (sold lines) coupler response considering Port 1 as the input which provides a differential phase output.

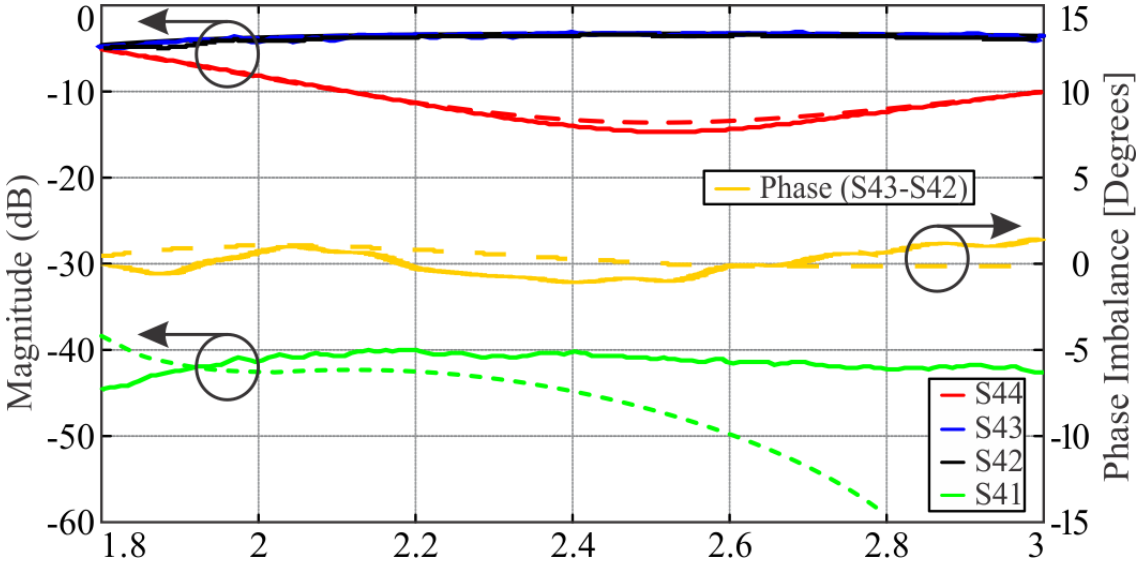

Figure 3.20: Simulated (dashed lines) and measured (sold lines) coupler response considering Port 4 as the input which provides an equal phase output.

competitive in size when compared to other FD antenna systems as found in the literature. Improved operating bandwidths for the antenna might also be possible with a third patch layer, however, misalignment could be a practical issue for the multi-layer design. Additionally, the developed differential feed circuits could be integrated within the proposed antenna system to avoid the need for external cables. This attractive solution for future work would hopefully minimize any phase imbalances introduced by the many

Table 3.5: Antenna (foam prototype) and coupler response comparison

Coupler Type	Beam Position	Frequency	Cross-pol. below Beam Max
Rat-Race	-1°	2.1 GHz	<-34 dB
Slot-line	0°	2.1 GHz	<-37 dB
Rat-Race	0°	2.2 GHz	<-27 dB
Slot-line	0°	2.2 GHz	<-32 dB
Rat-Race	1°	2.3 GHz	<-25 dB
Slot-line	0°	2.3 GHz	<-27 dB

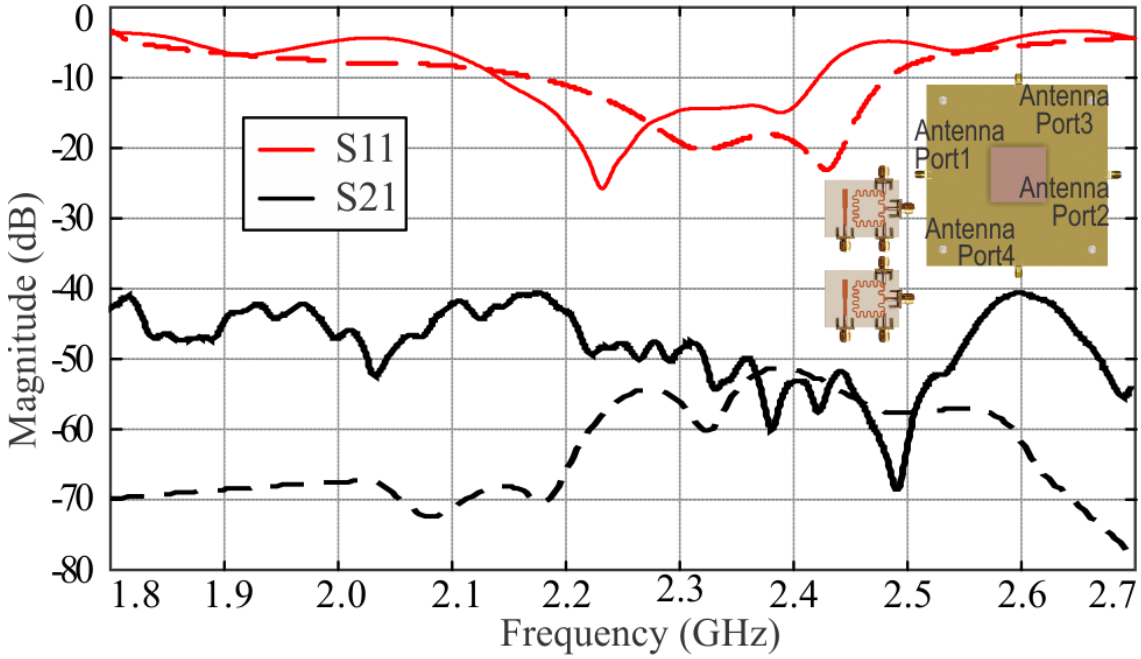

Figure 3.21: Simulated (dashed lines) and measured (solid lines) S-parameters of the antenna (nylon screws prototype, Fig. 3.13) with the newly proposed slot-line coupler (Fig. 3.18). Simulations are inline with the measurements which used the same experimental setup as outlined for Fig. 3.12.

required mechanical cable connections. Ideally, this effort for complete feed circuit integration when considering the developed differential couplers required for FD operation would also improve the practical inter-port isolation levels.

3.11 Dual-Polarized Antenna With Dual-Differential Integrated Feeding for Wideband Full-Duplex Systems

Following the need for simple feeding approaches and low-cost systems, this part of the thesis proposes an integrated feeding design (see Fig. 3.22, 3.23 and 3.24) with only two dividers within the same antenna system, and no external couplers, which can offer broadband operation while also employing elevated patches. As outlined in Section II, this design approach can simplify the feeding and reduce the number of required cables, while also, eliminating the requirement of external Rat-race couplers or other hybrids (where one port is typically not used and loaded with 50-Ω). Previously, some more narrowband IBFD antennas used two external hybrid couplers [71], [72] and connecting phase-matched cables were required making the system cumbersome, bulky, and involved to measure mainly due to the external feeding requirements.

In comparison to existing FD antennas and supporting circuit systems as found in the literature the new two-port single-element antenna offers high isolation levels, employs two slot-based internal power dividers for simple double-differential feeding, requires no external cables for antenna operation (i.e cable-less feeding) while also provides a wideband response and low magnitude and phase imbalances for the circuit feeding system. This dual-differential feeding approach is further outlined in Section 3.9.2 while antenna system simulations and measurements are reported in Section 3.9.3. In addition, by advancing on this single-element design and the need for higher BW communications and FD beam steering, an extension to 4×1 array is presented in Section 3.11. Some brief conclusions follow in Section 3.12.

3.11.1 Single-element Design

The IBFD antenna with the proposed integrated feeding network consists of four H-shaped slots connected to two power dividers, and two patch antennas placed on top of the slot arrangement. The antenna design dimensions are outlined in Fig. 3.23 and Table 3.8. In particular, the feeding system consists of two slot-line dividers and strut-like vertical connectors for simple manufacturing and assembly. The optimized dimensions for the patch layers and the ground plane are outlined by a through d (see Table 3.8), while the parameters for the H-shaped slots are as follows: e = 0.2 mm, f = 14.6 mm, g = 19 mm, h = 4 mm and the distance between the opposite elements is i = 20.7 mm.

Table 3.6: Comparison to other High Isolation Antennas and Arrays for FD Applications (Measured Results Unless Stated)

Reference	Frequency	[1]Imped. BW	[2]Isolation Range	Element Size (Lowest Freq.)	Ground Plane (Lowest Freq.)	Height (Lowest Freq.)	Max Gain (Real.)	Boresight Cross-pol.	Circuit Feeding	Feeding Type	Polarization	Antenna Description (Single-element or Array)	Radiation Mechanism & Feeding Configuration
[71]	2.38 to 2.43 GHz	2%	72 to 98 dB	0.23 by 0.23 λ_0	1 by 0.67 λ_0	0.01 λ_0	4 dBi	<-50 dB	Both	Double-Diff.	dual-LP	Planar (Single, 2-port)	Single Rectangular Patch, Microstrip Feed
[98]	2.2 to 2.69 GHz	20%	45 to 52 dB	0.55 by 0.55 λ_0	0.7 by 0.7 λ_0	0.2 λ_0	9 dBi	<-30 dB	Integrated	Single-Diff.	dual-LP	Non-Planar (Single, 2-port)	Metallic Probe-like Elements and H-shaped Slot, Loaded Patch
[72]	2.45 to 2.55 GHz	4%	40 to 75 dB	0.22 by 0.22 λ_0	N/A	0.012 λ_0	4.4 dBi	<-24 dB	Integrated	Single-Diff	dual-LP	Planar (Single, 2-port)	Single Rectangular Patch, Microstrip Feed
[73]	4.75 to 5.18 GHz	9%	50 to 58 dB	N/A	3 by 2 λ_0	0.07 λ_0	13.1 dBi	<-24 dB	Integrated	Single-Diff.	dual-LP	Planar (Array, 2-port)	Four Rectangular Patches, Probe Feed
[86]	0.5 to 2 GHz	98%	40 to 55 dB	3.5 by 3.5 λ_0	6 by 6 λ_0	0.2 λ_0	5.5 dBi	<-10 dB	External	-	dual-LP	Non-Planar (Array, 5-port)	Four Dipole-like Elements, Probe Feed
[88]	2.4 to 2.5 GHz	3%	50 to 65 dB	0.3 by 0.3 λ_0	1.6 by 1.6 λ_0	N/A	10 dBic	<-24 dB	External	SRA	dual-CP	Planar (Array, 4-port)	Four Rectangular Patches, Probe Feed
[90]	2.3 to 2.7 GHz	20%	37 to 45 dB	0.36 by 0.36 λ_0	N/A	0.13 λ_0	8 dBi	<-16 dB	Integrated	-	dual-LP	Planar (Single, 2-port)	Dipole-like Elements, Probe Feed
[91]	2.4 to 2.5 GHz	4%	41 to 54 dB	0.32 by 0.32 λ_0	2 by 2 λ_0	0.015 λ_0	10.5 dBic	<-15 dB	Integrated	SRA	dual-CP	Planar (Array, 2-port)	Four Rectangular Patches, Microstrip Feed
Proposed Antenna	2.25 to 2.48 GHz	10%	46 to 60 dB	0.32 by 0.32 λ_0	1.8 by 1.8 λ_0	0.3 λ_0	7.8 dBi	<-25 dB	Integrated	Double-Diff	dual-LP	Planar (Single, 2-port)	Four H-shaped Slots with Two Loaded Patches
[3]Proposed Array	2.25 to 2.48 GHz	10%	45 to 50 dB	0.32 by 0.32 λ_0	1.8 by 3.4 λ_0	0.3 λ_0	13.3 dBi	<-28 dB	Integrated	Double-Diff	dual-LP	Planar (Array, 8-port)	Sixteen H-shaped Slots with Eight Loaded Patches

[1]The transmit and receive ports -10 dB impedance; i.e. the -10 dB impedance bandwidth (BW) for ports 1 and 2 of the antenna system (or the shared BW).

[2]The corresponding isolation range refers to the external port isolation for the antenna system while the port reflection coefficients are -10 dB (or better).

[3]The developed 4×1 array offers external access to its 8-ports which can easily support beam steering (simulation results described only) and when dual-polarization is required. No similar beam steering features were reported in [86], [72] - [98].

Table 3.7: Circuit Feeding Performances (Planar) for Some of the FD Antennas in Table 3.6

Reference	Frequency Range	[1]Impedance BW (-10 dB)	Phase Imbalance	Mag. Imbalance	Numbers of Power Dividers	Numbers of Hybrid Couplers
[71]	2.2 to 2.7 GHz	20%	<5°	<0.5 dB	0	2
[98]	1.8 to 3 GHz	50%	<35°	<0.5 dB	1	0
[72]	2.2 to 2.7 GHz	20%	<5°	<0.5 dB	0	1
[73]	3.5 to 6.5 GHz	60%	<1°	<0.4 dB	0	1
[86]	1.15 to 1.65 GHz	35%	<5°	<0.5 dB	-	-
[88]	2.2 to 2.7 GHz	20%	<2°	<1.5 dB	0	6
Proposed Antenna	1.85 to 2.8 GHz	40%	<1°	<0.1 dB	2	0
Proposed Array	1.85 to 2.8 GHz	40%	<1°	<0.1 dB	8	0

[1]The -10 dB impedance bandwidth (BW) refers to the percentage frequency BW for which all ports of the feed system offer a -10 dB reflection coefficient (or better).

The PCB design material for the patches was FR-4 (see Fig. 3.22, stacked patch # 1 and # 2) with a relative permittivity of 4.6 and thickness of 1.6 mm. The H-shaped slots serve as an excitation mechanism for the top square patches with the dimensions of b = 48.3 mm for the bottom patch and a = 42.5 mm for the top patch. Other slot-feeding configurations are possible (such as the conventional aperture coupled slot with a length of $\lambda/2$ in the ground plane and with microstrip feeding), but the H-shaped slot can support wideband antenna operation whilst being compact [99, 100]. The optimized distances between patches # 1 and # 2 are t = 9.36 mm, and, defined by s (= 4.16 mm), for the separation between patch # 1 and the H-shaped slots. This multilayer configuration can increase the BW of the antenna system. A single parasitic patch configuration is also possible, but this was shown to reduce the operating BW for the antenna design (all results were not reported for brevity).

The overall dimension of the proposed mutli-layer antenna system with four H-shaped slots and two stacked parasitic patches (see Figs. 3.22 and 3.23) is c = 240 mm by d = 240 mm (which corresponds to 1.8 by 1.8 λ_0 at the lowest operating frequency of 2.25 GHz). The distance between the H-shaped layer and the feeding layer is u = 24 mm. The relatively large and extended ground plane increases the antenna gain whilst reducing the side lobe levels caused by any parasitic radiation from the H-shaped slots. The antenna dimensions including the feeding PCB are compiled in Tables 3.8 and 3.9.

Table 3.8: Antenna dimensions as Illustrated in Fig. 3.23 (all values in millimeters)

a	b	c	d	e	f	g	h	i	j	k	l	m	n	p	q	r	s	t	u
42.5	48.3	240	240	0.2	14.6	19	4	20.7	2.3	98.3	66.3	21.35	11	3.1	69.5	45	4.16	9.36	24

3.11.2 Antenna Feeding Network

The double-differential integrated feeding network for the antenna consists of two slot-line power dividers. They are designed using compact transmission line meandering

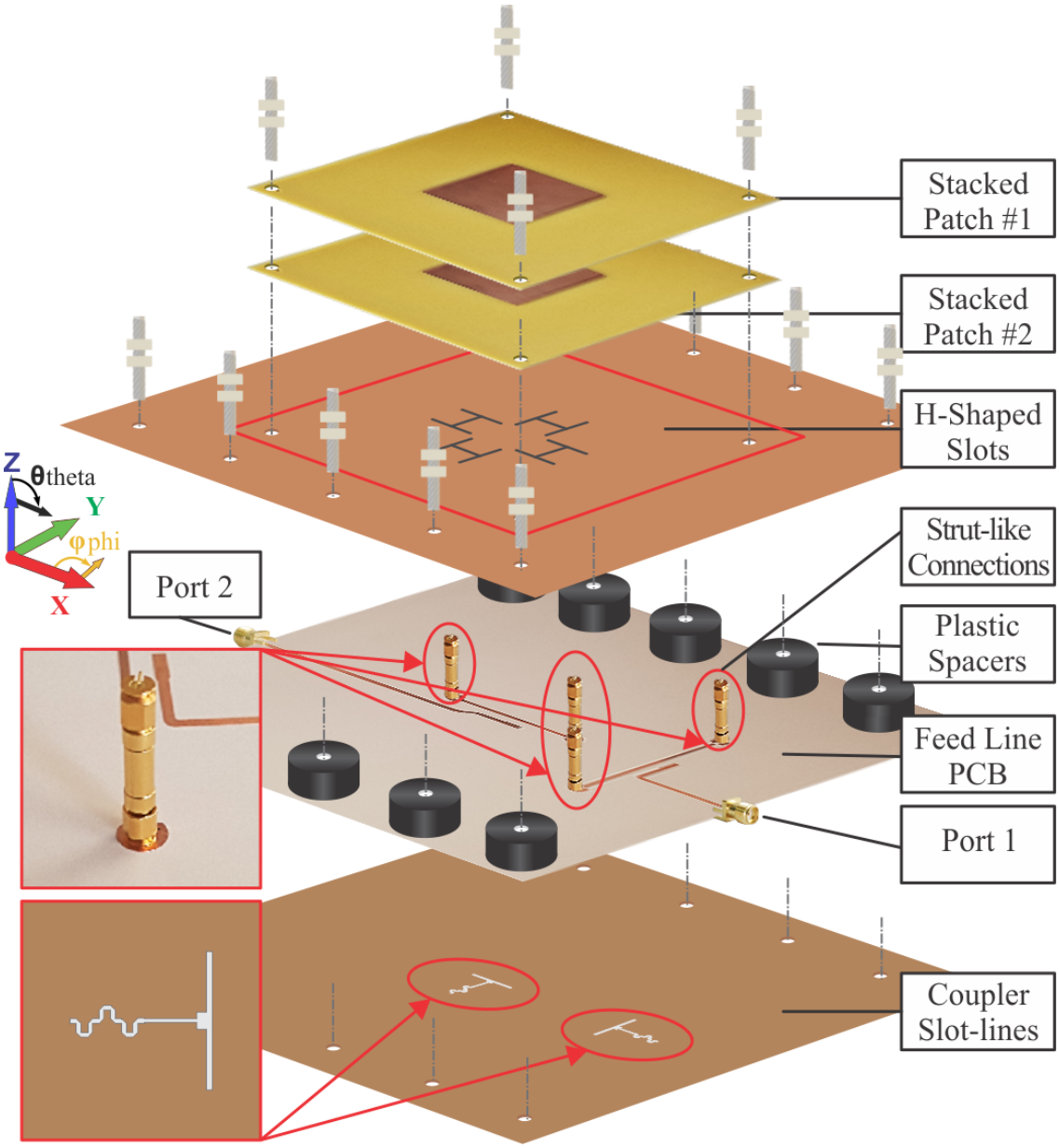

Figure 3.22: Antenna design exploded view: 2-port dual-linearly polarized antenna system with H-shaped slots and two parasitic square patch elements on top to increase BW. Bottom differential feeding network consisting of two dividers for 0° and 180° and this signal division circuit is made compact by meandering. Also, vertical strut-like transmission lines connect the multi-layer antenna.

considering a Rogers 3003c substrate which has a relative permittivity of 3 and thickness of 0.76 mm. Using this feeding approach the divider provides dual-differential feeding to the H-shaped slots with a signal shift of 0° and 180°. With this feeding network, two orthogonal linear polarizations are possible for the antenna. For example, by driving Port 1, the generated far-fields in the *x*-*z* plane will be linearly polarized (see Fig. 3.22). Similarly, by exciting Port 2, the dominant fields in the *y*-*z* plane will also be linearly polarized. When two dividers have perfect phase balance and the same amplitude, the

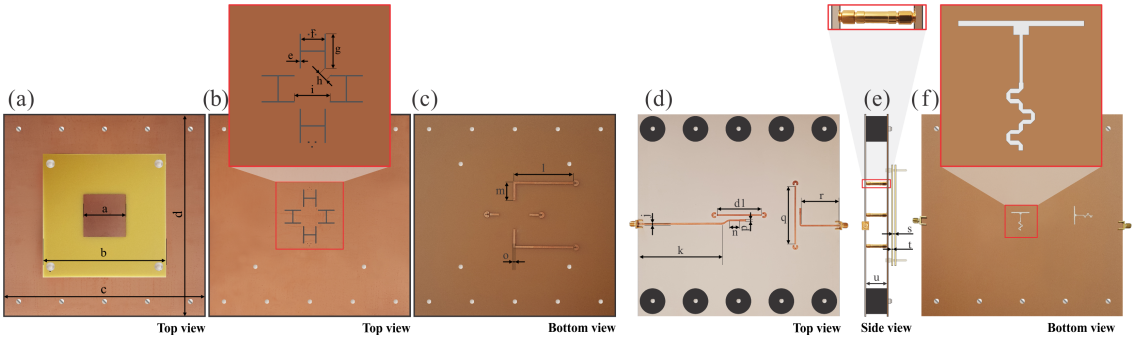

Figure 3.23: Antenna design overview. (a) Top view: loaded parasitic patches on top of the H-shaped slots, (b) Top view: four H-shaped slots, (c) Bottom view of the H-shaped board where strut-like connections are positioned for connectivity to the other layers, (d) Top view: feeding system on the second substrate, (e) Side view: strut-like structure connections to the H-shaped slots, (f) Bottom view of the lower substrate; i.e. T-shaped slots of the compact slot-line divider. The dimensions of the antenna and feeding elements can be seen in Table 3.8.

inter-port leakage of the transmitted and the received signals can be canceled. Thus, the employed slot-line based divider can be utilized for phase and magnitude stability.

The proposed slot-line power divider was designed and simulated in the commercial full-wave simulator CST microwave studio. The design of the divider can be seen in Fig. 3.24. From the simulations it can be observed that port 1 is well matched from 1.8 to 2.8 GHz with values below -10 dB with a center frequency at 2.28 GHz (see Fig. 3.25). Due to the employed symmetry, ports 2 and 3 can provide an equal power split ratio with values of -3.5 dB. However, it should be mentioned that ports 2 and 3 are not well matched to 50-Ω and only reach -6 dB (for when 0° phase shifts are applied to both ports). At first glance, it may seem that ports 2 and 3 are not well matched over frequency. However, both ports need to be analyzed together; i.e. ports 2 and 3 operate simultaneously. For this, the divider is required to be analyzed using active S-parameters (or active F-parameters in the CST). In particular, by applying signals to ports 2 and 3 with 0° and 180° phase offsets, the matching is improved and the active F-parameter is below -10 dB over the entire simulated range from about 1.8 GHz to 2.7 GHz. These results suggest that this divider is suitable for the proposed antenna system when port 1 of the slot-line divider circuit (see Fig. 3.24) is used as the transmitting port.

It should also be noted that in comparison to the conventional Rat-race hybrid coupler, the slot-line power divider magnitude and phase imbalance is much lower. The comparison between a Rat-race coupler with a center frequency of 2.3 GHz and the proposed slot-line divider as well as a Wilkinson power divider (and delay line as in [98]) can can

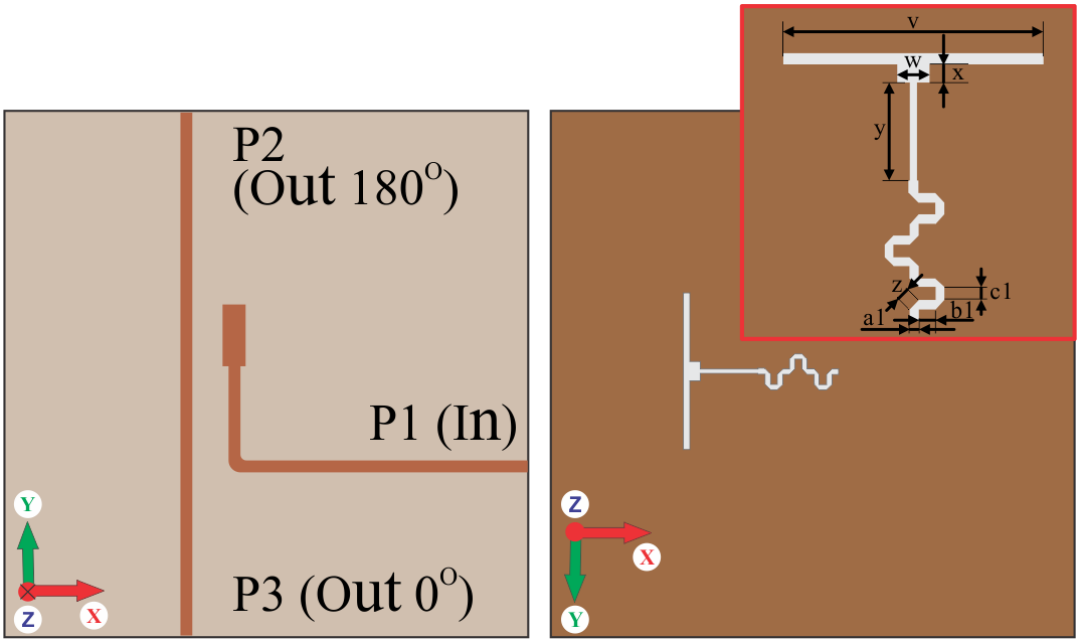

Figure 3.24: Top and bottom view for the proposed slot-line divider for the antenna feeding in Fig. 3.22. The slot-line divider dimensions are outlined in Table 3.9.

be seen in Fig. 3.26. The stability of the developed slot-line power divider is wideband over frequency, while the conventional Rat-race coupler and Wilkinson power divider can only provide stability at the center frequency. The full dimensions of the developed slot-type divider are also outlined in Table 3.9.

Table 3.9: Slot-line divider dimensions as Illustrated in Fig. 3.24
(all values in millimeters)

v	w	x	y	z	$a1$	$b1$	$c1$
22	2.5	1.5	8	1.07	1	1.37	0.76

3.11.3 Integration of the Antenna with the Feeding System & Results

The dividers were further integrated with the single antenna unit as depicted in Fig. 3.22. It should be mentioned that the integration of both dividers provides simplicity in the feeding system for the multi-layer antenna where only two ports are employed. Also, external couplers are not required. More importantly, this feeding system does not require additional cable connections between the elements whilst employing the strut-like connections. In comparison to more conventional feeding approaches [71, 72, 88], practical (and unavoidable) cable bending and twisting, as well as the cable connections themselves, could introduce additional phase and magnitude imbalances when external hybrid couplers are needed. This could introduce unwanted main beam tilting issues in

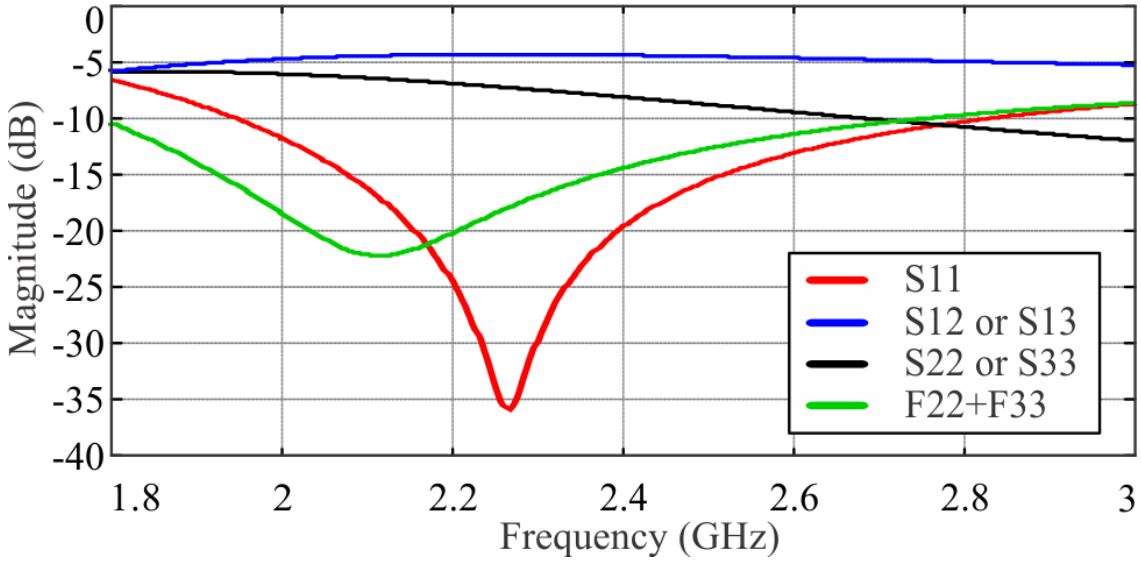

Figure 3.25: Simulated S-parameters of the slot-line divider proposed in Fig. 3.24. Port 1 provides a differential phase shift of 180° between ports 2 and ports 3. When analyzing such a structure, ports 2 and 3 operate considering a differential single shift. Therefore, S22 and S33 are only matched below -5 dB when studying conventional S-parameters. However, when the differential mode is properly considered (or active ports F22 + F33; i.e. when a differential phase is applied at ports 2 and 3) the active matching is well below -10 dB.

the far-field whilst reducing cross-polarization performances. Additionally, the employed slot-line coupler maintains stable magnitude and phase imbalances when compared to the conventional Rat-race couplers (see Fig. 3.26). Moreover, 50-Ω load terminations at the unused ports are not required as in [71, 72, 88].

The final antenna design was optimized in CST microwave studio (see results in Fig 3.27). The antenna is well matched with a simulated -10 dB impedance BW from 2.25 GHz to 2.48 GHz. Due to the employed feeding system, the matching is non-symmetrical, but still offers a significant impedance matching BW which is above 10%. The minimum simulated coupling (S21) is around 2.23 GHz with a value of -54 dB and maximum coupling occurs at 2.42 GHz with the value of -48 dB.

The simulated beam patterns for the Phi = 0° and Phi = 90° planes are presented in Figs. 3.29 and 3.30 for ports 1 and 2, respectively. As expected, the antenna is radiating at broadside with cross-polarization values well below 30 dB from the main beam maximum. Maximum realized gain for both ports is 7.8 dBi with port 1 having slightly higher values by about 0.2 dBi at 2.25 GHz (see Fig. 3.27).

Based on these findings, the proposed IBFD antenna with an integrated feeding system was manufactured and measured. The strut-like connections; i.e. the vertical trans-

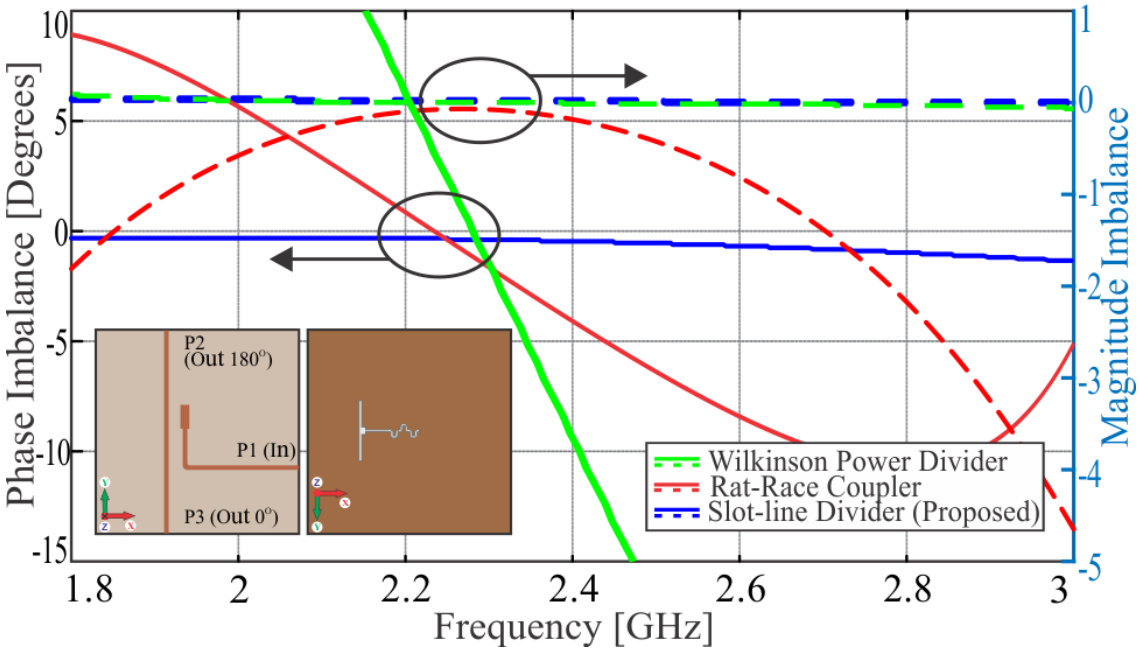

Figure 3.26: Simulated phase and magnitude imbalance comparison: Wilkinson power divider with delay line (as in [98]), conventional Rat-race hybrid coupler, and slot-line divider (see inset). It can be seen that the slot-line divider offers a 0.5° phase imbalance or less from 1.8 to 2.5 GHz and can approach 1.2° at 3 GHz (which is out of band of the antenna). Also, maximum magnitude imbalances are around 0.1 dB or less.

mission lines were realized using [101] from Cinch Connectivity while the transitions to microstrip were done using [102] from Amphenol. A photograph of the assembled unit can be seen in Fig. 3.28. Nylon screws were used to enhance the stability of the structure, provide spacing between the elements, while also reducing any interference between PCBs.

The S-parameter measurements were completed using Keysight PNAs N5225A and 5234A at the Heriot-Watt University Microwave Lab. From the measurements of the S-parameters (see Fig. 3.27) it can be observed that the coupling, S21, between ports is below -45 dB which is slightly higher than expected when compared to the simulations. The antenna ports are also well matched from 2.25 to 2.49 GHz with values below -10 dB. The slight discrepancy in the isolation is most likely related to a small alignment of the patches on top from the H-shaped structure. It can also be observed that the matching for both ports is not exactly the same. This is related to a needed and minor asymmetry in the feed system (see Fig. 3.23(d)) and the fact that vertical strut like connections were employed. Also, due to the minor back radiation from the H-shaped slots, the feedline PCB (see Fig. 3.22) is required to be positioned away from the H-shaped slot PCB

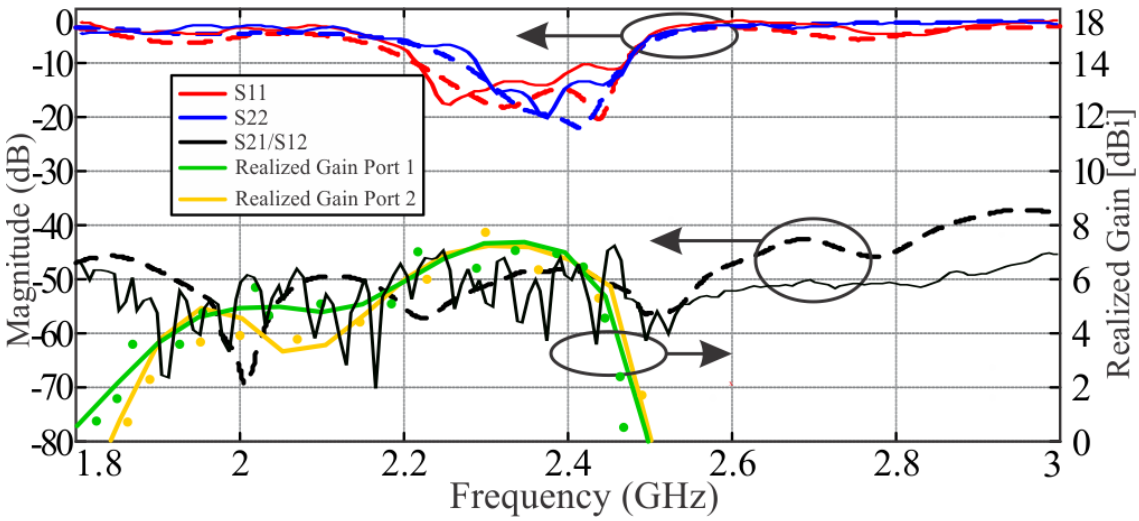

Figure 3.27: Simulated (dash line) and measured (solid line) S-parameters of the proposed integrated antenna design. The antenna is well matched from 2.25 to 2.48 GHz (-10 dB BW) while the coupling values are below -50 dB over this BW. The simulated (solid line) and measured (dots) realized gains of the antenna demonstrate a maximum of 7.8 dBi.

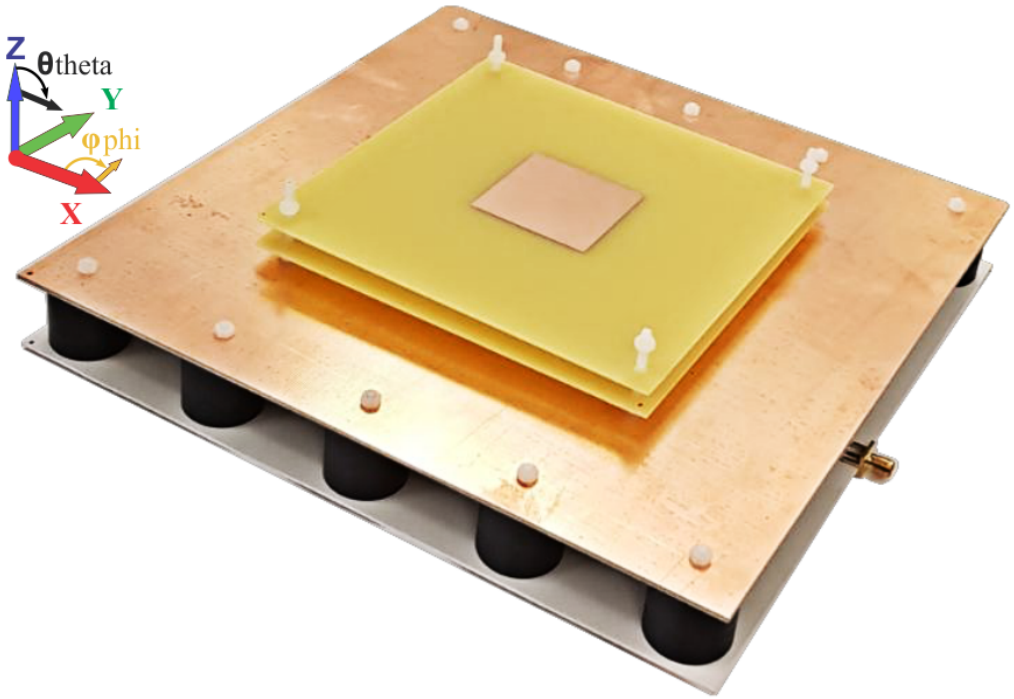

Figure 3.28: Manufactured and assembled antenna prototype. The antenna design overview can be seen in Figs. 3.22 and 3.23 with full dimensions in the Table 3.8.

layer by the distance u (see Table 3.8). Many optimizations in CST were carried out, however, because of the above noted design requirements, it was challenging to make the

reflection coefficients for each port exactly the same as observed in the simulations and measurements while also achieving high levels of isolation.

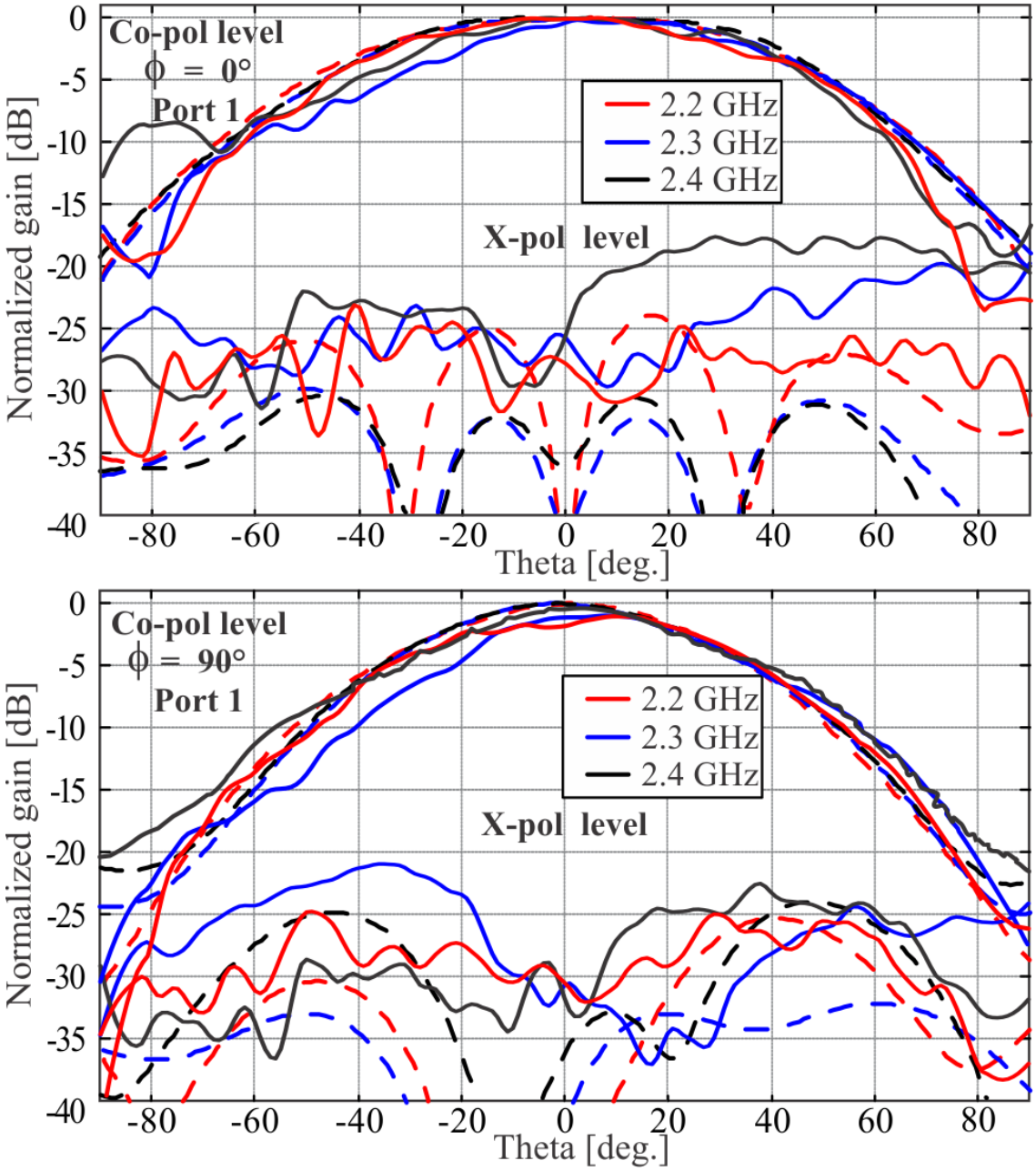

Figure 3.29: Simulated (dashed line) and measured (solid line) normalized beam patterns for port 1 at the operating frequencies for the antenna. The cross-polarization levels are below 25 dB at broadside.

The DAMS 7100 Diamond Engineering system was used for beam pattern measurements. The reference horn antenna (Flann Horn Antenna Type 08240) was employed. In Figs. 3.29 and 3.30 it can be observed that the simulated and measured beam patterns are in agreement. However, the cross-polarization values are higher than expected by about 5 to 10 dB depending on the frequency. This is most likely related to some interactions

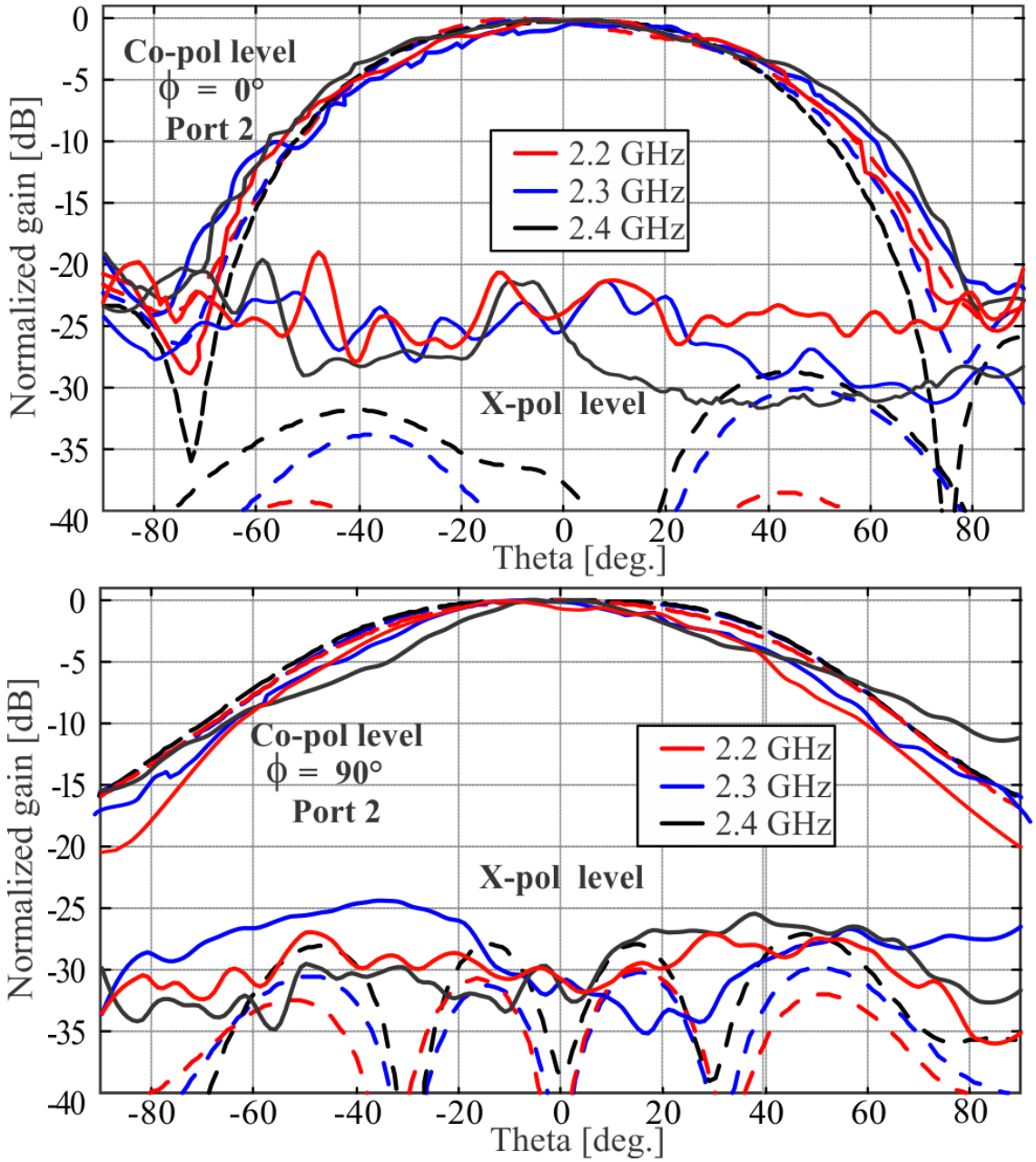

Figure 3.30: Simulated (dashed line) and measured (solid line) normalized beam patterns for port 2 at the operating frequencies for the antenna. The cross-polarization levels are below 20 dB at broadside.

with the metallic and plastic parts of the antenna positioner.

To compare the developed IBFD single-element with existing antennas and feed systems found in the literature (see Table 3.6 and 3.7), it can be observed that the proposed is the only planar antenna system that can offer an improved BW (10%), is fully integrated with its feed system (and double-differential), while also, offering sustained isolation with values reaching 60 dB. In addition, the structure does not require external hybrid couplers or external cables to achieve such isolation levels as in [71, 72, 88]. These comparisons

suggest that the proposed antenna is suitable for IBFD applications whilst providing a simple design approach with integrated feeding. Moreover, this feeding system has been realized with a reduced number of planar circuit elements as well as minimal magnitude and phase imbalances, and, has been demonstrated over a wide impedance BW.

3.12 Conclusion and Achievements

A dual-linearly polarized antenna with an integrated feeding network, for FD systems were reported. To summarize, the multilayer antenna consists of four H-shaped slots connected to two slot-line power dividers and two patch antennas placed on top of the slot arrangement. The antenna operates from about 2.2 GHz to 2.5 GHz with reflection coefficients below -10 dB. The maximum realized gain for the transmit and receive ports was 7.8 dBi, for the single-element, with isolation values approaching 60 dB.

As described, the newly reported designs are the only ones that realize double-differential feeding, are fully integrated with the antenna systems, provide wideband operation, and also, achieve the greatest levels of isolation as well as the minimal magnitude and phase imbalances for the planar feeding system. Most importantly, the antenna system does not require external hybrid couplers and the many supporting cable connections, etc. which define the more conventional feeding approach [71,72,88] to achieve similar design goals.

3.13 Full-duplex Antenna Array System Integration

While the antennas were looked at from the point of a single element, beam-steering FD antennas could be of further interest if tracking is required. This could be tracking users to provide charging, radar tracking, or other beam-steering systems. Thus, the proposed full-duplex antennas were configurated into arrays. Particular attention was given to maintaining the isolation and investigating beam steering characteristics.

The external feeding 2×2 antenna array was considered and investigated with some results presented in [103]. Based on that design, the antenna would consist of 16 antenna ports (AP) in total. To further investigate the 2×2 array element coupling, the feed system was simulated with a set of 8 hybrid couplers. The combined S-parameters showed that the cross-coupling between the elements is highest for AP1+AP2 and AP9+AP10 (which relate to antenna elements #1 and #3 indicative of the same polarization) which was at most -20 dB. However, for the orthogonal polarization, which is important when

considering FD operation, coupling between AP1+AP2 and AP7+AP8 (which relate to antenna elements #1 and #2) approaches -30 dB. Similar responses were observed for the other antenna elements due to the symmetry of the array. These results suggest that the antenna is capable of FD beam steering but that additional coupling reduction approaches might be required depending on the isolation levels needed. The remaining S-parameter results for all elements are presented in [103].

From these findings and the architecture of the array, it should be identified that such a beam steering antenna system can be fed in two different ways: 1) as a two-port system when only two couplers and a set of power dividers are employed, and, 2) as an 8-port system using 8 couplers to feed each element. Other feeding systems are possible as well. However, this design makes it not practical and too bulky. The attention was focused on an easier integrated feeding approach with a simplified antenna array feeding design. Thus, the focus shifted to a more feasible design with some integrated feeding systems.

Based on the earlier mentioned design considerations, a new integrated feeding IBFD antenna was proposed in the 4×1 configuration (see Fig. 3.31). The distance between the radiating elements (patches) is $e1$ = 84 mm (0.67 λ_0 at 2.4 GHz) and the extended ground plane has a total size of $d1$ (= 240 mm) by $f1$ (= 452 mm). Similarly to the single element, the antenna array employs 8 integrated differential power dividers realizing an 8-port feeding approach employed on one PCB, where ports 1,2,3,4 represents horizontal and linearly polarized far-fields and 5,6,7,8 represents vertical and linearly polarized far-fields, respectively.

The antenna was manufactured and constructed in-house. The antenna matching for ports 1, 2, 3, 4 of the array can be seen in Fig. 3.32. The antenna is well matched from 2.25 GHz to 2.45 GHz with the matching below -10 dB. Similar responses were observed for ports 5, 6, 7, and 8. Similarly to the 2×2, when designing the FD array, it is important to maintain high port-to-port isolation. From the S-parameter simulations and measurements in Fig. 3.33 of the co-polar elements which generate the same polarization (defining connections to ports 1, 2, 3, and 4), the maximum coupling is about -25 dB or lower (see S12, S13, S14). For the cross-coupling elements (i.e S15, S16, S17, and S18) the highest coupling is between port 1 to port 4 with a value of -42 dB at 2.25 GHz.

The normalized beam patterns for the array can be seen in Figs. 3.34. The cross-polarization values are below 30 dB. Similarly to the single element, the antenna is radiating at broadside for equal phase feeding. The side-lobe levels in the Phi = 90° plane

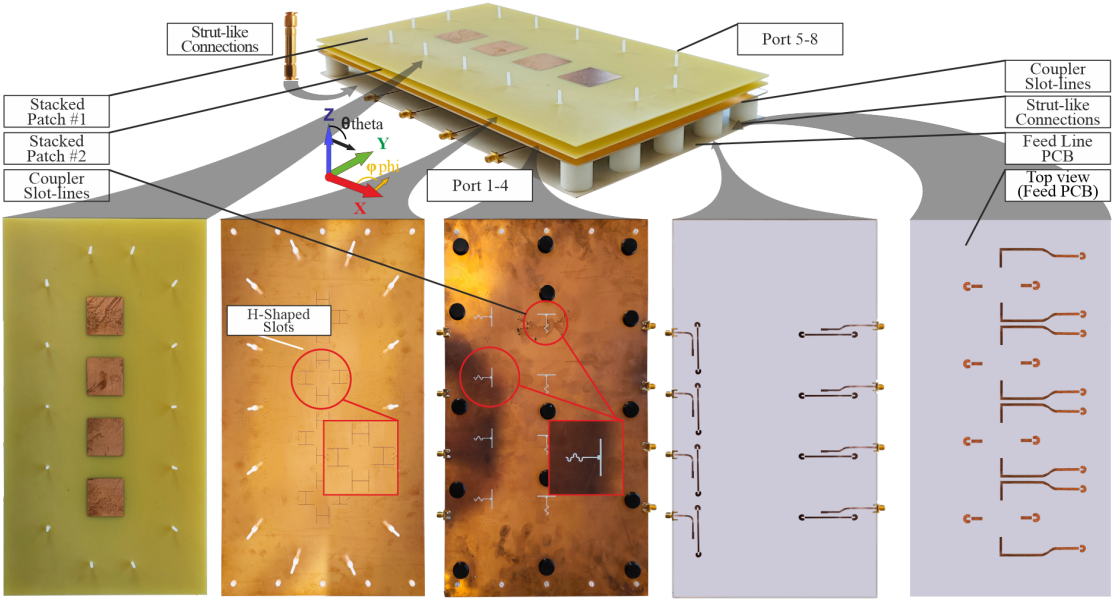

Figure 3.31: Top and bottom view of the proposed 4×1 FD array. The system consists of 4 elements with 2 ports for each element for transmitting and receiving defining 8-ports in total for the array. Here ports 1, 2, 3, and 4 are related to the horizontal and linearly polarized far-fields, while ports 5, 6, 7, and 8 define the other polarization.

are 12 dB below the main beam maximum. However, due to the presence of the strut-like connectors near the antenna elements of P2 and P8 (for example) and the aforementioned asymmetry in the feeding system for each element as well as the back radiation of the H-shaped slots, the matching is no longer consistent over frequency. Similarly, this can also be observed in the simulations of the array when ideal couplers are considered (see Fig. 3.38). It should also be mentioned that when the array was simulated without the external feed system and the many strut-like connectors, the maximum realized gain was about 13 dBi for both polarization states.

Using progressive phase shifts applied to the ports, the simulated antenna array beam steering capabilities are summarized in Tables 3.10 and 3.11 with beam patterns in Figs. 3.36 (similar responses were observed for orthogonal polarization ports). It can be seen that the antenna array is capable of beam steering to 32° for both ports with side-lobe levels 7 dB below, or better, from the main beam maximum (which is related to the element spacing of $0.67\lambda_0$ at 2.4 GHz). As described previously, ports 1,2,3,4 are for linearly polarized radiation in the *x*-*z* plane, and ports 5,6,7,8 are for the orthogonal polarization. Basically, for the array, ports 1, 2, 3, 4 (or 5, 6, 7, 8) can work together to excite the elements and generate the far-field beam patterns which can be steered. When consider-

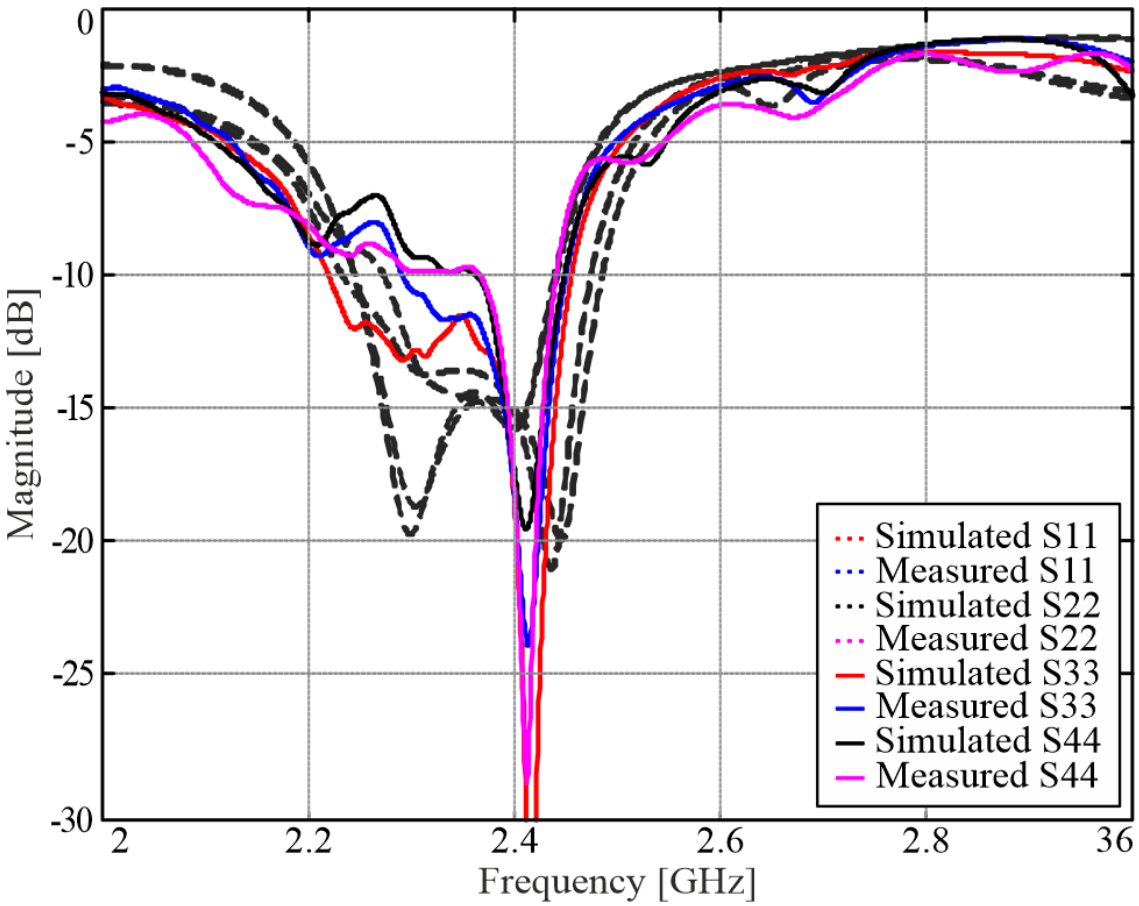

Figure 3.32: Simulated and measured reflection coefficients for ports 1, 2, 3 and 4. The antenna is well matched from 2.25 to 2.45 GHz. Similar responces were observed for ports 5, 6, 7 and 8.

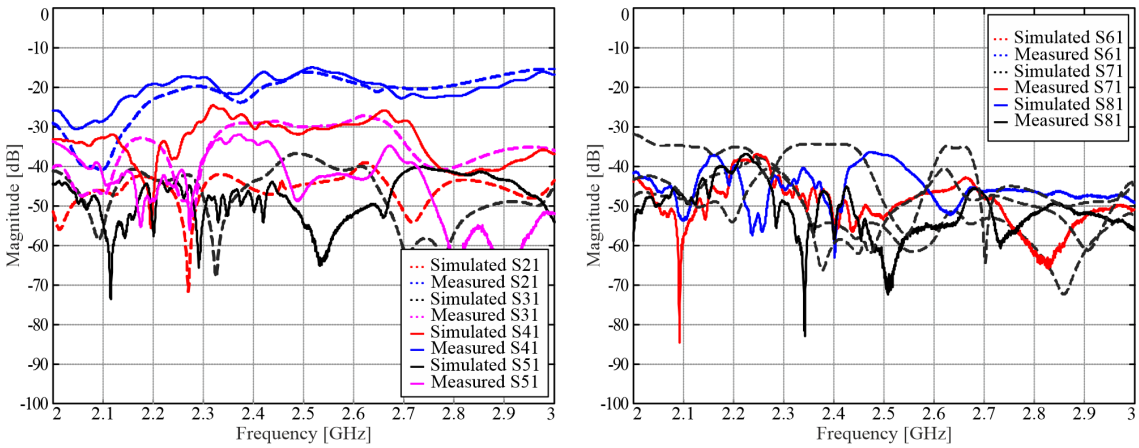

Figure 3.33: Simulated and measured coupling response for port 1. The higher coupling values are related to the same polarization. Thus, the coupling between same polarizaion ports 1 and 2 is around -25 dB.

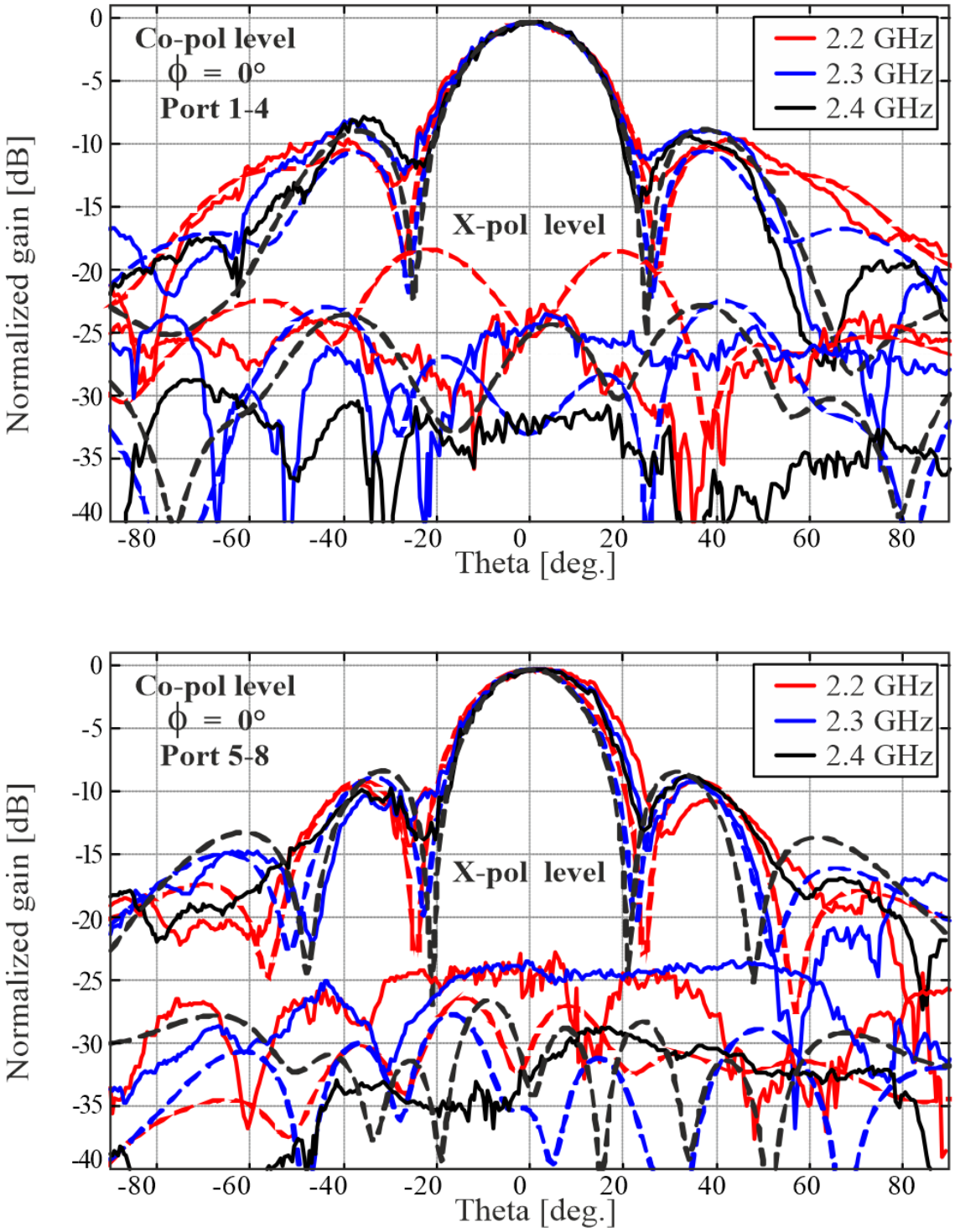

Figure 3.34: Simulated (dash line) and measured (solid lines) normalized beam patterns for ports 1-4 and ports 5-8 at some frequencies.

ing array feeding with ideal power dividers for the system, the isolation is well above 45 dB which is similar to the single-element (see Fig. 3.38). With those considerations, the isolation between the orthogonal polarizations is well above 45 dB.

The antenna beam steering characteristics were investigated with measurements for

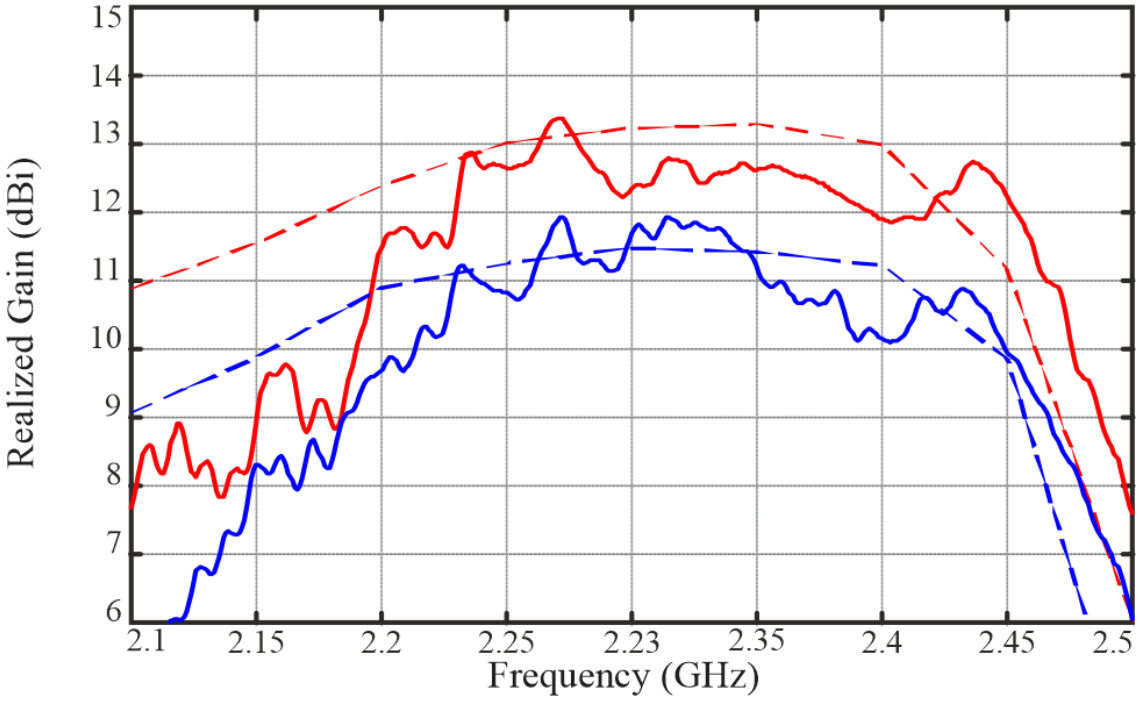

Figure 3.35: Simulated (dash line) and measured (solid lines) realized gain of ports 1-4 and ports 5-8.

Table 3.10: Full-duplex Antenna Array Characteristics Considering Different Steered Beam Positions in the *y-z* Plane for Ports 1, 2, 3, 4

	2.2 GHz				2.3 GHz				2.4 GHz			
Applied Phase	Beam Position	Max. Realized Gain (dBi)	SLL (dB)	Cross-pol. below Beam Max (dB)	Beam Position	Max. Realized Gain (dBi)	SLL (dB)	Cross-pol. below Beam Max (dB)	Beam Position	Max. Realized Gain (dBi)	SLL (dB)	Cross-pol. below Beam Max (dB)
0°	0°	11	-16.3	-38	0°	11.4	-14.7	-31.4	0°	11.2	-12.8	-34
30°	7°	11	-15.3	-30	7°	11.4	-14.7	-30	7°	11.2	-13.1	-30
60°	13°	10.5	-12.7	-28	13°	11.4	-12.1	-31	13°	11.1	-10.5	-27
90°	21°	10	-11.3	-27.9	21°	10.5	-10.7	-31.5	20°	10.7	-9.2	-25
120°	27°	9.4	-11	-29.4	27°	10.3	-12.2	-38	27°	10.7	-9.7	-20.4
135°	29°	8.5	-8.9	-25.8	29°	9.7	-10.4	-42	30°	10.4	-7.7	-24.4

Table 3.11: Full-duplex Antenna Array Characteristics Considering Different Steered Beam Positions in the *y-z* Plane for Ports 5, 6, 7, 8

	2.2 GHz				2.3 GHz				2.4 GHz			
Applied Phase	Beam Position	Max. Realized Gain (dBi)	SLL (dB)	Cross-pol. below Beam Max (dB)	Beam Position	Max. Realized Gain (dBi)	SLL (dB)	Cross-pol. below Beam Max (dB)	Beam Position	Max. Realized Gain (dBi)	SLL (dB)	Cross-pol. below Beam Max (dB)
0°	0°	12.3	-13.3	-45.6	0°	13.1	-13	-53	0°	13	-12.1	-51
30°	8°	12.3	-12.8	-42.3	8°	13.1	-10.9	-45	7°	13	-10.9	-50
60°	15°	12.2	-12.3	-36.2	15°	13.1	-10.4	-39	14°	12.9	-10.8	-39
90°	22°	11.8	-11.4	-34	21°	13.1	-10.6	-37	21°	12.8	-10.8	-36
120°	30°	10.9	-10	-36	28°	12.6	-9.4	-51	27°	12	-7.5	-35
135°	34°	10.45	-7.7	-35.2	32°	9.7	-10.4	-49	31°	12	-5	-37

ports 1-4 and 5-8. The consecutive phase shifts of 90° and 120° were chosen with delay lines attached to the antenna. Measurements for ports 1-4 for frequencies 2.35 and 2.45 GHz are presented. Some higher size beamwidth responses for the 120° delay lines are related to the slight shift by about 4° of the delay lines.

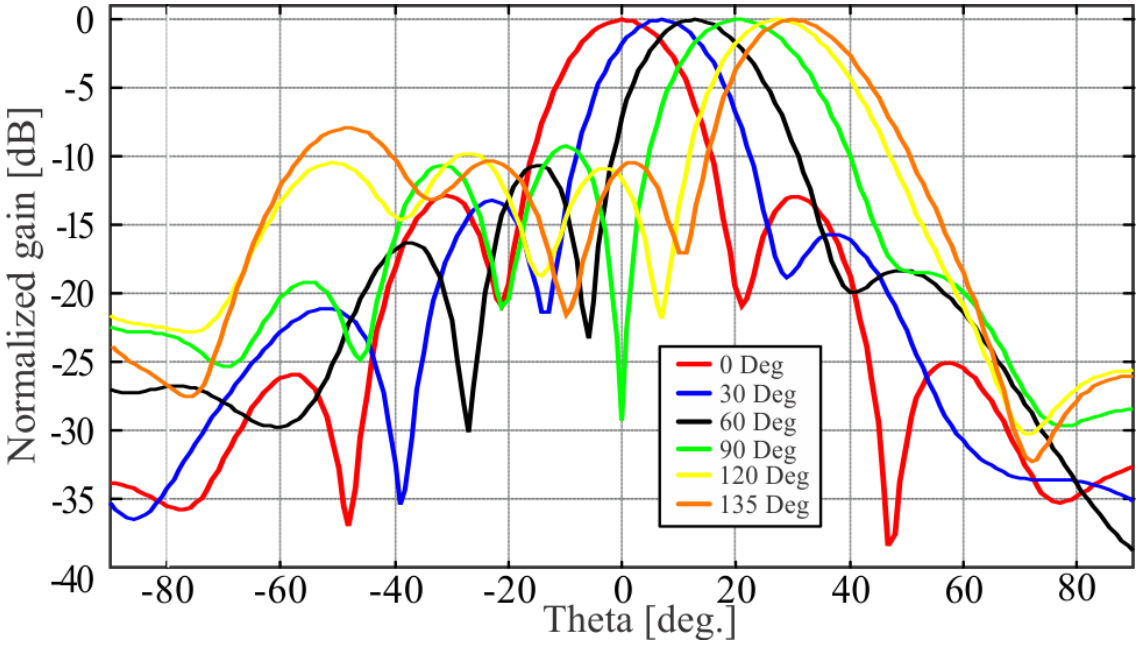

Figure 3.36: Simulated beam steering capabilities at 2.4 GHz whilst driving ports 1, 2, 3, and 4 for the 4×1 array using the considered phase shift definitions as in Table 3.10. Similar responces were obtained when steered driving ports 5, 6, 7, and 8.

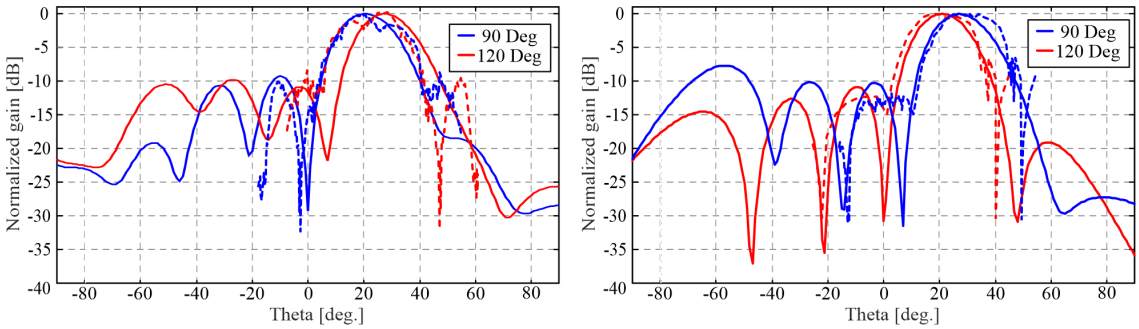

Figure 3.37: Simulated (dash line) and measured (solid lines) beam steering for ports 1-4 of the frequencies of 2.35 GHz and 2.45 GHz using delays lines defined in the inset. Simular responces were observed for ports 5-8.

3.14 Manufactured Results of the Integrated Feeding 4×1 Array

The proposed multi-layer antenna array structure was manufactured and measured. The photo of the array in the exploded view can be seen in Fig. 3.31. The antenna was configured for a dual-polarization setup, in particular, a two-port system measurement using two 4×1 power dividers connected to every 4 ports on the antenna sides (P1-P4 and P5-P8). The response of the antenna in this configuration can be seen in Fig. 3.38. The antenna is well matched from 2.2 to 2.45 GHz with reflection coefficients below -10

dB. The isolation levels vary from 42 to 65 dB over the operational bandwidth. This response is similar to a single element. The antenna gain beam patterns at frequencies 2.2, 2.3, and 2.4 GHz are close to what was simulated with side lobe levels below -9 dB (see Fig. 3.34). The measured and simulated realized gain can be seen in Fig. 3.37, showing that P1-P4 gain is higher than P5-P8 by almost 2 dBi. This is related to the fact that there is slight strut interference, the distance between the elements for polarization ports P5-P8, and other manufacturing tolerances.

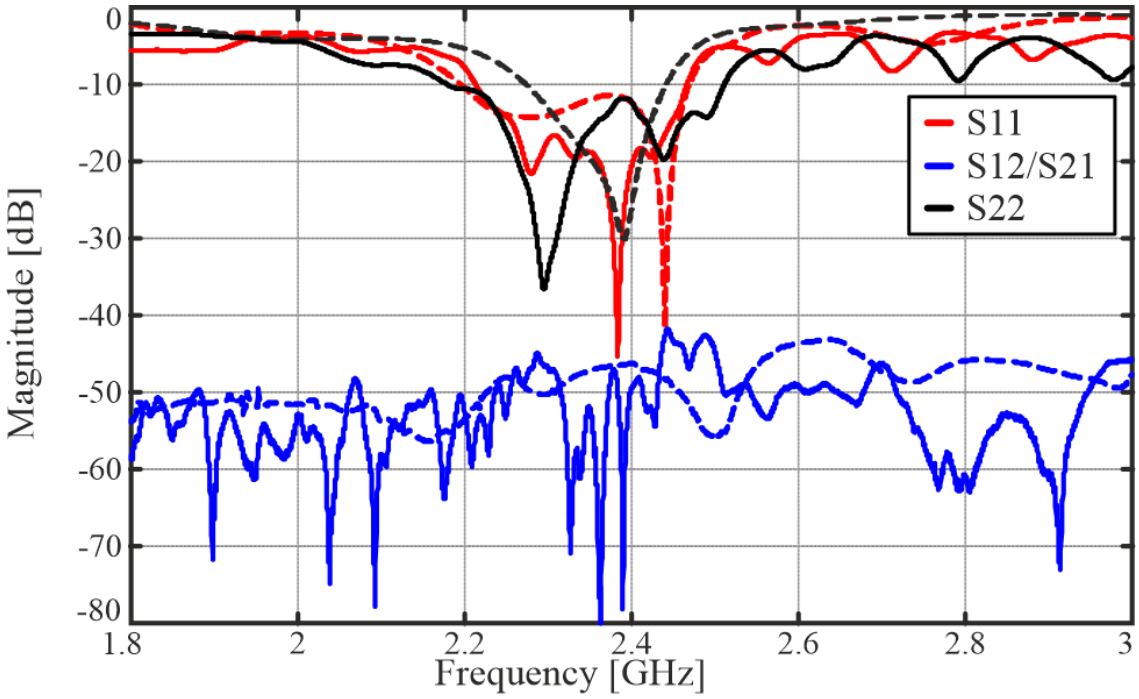

Figure 3.38: Simulated (dash line) and measured (solid lines) S-parameters of the array configurated into the dual-polarized mode using a set of external 1×4 power dividers.

3.15 Chapter Summary

In this chapter, in-band Full-duplex antennas were proposed and investigated. Those antennas can be well used in the WiFi S-band and deliver high port-to-port isolation. A novel meandered slot-line coupler for phase and magnitude stability was also proposed. The reported multilayer antenna, which was expanded to arrayed configurations for beam steering, can be considered a good alternative to the other full-duplex single-element and array systems previously reported in the literature. Good matching and wideband response will help to relax the isolation layers for full-duplex systems. This foundation will be helpful in new IBFD antennas and other RF circuitry designs. In the next thesis

chapter, other antenna systems will be investigated which operate at millimeter-wave frequencies. These designs are also applicable to 5G/6G systems and the related for FD communications.

Chapter 4

Full-duplex Antenna Systems which Operate at Millimeter-wave Frequencies

4.1 Introduction

In this chapter, 5G dual-polarized slot antennas and arrays for Full-duplex systems will be investigated. The first part will focus on 5G communication systems in this band and its potential benefits related Internet of Things (IoT) technologies. Additionally, theoretical considerations for the proposed prototype such as substrate integrated waveguide (SIW) and tapering techniques are investigated. Also, some recent works in the mm-wave frequency range for FD will also be compared against the proposed.

The second part will present developments of a new single-layer dual-polarized slot antenna with sum and difference beam patterns and high isolation at the ports. Antenna reconfigurability will also be investigated showing isolation for common and differential feeding configurations. The antenna was also compared with existing in the literature review showing design simplicity and phase control via the external coupler. The third part focuses on the redesign of the antenna and configuration into the 4×1 array for beam steering scenarios. The array retains a similar sum and difference beam pattern response and also provides reasonable isolation levels. An external Butler matrix beamformer was also used to investigate beam-steering capabilities, and up to $\pm55^{\circ}$ angles. This can be used in retro-directive arrays, dual-polarized radar systems, or other user-tracking communication interfaces. In the final part, the achievements of this work will be highlighted and potential antenna improvements are proposed.

4.2 5G Communications and Full-duplex for Millimeter-wave Frequencies

The microwave and millimeter-wave frequency bands can offer high data capacity throughputs and Gigabit transmission speeds for modern 5G communications, monopulse radar tracking systems, and direction of arrival estimation [104–109]. Additionally, 5G offers lower latencies and high data rates suitable for Internet of things (IoT) devices

and automotive radar with communications, for example, where information can be analyzed on flight [110, 111]. For these modern and complex scenarios, monopulse and dual-polarization antennas as well as full-duplex (FD) setups can offer significant advancements when compared to more standard single-polarization, half-duplex, and simplex versions. This has made polarization-diverse systems and in-band FD antennas a topic of interest.

5G applications can be useful in many different fields [112] such as in the entertainment sector to the high speed of data transfer. 5G networks are also applicable in cloud gaming. Games are streamed from the cloud with such 5G connectivity. This can mean that there is no significant input lag (delay in control) and this is critical for gaming. 5G is also associated with the smart homes and (IoT) technologies. Today you can find many devices that connect to the IoT: light bulbs, sockets, locks, speakers, and household appliances. For everything to work in a single technology ecosystem without delay, you need a good connection with a high data transfer rate. In the medical sector with the help of 5G, it is possible to conduct surveys with patients that may be of interest to people. The doctor will receive all the important information before the tactile connection, as at present. In transportation systems, 5G can help in the development of smart or unmanned vehicles. It will be possible to interact with smart roads, traffic lights, parking lots, and road signs. All data will be transferred and stored in the cloud [113].

However, while 5G is a well-established concept and currently under deployment in some countries, full-duplex (FD) antennas can offer critical physical layer advancement when compared to more standard half-duplex and simplex versions, making once again, antenna design a topic of interest. FD is also a well established concept which can offer simultaneous signal reception and transmission with applications to both communications and radar, however, some challenges still remain [104–106, 114–117]. For example, self-interference (SI) is a problem that must be overcome to support further 5G/6G development and make FD systems practical. Mitigation techniques for SI by approaches in the digital domain or by the appropriate signal processing [118], [119], are known, but there are still outstanding technical challenges.

4.3 Design Considerations for Millimeter-Wave Technologies and Antennas

In the millimeter-wave frequencies (mm) the low-frequency techniques could be challenging to apply. Particularly, the high manufacturing tolerances, higher cost, and overall

higher losses could be an issue when designing microwave components at mm-wave frequencies. Such barriers are also seen in the construction of 5G networks. The cost of equipment and electricity consumption of those devices are high which delays the expansion of the network in the developed countries. Thus, new types of technologies need to be used to reduce the overall cost and improve manufacturing. Particularly, in the antenna field, the narrow-band patch antennas can not be well used at mm-wave frequencies. This would require precise manufacturing as the narrow bandwidth might shift the frequency. The feeding network such as probe feeding is also not easy to implement such as pockets of air or small misalignments can be crucial in the antenna design, resulting in the beam tilting or cross-polarization issues.

In the world of antennas, a new well established technique and technologies in the mm-wave frequencies could be Substrate Integrated Waveguide (SIW) technology [120]. The SIW waveguides are relatively new microwave components that represent conventional metallic waveguides, but use lower cost substrate materials with metalized via elements. Other options could be leaky-wave antennas which have wideband response over frequency [121]. The first such antennas used metal structures [122]. Earlier in the 90s, these types of antennas were not very popular. The material was very expensive and such antennas were too complicated. To date, LWAs are experiencing a second birth, which to a large extent is associated with the use of modern and inexpensive dielectric materials and appearance of modern calculation capabilities. The modern development of low-cost basic dielectric materials allows the development of new types of effective LWAs with very high performance indicators [121]. Finally, the metasurface or metamaterial antennas [123], where the unit-cell acts like artificial layer elements serving to compliment radiation. Those antennas, similarly to LWAs can use surface waves for feeding and radiation.

4.4 SIW Waveguide and Taper

A waveguide is an artificial or natural channel capable of supporting waves propagating along it, whose fields are concentrated inside the channel or in the area adjacent to it [124], [125]. A post-wall waveguide (also known as an SIW, or a layered waveguide) is a synthetic rectangular electromagnetic waveguide formed in a dielectric base, tightly aligning metallized vias or through holes that connect the upper and lower metal base plates. A waveguide can be easily manufactured with low-cost and mass production us-

ing methods through a hole, where the postal walls consist of through fences. The SIW, as is known, has a similar controlled wave and has features similar to a conventional rectangular waveguide with an equivalent controlled wavelength. Also, SIW has low conductor loss and high power capabilities but potential drawbacks include leakage and dielectric losses when compared to bulky rectangular waveguides [125]. SIW structures also retain their benefits as compared to classic waveguides; i.e. high transmit power, low loss, fully shielded structure, high quality resonators [126]. SIW also acquires the features of planar structures: small size and weight as well as low production costs [127].

The design of the SIW line is analogous to the rectangular waveguide for TE_{10} mode propagation. The design approach consists of choosing dimensions for the pitch (distance between vias) and diameter of the vias [120], [124]. The first step is to determine the frequency at which the device will operate and this should be above the cutoff frequency f_c for the waveguide. With this, the major dimensions of the waveguide a and b can be found. The next step is to calculate the guided wavelength based on the type of material choice [124]:

$$\lambda_g = \frac{2\pi}{\sqrt{\frac{\varepsilon_r(2\pi f_c)^2}{c^2} - (\frac{\pi}{a})^2}} \tag{4.1}$$

where: λ_g - guided wavelength, ε_r - relative permittivity of the material, c - speed of light it the vacuum.

The design of the SIW line should also be verified by simulations in a commercial full-wave solver such as CST. For example, these equations do not take into consideration the possible leakage between the vias, and this can make the SIW lines not function as expected. Also when manufacturing SIW devices, it is important to consider the possible errors that can be associated. For example, among the main reasons the occurrence of inaccuracies is related to the geometric dimensions. This can be related to the size of the holes, errors in the thickness of the waveguide and the via location. Regardless of these challenges, the design of SIW and FD antennas was reported in this chapter.

To connect the SIW line it is also important to design a mating to a 50-Ω microstrip line. This can be made possible using a taper, and this allows connections to coaxial probes for external measurements. Such a tapering can also connect the microstrip line part to the SIW line [128], [129]. In practice, good design of the taper consists of a quarter-wave line and width (for the connection side of the tapper) to be a 50-Ω line with minimum losses. Typically, the impedance of the SIW line is around 320-Ω. Ta-

pering also allows for a better impedance matching of the microstrip line to SIW. Also, microstrip supports a quasi-TEM mode while the dominant mode for SIW is the TE_{10} mode.

4.5 Slotted Waveguide Antenna Arrays or Series-fed Slot Arrays

Series-fed slot arrays, also called slotted waveguide antenna arrays, are typically made using some type of waveguide. They have been popular for communication systems or radar applications due to their high-power capability [22]. These types of antenna arrays offer some advantages such as high efficiency, low profile, and high gain. To maximize these parameters it is important to optimize the slot positions and dimensions [130]. This typically depends on what radiation angle or pattern needs to be achieved. One of the first implementations was reported in [131]. That work considered every slot module and its load impedance in the design. Furthermore, an equivalent circuit model was developed with a focus to analyze the mutual coupling between slot elements. Also, classical array theory was adopted and implemented based on the array factor for a network of dipole antenna elements [22].

There are two conventional types of slot antenna arrays. The first being the standing-wave type [22] which is usually terminated with the wall, while the second is the traveling-wave type which is usually terminated with a load [132]. The traveling wave implementation can be used in leaky-wave antenna design and these apertures offer beam scanning characteristics over frequency, while the standing wave type usually offers broadside radiation.

For the full-duplex communication systems, it would be preferable to use broadside radiation which makes the standing-wave design preferable (see Fig. 4.1 for a representation). The first step in the implementation of the array is to design a single slot of length L which will dictate the operating frequency. The design process for the individual slot antenna element was discussed earlier in the thesis. The second step is to introduce the next slot and add offsets in the x- and y-directions to reduce coupling between slots. Typically, the distance between slots is around $\lambda_g/2$. Finally, the distance between the wall and the last slot is usually around $\lambda_g/4$. The width W can control the leakage rate of the antenna, while tapering techniques can improve performance such as reducing reflections at the input port and minimizing side-lobe levels [133], [134]. With the increase in the number of slots n, the antenna gain increases due to the increased aperture size, and band-

width narrows [135], [136]. Thus a balance must be considered depending on the design requirements between bandwidth, gain, array size.

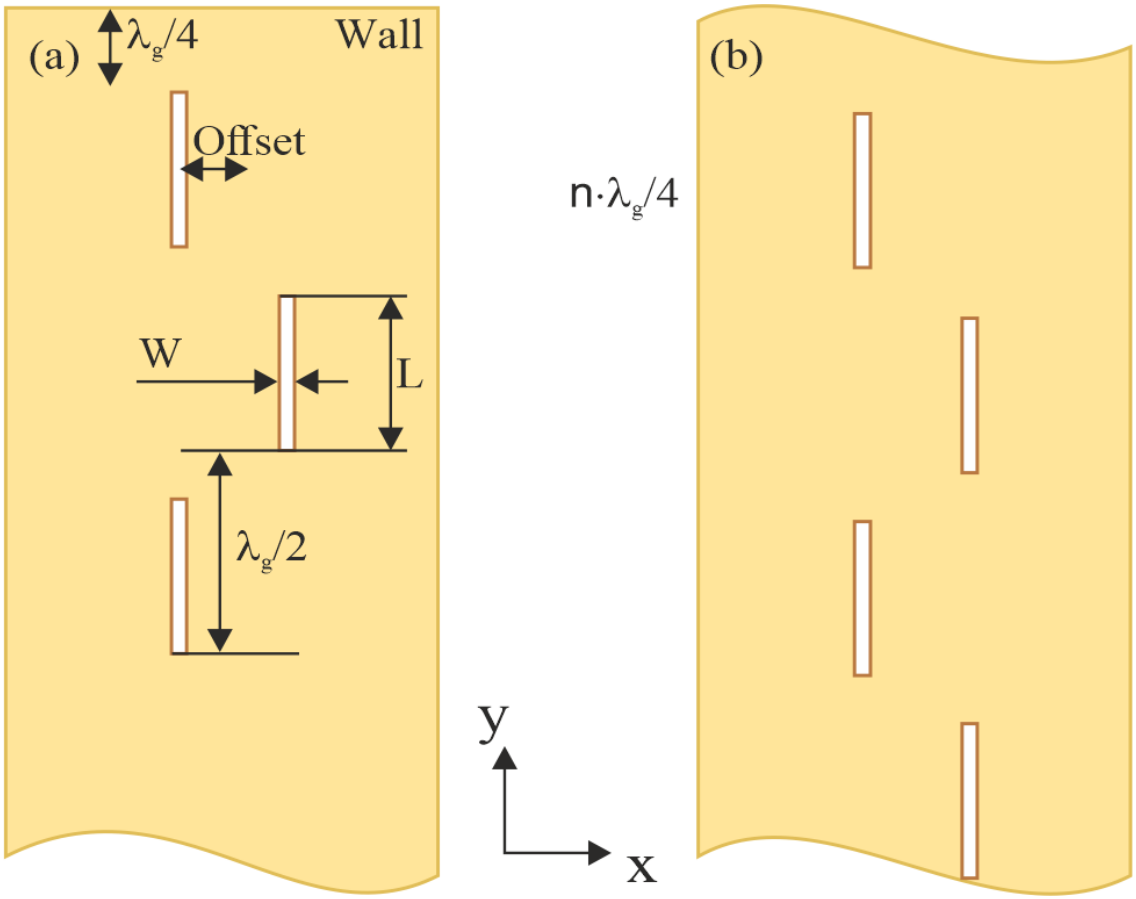

Figure 4.1: Example of slots in a waveguide defining a series-fed slot antenna array: a) standing-wave slot type due a shorting-wall termination, b) traveling-wave type which is representative of leaky-wave antennas (no load termination shown in the diagram). Based on [22] and [132].

4.6 Literature Review

Polarization diversity and FD systems are well established concepts which can support simultaneous signal reception and transmission by signal orthogonality, however, some technical challenges still remain [104–106, 114–117]. As previously mentioned, isolation and self-interference (SI) are problems that must be overcome and mitigation techniques can include the appropriate signal processing [118], [119]. These are needed to achieve efficient simultaneous transmission and reception (STAR). One such antenna using a multi-layer configuration was proposed in [137]. The structure was matched from 27.6 to 29.5 GHz with isolation levels up to 60 dB. In [86] an ultra-wideband antenna with

monocones and bent loops was proposed. Using an external coupler system, the reported antenna matching bandwidth (BW) was 98% with isolation over 50 dB. Another Ka-band design was reported in [138] where a dual-polarized antenna with a lens system was proposed. The antenna consisted of a circulator-based feeding network, a dual-polarized horn, and a spherical lens. Isolation values were 30 to 50 dB. In [139] a W-band reflectarray was reported with isolation levels of almost 70 dB. Similar to [137], [139] also employed a multi-layer pillbox transition system for feeding.

4.7 SIW Sub-arrays with Dual-polarized Monopulse Patterns for Full-duplex or Diversity Applications

Following these developments, and in this thesis part, a new high isolation slot array antenna offering dual-polarization, equal and differential feeding, and high isolation for 5G in-band full-duplex (IBFD) applications is presented (see Fig. 4.2). The single-layer structure consists of series-fed SIW slot arrays oriented in a cross-shaped setup. Also, the proposed design exploits dual-differential feeding to achieve -10 dB matching from 23.2 GHz to 25.3 GHz and the isolation between activated and passive ports in differential mode is around 70 dB. In the equal power split mode, it is above 34 dB. For differential feeding, the maximum simulated realized gain is around 14 dBi while the simulated cross-polarizations are well below 30 dB or lower from the main beam maximum. With an equal power split the maximum realized gain is around 13 dBi with the cross-polarization levels below -20 dB. To the best knowledge of the author, no similar antenna configuration has been previously reported offering high isolation in the K-band, capable to produce sum (equal power split) and difference (differential power split) beam patterns, and can enable high-data-rate transfer for in-band full-duplex systems.

In an effort to provide a new antenna design suitable for 5G communications, FD systems, radar tracking systems, etc., which offers dual-linear polarization and high isolation (reaching values of 95 dB), this chapter reports on an alternative and more advanced configuration when compared to the classic monopulse antenna presented earlier in [140], for example. That work employed a 1-D linear array of series-fed microstrip patches and bi-directional feeding. The newly proposed dual-polarization 2-D antenna is outlined in Figs. 4.2 and 4.3, and uses series-fed slot arrays in substrate integrated waveguide (SIW) technology. Moreover, the SIW structure is realized by the appropriate placement of four sub-arrays orientated in a cross-shaped network. With this configuration, and

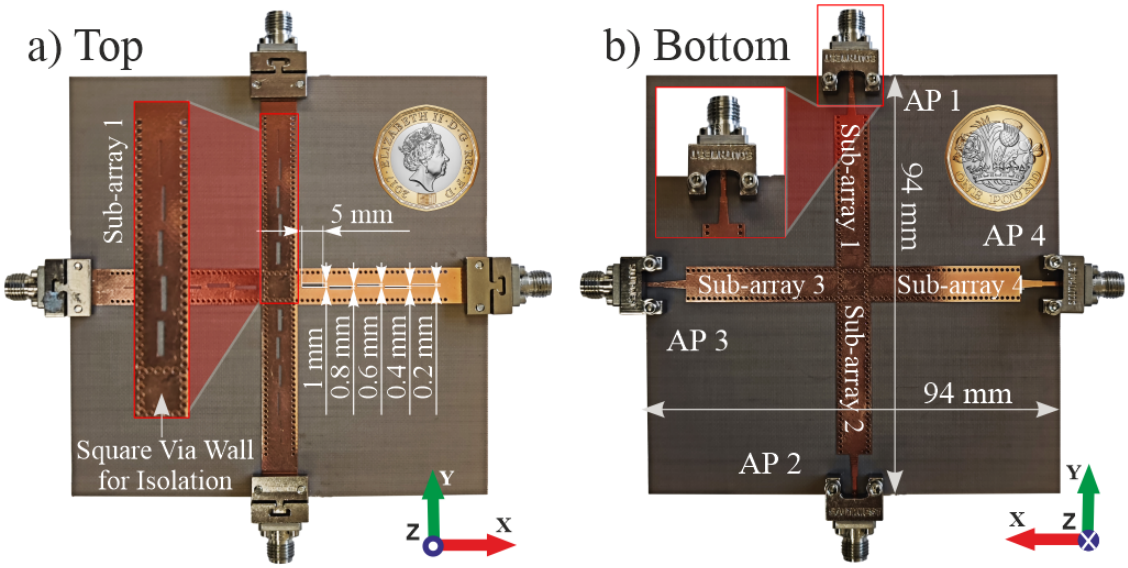

Figure 4.2: Proposed planar SIW-based antenna. The structure is defined by two pairs of sub-arrays, one for each polarization. Also, the series-fed slots have tapering for improved radiation. With dual-differential feeding and co-location of the sub-arrays, the four-port SIW array can support FD operation.

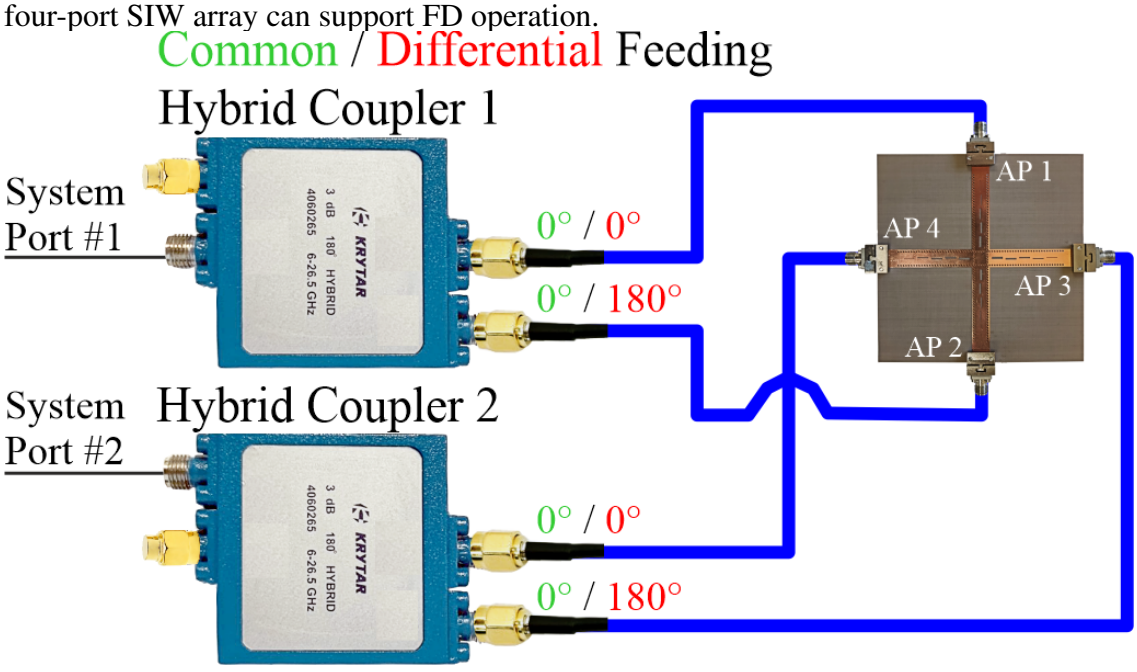

Figure 4.3: Possible feeding configurations for AP1+AP2 and AP3+AP4 defining the vertical (y-z) and horizontal (x-z) states of antenna operation, respectively. See also Table 4.2 which outlines the generated far-field patterns.

also by the appropriate dual-differential or dual-common feeding (see Table 4.2), sum or difference FF beam patterns; i.e. Σ or Δ (or both) are respectively made possible with dual-polarization.

As outlined in Table 4.1, the newly reported design is compared to existing K-band antenna systems as found in the literature. As it can be observed, the proposed SIW

antenna offers the highest levels of isolation with the lowest cross-polarization levels (-30 dB or more) for the monopulse sum and difference patterns, and, over the largest BW (≈10%). To the best knowledge of the authors no similar antenna configuration, with similar metrics and possible beam patterns with different polarization states, has been reported previously.

4.7.1 Design Considerations and Simulations

The proposed planar antenna consists of a simple and compact arrangement of sub-array SIW slots (series-fed), positioned in a cross-shape orientation as shown in Fig. 4.2. The SIW lines can be driven with an internal feeding circuit or connected to a conventional 50-Ω microstrip transition for external feeding (see Figs. 4.2 and 4.3). In addition, tapering is used when designing the slot widths for each sub-array to improve matching and decrease the sidelobe-levels (SLLs). By this configuration, the horizontal and vertical SIW branches offer controlled leakage, and isolation values are 50 dB (or more) over the operating band of the antenna. The PCB material choice was Taconic TLY-5 with a relative permittivity of 2.2 and a thickness of 0.51 mm. Should it be required, antenna gain can also be improved by increasing the number of slots and this follows conventional SIW series-fed slot array design. Also, the antenna structure was designed and simulated in CST microwave studio and the results are in Figs. 4.4 to 4.6.

The antenna configurations for different polarization states can be seen in Fig. 4.3 with responses compiled in Table 4.2. When the antenna was excited considering dual-common feeding as applied to antenna ports 1 (AP1) and 2 (AP2), or antenna ports 3 (AP3) and 4 (AP4), a difference-like FF beam pattern (Δ) can be realized in both principal planes. In addition, this setup defines a dual-linearly polarized antenna which can be useful for monopulse. The F-parameters (or active S-parameters) can be observed in Fig. 4.4 where the antenna is well matched from 23.2 GHz to 25.3 GHz and the isolation reaches 40 dB at 23.5 GHz. The antenna beam patterns are reported in Fig. 4.6 and the cross-polarization levels are 30 dB below (or more). The realized gain of the antenna reaches 13 dBi while the simulated total efficiency is more than 85% and 90% when connectors were respectively included and excluded in CST.

When dual-differential feeding is applied, dual-linearly polarized radiation is made possible with a FF sum pattern (Σ). The F-parameters can be observed in Fig. 4.4 with -10 dB matching from 23.2 GHz to 25.3 GHz and with isolation levels of more than 85

Table 4.1: Comparison of the Proposed Design to other High Isolation Structures with Dual-polarization (Measured Results)

	Frequency Range	[1]Matching 50-Ω BW	[2]Isolation Range	Element Size (Lowest Freq.)	Structure Size (Lowest Freq.)	Max Gain (Realized)	Radiating 3 dB BW	X-pol. Level	Feeding Type	Single-element or Array (External Ports)	FF Beam Patterns
[73]	4.75 to 5.18 GHz	9%	50 to 58 dB	N/A	3 by 2 λ_0	13.1 dBi	20%	<-24 dB	Single-diff.	Planar (Array, 2-port)	Directive
[86]	0.5 to 2 GHz	98%	40 to 55 dB	3.5 by 3.5 λ_0	6 by 6 λ_0	5.5 dBi	43%	<-10 dB	-	Metal (Array, 5-port)	Broad
[137]	27.8 to 29.5 GHz	5%	51 to 78 dB	7 by 0.37 λ_0	11.7 by 11.7 λ_0	24 dBi	6%	<-27 dB	Dual-diff.	Planar (LWAs, 2-port)	Directive
[138]	26.5 to 29.5 GHz	10.7%	28 to 50 dB	1.4 by 0.7 λ_0	10 by 20 λ_0	25.5 dBi	7%	<-10 dB	-	Metal (Single, 2-port)	Directive
[139]	93 to 96 GHz	3.2%	55 to 72 dB	0.37 by 0.37 λ_0	22.3 by 22.3 λ_0	31.8 dBi	3.2%	<-28 dB	Dual-diff.	Metal/Planar (Array-like, 2-port)	Directive
Prop.	23.2 to 25.4 GHz	9%	48 to 62 dB	0.38 by 0.07 λ_0	7.2 by 7.2λ_0	13.0 / 14.0 dBi	10%	<-30 dB	Diff. + Comm.	Planar (Sub-arrays, 4-port)	Σ+Δ (Directive)
Prop.	23.2 to 25.4 GHz	9%	32 to 52 dB	0.38 by 0.07 λ_0	7.2 by 7.2λ_0	14.0 dBi	10%	<-30 dB	Dual-comm.	Planar (Sub-arrays, 4-port)	Δ (Directive)
Prop.	23.2 to 25.4 GHz	9%	60 to 90 dB	0.38 by 0.07 λ_0	7.2 by 7.2λ_0	13.0 dBi	10%	<-35 dB	Dual-diff.	Planar (Sub-arrays, 4-port)	Σ (Directive)

[1]The transmit and receive ports -10 dB impedance BW; i.e. where the reflection coefficients are -10 dB (or below) for the external ports of the antenna system (defining the shared BW). For an illustration of such external ports, see Fig. 4.3.

[2]The corresponding isolation range refers to the external port isolation for the antenna system while the port reflection coefficients are -10 dB (or better)[1].

Table 4.2: Possible Feeding Configurations and Generated Patterns

Circuit Phase Feeding	Vertical y-z Plane (Polarization State #1)	Horizontal x-z Plane (Polarization State #2)	Far-field Patterns in the y-z and x-z Planes
Dual-Common	AP1+AP2 (0°)	AP3+AP4 (0°)	Difference
Dual-Differential	AP1+AP2 (180°)	AP3+AP4 (180°)	Sum
Differential + Common	AP1+AP2 (180°)	AP3+AP4 (0°)	Sum and Difference
Common + Differential	AP1+AP2 (0°)	AP3+AP4 (180°)	Difference and Sum

dB. Also, the simulated electric field within the substrate is shown in Fig. 4.5a) and it can be observed that minimal leakage occurs to the vertical SIW transmission line branch. Like this dual-differential feeding case, leakage of the fields is also minimal (see Fig. 4.5b)) for dual-common feeding. Also, the sum patterns are reported in Fig. 4.6b).

To further discuss the design choices for the proposed structure, it should also be mentioned that additional studies were completed prior to fabrication. For example, when the antenna was simulated with practical connectors (SuperSMA [141]), it was noticed that minor ripples were observed in the beam pattern. Further simulations indicated that parasitic surface-wave fields were generated by the connector and transition (similar to [142]). To minimize these effects, the majority of the ground planes were removed (whilst maintaining the SIW transmission lines and the square PCB shape). This slightly reduced antenna gain by about 0.4 dBi and increased the SLL by at most 1.2 dB. However, alternative design choices increased the SLL by more than 1.5 dB; i.e. SLLs increased to 7 dB which we deemed not acceptable. Regardless of these considerations, the main SLL for the final design with connectors was 7 dB (see Fig. 4.6(b), at 24 GHz) in the worst case and more than 12 dB at 25 GHz (at best).

It should also be noted that the center radiating slots elements for the vertical and horizontal SIW branches were removed and isolation vias were added, mainly, to enable array co-location whilst maintaining symmetry and defining the sub-arrays. Moreover, this square via ring arrangement (see inset Fig. 4.2a)) supports isolation and dual-polarization as in [143]. This an important design feature, which in our understanding has not been employed previously for SIW slot arrays.

If a more conventional design and feeding approach was implemented for the series-fed arrays, as in [140], all the SIW transmission line sections would need to maintain the center radiating slots and no center square via ring would be included. Most importantly, and without this simple isolation element (see Fig. 4.2a), the co-location of the vertical and horizontal SIW branches would not be possible. It should also be mentioned that we carried out studies without this square via wall, and results suggest that the isolation can increase to more than 6 dB (results not reported for brevity). This significantly decreased

the performance of the antenna making it not suitable for polarization diversity and FD applications.

Due to the noted missing elements at the center of the structure, a higher SLL is observed in the FF, which is more problematic for the dual-differential feeding case. For example, SLLs are about 7 dB (or lower) as shown in Fig. 4.6(b). While it is indeed possible to design a dual-polarized slot [144], the required dual-layer configuration will contribute to a higher cost, potential alignment errors, and other manufacturing tolerances that could be problematic when operating at microwave and millimeter-wave frequencies.

In an effort to improve the SLLs, tapered radiation of the slots was introduced and it was noticed that this helped to provide better matching than without. Also, additional simulations were completed to investigate how the number of slots can help to minimize the SLL. In our prototype, there are 10 elements in total for the vertical and horizontal SIW branches (5 per each sub-array), and as mentioned, SLLs of about 7 dB (in the worst case) were observed at 24 GHz. When considering 20 elements per branch, the SLL level improved to 8.5 dB, and finally, when considering 32 slot elements the SLL level reached 10 dB (in the worst case) at this same frequency. However, the matching impedance BW became narrower and since we are trying to make a competitive design when compared to other dual-polarization antennas in the literature (see Table 4.1), we chose to manufacture a prototype for proof-of-concept with 5 slots per sub-array (10 per branch, see Figs. 4.2 and 4.3). Basically, a compromise was chosen between SLL and the -10 dB impedance matching BW.

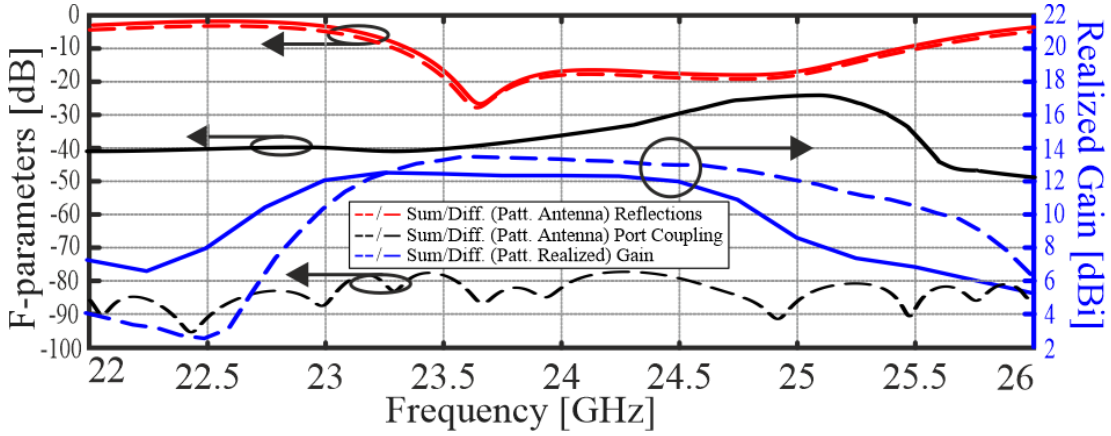

Figure 4.4: Simulated active S-parameters (or F-parameters from CST) for the different pattern types: sum pattern (dashed line) and difference pattern (solid line). This respectively corresponds to 0°+180° and 0°+0° phase shifts applied to AP1 and AP2 (see Table 4.2). The peak realized gain is also shown (right axis). Analogous results are observed when feeding AP3 and AP4.

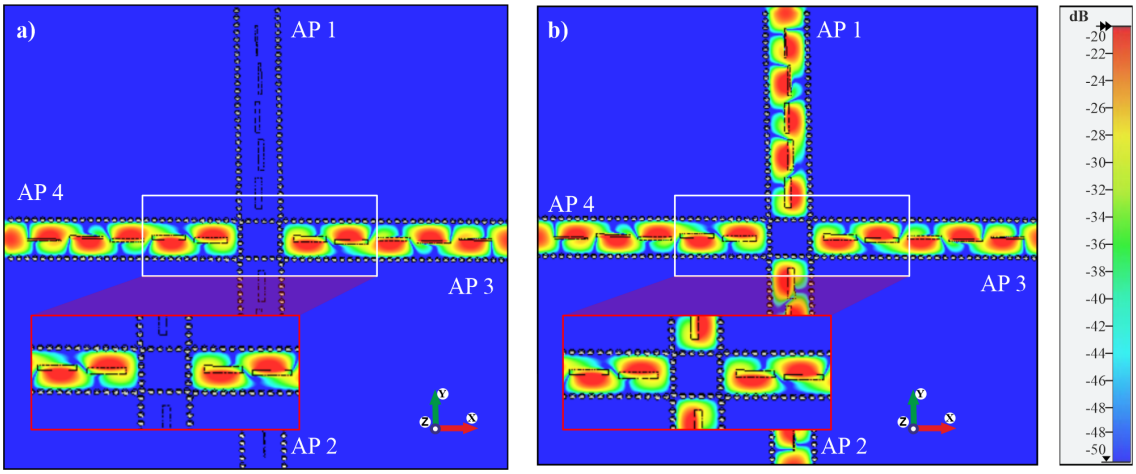

Figure 4.5: Simulated electric field at 24 GHz (inside substrate) a) 0° and 180° applied to AP3 and AP4 (differential feeding), b) 0° and 180° phase shifts applied to AP3 and AP4, 0° and 0° applied to ports AP1 and AP2 (common and differential feeding). Good isolation can be observed for both cases.

4.7.2 Antenna Measurements and Discussions

The radiation performance of the antenna was measured using the NSI-2000 near-field planar scanner and the diamond engineering DAMS-7000 FF positioner. The measurements for common and differential feeding (as applied to AP1 and AP2) can be seen in Fig. 4.7. Similar results were observed for AP3 and AP4 for the other polarization states. The slighly higher cross-polarization levels (when compared to the simulations) are most likely related to some minor phase imbalances of the coupler, cable bending connections, and other practical tolerances. Regardless, the simulated and measured realized gain is in good agreement as observed in Fig. 4.8 with values about 14 dBi and 12 dBi for the sum pattern (differential feeding) and the difference patterns (common feeding).

The active S-parameters measurements were completed using a Keysight PNA (N5234A). Measurement results are compared with simulations in Fig. 4.9. The passive reflection coefficient was first measured for the antenna showing that the antenna is well-matched with a -10 dB impedance BW from 23.2 GHz to 25.4 GHz. To measure the coupling coefficients (or isolation) for the antenna system as outlined in Fig. 4.3, two external couplers (Krytar 4060265 [145]) were used for the common and differential feeding arrangements. It should also be mentioned that ideal couplers were defined in CST. Regardless, results are in general agreement.

When both couplers are connected for a common power split (difference beam pattern), the measured isolation is less than about 50 dB. When both couplers were configured for the dual-differential feeding case (sum patterns), the simulated response showed

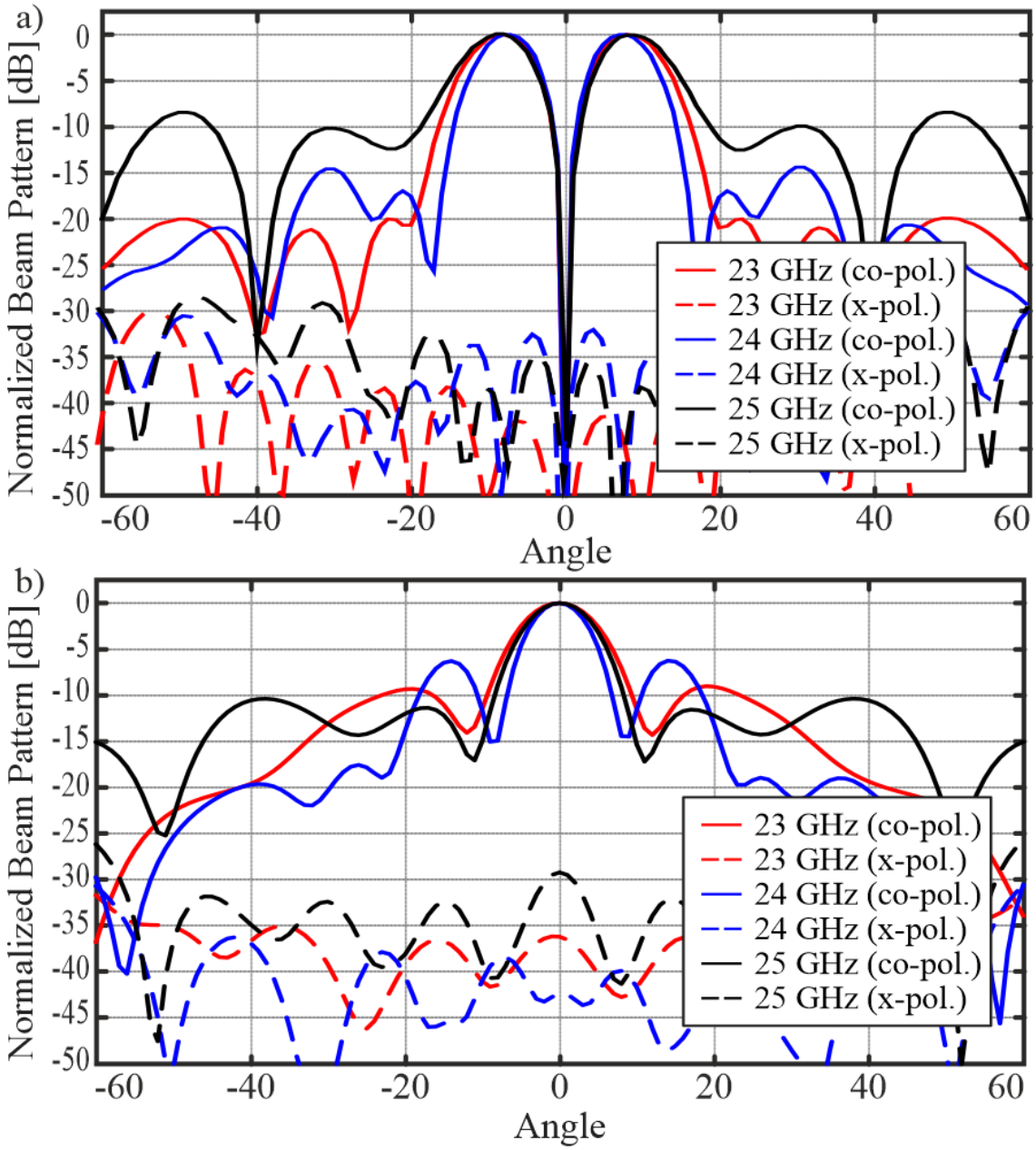

Figure 4.6: Simulated far-field patterns (normalized) in the *y*-*z* plane, with the applied phase shifts at AP1 and AP2: a) 0° and 0° (difference pattern), and b) 0° and 180° (sum pattern). Analogous results were observed in the *x*-*z* plane for AP3 and AP4 with similar feeding.

more than 80 dB of isolation, while the measurements only showed values of 60 dB (or more approaching 90 dB near 24 GHz). Lastly, when the system was configured for common and differential feeding, the isolation was below 50 dB and reached about 65 dB at the center frequency.

Those differences in simulations and measurements for the isolation responses are most likely related to the following factors: (i) the cable bending near the coupler, and (ii), non-ideal magnitude and phase imbalances from the coupler. For example, measurements and further investigations (not reported for brevity) showed that the coupler

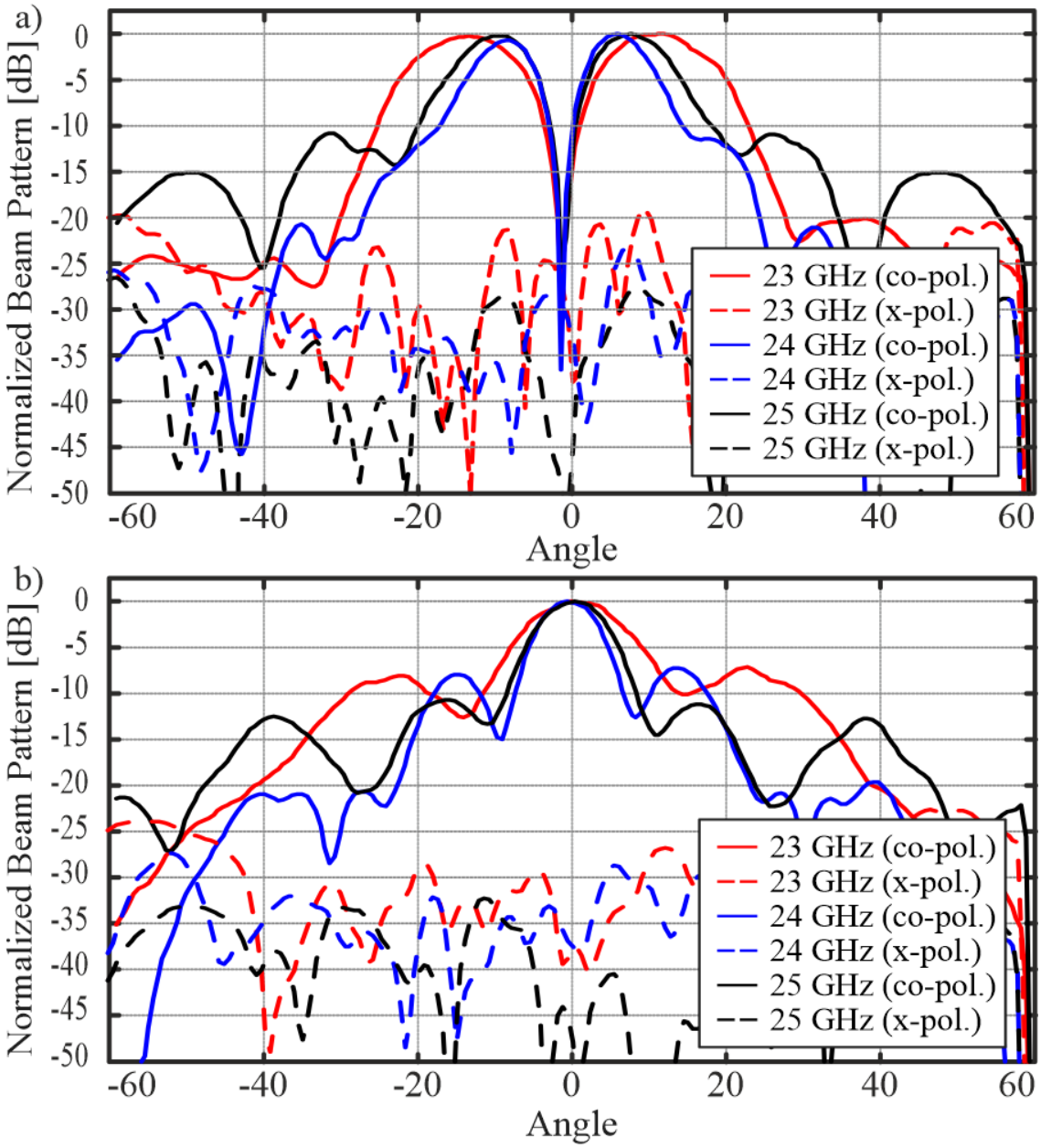

Figure 4.7: Measured far-field patterns (normalized) in the *y*-*z* plane, with the applied phase shifts at AP1 and AP2: a) 0° and 0° (difference pattern), and b) 0° and 180° (sum pattern). Similar results in the *x*-*z* plane for like feeding.

imbalances can reach up to ± 10° for frequencies where the antenna operates. Regardless of these practical effects, the general trend for the isolation responses for the feeding configurations are in agreement when comparing the simulations and measurements.

4.8 Summary and Discussions

A new and simple 4-port dual-polarized single-layer SIW slot antenna for IBFD applications is presented. The planar design uses a network of sub-arrays and external

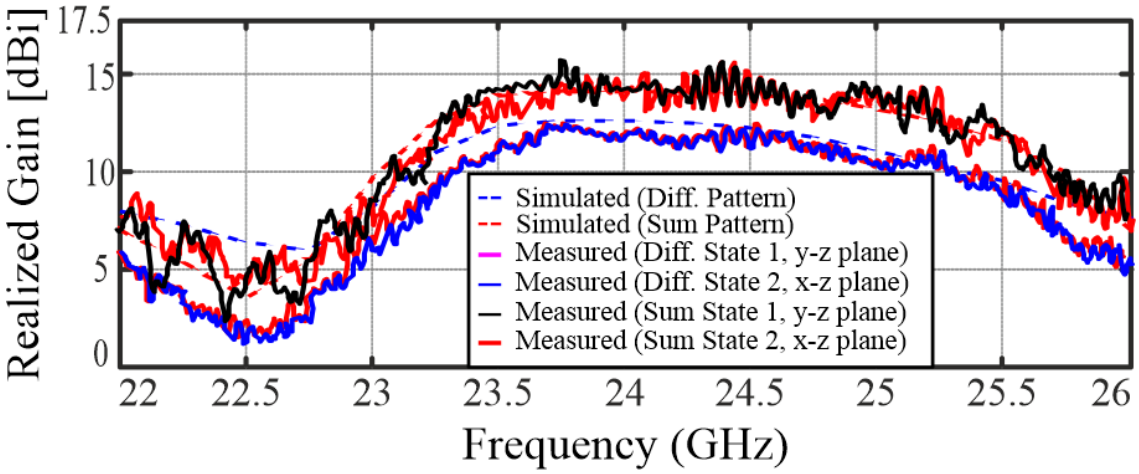

Figure 4.8: Maximum realized gain for the proposed antenna prototype for polarization state 1 and 2. Simulations and measurements are in good agreement with about 13 dBi (or more) for common or differential feeding.

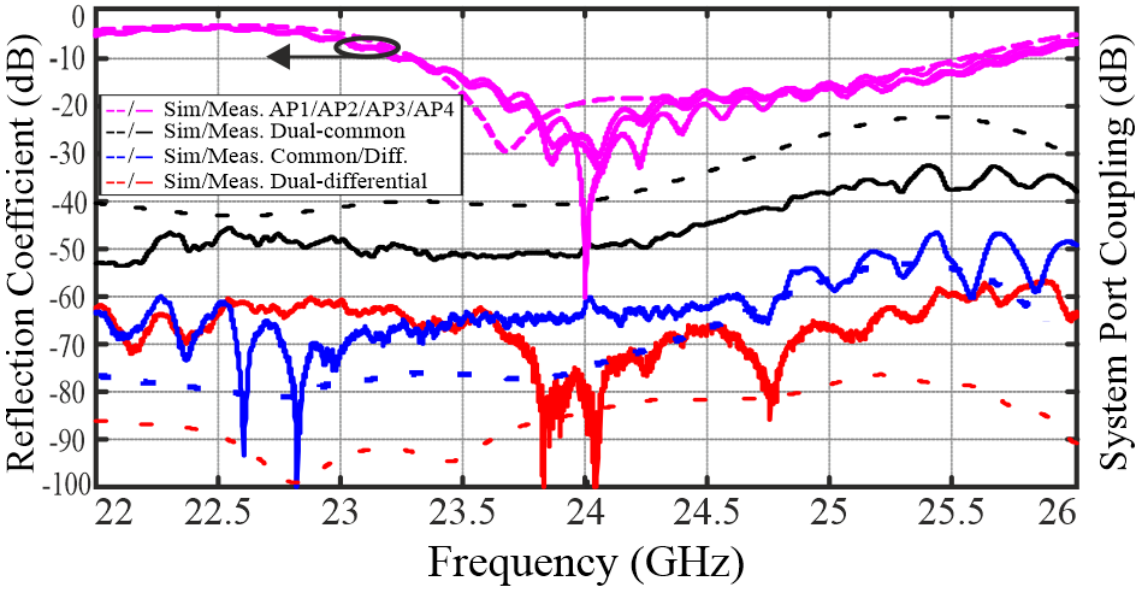

Figure 4.9: Simulated and measured reflection and coupling for the antenna itself (Fig. 4.2) and system ports (Fig. 4.3). For the simulations, an ideal coupler was considered while measurements employed a pair of 180° hybrid couplers.

couplers to provide dual-common and dual-differential feeding which generates sum and difference beam patterns respectively in the FF. Also, the antenna is well matched at millimeter-wave frequencies making it suitable for 5G communication applications, radar, and monopulse. Measured peak isolation levels values are about 50 dB and 90 dB for the dual-common and dual-differential feeding arrangements, respectively. The simple design approach makes it attractive for low-cost integration within FD systems and diversity scenarios and where high isolation levels and broad BWs are required.

The attractive addition to the antenna system would be an implementation of the an-

tenna array. This would allow a communication system with beam-steering capabilities. In such a frequency range, this would provide higher resolution and good reconfigurability for radar applications.

4.9 SIW Sub-arrays Antenna Array Dual-Polarized Sum and Difference Patterns Antenna Array for Full-duplex Systems

In this work, a new high isolation slot array antenna array offering dual-polarization, sum, and difference with high isolation for 5G in-band full-duplex (IBFD) applications is presented. The 16-port 4×1 single-layer antenna consists of sub-array slots (which are series-fed) with a cross-shaped orientation where 8 ports can produce linearly polarized radiation and the opposite 8 ports can produce orthogonal linear polarization. The antenna can be configured into the dual-differential (differential power split), dual-common (equal power split), or common/differential (equal and differential power split) modes to produce sum and difference beam patterns. Also, the matching is below -10 dB from 24 GHz to 25 GHz. The passive S-parameter coupling between the closest 4 ports is below -18 dB while coupling to the opposite ports and opposite polarization is well below -48 dB. When the antenna is configurated into the sum mode the coupling between non-active ports is below -55 dB, in the differential mode the antenna coupling is below -60 dB and when the antenna is in the common/differential mode the coupling is below -59 dB. The simulated and measured maximum realized gain for both configurations is around 22.4 dBi. The antenna beam-steering characteristics were measured with a Butler matrix showing the possibility to steer the beam up to 55° Such antenna arrays with high isolation can be well used in full-duplex communication systems with high data rates, dual-polarized radar applications, or other tracking applications.

4.9.1 Array Considerations

In the past chapter it was shown that a single-element antenna can offer a dual-polarized sum and difference beam patterns defining reconfigurability. When reviewing the literature, they are very limited antennas capable of beam steer in the FD mode. Therefore, the single-element was extended to the 4×1 antenna array to shift the beam in the *x*-*z* or *y*-*z* planes depending on polarization. The final antenna design retains pattern reconfigurability as a single element and provides good isolation levels, making it suit-

able for user tracking, radar applications and other communication systems. The antenna beam steering characteristics were measured using a Butler matrix beamformer capable to provide a consecutive phase shift of $\pm 45^{\circ}$ to $\pm 135^{\circ}$ and a set of power dividers connected to the antenna ports (AP).

The proposed planar antenna consists of an arrangement of four series-fed Sub-Arrays (SAi) substrate integrated waveguide (SIW) slots with each SA having four antenna ports (APi) positioned in the cross-shape-like orientation. The SIW lines are connected to the 50-Ω microstrip transitions. Tapering techniques were used for sub-arrays to improve the matching and reduce side-lobe levels (SLLs). Similarly to the past work, the antenna gain can be increased or reduced by changing the number of series-fed slots. The material choice was Taconic TLY-5 with a relative permittivity of 2.2 and a thickness of 0.51 mm. The manufactured antenna prototype can be seen in Fig. 4.10.

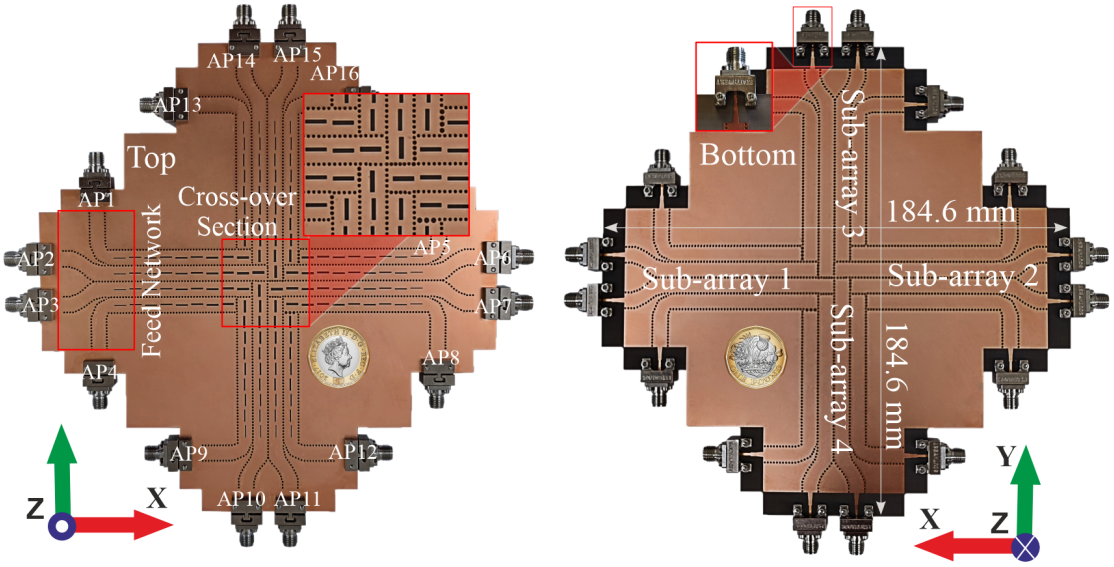

Figure 4.10: Top and bottom view of the manufactured 16 port Antenna array. The antenna consists of four Series-fed Sub-arrays (SA) lines slots with four ports for each SA.

The antenna was designed in the CST microwaves studio. The antenna configurations for different polarization states can be seen in Fig. 2 with responses compiled in Table I. The external couplers are connected to the 4×1 power dividers. When the antenna was excited considering dual-common feeding as applied to Sub-Array 1 (SA1) and 2 (SA2), or Sub-Array 3 (SA3) and 4 (SA4), a difference-like beam pattern can be realized in the far-field. When the antenna system is excited in dual-differential mode, a sum-like beam pattern will be produced in the farfield.

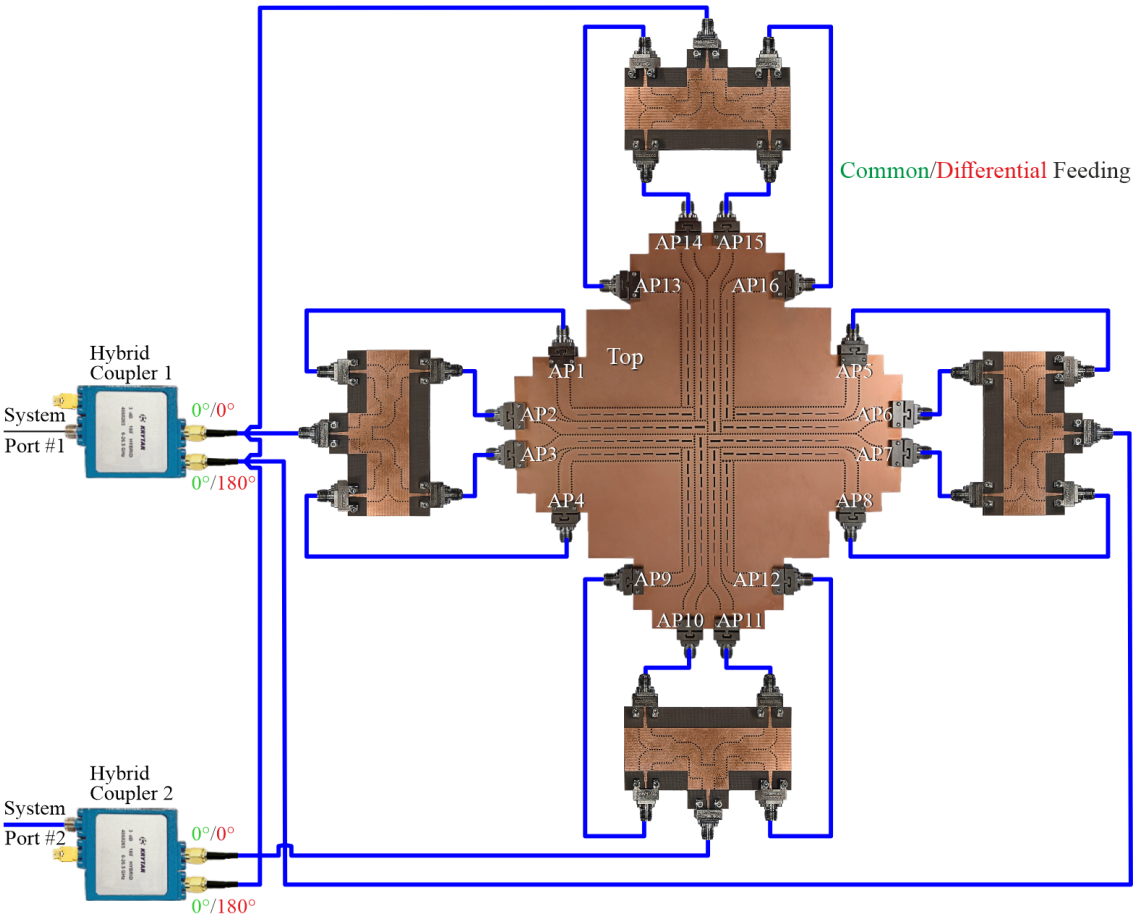

Figure 4.11: Possible feeding configurations for SA1+SA2 and SA3+SA4 defining the vertical (*y*-*z*) and horizontal (*x*-*z*) states of antenna operation, respectively. See also Table 4.3 which outlines the generated far-field patterns. The Krytat power dividers connected to the in-house made 1×4 power dividers to achieve equal power and phase split. Note: cables connections and lengths are just for illustrative purposes. In practice, common lengths were used to ensure consistent phase at the relative ports.

Table 4.3: Possible Feeding Configurations and Generated Patterns

Circuit Phase Feeding	Vertical *y*-*z* Plane (Polarization State #1)	Horizontal *x*-*z* Plane (Polarization State #2)	Far-field Patterns in the *y*-*z* and *x*-*z* Planes
Dual-Common	SA1+SA2 (0°)	SA3+SA4 (0°)	Difference
Dual-Differential	SA1+SA2 (180°)	SA3+SA4 (180°)	Sum
Differential + Common	SA1+SA2 (180°)	SA3+SA4 (0°)	Sum and Difference
Common + Differential	SA1+SA2 (0°)	SA3+SA4 (180°)	Difference and Sum

4.9.2 Antenna Measurements and Discussions

To assess the antenna performance and investigate the coupling, the antenna was measured in the passive single port approach using a Keysight PNA (N5234A). The passive reflection coefficients for AP1, AP2, AP3, and AP4 can be seen in Fig 4.12. Similar responses were observed for SA2, SA3, and SA4. The APi values are well matched from 24 to 25 GHz with values below -10 dB with a slightly higher mismatch on AP4. This is most likely related to manufacturing challenges or connector response. The passive

responses for the coupling for all AP1 to other APis can be seen in Fig 4.13. The coupling between AP1 to AP4 in the SA1 branch is well below -18 dB, while the isolation to other APi from the opposite and orthogonal Sub-arrays is below -48 dB. This shows that in general, the coupling coefficients have good isolation between the ports.

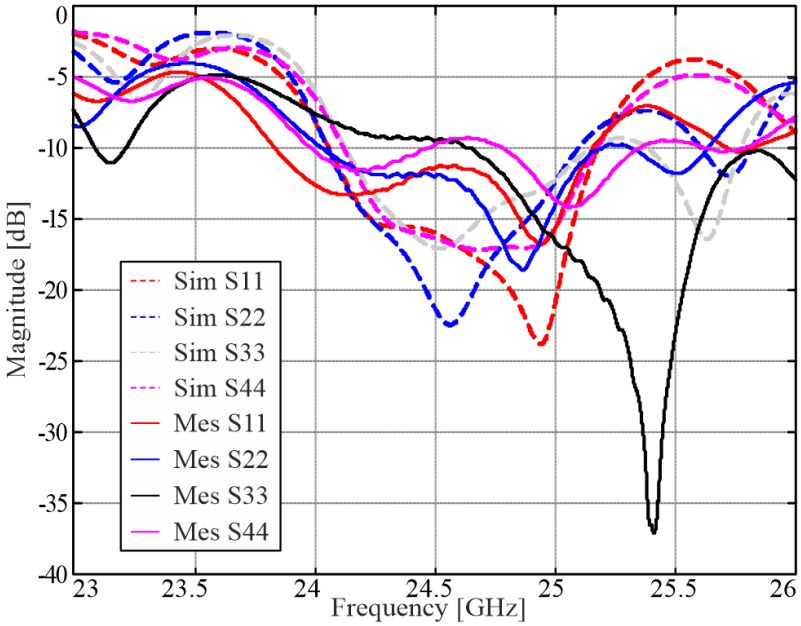

Figure 4.12: Simulated and measured the reflection coefficient of the ports AP1-AP4 of Sub-array 1. Similar responses were observed for other APs of Sub-arrays.

Further, the antenna was configurated in the two-port mode as presented in Table 4.3. The 2-ports of the analyzers (system ports 1 and 2) were connected to the power dividers (Krytar 4060265) and to external in-house made 1×4 equal power dividers. Additionally, the Miteq power divider (PD08-12002650) was also considered in the common and common+differential setup to investigate how the magnitude and phase imbalances can influence the isolation levels. Both couplers have similar responses in the Phase imbalance $\pm 11^{\circ}$ the magnitude imbalances are slightly higher on the Miteq power divider. As a result, the performance for the dual-common response can be observed in Fig. 4.14. There is a significant difference in the isolation response from 6 to 10 dB over the simulated and measured responses. A similar response was observed for a single-element when the antenna was connected for dual-common mode operation. As expected when both ports were configurated with both Krytar power dividers the isolation was higher than the Miteq power divider by about 3 to 10 dB. When the antenna was configurated in common and differential mode, the isolation levels were close to what was simulated for both couplers (see Fig. 4.15). In general, the isolation was below 58 dB. Finally, as only Krytar power dividers can be used for dual-differential mode, the isolation levels match

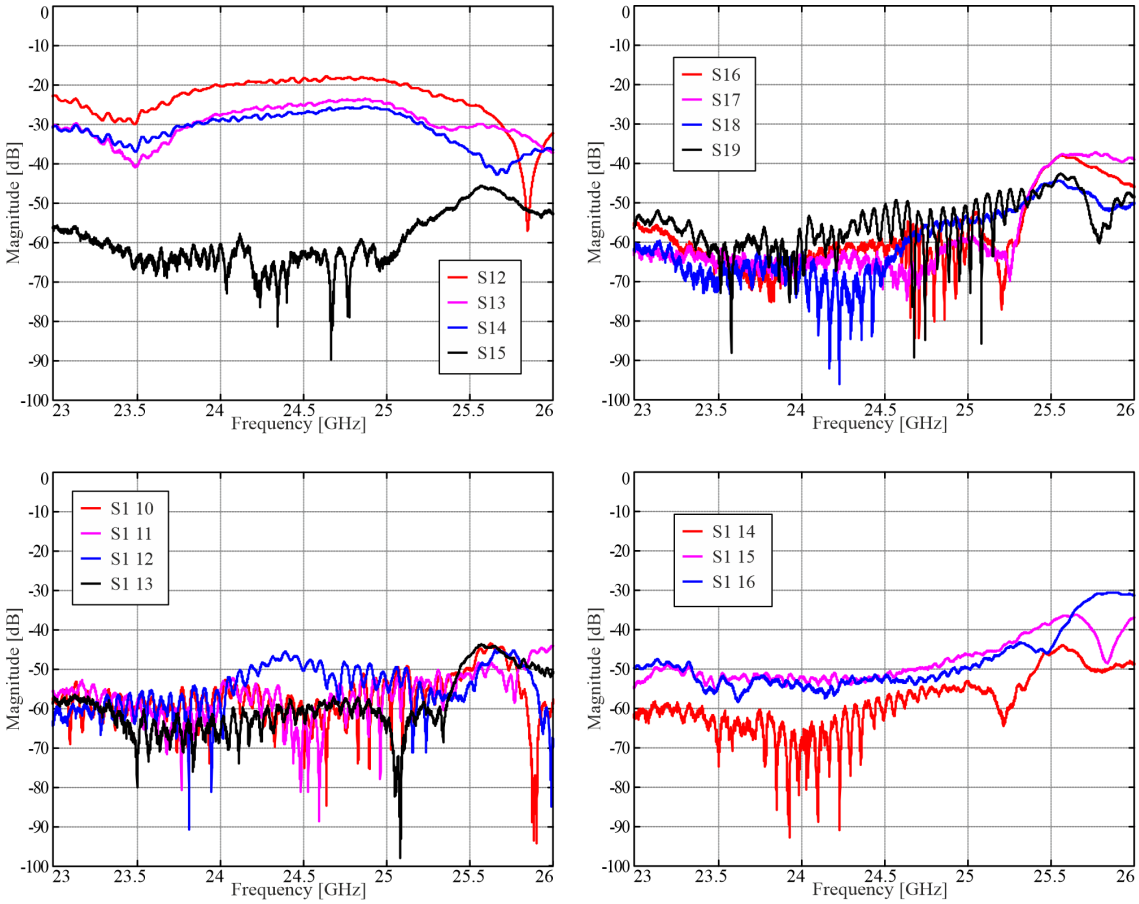

Figure 4.13: Simulated and measured passive coupling to all APi from the port AP1. Maximum coupling can be observed at around 18 dB of the APs of the same Sub-array. Other coupling coefficients of the opposite and cross-positioned APi are well below 50 dB.

the simulated with the coupling below -60 dB over operating bandwidth as in Fig. 4.16.

The antenna was measured in the NSI-2000 near-field planar system and DAMS-7000 far-field positioner. The antenna was configurated in the modes described in Table 4.3 to produce the sum-like and difference-like beam patterns. Simulated a) and measured b) beam-patterns for antenna array configurated in the common mode can be seen in Fig. 4.17. Good agreement between the simulations and measured can be observed. Cross-polarization levels are below -25 dB. Afterward, the antenna was configurated in the differential mode to produce sum-like beam patterns. Simulations a) and measurements b) can be seen in Fig. 4.18. The beam pattern response is close to what was simulated. Cross-polarization is well below -25 dB. Side-lobe levels are around -8 dB. Similar beam-pattern responses were observed for the orthogonal *y*-*z* plane polarization state. Those slightly higher cross-polarization levels are most likely related to measurement tolerances and phase and magnitude imbalances. Finally, the realized gain measurements can be seen in Fig. 4.19. Both common and differential modes with orthogonal polarization

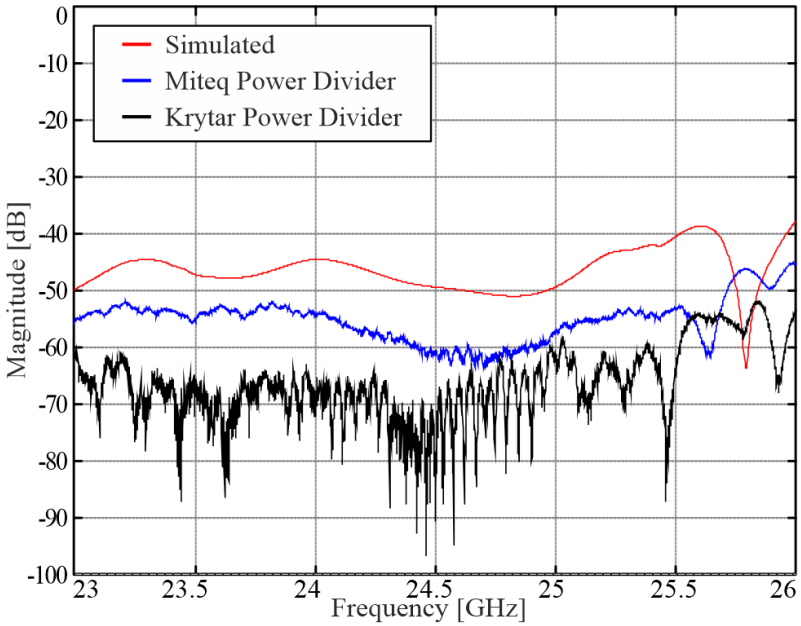

Figure 4.14: Simulated and measured coupling responses when the antenna was configurated in dual-common mode using two 1×8 Miteq power dividers or two 1×2 Krytar power dividers with 1×4 in-house power dividers. Slightly better isolation is most likely related to magnitude imbalances in the Krytar power divider. The isolation levels are slightly better by about 10 dB.

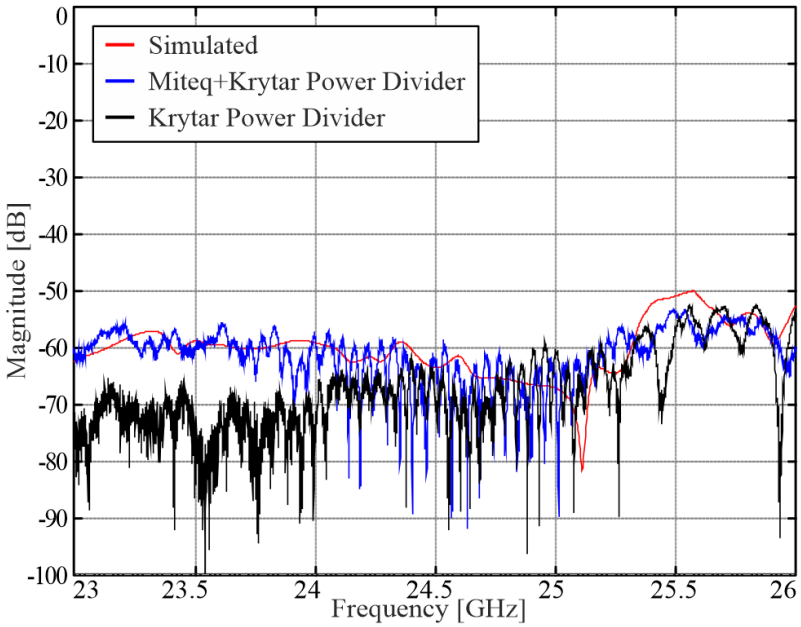

Figure 4.15: Simulated and measured coupling responses when the antenna was configurated in common and differential modes using a combination of Miteq power divider and Krytar or both Krytar power dividers. The isolation levels are slightly closer to what is measured with values below 58 dB.

have similar gain responses.

To investigate the beam steering response, a combination of the Butler matrix from [146] and Krytar power dividers were connected to the antenna. The photo of the Butler matrix can be seen in Fig. 4.20. The antenna system was configured to provide consequential shifts: i.e. when System Port 1 is excited, the resulting output of the Butler

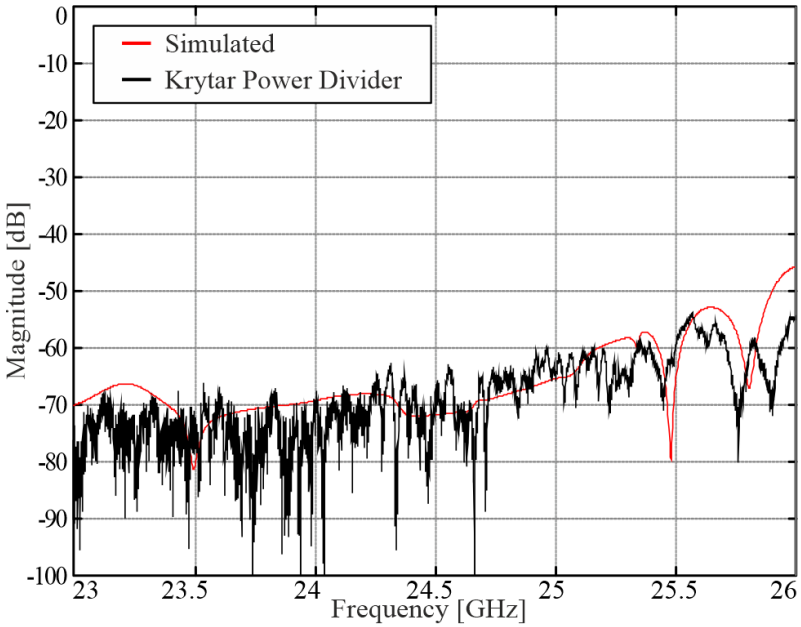

Figure 4.16: Simulated and measured coupling responses when the antenna was configurated in a dual-differential configuration with Krytar power dividers. Generally, the simulations and measurements are in agreement with isolation below 60 dB.

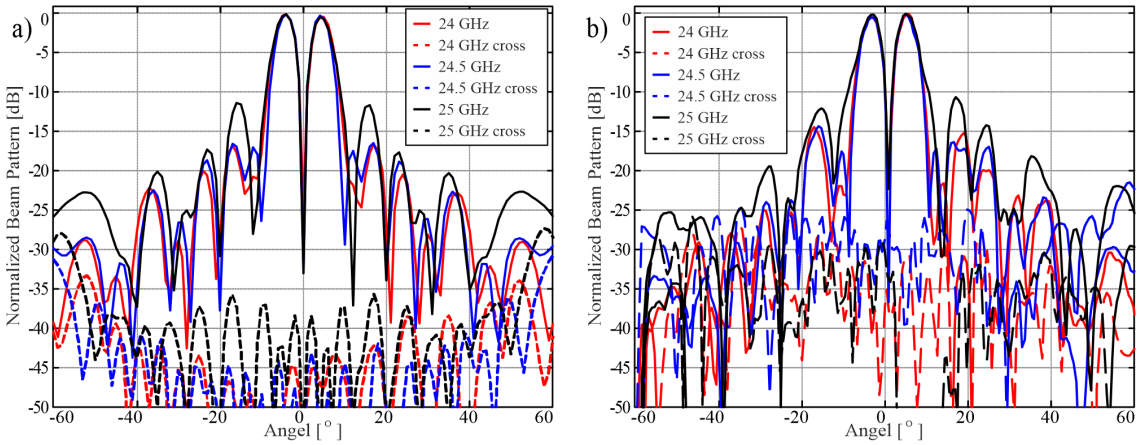

Figure 4.17: Simulated a) and measured b) antenna array configurated in the common mode to produce difference-like beam patterns. Slightly higher cross-polarization levels are most likely related to the measurement tolerances and phase and magnitude imbalances.

Matrix port 1 (BM P1) will be with the phase shift of $1\times\delta$, BM P2 - $2\times\delta$, BM P3 - $3\times\delta$ and BM P4 - $4\times\delta$, where δ is the designed delays as in compiled Table 4.4. The outputs of the Butler matrix ports are then connected to the Krytar power dividers to achieve the required phase shifts for sum and difference beam pattern configurations. The circuit system can be seen in Fig. 4.21. Some additional simulations were performed to observe the response of the array for the different beam steering configurations.

The farfield with the enforced phase as in Table 4.4 was simulated and measured. The beam patterns responce for difference and sum for frequencies a) 24 GHz b) 24.5 GHz and c) 25 GHz can be seen in Figs. 4.24 and 4.25. Simulated at 23.5 the 3-D

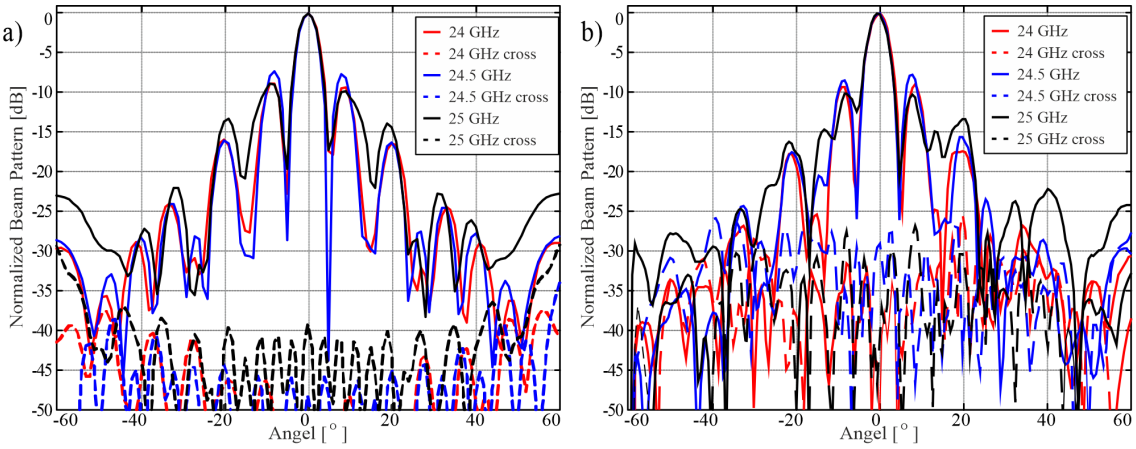

Figure 4.18: Simulated a) and measured b) antenna array configurated in the differential mode to produce sum-like beam patterns. Good agreements between measurements and simulations.

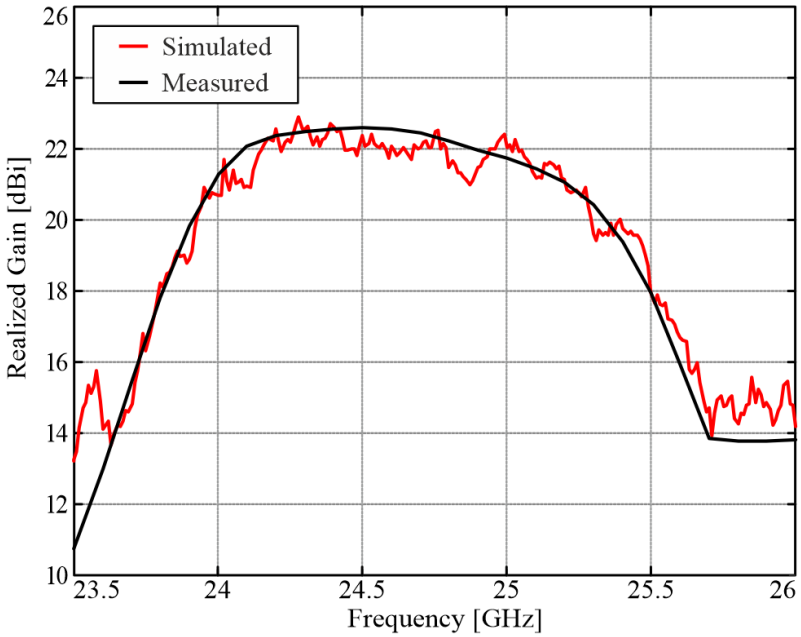

Figure 4.19: Simulated and measured realized gain. Maximum realize gain was around 22.5 dBi. Both polarization states have similar gain responses.

Table 4.4: Butler Matrix response depending on the excited port

Excited System Port	Phase shift, δ
1	45
2	-135
3	+135
4	-45

Beam steering responses for sum and difference beam patterns using the Butler matrix can be seen in Figs. 4.22 and 4.23. Similar responses were observed for the orthogonal polarization in the x-z plane. In general, measurements and simulations are close to what was expected.

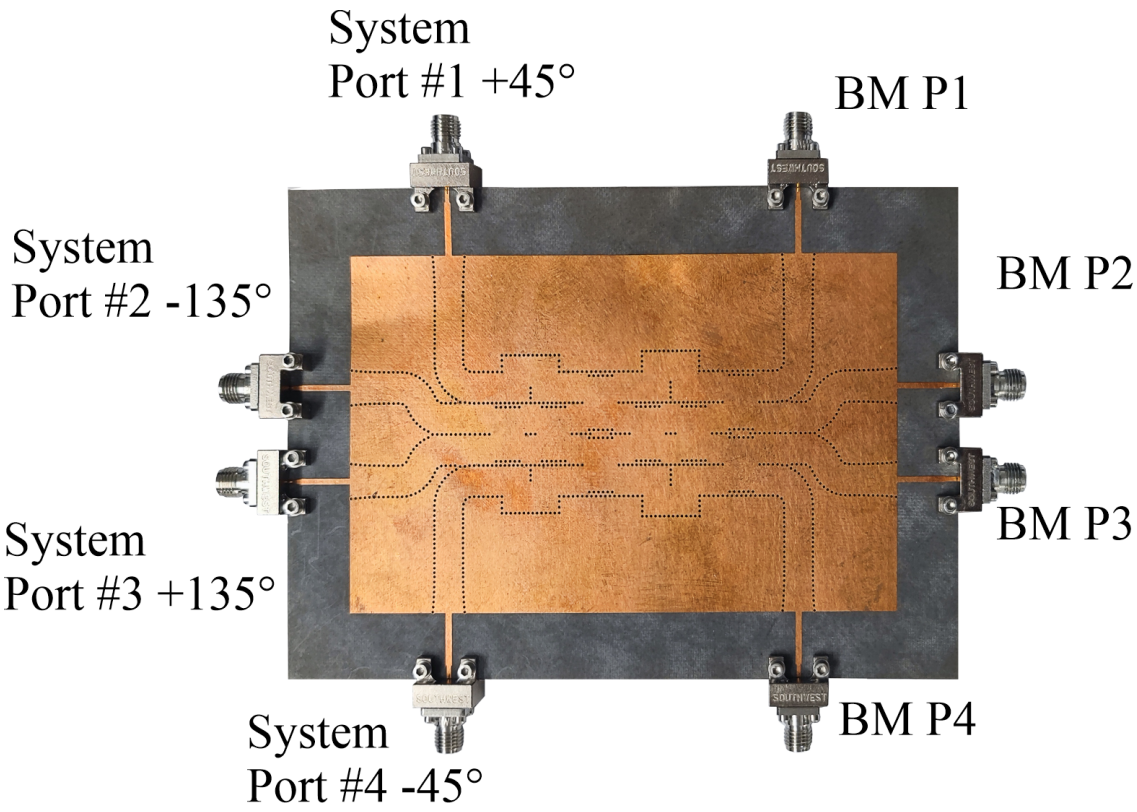

Figure 4.20: Photo of the Butler matrix from [146]. Depending on the excited system port, the resulting consequential shift can be achieved. Possible phase shifts can be seen in Table 4.4.

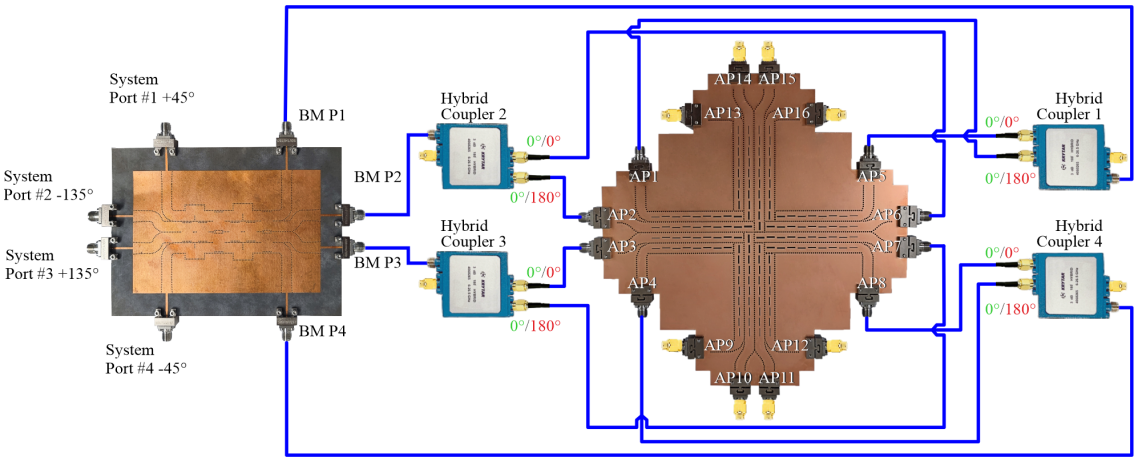

Figure 4.21: Assembled antenna system to investigate beam steering performance of the proposed IBFD antenna array. Depending on the port excited of the Butler matrix, the consecutive phase shift will be applied to the ports. Combining the differential power divider response of the Krytar power divider, the required sum and difference beam pattern shifts can be achieved. Note: cables connections and lengths are just for illustrative purposes. In practice, common lengths were used to ensure consistent phase at the relative ports.

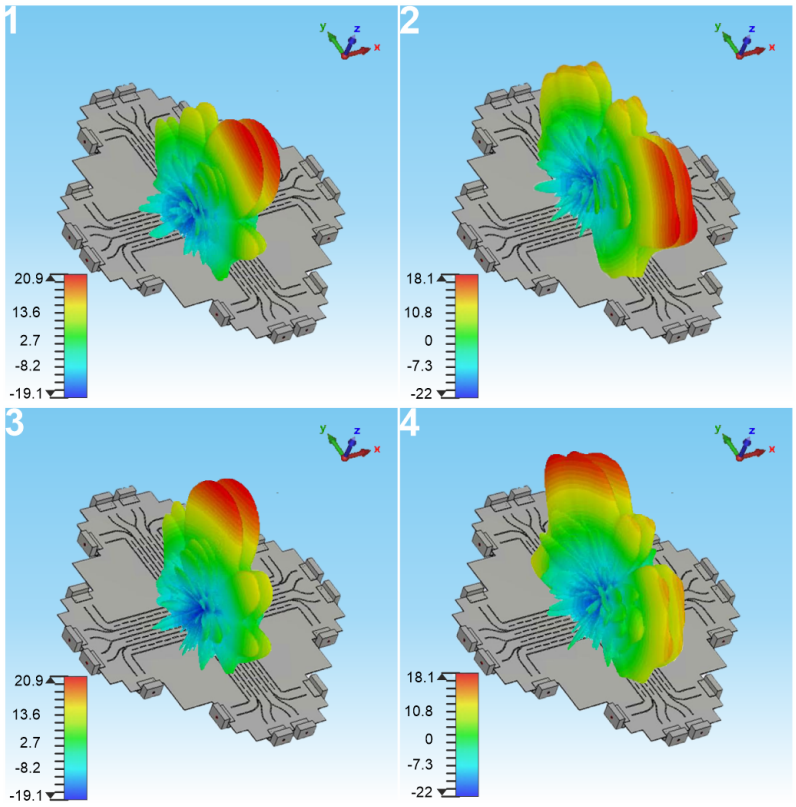

Figure 4.22: Simulated 3-D beam patterns at 23.5 GHz considering phase shifts 1) -45° 2) -135° 3) 45° and 4) 145° to enable the beam steering in the *y*-*z* planes in the common mode to produce difference-like beam patterns.

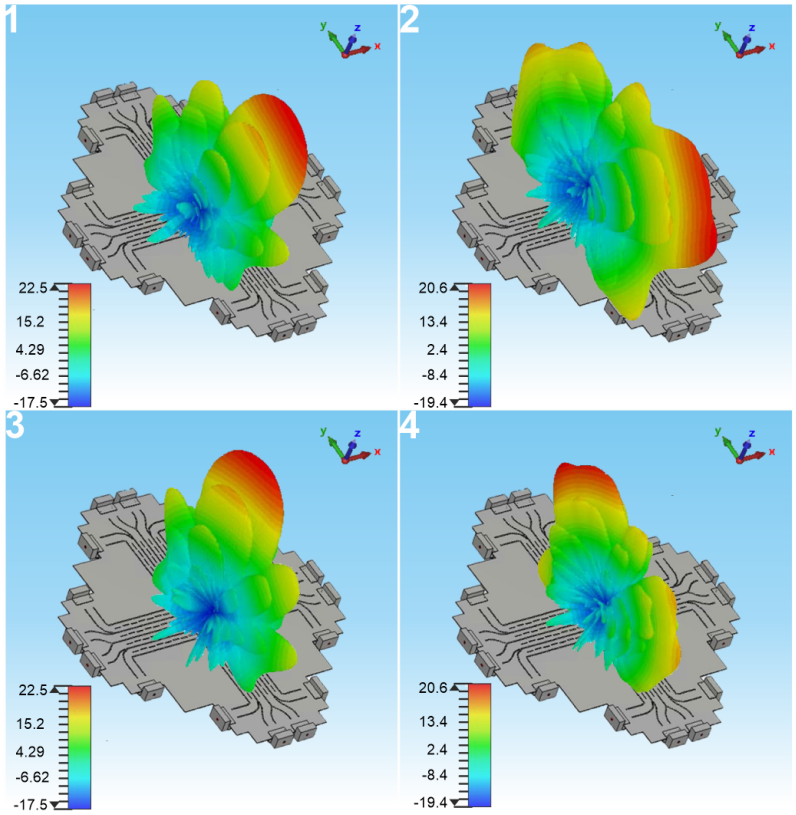

Figure 4.23: Simulated 3-D beam patterns at 23.5 GHz considering phase shifts 1) -45° 2) -135° 3) 45° and 4) 145° to enable the beam steering in the *y*-*z* planes in the differential mode to produce sum-like beam patterns.

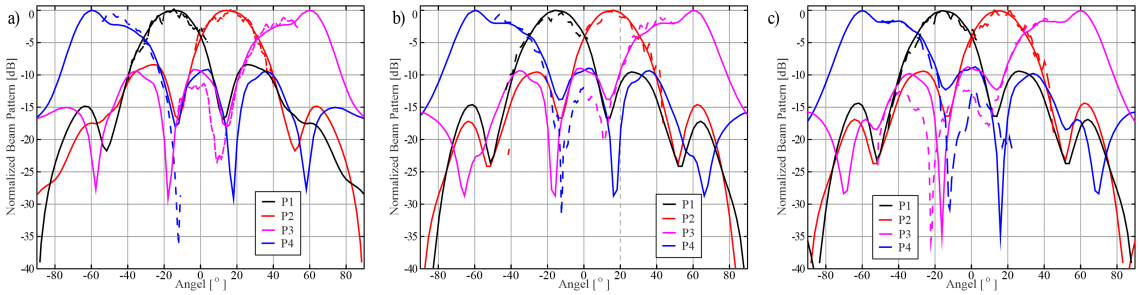

Figure 4.24: Simulated and measured antenna beam patterns considering excited ports of the Butler matrix of frequencies a) 24 GHz b) 24.5 GHz and c) 25 GHz when antenna configuration into the common mode to produce difference like beam patterns with steering in *y*-*z* plane.

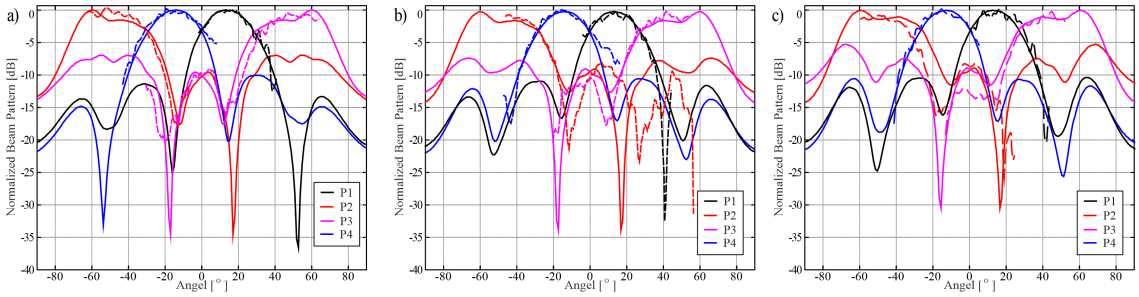

Figure 4.25: Simulated and measured antenna beam patterns considering excited ports of the Butler matrix of frequencies a) 24 GHz b) 24.5 GHz and c) 25 GHz when antenna configurated into differential mode to produce sum-like beam patterns with steering in *y*-*z* plane.

4.10 Chapter Summary

In this chapter, a new dual-polarized high isolation antenna and array for Full-duplex communication systems with sum-like and difference-like beam patterns and beam-steering was presented. The antenna is well matched from 24 to 25 GHz with isolation levels above 48 dB for the dual-common mode, 60 dB for the dual-differential mode, and about 60 dB for the common-differential mode. The simulated and measured peak realized gain was around 22.4 dBi. Cross-polarization levels are well below -20 dB. The antenna is capable of beam steering showing angles up to 55° using the Butler matrix beamformer. Such antenna array systems can be well used in the Retro Directive arrays, 5G Full-duplex communication systems, or any other radar systems.

Based on this work, the antenna design system could be expanded further by providing more steering options for 5G systems. Further research could be done integrating those antenna systems into real-life software-defined radios or RDA systems. Other improvements could be done by considering circular polarizations or increasing the bandwidth by using different slot antenna elements as well as more integrated feeding systems.

Chapter 5

Conclusion and Future Work

5.1 Conclusion

This thesis presented new polarization reconfigurable antennas and full-duplex (FD) antenna and circuit systems. The phase control and feeding of the structures was the main design aspect for the dielectric resonator antennas (DRAs). Using this experience, high isolation antennas were further designed as required for FD antennas. Additionally, the possibility of FD beam-steering was also reported for the first time. Those antenna studies can be useful for S-band and mm-wave 5G systems where high isolation, multiple polarizations, and antenna co-locations are required.

A new novel 8-port DRA antenna was introduced. The feeding system can provide dual-circular polarization and two orthogonal linear polarizations depending on the phase and amplitude excitation at the port. This approach offers polarization control for the dielectric resonator. Such polarization control can be useful for radio frequency (RF) challenged environments. However, such multi-port feeding makes it challenging for system integration. As examined in the thesis, further work integrated the feed system and used a higher dielectric resonator element. This made the system much more compact while offering two circular polarizations. Those presented antenna and circuit systems can be useful for GNSS and GPS helping to ensure accurate location and positioning.

Using the developed approaches for the DRAs, a new FD antenna systems for the S-band were presented. Applications include advanced Wi-Fi systems. As outlined in the chapter, in-band FD solutions are a popular research topic for these intended wireless systems. The chapter reported on phase control and coupler-based antenna systems with dual-polarization as well as dual-differential feeding systems. The developed H-shaped slot antenna was also proposed with an external network, and this design also offered high isolation levels. The antenna was extended by integrating the feeding circuit with a slot-line coupler which offered simple two-port feeding whilst maintaining isolation levels. The antenna array configurations were also examined for beam-steering FD systems.

A new FD antenna and beam-steering array for also proposed for 5G systems and

operation at mm-wave frequencies. The developed sub-array slot antenna offered reconfiguration of the beam patterns. The antenna was manufactured and measured, and the isolation levels for all operating modes was recorded. Such an antenna can also be used in continuous wave radars where the transmission leakage could be a challenge. This research demonstrated that state-of-the-art designs can be achieved and that antenna technology can be advanced. Application include polarization control and high-isolation systems with dual-polarization functionality. These features suggest that the developed FD antennas can be commercially employed for current and existing day-to-day systems, mainly in an effort to offer communications with high speeds and no delays [147].

5.2 Future Work

There are a number of potential future studies that can be highlighted.

1. For the DRAs, it might be possible to explore these structures and new feed systems to also offer dual-linear polarization with improved functionality. Currently, it is required to have external phase shifters. A possible multi-layer approach can be designed without additional circuitry. Another improvement could be designing the array systems for further beam-steering and tracking.

2. The DRA systems could be integrated into the stations to test and analyze the performance. Additionally, some algorithms for stable communications could be explored using those DRAs.

3. Other DRA improvements could be done by exploring other modes and control of it. Particulate TE modes excitation on the dielectric element.

4. As FD antenna systems are a topic of interest, the main challenge can be integration into commercial FD systems. Also, due to the isolation levels changing in the different environments, it is important to analyze this behaviour and take into account the reduction of the isolation levels whenever possible. This is because commercial simulators often provide higher isolation levels when in comparison to real-life measurements.

5. It would also be of benefit to analyze the antenna performance with a fully assembled system consisting of digital, analog, and antenna cancellations.

6. Other possible approaches could be an in-band retro-directive array where the self-tracking and beam-steering occurs at the same frequency. This would require further isolation in the analog part to reduce the self-interference.

7. Possible modulation techniques for the developed IBFD antennas would be another approach to investigate and integrate into a full system, while also exploring simultaneous radar and communications.

8. Other possible studies could be explored which investigate the integration of analog cancellation systems (and its bandwidth performances) when working with the developed broadband of this antennas.

Bibliography

[1] R. Bajaj, S. Ranaweera, and D. Agrawal, "Gps: location-tracking technology," *Computer*, vol. 35, no. 4, pp. 92–94, 2002.

[2] C. C. Counselman and S. A. Gourevitch, "Miniature interferometer terminals for earth surveying: Ambiguity and multipath with global positioning system," *IEEE Transactions on Geoscience and Remote Sensing*, vol. GE-19, no. 4, pp. 244–252, 1981.

[3] J. Abel and J. Chaffee, "Existence and uniqueness of gps solutions," *IEEE Transactions on Aerospace and Electronic Systems*, vol. 27, no. 6, pp. 952–956, 1991.

[4] S. Akesson, "Gprs, general packet radio service," in *Proceedings of ICUPC '95 - 4th IEEE International Conference on Universal Personal Communications*, 1995, pp. 640–643.

[5] J. Soubielle, I. Fijalkow, P. Duvaut, and A. Bibaut, "Gps positioning in a multipath environment," *IEEE Transactions on Signal Processing*, vol. 50, no. 1, pp. 141–150, 2002.

[6] I. Joo and C. Sin, "Design of gnss jamming propagation simulator using itu-r p.1546 propagation model," in *2015 15th International Conference on Control, Automation and Systems (ICCAS)*, 2015, pp. 1359–1362.

[7] J. Moon and Y. Kim, "Antenna diversity strengthens wireless LANs," *Communication Systems Design*, vol. 9, no. 1, pp. 14–24, 2003.

[8] T. Kumberg, R. Tannhaeuser, and L. Reindl, "Wake-up receiver with equal-gain antenna diversity," *Sensors*, vol. 17, p. 1961, 08 2017.

[9] R. Vaughan, "Polarization diversity in mobile communications," *IEEE Transactions on Vehicular Technology*, vol. 39, no. 3, pp. 177–186, 1990.

[10] X.-P. Mao and J. W. Mark, "On polarization diversity in mobile communications," in *2006 International Conference on Communication Technology*, 2006, pp. 1–4.

[11] D. Korpi, M. Heino, C. Icheln, K. Haneda, and M. Valkama, "Compact inband full-duplex relays with beyond 100 db self-interference suppression: Enabling techniques and field measurements," *IEEE Transactions on Antennas and Propagation*, vol. 65, no. 2, pp. 960–965, 2017.

[12] J. Flood, "Alexander graham bell and the invention of the telephone," *Electronics and Power*, vol. 22, no. 3, pp. 159–162, 1976.

[13] "Simplex, half-duplex, full-duplex: Definition, comparison and information," Dec 2021. [Online]. Available: https://teachcomputerscience.com/simplex-half-duplex-full-duplex/

[14] A. Sabharwal, P. Schniter, D. Guo, D. W. Bliss, S. Rangarajan, and R. Wichman, "In-band full-duplex wireless: Challenges and opportunities," *IEEE Journal on Selected Areas in Communications*, vol. 32, no. 9, pp. 1637–1652, 2014.

[15] A. Stove, "Linear fmcw radar techniques," *IEE Proceedings F (Radar and Signal Processing)*, vol. 139, pp. 343–350(7), October 1992. [Online]. Available: https://digital-library.theiet.org/content/journals/10.1049/ip-f-2.1992.0048

[16] K. E. Kolodziej, "In-band full-duplex wireless systems overview," in *ICC 2021 - IEEE International Conference on Communications*, 2021, pp. 1–6.

[17] D. Su, J. Qian, H. Yang, and D. Fu, "A novel broadband polarization diversity antenna using a cross-pair of folded dipoles," *IEEE Antennas and Wireless Propagation Letters*, vol. 4, pp. 433–435, 2005.

[18] A. Iqbal, I. B. Mabrouk, M. Al-Hasan, M. Nedil, and T. A. Denidni, "Wideband substrate integrated waveguide antenna for full-duplex systems," *IEEE Antennas and Wireless Propagation Letters*, vol. 21, no. 1, pp. 212–216, 2022.

[19] A. Tamayo-Dominguez, J.-M. Fernandez-Gonzalez, and M. S. Castaner, "Low-cost millimeter-wave antenna with simultaneous sum and difference patterns for 5g point-to-point communications," *IEEE Communications Magazine*, vol. 56, no. 7, pp. 28–34, 2018.

[20] M. V. Kuznetcov, S. K. Podilchak, M. Clénet, and Y. M. M. Antar, "Hybrid dielectric resonator antenna for diversity applications with linear or circular polariza-

tion," *IEEE Transactions on Antennas and Propagation*, vol. 69, no. 8, pp. 4457–4465, 2021.

[21] M. V. Kuznetcov, S. K. Podilchak, J. C. Johnstone, M. Clenet, and Y. M. M. Antar, "Planar Feeding Circuit Integrated With a Compact Dielectric Resonator for Polarization Diversity," *IEEE Transactions on Microwave Theory and Techniques*, vol. 69, no. 4, pp. 2229–2240, 2021.

[22] C. A. Balanis, *Antenna theory: analysis and design*. Wiley-Interscience, 2005.

[23] J. Shipman, J. Wilson, and C. Higgins, *An Introduction to Physical Science*, ser. Textbooks Available with Cengage Youbook. Cengage Learning, 2012.

[24] L. J. Ippolito, *Depolarization on Satellite Paths*. Dordrecht: Springer Netherlands, 1986, pp. 93–121. [Online]. Available: https://doi.org/10.1007/978-94-011-7027-7_6

[25] K. Grover, A. Lim, and Q. Yang, "Jamming and anti–jamming techniques in wireless networks: a survey," *International Journal of Ad Hoc and Ubiquitous Computing*, vol. 17, no. 4, pp. 197–215, 2014. [Online]. Available: https://www.inderscienceonline.com/doi/abs/10.1504/IJAHUC.2014.066419

[26] B. Lim, "Dielectric resonator antennas : theory and design." Springer, 1999. [Online]. Available: http://hdl.handle.net/1721.1/36782

[27] A. Petosa and A. Ittipiboon, "Dielectric resonator antennas: A historical review and the current state of the art," *IEEE Antennas and Propagation Magazine*, vol. 52, no. 5, pp. 91–116, 2010.

[28] A. Petosa, *Dielectric Resonator Antenna Handbook*. Norwood, MA: Artech House,, 2007.

[29] M. Aras, M. Rahim, A. Asrokin, and M. Abdul Aziz, "Dielectric resonator antenna (dra) for wireless application," in *2008 IEEE International RF and Microwave Conference*, 2008, pp. 454–458.

[30] Y. Zhou, Y. Jiao, Z. Weng, and T. Ni, "A novel single-fed wide dual-band circularly polarized dielectric resonator antenna," *IEEE Antennas and Wireless Propagation Letters*, vol. 15, pp. 930–933, 2016.

[31] K. Gong and X. H. Hu, "Low-profile substrate integrated dielectric resonator antenna implemented with PCB process," *IEEE Antennas and Wireless Propagation Letters*, vol. 13, pp. 1023–1026, 2014.

[32] Q. Rao, T. A. Denidni, and A. R. Sebak, "Broadband compact stacked T-shaped dra with equilateral-triangle cross sections," *IEEE Microwave and Wireless Components Letters*, vol. 16, no. 1, pp. 7–9, Jan 2006.

[33] T. A. Denidni, Qinjiang Rao, and A. R. Sebak, "Broadband L-shaped dielectric resonator antenna," *IEEE Antennas and Wireless Propagation Letters*, vol. 4, pp. 453–454, 2005.

[34] G. Varshney, V. S. Pandey, R. S. Yaduvanshi, and L. Kumar, "Wide band circularly polarized dielectric resonator antenna with stair-shaped slot excitation," *IEEE Transactions on Antennas and Propagation*, vol. 65, no. 3, pp. 1380–1383, March 2017.

[35] R. Chair, S. L. S. Yang, A. A. Kishk, Kai Fong Lee, and Kwai Man Luk, "Aperture fed wideband circularly polarized rectangular stair shaped dielectric resonator antenna," *IEEE Transactions on Antennas and Propagation*, vol. 54, no. 4, pp. 1350–1352, April 2006.

[36] Chih-Yu Huang, Jian-Yi Wu, and Kin-Lu Wong, "Cross-slot-coupled microstrip antenna and dielectric resonator antenna for circular polarization," *IEEE Transactions on Antennas and Propagation*, vol. 47, no. 4, pp. 605–609, April 1999.

[37] B. Li, C. Hao, and X. Sheng, "A dual-mode quadrature-fed wideband circularly polarized dielectric resonator antenna," *IEEE Antennas and Wireless Propagation Letters*, vol. 8, pp. 1036–1038, 2009.

[38] W. M. Abdel Wahab, D. Busuioc, and S. Safavi-Naeini, "Low cost planar waveguide technology-based dielectric resonator antenna (DRA) for millimeter-wave applications: Analysis, design, and fabrication," *IEEE Transactions on Antennas and Propagation*, vol. 58, no. 8, pp. 2499–2507, Aug 2010.

[39] W. M. Abdel-Wahab, Y. Wang, and S. Safavi-Naeini, "SIW hybrid feeding network-integrated 2-D DRA array: Simulations and experiments," *IEEE Antennas and Wireless Propagation Letters*, vol. 15, pp. 548–551, 2016.

[40] X. Liang and T. A. Denidni, "H-shaped dielectric resonator antenna for wideband applications," *IEEE Antennas and Wireless Propagation Letters*, vol. 7, pp. 163–166, 2008.

[41] M. Abedian, S. K. A. Rahim, and M. Khalily, "Two-segments compact dielectric resonator antenna for UWB application," *IEEE Antennas and Wireless Propagation Letters*, vol. 11, pp. 1533–1536, 2012.

[42] J. H. Winters, J. Salz, and R. D. Gitlin, "The impact of antenna diversity on the capacity of wireless communication systems," *IEEE Transactions on Communications*, vol. 42, no. 234, pp. 1740–1751, Feb. 1994.

[43] B. J. Wysocki, T. A. Wysocki, and J. Seberry, "Modeling dual polarization wireless fading channels using quaternions," in *Joint IST Workshop on Mobile Future, 2006 and the Symposium on Trends in Communications. SympoTIC '06.*, June 2006, pp. 68–71.

[44] R. G. Vaughan and J. B. Andersen, "Antenna diversity in mobile communications," *IEEE Transactions on Vehicular Technology*, vol. 36, no. 4, pp. 149–172, Nov 1987.

[45] S. K. Yoo, S. L. Cotton, and W. G. Scanlon, "Switched diversity techniques for indoor off-body communication channels: An experimental analysis and modeling," *IEEE Transactions on Antennas and Propagation*, vol. 64, no. 7, pp. 3201–3206, 2016.

[46] S. S. Ikki and M. H. Ahmed, "Performance of cooperative diversity using equal gain combining (EGC) over nakagami-m fading channels," *IEEE Transactions on Wireless Communications*, vol. 8, no. 2, pp. 557–562, 2009.

[47] Y. Gao, Z. Feng, and L. Zhang, "Compact CPW-fed dielectric resonator antenna with dual polarization," *IEEE Antennas and Wireless Propagation Letters*, vol. 10, pp. 544–547, 2011.

[48] Z. Chen, I. Shoaib, Y. Yao, J. Yu, X. Chen, and C. G. Parini, "Pattern-reconfigurable dual-polarized dielectric resonator antenna," *IEEE Antennas and Wireless Propagation Letters*, vol. 15, pp. 1273–1276, 2016.

[49] S. K. Podilchak, M. Clénet, and Y. M. M. Antar, "A hybrid dielectric resonator antenna with polarization-agility and wideband operation," in *The 8th European Conference on Antennas and Propagation (EuCAP 2014)*, April 2014, pp. 3162–3163.

[50] U. Kraft, "An experimental study on 2 by 2 sequential-rotation arrays with circularly polarized microstrip radiators," *IEEE Transactions on Antennas and Propagation*, vol. 45, no. 10, pp. 1459–1466, 1997.

[51] S. K. Podilchak, J. C. Johnstone, M. Caillet, M. Clénet, and Y. M. M. Antar, "A compact wideband dielectric resonator antenna with a meandered slot ring and cavity backing," *IEEE Antennas and Wireless Propagation Letters*, vol. 15, pp. 909–913, 2016.

[52] K. U-yen, E. J. Wollack, J. Papapolymerou, and J. Laskar, "A broadband planar magic-t using microstrip–slotline transitions," *IEEE Transactions on Microwave Theory and Techniques*, vol. 56, no. 1, pp. 172–177, 2008.

[53] G. Brzezina and L. Roy, "Miniaturized 180° hybrid coupler in ltcc for l-band applications," *IEEE Microwave and Wireless Components Letters*, vol. 24, no. 5, pp. 336–338, 2014.

[54] J. C. Johnstone, S. K. Podilchak, M. Clénet, and Y. M. M. Antar, "A compact cylindrical dielectric resonator antenna for MIMO applications," in *2014 IEEE Antennas and Propagation Society International Symposium (APSURSI)*. IEEE, 2014, pp. 1938–1939.

[55] W. M. Dyab, A. A. Sakr, and K. Wu, "Dually-polarized butler matrix for base stations with polarization diversity," *IEEE Transactions on Microwave Theory and Techniques*, vol. 66, no. 12, pp. 5543–5553, 2018.

[56] J. A. Ruiz-Cruz, M. M. Fahmi, S. A. Fouladi, and R. R. Mansour, "Waveguide antenna feeders with integrated reconfigurable dual circular polarization," *IEEE Transactions on Microwave Theory and Techniques*, vol. 59, no. 12, pp. 3365–3374, 2011.

[57] J. Zhang, S. Zhang, Z. Ying, A. S. Morris, and G. F. Pedersen, "Radiation-pattern reconfigurable phased array with p-i-n diodes controlled for 5g mobile terminals,"

IEEE Transactions on Microwave Theory and Techniques, vol. 68, no. 3, pp. 1103–1117, 2020.

[58] J. C. Johnstone, S. K. Podilchak, M. Clénet, and Y. M. M. Antar, "A compact cylindrical dielectric resonator antenna for MIMO applications," in *2014 IEEE Antennas and Propagation Society International Symposium (APSURSI)*, 2014, pp. 1938–1939.

[59] EETimes, "Antenna Diversity Strengthens Wireless LANs," Jan 2003. [Online]. Available: https://www.eetimes.com/antenna-diversity-strengthens-wireless-lans

[60] Hemalatha, M and Prithiviraj, Venkatapathy and Jayalalitha, S and Thenmozhii, K, "Diversity analysis in WiFi system," *Journal of Theoretical and Applied Information Technology*, vol. 15, p. , 11 2011.

[61] S. M. Lindenmeier and L. M. Reiter and D. E. Barie and J. F. Hopf, "Antenna Diversity for Improving the BER in Mobile Digital Radio Reception Especially in Areas with Dense Foliage," in *2007 2nd International ITG Conference on Antennas*, 2007, pp. 45–48.

[62] G. Liu, F. R. Yu, H. Ji, V. C. M. Leung, and X. Li, "In-Band Full-Duplex Relaying: A Survey, Research Issues and Challenges," *IEEE Communications Surveys Tutorials*, vol. 17, no. 2, pp. 500–524, 2015.

[63] J. Cowley, *Communications and Networking: An Introduction*, ser. Undergraduate Topics in Computer Science. Springer London, 2012.

[64] T. Riihonen, "Design and analysis of duplexing modes and forwarding protocols for ofdm(a) relay links," 2014.

[65] D. M. Pozar, *Microwave engineering; 3rd ed.* Hoboken, NJ: Wiley, 2005.

[66] G. J. R. Povey, "Frequency and time division duplex techniques for cdma cellular radio," in *Proceedings of IEEE 3rd International Symposium on Spread Spectrum Techniques and Applications (ISSSTA'94)*, 1994, pp. 309–313 vol.1.

[67] R. Esmailzadeh, M. Nakagawa, and E. A. Sourour, "Time-division duplex cdma communications," *IEEE Personal Communications*, vol. 4, no. 2, pp. 51–56, 1997.

[68] K. E. Kolodziej, B. T. Perry, and J. S. Herd, "In-band full-duplex technology: Techniques and systems survey," *IEEE Transactions on Microwave Theory and Techniques*, vol. 67, no. 7, pp. 3025–3041, 2019.

[69] A. Grami, "Chapter 2 - fundamental aspects of digital communications," in *Introduction to Digital Communications*, A. Grami, Ed. Boston: Academic Press, 2016, pp. 11 – 39.

[70] H. Wymeersch and A. Eryilmaz, "Chapter 12 - multiple access control in wireless networks," in *Academic Press Library in Mobile and Wireless Communications*, S. K. Wilson, S. Wilson, and E. Biglieri, Eds. Oxford: Academic Press, 2016, pp. 435 – 465.

[71] H. Nawaz and I. Tekin, "Double-differential-fed, dual-polarized patch antenna with 90 dB interport RF isolation for a 2.4 GHz in-band full-duplex transceiver," *IEEE Ant. and Wire. Prop. Lett.*, vol. 17, no. 2, pp. 287–290, Feb 2018.

[72] ——, "Compact dual-polarised microstrip patch antenna with high interport isolation for 2.5 ghz in-band full-duplex wireless applications," *IET Microwaves, Antennas Propagation*, vol. 11, no. 7, pp. 976–981, 2017.

[73] Y. Zhang, S. Zhang, J. Li, and G. F. Pedersen, "A dual-polarized linear antenna array with improved isolation using a slotline-based 180° hybrid for full-duplex applications," *IEEE Ant. and Wire. Prop. Lett.*, vol. 18, no. 2, pp. 348–352, 2019.

[74] T. A. Milligan, *Modern antenna design*. Wiley-IEEE Press, 2005.

[75] B. Liu, R. Zhao, Y. Ma, Z. Guo, X. Wei, W. Xing, and Y. Wang, "A 45° linearly polarized slot array antenna with substrate integrated coaxial line technique," *IEEE Antennas and Wireless Propagation Letters*, vol. 17, no. 2, pp. 339–342, Feb 2018.

[76] K. Gong, Z. N. Chen, X. Qing, P. Chen, and W. Hong, "Substrate integrated waveguide cavity-backed wide slot antenna for 60-ghz bands," *IEEE Transactions on Antennas and Propagation*, vol. 60, no. 12, pp. 6023–6026, 2012.

[77] S. Ebadi and K. Forooraghi, "An annular waveguide slot antenna," *IEEE Antennas and Wireless Propagation Letters*, vol. 6, pp. 525–528, 2007.

[78] W. Li, Z. Xia, B. You, Y. Liu, and Q. H. Liu, "Dual-polarized h-shaped printed slot antenna," *IEEE Antennas and Wireless Propagation Letters*, vol. 16, pp. 1484–1487, 2017.

[79] Yun Liu, Zhenyi Niu, and Xiaojun Wang, "Design of dual-band h-shaped slot antenna for 2.4 and 5 ghz wireless communication," in *2009 International Conference on Microwave Technology and Computational Electromagnetics (ICMTCE 2009)*, 2009, pp. 95–97.

[80] T. Chang and J. Kiang, "Compact multi-band h-shaped slot antenna," *IEEE Transactions on Antennas and Propagation*, vol. 61, no. 8, pp. 4345–4349, 2013.

[81] M. El Yazidi, M. Himdi, and J. P. Daniel, "Transmission line analysis of nonlinear slot coupled microstrip antenna," *Electronics Letters*, vol. 28, no. 15, pp. 1406–1408, 1992.

[82] W. Afzal, U. Rafique, M. M. Ahmed, M. A. Khan, and F. A. Mughal, "A tri-band h-shaped microstrip patch antenna for dcs and wlan applications," in *2012 19th International Conference on Microwaves, Radar Wireless Communications*, vol. 1, 2012, pp. 256–258.

[83] Kin-Lu Wong, Hao-Chun Tung, and Tzung-Wern Chiou, "Broadband dual-polarized aperture-coupled patch antennas with modified h-shaped coupling slots," *IEEE Transactions on Antennas and Propagation*, vol. 50, no. 2, pp. 188–191, 2002.

[84] C. Mao, S. Gao, and Y. Wang, "Dual-band full-duplex tx/rx antennas for vehicular communications," *IEEE Transactions on Vehicular Technology*, vol. 67, no. 5, pp. 4059–4070, May 2018.

[85] J. Li, D. Wu, G. Zhang, Y. Wu, and C. Mao, "Compact dual-polarized antenna for dual-band full-duplex base station applications," *IEEE Access*, vol. 7, pp. 72 761–72 769, 2019.

[86] R. Lian, T. Shih, Y. Yin, and N. Behdad, "A high-isolation, ultra-wideband simultaneous transmit and receive antenna with monopole-like radiation characteristics," *Trans. Ant. Prop.*, vol. 66, no. 2, pp. 1002–1007, Feb 2018.

[87] E. Yetisir, C. Chen, and J. L. Volakis, "Wideband low profile multiport antenna with omnidirectional pattern and high isolation," *IEEE Transactions on Antennas and Propagation*, vol. 64, no. 9, pp. 3777–3786, Sep. 2016.

[88] J. Ha, M. A. Elmansouri, P. Valale Prasannakumar, and D. S. Filipovic, "Monostatic co-polarized full-duplex antenna with left- or right-hand circular polarization," *Trans. on Ant. and Prop.*, vol. 65, no. 10, pp. 5103–5111, Oct 2017.

[89] R. B. Waterhouse, "Design of probe-fed stacked patches," *Trans. on Ant. and Prop.*, vol. 47, no. 12, pp. 1780–1784, Dec 1999.

[90] L. Sun, Y. Li, Z. Zhang, and Z. Feng, "Compact co-horizontally polarized full-duplex antenna with omnidirectional patterns," *IEEE Antennas and Wireless Propagation Letters*, vol. 18, no. 6, pp. 1154–1158, June 2019.

[91] Z. Zhou, Y. Li, J. Hu, Y. He, Z. Zhang, and P. Chen, "Monostatic copolarized simultaneous transmit and receive (star) antenna by integrated single-layer design," *IEEE Antennas and Wireless Propagation Letters*, vol. 18, no. 3, pp. 472–476, 2019.

[92] H. Saeidi-Manesh, S. Saeedi, and G. Zhang, "Dual-Polarized Perpendicularly Fed Balanced Feed Antenna With High Polarization Purity," *IEEE Antennas and Wireless Propagation Letters*, vol. 19, no. 2, pp. 368–372, 2020.

[93] N. A. Nguyen, V. H. Le, N. Nguyen-Trong, M. Radfar, A. Ebrahimi, K. Phan, and A. Desai, "Dual-Polarized Slot Antenna for Full-Duplex Systems with High Isolation," *IEEE Transactions on Antennas and Propagation*, pp. 1–1, 2020.

[94] Lu Fan, Chien-Hsun Ho, S. Kanamaluru, and Kai Chang, "Wide-band reduced-size uniplanar magic-t, hybrid-ring, and de ronde's cpw-slot couplers," *IEEE Transactions on Microwave Theory and Techniques*, vol. 43, no. 12, pp. 2749–2758, 1995.

[95] M. Caillet, M. Clenet, A. Sharaiha, and Y. M. M. Antar, "A compact wide-band rat-race hybrid using microstrip lines," *IEEE Microwave and Wireless Components Letters*, vol. 19, no. 4, pp. 191–193, 2009.

[96] W. Feng, W. Che, and K. Deng, "Compact planar magic-t using e-plane substrate integrated waveguide (siw) power divider and slotline transition," *IEEE Microwave and Wireless Components Letters*, vol. 20, no. 6, pp. 331–333, 2010.

[97] H. Liu, S. Fang, and Z. Wang, "Modified coupled line trans-directional coupler with arbitrary power divisions and its application to a 180° hybrid," *IET Microwaves, Antennas Propagation*, vol. 9, no. 7, pp. 682–688, 2015.

[98] K. Luo, W.-P. Ding, Y.-J. Hu, and W.-Q. Cao, "Design of dual-feed dualpolarized microstrip antenna with high isolation and low cross polarization," *Progress In Electromagnetics Research Letters*, vol. 36, pp. 31–40, 01 2013.

[99] V. Rathi, G. Kumar, and K. Ray, "Improved Coupling for Aperture Coupled Microstrip Antennas," *IEEE Transactions on Antennas and Propagation*, vol. 44, no. 8, pp. 1196–1198, 1996.

[100] A. Zarreen and S.C.Shrivastava, "An Introduction of Aperture Coupled Microstrip Slot Antenna," *International Journal of Engineering Science and Technology*, vol. 2, 01 2010.

[101] C. C. S. Johnson, "127-0901-811 cinch connectivity solutions johnson: Connectors, interconnects." [Online]. Available: https://www.digikey.com/en/products/detail/cinch-connectivity-solutions-johnson/127-0901-811/1755819

[102] A. S. Microwave, "1211-40001 amphenol sv microwave: Connectors, interconnects." [Online]. Available: https://www.digikey.com/en/products/detail/amphenol-sv-microwave/1211-40001/6050825

[103] M. V. Kuznetcov, S. K. Podilchak, A. J. McDermott, and M. Sellathurai, "Dual-polarized high-isolation antenna design and beam steering array enabling full-duplex communications for operation over a wide frequency range," *IEEE Open Journal of Antennas and Propagation*, vol. 2, pp. 521–532, 2021.

[104] C. R. Storck and F. Duarte-Figueiredo, "A Survey of 5G Technology Evolution, Standards, and Infrastructure Associated With Vehicle-to-Everything Communications by Internet of Vehicles," *IEEE Access*, vol. 8, pp. 117 593–117 614, 2020.

[105] D. Comite, S. K. Podilchak, P. Baccarelli, P. Burghignoli, A. Galli, A. P. Freundorfer, and Y. M. M. Antar, "Design of a Polarization-Diverse Planar Leaky-Wave Antenna for Broadside Radiation," *IEEE Access*, vol. 7, pp. 28 672–28 683, 2019.

[106] C. Chu, J. Zhu, S. Liao, Q. Xue, and A. Zhu, "Dual-Polarized Substrate-Integrated-Waveguide Cavity-Backed Monopulse Antenna Array for 5G Millimeter-Wave

Applications," in *2019 IEEE MTT-S International Microwave Conference on Hardware and Systems for 5G and Beyond (IMC-5G)*, 2019, pp. 1–3.

[107] H. Wang, D.-G. Fang, and X. Chen, "A compact single layer monopulse microstrip antenna array," *IEEE Transactions on antennas and propagation*, vol. 54, no. 2, pp. 503–509, 2006.

[108] Z.-C. Hao, H.-H. Wang, and W. Hong, "A novel planar reconfigurable monopulse antenna for indoor smart wireless access points' application," *IEEE Transactions on Antennas and Propagation*, vol. 64, no. 4, pp. 1250–1261, 2016.

[109] A. Tamayo-Dominguez, J.-M. Fernandez-Gonzalez, and M. S. Castaner, "Low-cost millimeter-wave antenna with simultaneous sum and difference patterns for 5g point-to-point communications," *IEEE Communications Magazine*, vol. 56, no. 7, pp. 28–34, 2018.

[110] P. Samczynski, K. Abratkiewicz, M. Plotka, T. P. Zielinski, J. Wszolek, S. Hausman, P. Korbel, and A. Ksiezyk, "5G Network-Based Passive Radar," *IEEE Transactions on Geoscience and Remote Sensing*, vol. 60, pp. 1–9, 2022.

[111] S. Pandit, F. H. P. Fitzek, and S. Redana, "Demonstration of 5G connected cars," in *2017 14th IEEE Annual Consumer Communications Networking Conference (CCNC)*, 2017, pp. 605–606.

[112] A. Nordrum, K. Clark, and I. Spectrum, "Everything you need to know about 5g," Sep 2021. [Online]. Available: https://spectrum.ieee.org/everything-you-need-to-know-about-5g

[113] R. Siddavaatam, I. Woungang, G. H. S. Carvalho, and A. Anpalagan, "Mobile cloud storage over 5g: A mechanism design approach," *IEEE Systems Journal*, vol. 13, no. 4, pp. 4060–4071, 2019.

[114] J. Xue, S. Biswas, A. C. Cirik, H. Du, Y. Yang, T. Ratnarajah, and M. Sellathurai, "Transceiver Design of Optimum Wirelessly Powered Full-Duplex MIMO IoT Devices," *IEEE Trans. on Com.*, vol. 66, no. 5, pp. 1955–1969, 2018.

[115] J. M. B. da Silva, G. Fodor, and C. Fischione, "On the spectral efficiency and fairness in full-duplex cellular networks," in *2017 IEEE International Conference on Communications (ICC)*, 2017, pp. 1–6.

[116] H.-L. Peng, W.-Y. Yin, J.-F. Mao, and Y.-T. Xie, "A Compact Single/Dual-Polarized Broadband Antenna With SUM and Difference Beam Capabilities," *IEEE Antennas and Wireless Propagation Letters*, vol. 9, pp. 990–993, 2010.

[117] H. Sun, X. Ge, W. He, and L. Zhao, "A Reconfigurable Antenna With Sum and Difference Patterns for WLAN Access Points," *IEEE Antennas and Wireless Propagation Letters*, vol. 19, no. 7, pp. 1073–1077, 2020.

[118] N. H. Mahmood, I. S. Ansari, G. Berardinelli, P. Mogensen, and K. A. Qaraqe, "Analysing self interference cancellation in full duplex radios," in *2016 IEEE Wireless Com. and Networking Conf.*, 2016, pp. 1–6.

[119] A. Thangaraj, R. K. Ganti, and S. Bhashyam, "Self-interference cancellation models for full-duplex wireless communications," in *2012 International Conference on Signal Processing and Communications (SPCOM)*, 2012, pp. 1–5.

[120] D. Deslandes and K. Wu, "Integrated microstrip and rectangular waveguide in planar form," *IEEE Microwave and Wireless Components Letters*, vol. 11, no. 2, pp. 68–70, 2001.

[121] D. R. Jackson, C. Caloz, and T. Itoh, "Leaky-wave antennas," *Proceedings of the IEEE*, vol. 100, no. 7, pp. 2194–2206, 2012.

[122] L. Goldstone and A. Oliner, "Leaky-wave antennas i: Rectangular waveguides," *IRE Transactions on Antennas and Propagation*, vol. 7, no. 4, pp. 307–319, 1959.

[123] C. L. Holloway, E. F. Kuester, J. A. Gordon, J. O'Hara, J. Booth, and D. R. Smith, "An overview of the theory and applications of metasurfaces: The two-dimensional equivalents of metamaterials," *IEEE Antennas and Propagation Magazine*, vol. 54, no. 2, pp. 10–35, 2012.

[124] F. Xu and K. Wu, "Guided-wave and leakage characteristics of substrate integrated waveguide," *IEEE Transactions on Microwave Theory and Techniques*, vol. 53, no. 1, pp. 66–73, 2005.

[125] D. Deslandes and K. Wu, "Accurate modeling, wave mechanisms, and design considerations of a substrate integrated waveguide," *IEEE Transactions on Microwave Theory and Techniques*, vol. 54, no. 6, pp. 2516–2526, 2006.

[126] S. Adhikari, Y.-J. Ban, and K. Wu, "Magnetically tunable ferrite loaded substrate integrated waveguide cavity resonator," *IEEE Microwave and Wireless Components Letters*, vol. 21, no. 3, pp. 139–141, 2011.

[127] Z.-C. Hao, W. Hong, J.-X. Chen, X.-P. Chen, and K. Wu, "Compact super-wide bandpass substrate integrated waveguide (siw) filters," *IEEE Transactions on Microwave Theory and Techniques*, vol. 53, no. 9, pp. 2968–2977, 2005.

[128] D. Deslandes, "Design equations for tapered microstrip-to-substrate integrated waveguide transitions," in *2010 IEEE MTT-S International Microwave Symposium*, 2010, pp. 704–707.

[129] E. Miralles, H. Esteban, C. Bachiller, A. Belenguer, and V. E. Boria, "Improvement for the design equations for tapered microstrip-to-substrate integrated waveguide transitions," in *2011 International Conference on Electromagnetics in Advanced Applications*, 2011, pp. 652–655.

[130] L. Yan, W. Hong, G. Hua, J. Chen, K. Wu, and T. J. Cui, "Simulation and experiment on siw slot array antennas," *IEEE Microwave and Wireless Components Letters*, vol. 14, no. 9, pp. 446–448, 2004.

[131] R. Elliott, "An improved design procedure for small arrays of shunt slots," *IEEE Transactions on Antennas and Propagation*, vol. 31, no. 1, pp. 48–53, 1983.

[132] J. Liu, D. R. Jackson, and Y. Long, "Substrate integrated waveguide (siw) leaky-wave antenna with transverse slots," *IEEE Transactions on Antennas and Propagation*, vol. 60, no. 1, pp. 20–29, 2012.

[133] J. Gomez-Tornero, A. Martinez, D. Rebenaque, M. Gugliemi, and A. Alvarez-Melcon, "Design of tapered leaky-wave antennas in hybrid waveguide-planar technology for millimeter waveband applications," *IEEE Transactions on Antennas and Propagation*, vol. 53, no. 8, pp. 2563–2577, 2005.

[134] F. Taringou, D. Dousset, J. Bornemann, and K. Wu, "Broadband cpw feed for millimeter-wave siw-based antipodal linearly tapered slot antennas," *IEEE Transactions on Antennas and Propagation*, vol. 61, no. 4, pp. 1756–1762, 2013.

[135] S. Cheng, H. Yousef, and H. Kratz, "79 ghz slot antennas based on substrate integrated waveguides (siw) in a flexible printed circuit board," *IEEE Transactions on Antennas and Propagation*, vol. 57, no. 1, pp. 64–71, 2009.

[136] S. Moitra and A. Mukhopadhyay, "Ku-band substrate integrated waveguide (siw) slot array antenna for next generation networks," *Global Journal of Computer Science and Technology: E Network, Web and Security*, vol. 13, pp. 11–15, 10 2013.

[137] Q.-C. Ye, Y.-M. Zhang, J.-L. Li, G. F. Pedersen, and S. Zhang, "High-Isolation Dual-Polarized Leaky-Wave Antenna With Fixed Beam for Full-Duplex Millimeter-Wave Applications," *IEEE Trans. on Antennas Propagat.*, vol. 69, no. 11, pp. 7202–7212, 2021.

[138] C. A. M. Hernandez, L. B. Boskovic, M. A. Elmansouri, M. Ignatenko, and D. S. Filipovic, "Fixed and Steerable Beam Dual-Polarized Lens Antenna With High Tx to Rx Isolation," *IEEE Trans. on Antennas Propagat.*, vol. 69, no. 11, pp. 7213–7221, 2021.

[139] R. S. Hao, Y. J. Cheng, Y. F. Wu, and Y. Fan, "A W-Band Low-Profile Dual-Polarized Reflectarray With Integrated Feed for In-Band Full-Duplex Application," *IEEE Trans. on Antennas Propagat.*, vol. 69, no. 11, pp. 7222–7230, 2021.

[140] Kim, Sang-Gyu and Chang, Kai, "Low-cost monopulse antenna using bi-directionally-fed microstrip patch array," *Electronics Letters*, vol. 39, no. 20, pp. 1428–1429, 2003.

[141] "End launch supersma 27 GHz jack (female) standard block (.500)," Jan. 2022. [Online]. Available: https://mpd.southwestmicrowave.com/product/292-04a-6-end-launch-supersma-27-ghz-jack-female-standard-block/

[142] M. V. Kuznetcov, V. G.-G. Buendía, Z. Shafiq, L. Matekovits, D. E. Anagnostou, and S. K. Podilchak, "Printed Leaky-Wave Antenna With Aperture Control Using Width-Modulated Microstrip Lines and TM Surface-Wave Feeding by SIW Technology," *IEEE Antennas and Wireless Propagation Letters*, vol. 18, no. 9, pp. 1809–1813, 2019.

[143] M. V. Kuznetcov, S. K. Podilchak, A. J. McDermott, and M. Sellathurai, "Dual-polarized antenna with dual-differential integrated feeding for wideband full-

duplex systems," *IEEE Transactions on Antennas and Propagation*, vol. 69, no. 11, pp. 7192–7201, 2021.

[144] G. Srivastava and A. Mohan, "A Differential Dual-Polarized SIW Cavity-Backed Slot Antenna," *IEEE Transactions on Antennas and Propagation*, vol. 67, no. 5, pp. 3450–3454, 2019.

[145] "krytar - 6.0-26.5 ghz 180 degree hybrid coupler model 4060265." [Online]. Available: https://www.krytar.com/pdf/4060265.pdf

[146] P. D. Hilario Re, D. Comite, S. K. Podilchak, C. A. Alistarh, G. Goussetis, M. Sellathurai, J. Thompson, and J. Lee, "Fmcw radar with enhanced resolution and processing time by beam switching," *IEEE Open Journal of Antennas and Propagation*, vol. 2, pp. 882–896, 2021.

[147] B. Debaillie, B. van Liempd, B. Hershberg, J. Craninckx, K. Rikkinen, D. J. van den Broek, E. A. M. Klumperink, and B. Nauta, "In-band full-duplex transceiver technology for 5g mobile networks," in *ESSCIRC Conference 2015 - 41st European Solid-State Circuits Conference (ESSCIRC)*, 2015, pp. 84–87.